

# Metabolomics as a tool for the study of drug-induced hepatotoxicity

Juan Carlos García Cañaveras



VNIVERSITAT  
DE VALÈNCIA

TESIS DOCTORAL

**Metabolomics as a tool for the study of drug-induced  
hepatotoxicity**

JUAN CARLOS GARCÍA CAÑAVERAS

DIRECTORES:

Dr. AGUSTÍN LAHOZ RODRÍGUEZ

Dra. MARÍA TERESA DONATO MARTÍN

PROGRAMA DE DOCTORADO: BIOQUÍMICA Y BIOMEDICINA

Departamento de Bioquímica y Biología Molecular

Facultat de Ciències Biològiques

**2015**



La presente tesis doctoral ha sido realizada dentro del programa VALi+d para investigadores en formación de la Conselleria d'Educació, Cultura i Esport de la Generalitat Valenciana en la Unidad Mixta de Hepatología Experimental, adscrita al Departamento de Bioquímica y Biología Molecular de la Facultad de Medicina y Odontología de la Universidad de Valencia y al Instituto de Investigación Sanitaria La Fe bajo la dirección de los doctores Agustín Lahoz Rodríguez y María Teresa Donato Martín. Asimismo, como parte de la actividad investigadora asociada, se incluye una estancia de 3 meses en el grupo Quantitative Biology and Bioinformatics perteneciente al VTT Technical Research Center of Finland (Espoo, Finlandia) bajo la tutela de los doctores Matej Orešič y Marko Sysi-Aho.



Instituto de  
Investigación  
Sanitaria La Fe





D. AGUSTÍN LAHOZ RODRÍGUEZ, Doctor en Farmacia Investigador Principal en el Instituto para la Investigación del Hospital Universitario La Fe de Valencia,

INFORMA:

Que la presente memoria titulada "**Metabolomics as a tool for the study of drug-induced hepatotoxicity**", realizada por el licenciado en Bioquímica **Juan Carlos García Cañaveras**, bajo su dirección, en la Unidad Mixta de Hepatología Experimental de la Universidad de Valencia y del Instituto de Investigación Sanitaria La Fe, corresponde a su Tesis Doctoral y autoriza mediante este escrito la presentación de la misma para la obtención del grado de Doctor.

Fdo. Dr. Agustín Lahoz Rodríguez



Dña. MARÍA TERESA DONATO MARTÍN, Doctora en Farmacia y Profesora Contratada Doctora adscrita al Departamento Bioquímica y Biología Molecular de la Facultad de Medicina y Odontología de la Universidad de Valencia

INFORMA:

Que la presente memoria titulada "**Metabolomics as a tool for the study of drug-induced hepatotoxicity**", realizada por el licenciado en Bioquímica **Juan Carlos García Cañaveras**, bajo su dirección, en la Unidad Mixta de Hepatología Experimental de la Universidad de Valencia y del Instituto de Investigación Sanitaria La Fe, corresponde a su Tesis Doctoral y autoriza mediante este escrito la presentación de la misma para la obtención del grado de Doctor.

Fdo. Dra. María Teresa Donato Martín





## AGRADECIMIENTOS

A todos aquellos que han tenido la paciencia de enseñarme y corregir mis errores a lo largo de mi aprendizaje y mi carrera investigadora.

A los doctores Luis Franco y Maribel Rodrigo por ser los primeros en acogerme en un laboratorio de investigación. En el Laboratorio de Cromatina del Departamento de Bioquímica y Biología Molecular de la Facultad de Ciencias Biológicas de la Universidad de Valencia empecé a conocer en qué consistía el trabajo de un investigador y de la mano de Andy aprendí una gran cantidad de lecciones no solamente relacionadas con las técnicas empleadas en Bioquímica y Biología Molecular, sino herramientas imprescindibles en cualquier trabajo o tarea vital como son la curiosidad, la paciencia, el tesón, la humildad de aprender de quien tiene algo que enseñarte...

Al Dr. Pedro A. Lazo, investigador principal del Instituto de Biología Molecular y Celular del Cáncer de Salamanca y a todos los miembros de su laboratorio, en especial a Marta y Alberto.

A los doctores M<sup>a</sup> José Gómez-Lechón y José Vicente Castell por haberme dado la oportunidad de incorporarme al grupo de Hepatología Experimental. A los doctores Teresa Donato y Agustín Lahoz, por permitirme descubrir un mundo completamente nuevo para mí, el de la metabonomía y de los problemas sanitarios y económicos derivados de la hepatotoxicidad provocada por fármacos, lleno de retos inmensamente interesantes y relevantes. Ellos me han guiado en el camino hacia la consecución de esta tesis, me han hecho partícipe de sus proyectos e ideas, han confiado en mi trabajo y han puesto todo su entusiasmo y conocimiento en ayudarme a crecer tanto a nivel profesional como personal. A todos mis compañeros del grupo de Hepatología Experimental y de la Unidad Analítica con los que he coincidido en esta etapa, tanto a los que todavía están, como a los que

han dado o tenido que dar un giro a sus carreras que les ha alejado de este grupo. A Silvia y Nuri, por su impagable ayuda tanto en cultivos celulares como en otras muchas tareas y situaciones. A Sandra por estar siempre ahí, trabajando duro, ayudando, apoyando, animando, dando consejos y vigilando que todo vaya sobre ruedas.

A mis compañeros del grupo Quantitative Biology and Bioinformatics perteneciente al VTT Technical Research Center of Finland (Espoo, Finlandia). Aunque la experiencia no fue todo lo satisfactoria que cabría esperar, hubo personas que estuvieron a mi lado durante los tres meses y me ayudaron a dar algunos pasos importantes en el campo de la bioestadística y de la bioinformática, además de permitirme aprender una gran lección vital.

A mis amigos, porque no todo en la vida es ciencia... aunque con alguno de ellos sea el principal tema de conversación.

A mi padres. Porque han puesto todo su trabajo y cariño en que yo pudiera tener las oportunidades que ellos nunca tuvieron. Siempre me han dejado elegir el camino que he creído conveniente y no han hecho otra cosa más que apoyarme en las decisiones tomadas y animarme a conseguir los objetivos que me he ido fijando.

A Alicia. La investigación científica es una disciplina donde las alegrías son escasas en comparación con los momentos duros, los experimentos fallidos, las dudas... su paciencia, comprensión y apoyo han sido esenciales para poder avanzar en este camino.

### LIST OF CONTENTS

<b>LIST OF ABBREVIATIONS</b>	15
<b>ABSTRACT</b>	21
<b>1. INTRODUCTION</b>	25
1.1 General aspects of liver structure and function	27
1.2 Cells of the liver	29
1.3 Drug-induced liver injury	31
1.4 Mechanism-based classification of DILI	35
1.4.1 Steatosis	35
1.4.2 Phospholipidosis	36
1.4.3 Cholestasis	37
1.4.4 Oxidative Stress	38
1.5 Experimental models for the study of hepatotoxicity	40
1.5.1 Human hepatocytes	41
1.5.2 Hepatoma cell lines	42
1.6 Methods for the evaluation of DILI using <i>in vitro</i> models	45
1.6.1 Conventional hepatotoxicity assays	45
1.6.2 Multiparametric approaches	46
1.7 Metabolomics	49
1.7.1 Basic structure of a metabolomic study	51
1.7.2 Techniques for the study of the metabolome	52
1.7.3 LC-MS-based metabolomics	53
1.7.4 Data analysis in metabolomics	58
1.7.5 State of the art in the application of metabolomics to hepatotoxicity prediction	61
1.8 Hypothesis of work and objectives	63
<b>2. METHODOLOGY</b>	65
2.1 General procedures, equipment and reagents	67

## List of Contents

---

2.2	Instrumentation used in MS-based metabolomics analysis	68
2.2.1	Waters Acquity UPLC system	68
2.2.2	Waters Synapt HDMS QToF mass spectrometer	69
2.2.3	Waters Xevo TQ-S mass spectrometer	71
2.3	Analytical conditions for LC-MS untargeted analysis	72
2.3.1	Generic RP untargeted analysis	72
2.3.2	Lipidomic RP untargeted analysis	73
2.3.3	HILIC untargeted analysis	74
2.4	Raw data processing and metabolite identification in untargeted metabolomic analysis	75
2.5	Data analysis	78
2.5.1	Detection of outliers	79
2.5.2	Identification of metabolomic alterations	82
2.5.3	Predictive model development	84
2.6	Culture and treatment of HepG2 cells with model hepatotoxic compounds	93
2.7	Sample processing and analysis optimization for HepG2 cells	96
2.7.1	Sample analysis	97
2.7.2	Metabolome extraction	99
2.7.3	Sample processing strategy optimization	101
2.8	Optimized sample extraction protocols for untargeted metabolomic analysis in HepG2 cells	104
2.8.1	Generic protocol	104
2.8.2	Steatosis/Phospholipidosis specific protocol	105
2.9	<i>In vivo</i> hepatotoxicity studies in medaka ( <i>Oryzias latipes</i> )	107
2.9.1	Animal handling	107
2.9.2	Sample processing and analysis	108
2.10	<i>In vivo</i> hepatotoxicity studies in rats	110
2.10.1	Animal handling	110

## List of Contents

---

2.10.2	Sample processing and untargeted LC-MS analysis	111
2.11	Method validation for LC-MS/MS targeted analyses	113
2.12	Targeted analysis of bile acids	114
2.12.1	Bile acids included in the method	114
2.12.2	UPLC-MS analysis	115
2.12.3	Sample processing	118
2.13	Targeted analysis of oxidative stress biomarkers	119
2.13.1	OS markers included in the method	119
2.13.2	UPLC-MS analysis	119
2.13.3	Sample processing	121
2.14	Targeted analysis of $\gamma$ -glutamyl dipeptides	124
2.14.1	Compounds included in the method	124
2.14.2	UPLC-MS analysis	124
2.14.3	Sample processing	128
<b>3.</b>	<b>RESULTS &amp; DISCUSSION</b>	<b>131</b>
3.1	Quality assurance strategy in untargeted metabolomic analysis	133
3.2	Optimization of metabolome coverage for mammalian cells in adherent culture by using LC-MS	142
3.2.1	Optimization of endometabolome analysis by LC-MS	142
3.2.2	Optimization of endometabolome extraction	147
3.2.3	Optimization of cell harvesting and processing	149
3.2.4	Assembling an appropriate protocol for sample processing and analysis	151
3.3	Metabolomic analysis of HepG2 cells exposed to model hepatotoxic compounds	155
3.3.1	Identification of markers of hepatotoxicity	157
3.3.2	Development of a metabolomic approximation focused on the detection of lipidomic alterations induced by steatogenic and phospholipidogenic drugs	174

## List of Contents

---

3.3.3	Targeted analysis of OS markers	184
3.3.4	Development of predictive/classificatory models of hepatotoxicity	188
3.4	Extrapolation of <i>in vitro</i> results to <i>in vivo</i> models	200
3.4.1	Differential metabolomic profiling analysis of medaka	200
3.4.2	Differential metabolomic analysis of rats exposed to tetracycline and paracetamol	216
3.4.3	Targeted analysis of non-invasive serum markers of hepatotoxicity in rats	223
<b>4.</b>	<b>CONCLUSIONS &amp; OUTLOOK</b>	<b>231</b>
4.1	Conclusions	233
4.2	Outlook	235
	<b>RESUMEN EN CASTELLANO</b>	<b>237</b>
	<b>REFERENCES</b>	<b>243</b>
	<b>LIST OF FIGURES</b>	<b>271</b>
	<b>LIST OF TABLES</b>	<b>279</b>
	<b>LIST OF PUBLICATIONS</b>	<b>281</b>

## List of Abbreviations

---

### LIST OF ABBREVIATIONS

<b>2CV</b>	Double cross validation
<b>2-dG</b>	2-deoxyguanosine
<b>8-OH-dG</b>	8-hydroxy-2'-deoxyguanosine
<b>ALT</b>	Alanine aminotransferase
<b>ANOVA</b>	Analysis of variance
<b>AST</b>	Aspartate aminotransferase
<b>AUROC</b>	Area under the receiver operating characteristic curve
<b>BA</b>	Bile acid
<b>BSEP</b>	Bile Salt Export Pump
<b>CA</b>	Cholic acid
<b>CAD</b>	Cationic amphiphilic drug
<b>CA-D4</b>	Cholic acid-2,2,4,4-D4
<b>CDCA</b>	Chenodeoxycholic acid
<b>CE</b>	Capillary electrophoresis
<b>ChE</b>	Cholesterol ester
<b>Cl-Tyr</b>	3-chloro-L-tyrosine
<b>CSSG</b>	Cysteine-glutathione disulfide
<b>CV</b>	Cross validation
<b>CYP</b>	Cytochrome P-450
<b>DCA</b>	Deoxycholic acid
<b>DCA-D4</b>	Deoxycholic acid-2,2,4,4-D4
<b>DG</b>	Diacylglyceride
<b>DHCA</b>	Dehydrocholic acid
<b>DILI</b>	Drug-induced liver injury
<b>DMSO</b>	Dimethyl sulfoxide



## List of Abbreviations

---

<b>DNPH</b>	2,4-dinitrophenylhydrazine
<b>DP</b>	Dipeptidase
<b>EMA</b>	European Medicines Agency
<b>ESI</b>	Electro spray ionization
<b>FA</b>	Fatty acid
<b>FDA</b>	US Food and Drug Administration
<b>FDR</b>	False discovery rate
<b>FWHM</b>	Full width at half maximum
<b>FXR</b>	Farnesoid X receptor
<b>GC</b>	Gas chromatography
<b>GCA</b>	Glycocholic acid
<b>GCA-D4</b>	Glycocholic acid-2,2,4,4-D4
<b>GCDCA</b>	Glycochenodeoxycholic acid
<b>GCDCA-D4</b>	Glycochenodeoxycholic acid-2,2,4,4-D4
<b>GCL</b>	Glutamate cysteine ligase
<b>GDCA</b>	Glycodeoxycholic acid
<b>GDHCA</b>	Glycodehydrocholic acid
<b>GGT</b>	$\gamma$ -glutamyl transpeptidase
<b>GHCA</b>	Glycohyochocholic acid
<b>GHDCA</b>	Glychoyodeoxycholic acid
<b>GLCA</b>	Glycolithocholic acid
<b>GS</b>	Glutathione synthase
<b>GSH</b>	Glutathione
<b>GSSG</b>	Oxidized glutathione
<b>GUDCA</b>	Glycoursodeoxycholic acid
<b>HCA</b>	Hierarchical cluster analysis
<b>HCA</b>	Hyochocholic acid

## List of Abbreviations

---

<b>HCS</b>	High content screening
<b>HDCA</b>	Hyodeoxycholic acid
<b>HDL</b>	High density lipoprotein
<b>HILIC</b>	Hydrophilic interaction chromatography
<b>HLC</b>	Hepatocyte-like cell
<b>HMDB</b>	Human Metabolome Database
<b>HPLC</b>	High performance liquid chromatography
<b>HSC</b>	Hepatic stellate cell
<b>IS</b>	Internal standard
<b>I-Tyr</b>	3-iodo-L-tyrosine
<b>KC</b>	Kupffer cell
<b>LC</b>	Liquid chromatography
<b>LCA</b>	Lithocholic acid
<b>LCA-D4</b>	Lithocholic acid-2,2,4,4-D4
<b>LCFA</b>	Long-chain fatty acid
<b>LDH</b>	Lactate dehydrogenase
<b>LLOQ</b>	Lower limit of quantification
<b>LOD</b>	Limit of detection
<b>LSEC</b>	Liver sinusoidal endothelial cell
<b>LV</b>	Latent variable
<b>LysoPA</b>	Lysophosphatidic acid
<b>LysoPC</b>	Lysophosphatidylcholine
<b>LysoPE</b>	Lysophosphatidylethanolamine
<b>LysoPG</b>	Lysophosphatidylglycerol
<b>LysoPI</b>	Lysophosphatidylinositol
<b><i>m/z</i></b>	Mass-to-charge ratio
<b>MCFA</b>	Medium-chain fatty acid

## List of Abbreviations

---

<b>MDA</b>	Malondialdehyde
<b>MG</b>	Monoacylglyceride
<b>MRM</b>	Multiple reaction monitoring
<b>MS</b>	Mass spectrometry
<b>mtDNA</b>	Mitochondrial DNA
<b>m-Tyr</b>	DL-m-tyrosine
<b>MuroCA</b>	Mucrocholic acid
<b>MVDA</b>	Multivariate data analysis
<b>NAFLD</b>	Non-alcoholic fatty liver disease
<b>NAPQI</b>	N-acetyl-p-benzoquinone imine
<b>NASH</b>	Non-alcoholic steatohepatitis
<b>NEM</b>	N-ethylmaleimide
<b>NMR</b>	Nuclear magnetic resonance
<b>N-Tyr</b>	3-nitro-tyrosine
<b>OPLS-DA</b>	Orthogonal projection to latent structures-discriminant analysis
<b>OS</b>	Oxidative stress
<b>o-Tyr</b>	DL-o-tyrosine
<b>PA</b>	Phosphatidic acid
<b>PBS</b>	Phosphate buffer saline
<b>PC</b>	Phosphatidylcholine
<b>PCA</b>	Principal component analysis
<b>PCLS</b>	Precision-cut liver slices
<b>PE</b>	Phosphatidylethanolamine
<b>PG</b>	Phosphatidylglycerol
<b>Phed5</b>	L-phenylalanine-d5
<b>PI</b>	Phosphatidylinositol

## List of Abbreviations

---

<b>PKC</b>	Protein kinase C
<b>PL</b>	Phospholipid
<b>PLA2</b>	Phospholipase A2
<b>PLS-DA</b>	Partial least squares–discriminant analysis
<b>ppm</b>	Parts per million
<b>PS</b>	Phosphatidylserine
<b>p-Tyr</b>	L-tyrosine
<b>Q<sup>2</sup></b>	Predictable y variation
<b>QC</b>	Quality control
<b>QTOF</b>	Quadrupole time of flight
<b>R<sup>2</sup></b>	Total y explained variance
<b>ROS</b>	Reactive oxygen species
<b>RP</b>	Reversed phase
<b>RSD</b>	Relative standard deviation
<b>RT</b>	Retention time
<b>SAH</b>	S-(5-adenosyl)-L-homocysteine
<b>SAM</b>	S-(5-adenosyl)-L-methionine
<b>SCFA</b>	Short-chain fatty acid
<b>SD</b>	Space of Disse
<b>SIMCA</b>	Soft independent modeling of class analogy
<b>SM</b>	Sphingomieline
<b>SNW</b>	Strong needle wash
<b>SW</b>	Seal wash
<b>TCA</b>	Taurocholic acid
<b>TCDCa</b>	Taurochenodeoxycholic acid
<b>TDCA</b>	Taurodeoxycholic acid
<b>TDHCA</b>	Taurodehydrocholic acid

## List of Abbreviations

---

<b>TG</b>	Triacylglyceride
<b>THCA</b>	Taurohyococholic acid
<b>THDCA</b>	Taurohyodeoxycholic acid
<b>TLCA</b>	Taurolithocholic acid
<b>TQ</b>	Triple quadrupole
<b>TUDCA</b>	Tauroursodeoxycholic acid
<b>T<math>\alpha</math>MCA</b>	Tauro- $\alpha$ -muricholic acid
<b>T<math>\beta</math>MCA</b>	Tauro- $\beta$ -muricholic acid
<b>T<math>\omega</math>MCA</b>	Tauro- $\omega$ -muricholic acid
<b>UDCA</b>	Ursodeoxycholic acid
<b>UPLC</b>	Ultra performance liquid chromatography
<b>VDR</b>	Vitamin D receptor
<b>VIP</b>	Variable importance in the projection
<b>WNW</b>	Weak needle wash
<b><math>\alpha</math>MCA</b>	$\alpha$ Muricholic acid
<b><math>\beta</math>MCA</b>	$\beta$ Muricholic acid
<b><math>\omega</math>MCA</b>	$\omega$ Muricholic acid

### ABSTRACT

Drug-induced liver injury (DILI) is a major health and economic problem and the leading cause of hepatic dysfunction, drug failure during clinical testing and post-market withdrawal of approved drugs. Pre-clinical testing should be able to detect potential hepatotoxins early in the drug development process in order to minimize health risks and financial losses. Several liver-derived *in vitro* models have been developed to be used in pharmacology and toxicology research to understand the mechanism of DILI and to evaluate potential hepatotoxicity of new chemical entities. Although they fail to reproduce the complexity of a whole organ, their low cost, high reproducibility, and the possibility of a human origin make them a good complement to traditional *in vivo* tests. Monoparametric strategies used in *in vitro* toxicity testing have been proved insufficient to predict human DILI. The application of the new 'omics' technologies allows the simultaneous determination of multiple parameters in a single biological sample and represents a more sensitive, comprehensive and powerful tool for the study of hepatotoxic events. Among them, metabolomics measures the downstream products of the 'omics cascade', thus representing a closer approximation to phenotype than the study of genes, transcripts or proteins.

Based on the previous evidences we decided to evaluate whether metabolomics, in combination with *in vitro* cellular models and *in vivo* animal models, could be a useful tool for the discovery of characteristic patterns associated to specific mechanisms of DILI.

First, we defined a suitable framework that, thanks to a careful design of sample analysis and the incorporation of different internal standards and quality controls, allowed us to perform metabolomic analysis within a quality assurance environment. Then, uni- and multivariate statistical tools were selected in order to be able to identify mechanism-specific

## Abstract

---

alterations and to develop predictive/classificatory models. Finally, we optimized a sample processing and analysis strategy that allowed the differential extraction and detection of a broad range of metabolites ranging from highly polar to highly apolar ones thus maximizing metabolome coverage.

The application of the developed tools to HepG2 cells exposed to subcytotoxic concentrations of model hepatotoxins acting through different mechanisms of toxicity allowed us to identify specific metabolomic patterns associated to each of the mechanisms of interest. Moreover, the application of multivariate data analysis techniques allowed the development of predictive/classificatory models able not only to distinguish between toxic and non-toxic compounds, but also to specifically classify drugs according to their mechanism of hepatotoxicity. The proposed strategy could be of interest for the identification of early markers of hepatotoxicity and for the prediction of mechanism of hepatotoxicity of new drug entities.

The usefulness of the analytical strategy was also confirmed by its application with *in vivo* models using both medaka (*Oryzias latipes*) and rat. Studies in medaka revealed common liver altered pathways with HepG2 cells, suggesting medaka as a useful model for human hepatotoxicity prediction. Toxicity studies in rats allowed us to identify common serum markers of hepatotoxicity which could be used as biomarkers in pre-clinical studies or even extrapolated to humans.

*"Nothing is hidden so much that it  
wouldn't be revealed through its fruit"*

Paracelsus

*"Data does not equal information;  
information does not equal knowledge;  
and, most importantly of all,  
knowledge does not equal wisdom.  
We have oceans of data,  
rivers of information,  
small puddles of knowledge,  
and the odd drop of wisdom."*

Prof. Henry Nix





# **1. Introduction**

---



### 1.1 General aspects of liver structure and function

The liver plays an essential role in a variety of functions to maintain homeostasis in the organism. This organ is able to synthesize, degrade or storage a wide variety of molecules in a regulated way. It is involved in the metabolism of substances as different as carbohydrates, lipids, amino acids, bile acids (BAs), vitamins, steroids or iron. The liver also produces most of the circulating plasma proteins, including the most abundant component, albumin. Moreover, the liver is the center organ in the detoxification of xenobiotics (1-3).

The liver is the largest solid organ in the human body (from 1300 to 1700 g in adults) and it is located in the abdominal cavity. Blood supply to the liver is performed by two different blood vessels: i) the hepatic portal vein, which represents about 80% of the hepatic blood supply, carries blood that, having already circulated through the gut, the pancreas and the spleen, is reduced in oxygen and enriched in nutrients, xenobiotics, hormones and growth factors; and ii) the hepatic artery, which supplies oxygen-rich blood from the aorta artery. The unusual pattern of blood supply in the liver is essential to understand its role in both nutrient and xenobiotic metabolism (2, 4). Two different efferent vessels coexist in the liver. On one hand, blood is drained into the central veins and leaves the liver through a number of hepatic veins, which enter the inferior vena cava. On the other hand, the bile produced in the liver is collected in bile canaliculi, which merge to form bile ducts.

The basic structural unit of the liver is the hepatic lobule (**Figure 1.1.A**). It has the shape of a polygon, usually a hexagon. Each corner of the polygonal hepatic lobule is occupied by a portal triad, consisting of the hepatic artery, bile duct and portal vein. At the center of each hepatic lobule is located the central vein. The area defined by this hexagon is occupied by hepatocyte plates that adopt a radial distribution from the central vein to the perimeter of the lobule. Hepatic plates or cords are

## Introduction

generally one hepatocyte thick and are separated from one another by the hepatic sinusoids (the capillaries of the liver) which are lined by sinusoidal endothelium (3, 5).

The functional unit of the liver, known as the acinus, is delimited by the elliptical or diamond-shaped space that comprises two adjacent central veins, connected by the long axis, and to adjacent portal triads, connected by the short axis (**Figure 1.1.A**) (5, 6). Two different fluid flows take place along this axis. Blood enters the liver from the portal veins and hepatic arteries at the portal triads, flows through the sinusoids and exits from the central vein. On the other hand, bile flows in the opposite direction, thus going through the canaliculi along the hepatocyte plates to the bile ducts situated in the portal triad (3, 5).

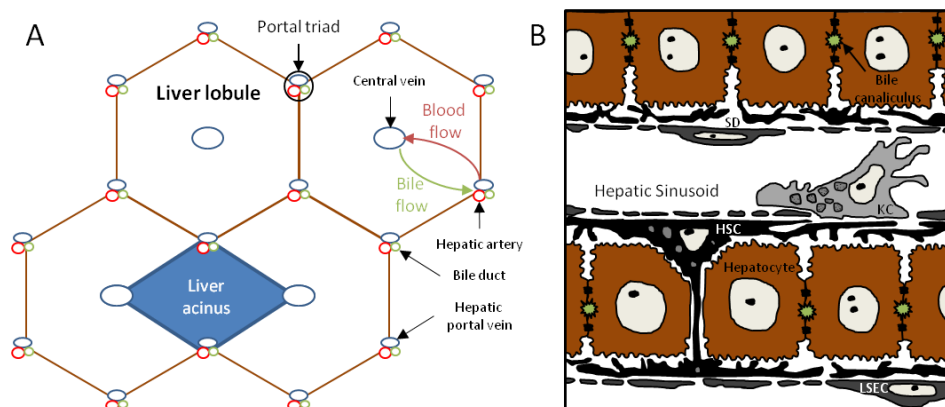


**Figure 1.1. A)** Diagram of the basic hepatic lobule and the acinus substructure. Hepatic lobules have hexagonal shape with the portal triads - formed by the hepatic artery, the hepatic portal vein and the bile duct - located at the corners and the central vein located at the center. **B)** Diagram illustrating the basic structure and composition of liver sinusoids. Liver sinusoids are lined by fenestrated liver sinusoidal endothelial cells (LSEC). Hepatocytes are disposed forming hepatic cords, with the basolateral membranes exposed to blood components through the space of Disse (SD), while the lateral membrane is in contact with adjacent hepatocytes attached by tight junctions and forms the bile canaliculus. Hepatic stellate cells (HSC) are located in the SD with numerous plasmatic extensions that allow them to be in close contact with other HSC as well with hepatocytes and LSEC. Finally, Kupffer cells (KC) are attached to the luminal surface of LSEC, in a strategic location that permits its continuous access to afferent blood. **Figure 1.1.A** adapted from reference (5). **Figure 1.1.B** adapted from reference (7).

### 1.2 Cells of the liver

The liver is comprised by a rich variety of cells. The hepatocytes, the most abundant cell type, carry out the majority of the functions associated with the liver (5). They are responsible of the synthesis and excretion of plasma proteins, coagulation factors, lipoproteins and acute phase reactants. Moreover, they control the homeostasis of glucose/glycogen, triacylglycerides (TG), cholesterol, BAs, vitamins A and D, and metabolize amino acids, metals, heme, bilirubin, and xenobiotics (1). Nevertheless, the hepatocytes alone are not competent to perform all the hepatic functions, and the cohort of non-parenchymal cells are essential to the maintenance of the liver structure and are important contributors to various roles that support and regulate hepatic growth and function. Major liver non-parenchymal cells are bile duct epithelial cells (or cholangiocytes), liver sinusoidal endothelial cells (LSEC), hepatic stellate cells (HSC), Kupffer cells (KC), and hepatic progenitor cells (5, 8) (**Figure 1.1.B**). The liver also contains a large and diverse population of residing immunocytes that in addition to KC and LSEC are essential components of the liver-centered immune system (2, 5, 9).

Hepatocytes are large cells and represent about 60% of the total cell population and about 80% of the liver mass/volume (2, 3, 5, 8). Hepatocytes possess one or more nuclei, as a result of mitotic division of the nucleus without cytokinesis, with prominent nucleoli, indicative of an active transcriptional activity. As corresponds to their numerous and varied metabolic, storage and secretory functions, hepatocytes contain abundant mitochondria, lysosomes, peroxisomes and Golgi complexes, mainly adjacent to the bile canaliculi. The cytoplasm is rich in rough endoplasmic reticulum, indicative of the hepatocyte's secretory nature, and smooth endoplasmic reticulum, where many of the enzymes involved in phase I and phase II biotransformation of endogenous and exogenous compounds are located (2, 5).

## Introduction

---

Hepatocytes are highly polarized cuboidal-shaped cells. Due to the particular configuration of cells in the hepatic cords, each hepatocyte is adjacent to two neighbor hepatocytes and possess two basolateral domains that interface with the sinusoids on opposite sides of the cell plates (5, 10). The basolateral domain of hepatocytes is formed by the sinusoidal and lateral plasma membrane. At the sinusoidal side, hepatocytes are directly in contact with most of the blood substances thanks to the fenestrations present in the membranes of the LSEC. At the lateral membrane, neighbor hepatocytes are connected through gap junctions, thus allowing the communication of adjacent hepatocytes by transfer of small molecules (2, 11). The apical domain of the hepatocyte represents a small portion of the plasma membrane and lies between cells, set off from the basolateral plasma membrane by tight junctions and forming the bile canaliculus (10). These membrane domains show structural, compositional and functional differences and are essential for the role of hepatocytes in the uptake, metabolism and biliary elimination of both endogenous and exogenous substrates (5). In general, the basolateral plasma membrane has transporters that remove substances (e.g. BAs, drugs) from the portal venous blood by facilitated diffusion along a concentration gradient, whereas the apical plasma membrane has transporters that pump substances against a steep concentration gradient from the cell interior into the bile canaliculus (10).

The liver architecture, cell composition and function are essential to understand its involvement in drug metabolism and toxicity. In particular, hepatocytes are the major players in biotransformation processes (phase I and II reactions and drug transport) and their function strongly impacts on the pharmacokinetic, side effects and toxicity of drugs. Therefore, the development of *in vitro* approaches for drug metabolism and hepatotoxicity studies is focused on the imitation of the functional status and disposition of hepatocytes, and other components, in the intact liver.

### 1.3 Drug-induced liver injury

The liver is an organ specially prone to suffer toxic damage due to its particular anatomic location and to its involvement in drug metabolism and detoxification. As described above, the liver is functionally interposed between the site of absorption of exogenous compounds and the systemic circulation. Thus, through its blood supply from the portal vein, the liver is directly exposed to all ingested substances that are present in the portal blood (12-14). On the other hand, the liver is quantitatively and qualitatively the most important site of drug metabolism due to the expression in the hepatocytes of phase I and phase II metabolizing enzymes and drug transporters. Thus the liver, along with drug-metabolizing enzymes and drug transporters expressed in the intestinal mucosa, provides an effective barrier that prevents xenobiotics from entering the systemic circulation (15). However, the high exposure of the liver to xenobiotics, its involvement in their metabolism and the possibility of formation of drug-derived reactive species make the liver an organ specially sensitive to drug-induced damage (16, 17).

Drug-induced liver injury (DILI) is a major health problem that challenges pharmaceutical companies, regulatory agencies and health care professionals and institutions (18). DILI is the most frequent basis for drug-related regulatory actions (19), including termination of clinical drug trials, failure to obtain US Food and Drug Administration (FDA) or European Medicines Agency (EMA) approval, restriction of use, as well as the major reason for post-market withdrawal of drugs (16, 20). The incidence of DILI in the general population has been estimated to be 10-15 cases per 100000 patients year (21), being the responsible of one third to one half of cases of acute liver failure and 15% of associated liver transplantations (20, 22, 23). DILI mimics all forms of acute and chronic hepatobiliary diseases and the most frequent clinical manifestations are



## Introduction

---

hepatocellular damage, cholestasis, mixed hepatocellular and cholestatic injury, and steatosis (17).

A major concern regarding DILI is the failure of the drug development process to detect potentially hepatotoxic drugs. Safety tests during drug development involve pre-clinical and clinical phases. Pre-clinical testing is based on toxicity assessments in *in vitro* models and in experimental animals. Unfortunately, these pre-clinical studies are not very predictive of human DILI. During clinical trials, the drug is administered to an increasing number of patients from phase I to phase III to reach approximately 3000 patients in a phase III study (24). Two of the main reasons leading to misdetection of DILI before drug approval are the lack of specific and reliable diagnostic markers or tests to verify an episode of DILI and the underpowered nature of clinical trials due to the limited number of patients involved (16). Liver function/damage monitoring during clinical trials includes measurement of serum liver enzyme levels. The discontinuation of testing is only advised in the case of finding frequent or severe increases in aminotransferase levels (greater than eight times the upper limit of normal) or accompanying increases in bilirubin without initial findings of cholestasis (25). In practice, it is very unlikely to detect those rare reactions before drug approval and most DILI appear post-approval. Once marketed, drugs are administered to a much larger and diverse group of patients than those included in controlled pre-approval trials, including patients at elevated risks for adverse effects (elderly persons, children, pregnant women, and patients with HIV infection or treated with multiple drugs) (13).

DILI is commonly classified into intrinsic versus idiosyncratic hepatotoxicity. Intrinsic hepatotoxicity is regarded as dose-dependent and predictable above an approximate threshold dose, thus causing a reproducible liver damage that is usually detected during pre-clinical safety testing. Idiosyncratic toxicity occurs without obvious dose-dependency, with a delayed onset and the participation of innate and

adaptive immune responses is required. Its development is strongly affected by the mix of unique characteristics - phase I and II drug-metabolizing activities, transporters or immune factors - specific to an individual (14, 26-28).

DILI progression involves complex multi-step mechanisms that are initiated by a chemical insult to cells in the liver (27). Drug exposure is determined by the dose and handling of the drug by the liver (phase I, II, III drug metabolism) (24). In phase I metabolic reactions, drugs are rendered more hydrophilic, primarily by oxidative pathways through the cytochrome P-450 (CYP) enzyme system. Phase II usually involves conjugation of the parent drug or its metabolites to glucuronide, sulfate or glutathione (GSH). Finally, the drug and/or its hydrophilic products are exported into plasma or bile by transport proteins located on the hepatocyte membrane (phase III) (13, 27). The metabolites obtained through biotransformation may be non-toxic, in which case drug metabolism and excretion is a detoxifying process, or may mediate toxicity, typically through the formation of chemically reactive species (27). Thus, the parent drug, or more often, reactive metabolites may cause GSH depletion, covalent binding to proteins, lipids or nucleic acids, induction of oxidative stress (OS), lipid peroxidation, or inhibition of the activity of biliary efflux transporters thus initiating the damage process (14, 16, 17, 27). All those have direct effects on organelles such as mitochondria, the endoplasmic reticulum, the cytoskeleton, or the nucleus. They may also have an indirect influence through the activation or inhibition of signaling kinases or transcription factors that may contribute to the protection against the damage or to its progression (17). The consequences of the amplification and progression of toxicity include hepatocellular damage and the initiation of immunological reactions. Innate immunity activation and inflammation seems to be a general feature in DILI, however some drugs have the ability to provoke the activation of the adaptive immune system (16, 27). The balance

## Introduction

between intracellular and cell-to-cell signaling determines the final extent of the damage, thus leading to an adaptation to the insult resulting in a mild but manageable damage or accelerating the damage leading to massive cell death (either through apoptosis or necrosis) and severe liver damage (14, 24). **Figure 1.2** summarizes the events and inputs determining DILI initiation, development and resolution. Although the focus of hepatotoxicity is mainly on hepatocytes, non-parenchymal cells such as cholangiocytes, LSEC or KC can be involved in the process of drug-induced hepatotoxicity. Moreover, some drugs can induce cholestasis by impairing bile secretion or causing obstruction of extra-hepatic bile ducts (26).

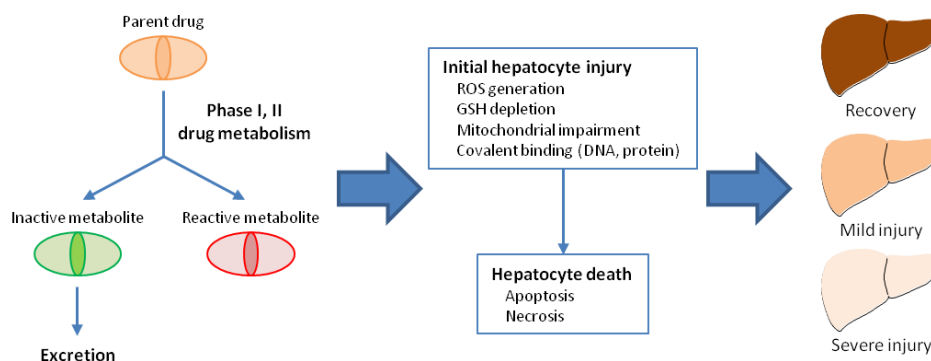


**Figure 1.2.** Schematic representation of the different steps involved in the initiation, development and resolution of drug-induced liver damage. Drug exposure in the liver is determined by the dose and phase I and II drug metabolizing reactions. Drug metabolism is considered to be a detoxifying process, however, it may result in the formation of reactive species. The parent drug, or more often, the reactive metabolites formed may cause an initial damage that sets in motion a series of intracellular and extracellular processes. The balance between protective versus injurious pathways determines the extent of the hepatocellular damage. Finally, the severity, duration and progression of the damage versus the capacity of the liver to regenerate damaged zones will determine the extent of the injury. Figure adapted from references (14, 24).

### 1.4 Mechanism-based classification of DILI

Several molecular mechanisms are primarily involved in hepatocyte injury induced by the drug itself or by any of its metabolites, and the manner in which the intracellular organelles, macromolecules and functions are affected defines the pattern of liver disease (13, 14, 24, 29). Several mechanism-based classifications of DILI have been proposed according to different criteria (12, 13, 18, 24, 28-30). We have adopted the classification proposed by *Gómez-Lechón et al* (29) in which, independently of the initial target causing the damage, mechanisms of DILI are grouped according to the initial clinical manifestation provoked by the drug. Thus, the following mechanisms will be described below: i) Steatosis; ii) Phospolipidosis; iii) Cholestasis; and iv) Oxidative stress

#### 1.4.1 Steatosis

Steatosis, or fatty liver disease, is characterized by an increased deposition of lipids, mainly TG, in hepatocytes above 5% in weight (31). Accumulation of TG in hepatocytes leads to micro- and macro-vesicular steatosis and balloon-cell degeneration (32). Steatosis is a complex process that has been associated to nutritional factors, genetic defects and drug intake. Impairment of  $\beta$ -oxidation leading to the accumulation of fatty acids (FA) as TG in the cytoplasm of hepatocytes is one of the major mechanisms involved in drug-induced steatosis (32, 33). Micro-vesicular steatosis is usually due to a severe impairment of  $\beta$ -oxidation and is characterized by the presence of multiple small lipid droplets within the cytoplasm of hepatocytes. It is an acute condition that may be associated with liver failure, coma and death due to the secondary damages associated to lipid peroxidation and energy depletion (32-35). On the other hand, macro-vesicular steatosis is due to milder and prolonged forms of mitochondrial dysfunction. In this case fat

## Introduction

---

accumulates in form of a single large droplet. Although it is considered a benign condition it can progress to liver fibrosis or cirrhosis after several years (31, 32).

Multiple drug-induced alterations can cause steatosis (29, 32): 1) Direct alteration of mitochondrial FA oxidation by the inhibition of any  $\beta$ -oxidation enzyme; 2) Indirect impairment of  $\beta$ -oxidation by sequestration of cofactors L-carnitine or coenzyme A; 3) Inhibition of carnitine palmitoyl transferase-1 altering FA transport across the mitochondrial membrane; 4) Inhibition of long-chain acyl-CoA synthase, thus impairing the mitochondrial entry of long-chain FA (LCFA); 5) Increased TG synthesis with or without lowered cholesterol and/or phospholipid (PL) synthesis; 6) Reduction in lipid export by the inhibition of microsomal triglyceride transfer protein activity; 7) Induction of mitochondrial permeability transition pore opening; 8) Dissipation of the mitochondrial transmembrane potential; 9) Direct impairment of mitochondrial respiratory chain, which can secondarily inhibit mitochondrial  $\beta$ -oxidation and enhance reactive oxygen species (ROS) formation; 10) Mitochondrial DNA (mtDNA) depletion, which can reduce the synthesis of mtDNA-encoded proteins, impair mitochondrial respiratory chain and increase ROS generation; 11) Increased *de novo* FA synthesis.

### 1.4.2 Phospholipidosis

Phospholipidosis is a lipid storage disorder characterized by the excessive accumulation of PL within cells and by the formation of membrane-bound cytosolic inclusions with a lamellar morphology (lamellar bodies), predominantly of a lysosomal origin (32, 36). In toxicity studies, phospholipidosis has been shown to occur in various tissues, being the liver one of the most common targets. Most drugs inducing phospholipidosis belong to a group of compounds known as cationic amphiphilic drugs (CADs). These compounds contain a hydrophobic

region (usually a ring structure) and a hydrophilic side chain (a primary or substituted nitrogen group) that is positively charged at a physiological pH. This chemical structure allows a direct binding of the molecule with PL (32). To date, it is not clear which are the biological effects caused by PL accumulation, however phospholipidosis is usually associated to a high intrahepatic accumulation of the causing drug (or a metabolite), which can produce potential toxicity after chronic exposure (29, 32, 37). Regulatory agencies generally consider phospholipidosis an adverse effect and the development of a drug can be delayed or terminated when pre-clinical studies in animals reveal PL accumulation in certain organs.

Different mechanisms have been proposed to explain the development of drug-induced phospholipidosis (29, 32): 1) Direct inhibition of lysosomal phospholipase; 2) Decreased degradation of PL due to the formation of degradation-resistant drug-PL complexes; 3) Decreased lysosomal enzyme transport; and 4) Increased synthesis of PL.

### **1.4.3 Cholestasis**

Drug-induced cholestasis is characterized by impaired bile flow, which leads to the accumulation of BAs in the liver and the subsequent toxicity to hepatocytes (28, 29). BAs are major components of bile formed from cholesterol through various enzymatic reactions in hepatocytes. BAs act as detergents involved in the process of solubilization and absorption of dietary fats and fat soluble vitamins and they also facilitate the excretion of bile pigments, cholesterol and other hydrophobic molecules (38). On the other hand, BAs are regulatory molecules able to control not only their own homeostasis but also FA, lipoprotein, glucose, and energy metabolism (39-41) by binding specific receptors (e.g., PXR, VDR or TGR5) and activating several cell signaling pathways (i.e., JNK, ERK, or AKT) (39, 40, 42-44). Abnormal accumulation of BAs in the hepatocytes

## Introduction

---

not only induces several changes in gene expression, but due to its detergent nature it also induces damages on cellular membranes, mitochondrial dysfunction and ultimately necrosis and apoptosis (38, 45, 46). It has been shown that the deleterious toxic effects of BAs depend on the profile of accumulated BAs, with higher toxic effects associated to more hydrophobic BAs (47). Thus, the rank order of BA cytotoxicity is: lithocholic acid (LCA) > chenodeoxycholic acid (CDCA) , deoxycholic acid (DCA) > cholic acid (CA) (46).

At the hepatocyte level, cholestasis is mainly produced through damage to the structure and/or function of bile canaliculi, thus altering bile flow (29). Several transport proteins have been identified as potential loci for drug-induced cholestasis. These include the basolateral uptake transporters (NTCP and OATPs), canalicular efflux transporters (BSEP, MRP2, and MDR3), and basolateral efflux transporters (MRP3 and MRP4) (38, 45, 48). Events leading to drug-induced cholestasis include (13, 29, 38): 1) Direct inhibition of transport proteins; 2) Altered localization of transport proteins; 3) Altered transport protein expression; 4) Disruption of actin filaments in the proximities of the canaliculus; and 5) Transport protein malfunction due to energy supply disruption.

### 1.4.4 Oxidative Stress

OS is produced when the generation of oxidant species (reactive molecules containing oxygen or nitrogen) exceeds the antioxidant protection of the cells (antioxidant enzymes or non-enzymatic scavengers/quenchers). This situation is produced by different physio-pathological conditions, including exposure to drugs able to induce an excessive generation of ROS or a depletion of GSH pool. The mitochondrion is one of the main sources of ROS within the cell, where superoxide radical is produced during oxidative phosphorylation. In addition, ROS can be generated by CYP-dependent microsomal

oxidations of drugs and other xenobiotics. GSH is a strong nucleophilic thiol that protects cells against damage caused by a variety of electrophiles (free radicals, ROS, etc.). In addition, it serves as an essential co-factor of GSH peroxidase which removes hydroperoxides formed during oxidative processes. Finally, GSH is involved in the conjugation and inactivation of the reactive metabolites produced by CYP-dependent oxidations (49). Enhanced ROS levels leading to GSH depletion and OS may cause a wide spectrum of oxidative damage to intracellular biomolecules (DNA, lipids and proteins), altering the structure and function of key cellular constituents that result in mutation, cell damage and cell death (14, 29, 50).

OS is produced by compounds that are able to undergo repeated oxidation and reduction cycles within the cell, or by molecules containing oxygen atoms that can either produce free radicals or are chemically activated by them (49, 51). Drugs may induce OS through different mechanisms (29): 1) Excessive ROS generation during drug oxidations catalyzed by CYPs; 2) GSH depletion due to the formation of GSH adducts with reactive electrophilic metabolites; 3) GSH depletion due to the formation of GSH conjugated metabolites catalyzed by GSH transferases; 4) Direct or indirect impairment of mitochondrial electron chain; and 5) Redox cycling inducing molecules.



### 1.5 Experimental models for the study of hepatotoxicity

As mentioned, DILI is a major health and economic problem and the hepatotoxicity is the main cause of safety problem leading to drug failure during clinical testing and after being launched to the market (16, 20). Furthermore, the limitation in the number of patients exposed to the drug during clinical testing hampers the detection of very low incidence drug-related adverse reactions (13). Pre-clinical testing should be able to detect potential hepatotoxins early in the drug development process in order to minimize health risks and financial losses. One drawback related to hepatotoxicity prediction is the low concordance between humans and commonly used experimental animals (49, 52, 53). Species differences in drug metabolism, target molecules and pathophysiology are important factors that hamper the usefulness of animal models (49). As an alternative to *in vivo* experiments, several liver-derived *in vitro* models have been developed for use in safety pharmacology and toxicology research to understand the mechanisms of DILI and to evaluate potential hepatotoxicity of new chemical entities (49, 54). Major advantages of *in vitro* models are the highly controlled environmental conditions in which experiments are performed, the possibility of using material from a human origin, the possibility of performing high-throughput experiments, its relative low cost in comparison with *in vivo* experiments and the reduction of the number of animals needed. Although *in vitro* approaches fail to reproduce the complexity of a whole organ, they are a good complement to traditional *in vivo* tests and may be useful in the prediction of toxicity in early stages of drug development (49).

Primary culture of freshly isolated human hepatocytes is considered the gold standard *in vitro* model for the study of DILI (55). However, many other liver-based models have been used in hepatotoxicity assessment including: immortalized tumor-derived cell lines, hepatocyte-

like cells (HLCs) derived from pluripotent stem cells and liver tissue preparations (slices, microsomes and S9 fractions) (49, 54). **Table 1.1** summarizes the advantages and disadvantages of the main experimental models. Detailed information about the characteristics of cultured hepatocytes and hepatoma cell lines, the most widely used liver-derived cell models, is provided below.

### 1.5.1 Hepatocytes

Among *in vitro* systems, cultured hepatocytes are recognized as the closest model to the *in vivo* situation (5, 49, 55). Hepatocytes cultured under the appropriate conditions retain most of differentiated liver-specific functions (i.e. gluconeogenesis, glycogen metabolism, urea formation, plasma protein synthesis and secretion, lipid metabolism...) and drug metabolism (phase I and phase II enzymes) and transporters for limited period (5, 49, 55). Many different culture conditions (medium formulation, cell density, extracellular matrix components and configuration, co-culture with other cell types, dynamic culture systems) have been described for the *in vitro* use of hepatocytes and they strongly influence hepatocyte's viability and functionality (5, 49, 55).

Isolated hepatocytes in suspension are the simplest culture system derived from hepatocytes. They allow to perform a complete set of functional analysis (viability, transport, drug-metabolism, excretion of plasma proteins...). However, its usefulness is very limited due to their very short-term viability (2-4 h) and the phenotypic changes induced by the loss of cell-cell and cell-matrix interactions (49, 55).

2D culture systems are the most common way of culturing hepatocytes. They involve the culture of the hepatocytes over a coated dish, what extends hepatocyte viability and functionality up to a week thanks to the establishment of cell-cell and cell-matrix interactions. The main strengths of this model are its simplicity, the extended hepatocyte

## Introduction

---

viability and the possibility of detecting metabolism mediated hepatotoxicity. However, phase I and II drug-metabolizing enzymes activity decay with the time in culture (5, 49, 55). An alternative to the classic monolayer cultures, in which transport studies cannot be performed due to the loss of hepatocyte polarity, is the culture of the hepatocytes in the commonly named 'sandwich' configuration. It involves the culture of the hepatocytes between two layers of matrix, thus reconstructing the opposing sinusoidal facing domains of hepatic plates *in vivo*. Under these conditions the hepatocytes repolarize and reestablish bile canaliculi and the expression of functional transporters. Moreover, they are characterized by an improved functionality and similarity to *in vivo* response and an increased viability (up to some weeks) (5, 49, 55).

### 1.5.2 Hepatoma cell lines

Hepatoma cell lines constitute a simple, readily accessible and almost unlimited source of cells from a human liver origin (49). Besides their differences with hepatocytes in many functional aspects, especially with respect the levels of drug-metabolizing enzymes, they represent a very common *in vitro* model used in toxicological studies. Although many different human hepatic cell lines have been tested (i.e. HuH7, HepaRG, Fa2N-4...), HepG2 cell line is the most commonly used and best characterized one (5, 49).

HepG2 cells are derived from a liver tissue sample of a donor with a well differentiated hepatocellular carcinoma (5). HepG2 are no tumorigenic cells with high proliferation rates and epithelial-like morphology and they show many differentiated hepatic functions: synthesis and secretion of plasma proteins, cholesterol and TG metabolism, lipoprotein metabolism and transport, BA synthesis, glycogen synthesis or insulin signaling (5, 56-58). The main inconvenient

of the use of HepG2 cells in toxicological studies is the reduced expression of several hepatic functions, especially those related to drug metabolism and transport. HepG2 cell line shows substantially lower levels of phase I and II biotransformation enzymes when compared to primary hepatocytes thus leading to a possible misdetection of metabolic-dependent toxicity for particular compounds (5, 49). An alternative to circumvent the low expression of drug-metabolizing enzymes in HepG2 cell line is their genetic engineering to achieve stable or transient expression of the desired genes. HepG2 cells stably expressing drug-metabolizing enzymes have been successfully generated. However, a major limitation of this strategy is that only one or two enzymes can be satisfactorily transfected to cells, thus limiting their application to the study of the contribution of a single enzyme in drug metabolism and related toxicity. On the other hand, transient expression has been achieved for multiple enzymes in a regulated manner, thus being able to customize enzyme expression to reproduce the desired activity pattern. However, transient expression is limited to a maximum of 24-72 h and yet the expression or function of other several genes/proteins involved in drug metabolism, clearance and toxicity cannot be restored with this strategy (59). Despite the limitations of the model, HepG2, by themselves or in combination with some strategy to upgrade their metabolic capacity, is the most used immortalized hepatic-derived cell line for the prediction of toxicological adverse effects. As a result of this widespread use, exhaustive data on the effects of a huge number of compounds (model hepatotoxins, drugs, chemicals) on many parameters indicative of toxicity to HepG2 cells (viability, membrane integrity, cell proliferation, ATP level, etc.) are available in the literature (52, 60, 61). Moreover, recent transcriptomic, proteomic and cytomic studies have confirmed the potential value of HepG2 cells as *in vitro* model for toxicity screenings (52, 62-64). In summary, its unlimited availability, easy culture and handle conditions, complete

## Introduction

---

characterization and wide bibliographic documentation makes HepG2 a very interesting option in toxicological studies, at least as a first approximation to the problem.

**Table 1.1.** *In vitro* models for hepatotoxicity studies.

<b><i>In Vitro</i> Model</b>	<b>Advantages</b>	<b>Limitations</b>
Liver Slices	<ul style="list-style-type: none"> <li>- Preserved liver architecture</li> <li>- Hepatocyte heterogeneity</li> <li>- Presence of non-parenchymal cells</li> <li>- Preservation of hepatocyte bipolarity</li> <li>- High-resemblance to the <i>in vivo</i> phenotype</li> <li>- Possibility of histological examination</li> </ul>	<ul style="list-style-type: none"> <li>- Limited viability and function</li> <li>- Scarce availability (fresh human liver)</li> <li>- High inter-donor variability</li> <li>- High intra-assay variability</li> <li>- Technically demanding</li> </ul>
Primary Cultured Hepatocytes	<ul style="list-style-type: none"> <li>- Easy to use</li> <li>- Expression of inducible biotransformation enzymes.</li> <li>- Correct function of transporters (depending on the culture conditions)</li> <li>- Reasonable resemblance to <i>in vivo</i> liver phenotype</li> <li>- Potential use for long-term studies</li> <li>- High versatility of culture conditions</li> </ul>	<ul style="list-style-type: none"> <li>- Limited availability (human tissue)</li> <li>- Early phenotypic changes</li> <li>- Loss of drug-metabolizing activities</li> <li>- Inter-donor variability</li> <li>- High influence of culture conditions (viability, transport, function...)</li> </ul>
HepG2 Cells	<ul style="list-style-type: none"> <li>- Unlimited availability</li> <li>- Easy to use</li> <li>- Most commonly used and best characterized human liver cell line</li> <li>- Expression of many differentiated hepatic functions</li> <li>- High reproducibility</li> <li>- Amenable to high throughput screening</li> <li>- Customizable expression of CYPs and phase II conjugating enzymes though permanent or transient modifications.</li> </ul>	<ul style="list-style-type: none"> <li>- Lack/scarce expression of transport proteins</li> <li>- Limited/partial expression of some relevant drug-metabolizing enzymes</li> <li>- No reproduction of <i>in vivo</i> hepatic phenotype</li> <li>- Low response to certain inducers.</li> </ul>
Hepatocyte Like Cells (HLCs)	<ul style="list-style-type: none"> <li>- Unlimited availability</li> <li>- Representative of phenotypic and genetic variation in population (induced pluripotent stem cells - derived HLCs)</li> </ul>	<ul style="list-style-type: none"> <li>- Complex culture conditions</li> <li>- Non-standardized differentiation procedures</li> <li>- High variability</li> <li>- Low expression of key hepatic functions</li> <li>- Non-complete characterization</li> </ul>

### 1.6 Methods for the evaluation of DILI using *in vitro* models

#### 1.6.1 Conventional hepatotoxicity assays

Toxicological *in vitro* studies have been usually performed by the employment of cytotoxicity assays that are based on an estimation of cell viability and/or functional or metabolic state of cells previously exposed to toxicants. Common cytotoxicity testing involves the analysis of cell number, membrane integrity (e.g. release of intracellular enzymes, membrane-impermeable DNA stain), apoptosis (e.g. activation of caspases), loss of critical biomolecules (e.g. ATP depletion), metabolic effects (e.g. tetrazolium salt assays, Alamar blue assay), or anti-proliferative assays (e.g. inhibition of DNA or protein synthesis) (49, 65). These assays monitor events that occur in late stages of cell injury, when the cell is near to death. They are useless for mechanistic studies and they are more likely to miss toxicities that produce adverse but non-lethal effects (27, 49). In contrast to this approximation, a variety of pre-lethal mechanistic assays have been proposed to study potential hepatotoxic adverse effects that occur before compromising cell viability including: OS (e.g. ROS generation, GSH depletion, lipid peroxidation), mitochondrial dysfunction (e.g. inner mitochondrial membrane depolarization), lipid accumulation, impairment of BA transport or liver-specific functions (e.g. plasma protein synthesis, ureogenesis...) (49, 65).

As a general protocol, conventional *in vitro* hepatotoxicity studies are performed in two steps. First, effects in cell viability are examined by cytotoxicity parameters. To this end, cells are incubated with a wide range of concentrations of the test compound to obtain a dose-viability curve and to calculate IC<sub>10</sub> or IC<sub>50</sub> values (concentrations causing 10% or 50% of cell death, respectively). In a second stage, non-lethal concentrations of the drug (e.g., lower than IC<sub>10</sub>) are used to perform

## Introduction

---

functional and/or mechanistic studies (49, 65). To achieve an accurate and reliable *in vitro* evaluation of drug-induced hepatotoxicity, several key markers need to be analyzed. Although many of the conventional tests have been adapted to multi-well culture formats, contributing to increase screening throughput, their main limitation is that each test evaluates a single parameter. Thus a wide battery of traditional tests, each performed in a different biological replicate, needs to be performed in order to obtain enough information to relate one problem drug to a specific mechanism of hepatotoxicity.

### 1.6.2 Multiparametric approaches

The application of the new '*omics*' technologies (i.e. transcriptomics, proteomics, cytomics and metabolomics) allows the simultaneous determination of multiple parameters in a single biological sample (49).

In a general sense, transcriptomics examines the levels of all coding and non-coding RNA molecules (transcriptome) in a given sample (e.g. cell population). However, the most common application of transcriptomics is usually referred as gene expression profiling as it is based on the determination of levels of mRNAs (49, 66, 67). The premise beyond the application of transcriptomics to the study of toxicity is that after an adverse effect produced by a toxicant, the cellular homeostasis is altered and the cell tries to restore it by switching on/off the expression of specific genes (11). A fingerprint (gene expression or RNA levels signature) can then be deciphered and used to predict the toxicity of a candidate drug based on the concept that similar toxins or similar mechanisms of toxicity elicit comparable changes in the gene expression (49, 67, 68). Moreover, transcriptional profiling can be used to identify potential markers of DILI for diagnosis purposes. The usefulness of this experimental approximation has been successfully demonstrated (67, 69-71). However, the correct interpretation of transcriptomic studies is

hampered by a number of experimental factors that can contribute to the observed changes in gene-expression data. A major difficulty is the differentiation of gene expression alterations related to drug toxicity from those associated to its pharmacological activity. Moreover, timing is a critical factor in the experimental design. The most valuable mechanistic information is obtained from early transcriptional changes preceding the occurrence of toxicity, because changes observed in later stages after drug exposure can be more related to an adaptive response to the toxicity (72).

The proteome is defined as the entire set of proteins produced or modified by an organism or system. It varies with time and the distinct requirements, or stresses, that a cell or organism undergoes (73). Thus, from a comprehensive point of view, proteomics is the large-scale study of proteins, particularly their structures and functions, although a more simple and practical definition could be the high-throughput separation, display and identification of proteins (74, 75). The main theoretical advantage of proteomics with respect transcriptomics is that gene expression is not the definitive determinant of the final protein content and function, as not all mRNAs are transcribed into proteins and, moreover, post-translational modifications and final location of proteins (targeting, trafficking) deeply influence protein abundance and activity (76, 77). Chemical exposure frequently modifies proteins and dysregulates critical biological pathways or processes leading to toxicity. Therefore, the main aims of proteomics when applied to toxicity studies are the discovery of key modified proteins, the identification of affected pathways, and the development of biomarkers for the eventual prediction of toxicity as it is assumed that toxicants that produce similar effects will induce similar changes in the proteome (49). Recent publications support the use of proteomics to evaluate or predict mechanism of hepatotoxicity using *in vitro* models (62, 78, 79). However, the applicability of proteomics is limited compared to other



## Introduction

---

'*omics*' due to its relative low throughput, the need of a high amount of sample, the high complexity of the proteome due to post-translational modifications of proteins and technical problems associated to some of the technologies employed that hinder the detection of low-abundant, hydrophobic, acidic, basic, small and large proteins (49, 80-82).

The cytomes can be defined as the heterogeneous cellular systems and functional components of the pluricellular organisms. Cytomics is the study of the heterogeneity of cytomes and aims to determine changes in the phenotype of single cells, which can be further related to a given stimulus or injury (83, 84). Within the '*omics*' framework, cytomics can be considered as the science of single cell-based analyses that links genomics and proteomics with the dynamics of cell and tissue function, as modulated by external influences (83-85). Cytomics technology is based on the use of specific fluorescent probes to assess the status of the cell. With a suitable combination of fluorescent markers, many different parameters of interest in toxicological studies such as nuclear morphology, mitochondrial function (transmembrane potential), cell viability, intracellular calcium concentration, ROS generation or lipid accumulation may be recorded simultaneously. Among cytomic technologies, a new image-based technology called high content screening (HCS) integrates the fluorescence microscopy with image analysis algorithms and informatics to automate cell analysis (49, 84, 86), what allows to record spatial information of the fluorescence signals while maintaining high throughput thanks to the automation (84). The nature of this technology makes it especially suitable for its application in drug toxicity as several parameters can be recorded simultaneously in individual cells. Many examples of the application of different methodological variants of cytomics applied to hepatotoxicity prediction or mechanistic classification can be found in the recent literature (52, 87-93).

### 1.7 Metabolomics

The term metabolome was initially defined as the quantitative complement of all the low molecular weight molecules present in a cell in a particular physiological or developmental state (94, 95). This definition has been updated to cover the broader range of applications that have arisen within this field and can be defined as the quantitative determination of all the low-molecular-weight (approximately below 1 kDa) endogenous metabolites in a specified biological sample. Each cell type/biological fluid has specific levels of metabolites depending on the specific environmental conditions and fluctuate through time according to physiological demands (96). Two different terms were initially coined to name the science focused on the study of the metabolome: metabolomics (97) and metabonomics (98). The term metabolomics was defined as “the comprehensive and quantitative analysis of all metabolites present in a specific cellular, tissue or biological sample” and it was originated by semantic analogy with other '*omics*' disciplines (97). On the other hand, the term metabonomics was defined as “the quantitative measurement of the time-related multiparametric metabolic response of living systems to pathophysiological stimuli or genetic modification” (98) and is derived from the Greek roots '*meta*' and '*nomos*' meaning changes and rules/laws, respectively, to describe the generation of pattern recognition-based models that have the ability to classify changes in metabolism (99). The initial discrepancy between the two definitions was mainly philosophical. While metabolomics aimed to characterize and quantify all the small molecules present in a biological sample, metabonomics was focused on the global changes in the metabolome as a response to a given stress, stimuli or genetic manipulation (100). Nowadays both terms are often used interchangeably to define those studies aimed at the untargeted analysis of the metabolites in a given biological system under study (100). Their

## Introduction

---

main applications include toxicity assessment, pharmaceutical drug development, cell culture monitoring, disease diagnosis, nutrition, oncology and transplantation (101-106).

Metabolomics measures the downstream products of the '*omics cascade*', thus providing information that is not accessible through other alternative '*omics*' such as genomics, transcriptomics or proteomics (103, 107) (**Figure 1.3**). Metabolites are the intermediates of biochemical reactions, thus their levels are determined by both the concentration and properties of the enzymes, these last being the result of the integration of transcription, translation, post-translational modifications and allosteric effects, thus resulting in an integrative effect between the capabilities of the system under study and its interaction with the environment (108). Therefore, thanks to amplification, as a result of being downstream of the activity of genes and proteins, the integration of intra- and extracellular signals and a more dynamic nature, the metabolome, and metabolomic changes, represent a closer approximation to phenotype than genes, transcripts or proteins (103, 107, 109). Thus, metabolomics is more informative of functional status of cells than other '*omics*'.

Within the classical approximations of the '*omics cascade*', each step closer to the phenotype represents a huge increase in the figures of entities of interest: from about 20000 genes to 100000 transcripts and 1000000 proteins. However, the number of metabolites in humans is estimated to be around 40000 (110), although the number of major metabolites, those being at higher concentrations and with the most relevant functions, is estimated to be around 2000 (111). Moreover, while genes, transcripts and proteins are species specific, and therefore different probes have to be designed for each species, most of the metabolites are common to all the species and only a part of the metabolome is species specific (81).

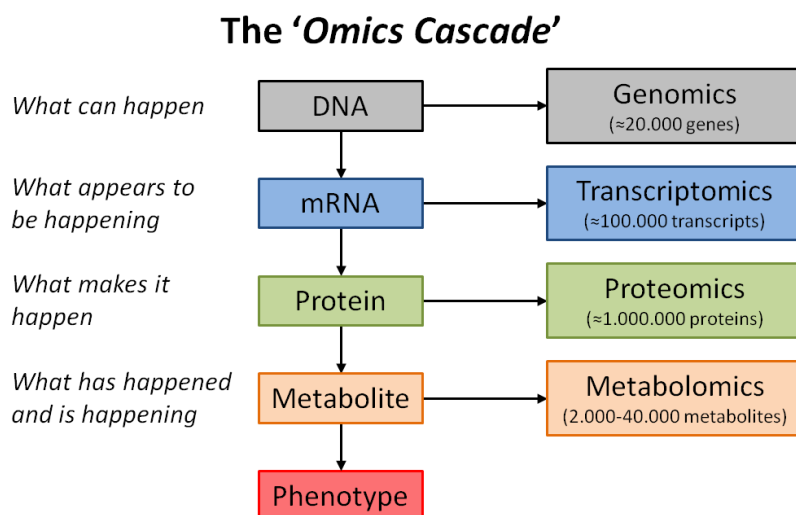


**Figure 1.3.** Representation of the 'omics cascade' along with the figures of the estimated number of components belonging to each of the levels. Metabolomics focus is on the last step of the information cascade thus amplifying and integrating the signals of the preceding levels of regulation and therefore being the closest approximation to the actual phenotype.

### 1.7.1 Basic structure of a metabolomic study

The typical structure of a metabolomic study is depicted in **Figure 1.4**. The first step is to establish the hypothesis of work and define the main objectives to be achieved with the study, that is, the biological question to be answered. Closely related to this point is the definition of the experimental conditions in order to achieve the proposed objectives. This step, with regards to a toxicological study, includes the selection of the experimental model (e.g. *in vitro* vs *in vivo*, immortalized cell lines vs primary cultured cells...), the drugs to be tested (e.g., model compounds associated to well known mechanisms of toxicity), the concentrations and the schedule/pattern of the treatment, and the analytical platform. In addition to that, it is necessary to perform a careful selection of the type of sample to be analyzed (e.g., cell monolayer and/or culture

## Introduction

---

medium; that is endometabolome vs exometabolome) and sampling protocol processing methods. One key pre-requisite is that samples have to be representative and informative of the phenomenon under study. Therefore sample processing has to allow the extraction of the metabolites of interest while providing a correct quenching of the cell metabolism in order to avoid metabolite degradation or alterations in their levels at the time of the sampling. After the samples have been generated, they have to be analyzed under the appropriate analytical platform in an environment that ensures the quality of the generated results. Finally, the use of suitable data analysis techniques will allow the generation of biologically meaningful results that with the correct interpretation and validation, will answer the question of interest. The decisions made at every step of the workflow are crucial in obtaining high quality and informative results (103).

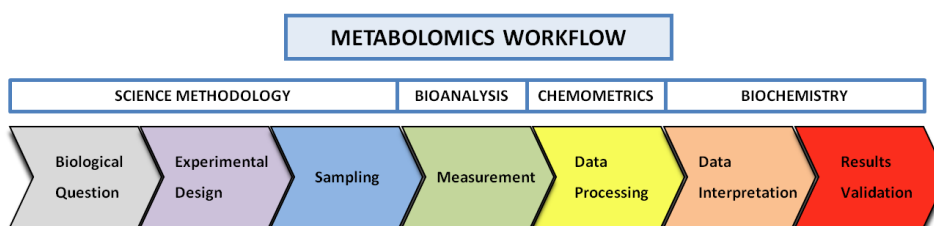


**Figure 1.4.** Scheme of a general workflow in a metabolomics study. Figure adapted from reference (103)

### 1.7.2 Techniques for the study of the metabolome

The metabolome presents a large diversity of components (aminoacids, carbohydrates, lipids, organic acids...) with highly different chemical structures and properties (from ionic or very polar to highly hydrophobic compounds). It is almost impossible to determine the complete metabolome using a single analytical platform and thus the

combination of complementary techniques (covering both sample preparation and analysis) is required to achieve a comprehensive coverage of the metabolome (108).

The most common analytical techniques used to study the metabolome are nuclear magnetic resonance (NMR) spectroscopy and mass spectrometry (MS), the later usually hyphenated to previous separation techniques (112). NMR and MS, in their different configurations, are complementary rather than opposite platforms and thus the use of different analytical techniques has a positive impact in widening the coverage of the metabolome.

<sup>1</sup>H-NMR spectroscopy is based on the detection of all the proton signals present in a given sample. The main advantages of NMR spectroscopy are: i) it is a non-destructive technique, therefore the samples may be used in further analysis; ii) it requires non or low sample preparation; iii) it is possible to perform analysis with solid samples; iv) it is an intrinsically quantitative technique; v) it is possible to perform structural analysis; and vi) its high robustness allows easy lab-to-lab comparisons. However the application of NMR is hampered by its low resolution and sensitivity, the difficulty in the interpretation of the obtained spectra and the presence of analytes deficient in protons or that possess protons that can be readily interchanged with the solvent (108, 113).

In MS, the analytes present in the sample are ionized and characterized by their mass-to-charge ratio ( $m/z$ ). MS detection is usually preceded by a separation technique in order to separate the individual components present in the complex biological matrices. The most popular separation techniques coupled to MS are: gas chromatography (GC), liquid chromatography (LC) and capillary electrophoresis (CE). GC is used to separate volatile (and no-volatile, after derivatization) metabolites. CE separate polar ionizable compounds based on their  $m/z$ . LC is by far the most popular separation technique used in metabolomics and allows the

## Introduction

---

separation of the metabolites based on their chemical properties as a function of the stationary phase of the selected chromatographic column. The main advantages of MS hyphenated to separation techniques are: i) its high sensitivity, several orders of magnitude lower than NMR; ii) its high resolution and selectivity; iii) the possibility of performing fragmentation analysis thus confirming the identity of the detected metabolites and the identification of unknown and unexpected compounds; and iv) the information is easier to handle than in the case of NMR spectroscopy (80, 103, 108).

### 1.7.3 LC-MS-based metabolomics

Currently two approaches are used for LC-MS-based metabolomic investigations: i) untargeted and ii) targeted. Although the latter may not be considered as a true '*omic*' approach because it basically consists in a biased analysis which is driven usually by a hypothesis or by *a priori* knowledge of the system under study, targeted analysis may be considered an important part of untargeted metabolomics. Once potential biomarkers have been deciphered by untargeted metabolomics analysis, they should be validated by performing targeted quantitative analysis (**Figures 1.4, 1.5**).

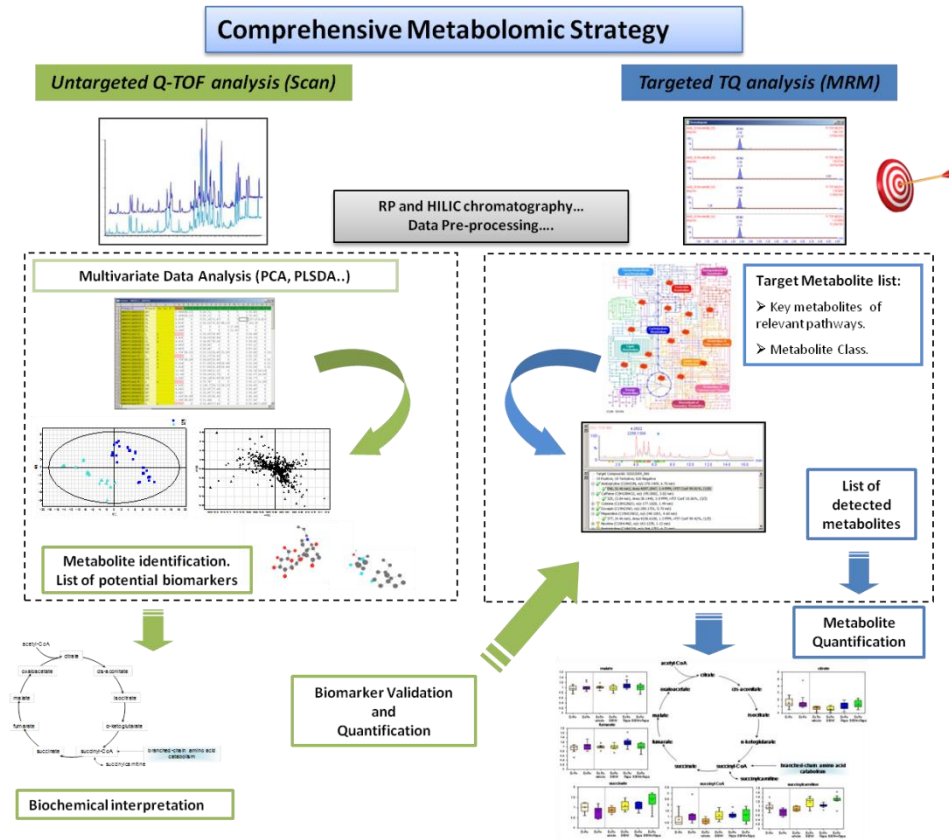


**Figure 1.5.** Scheme of the proposed global metabolite profile strategy. The strategy is based in the combination of both untargeted and targeted metabolomics analysis with the workflow described in **Figure 1.4** as starting point. Untargeted analysis is able to provide candidate biomarkers that can be validated by the use of targeted quantitative analysis. Moreover targeted analysis is a complementary tool to untargeted analysis when addressing metabolites belonging to a specific class. Adapted from reference (103)



## Introduction

---

### Untargeted metabolomics

Untargeted metabolomics aims to characterize the maximum possible number of metabolites in a given biological sample. It is focused on an unbiased profiling of the metabolome in order to link specific patterns of metabolites to a given treatment or condition (103, 108). As previously mentioned, the broad chemical and physical diversity of the metabolome renders the simultaneous analysis of all the existing metabolites in a given sample via a single technique impossible. In LC-MS-based metabolomics, this aim can be achieved with the combination of the right separation strategy with a detection system that covers a wide range of  $m/z$  in an unbiased way (103).

Traditional LC separations have been performed using reversed phase (RP) chromatography (107, 114, 115). RP columns, typically C18-bonded silicas, are able to retain and separate medium-polar and non-polar metabolites and are a good option as starting point in metabolomic studies. However, very polar compounds elute in the void volume or with minimal retention. Recent advances in column technology, such as hydrophilic interaction chromatography (HILIC) (116), allow the detection of polar/ionic analytes which, typically, are poorly retained by RP phases or indeed are not retained at all (117-119). Stationary phases used in HILIC chromatography include amine, amide or free silanol groups. The retention of a metabolite is a combination of liquid-liquid partitioning, adsorption, ionic interactions, and hydrophobic retention and is heavily dependent on the nature of the analyte and the composition of the mobile phase (117). Using HILIC chromatography coupled to MS may also offer higher sensitivity than conventional RP phases because of increased ionization efficiency resulting from the use of mobile phases containing a high proportion of organic solvents. No single separation technique is able to resolve and detect the complete range of metabolites that may be present in a complex biological sample; therefore, achieving the most

comprehensive metabolome coverage may require the use of several column chemistries (103, 107).

With respect to MS detection, untargeted metabolomics require instruments with a sensitive full scan mode and accurate mass measurement. The quadrupole time of flight (QTOF) mass spectrometer meets such requirements as it combines the stability of a quadrupole with the high efficiency, sensitivity and accuracy (< 5ppm) of a TOF. It also offers mass fragmentation capabilities for unknown metabolite identification. Thanks to its capabilities, the QTOF mass spectrometer has become the instrument of choice for untargeted analysis approaches, although other instruments such as Orbitrap or Fourier Transform Ion Cyclotron Resonance also meet high mass resolution capabilities (103).

### Targeted metabolomics

Targeted metabolomics aims at the quantitative determination of a previously selected set or class of metabolites. The recent advances in MS instruments along with the development of ultra performance liquid chromatography (UPLC) have permitted the simultaneous quantification of dozens to hundreds of target metabolites in a single chromatographic run (103, 108). The usefulness of targeted metabolomics resides in mapping some metabolites of interest, instead of the whole metabolome. This approach is especially suitable in hypothesis-driven studies, where the focus is on a specific pathway or class of compounds, or to validate previously discovered biomarkers (**Figure 1.5**).

Targeted metabolomics requires the unambiguous identification and the quantification of the metabolites of interest. With respect LC, the chromatographic separation is optimized according to the chemical properties of the group of metabolites of interest. Triple quadrupole (TQ) mass spectrometers, mostly working in multiple reaction monitoring

## Introduction

---

(MRM) mode, are the most common platform to perform targeted analysis. TQ mass spectrometers have a lower mass resolution than QTOF, however they have greater sensitivity, specificity, robustness, and a broader dynamic range. In TQ operating in MRM, the first quadrupole selects a parent ion that is fragmented in the second quadrupole (collision cell) to give specific fragments (daughter ions) that are selected in the third quadrupole before arriving to the detector. Thus in UPLC-TQ targeted metabolomics the high selectivity, that ultimately favors its high sensitivity, is provided by a triple filter: 1) retention time (RT) in the UPLC; 2) molecular formula/mass, determined by the first quadrupole; and 3) structure, determined by the fragmentation process and the selection of daughter ions in the third quadrupole (103, 120).

### 1.7.4 Data analysis in metabolomics

LC-MS untargeted analysis generates huge amounts of data in form of a three-dimensional matrix (RT,  $m/z$  and signal intensity). The ultimate goal of data analysis applied to metabolomics is to transform the raw data provided by the analytical platform into reliable, useful and intelligible biological information (103, 121). After several preprocessing steps, the result is a two-dimensional matrix (usually RT\_ $m/z$ , signal intensity) in which the data from all the samples have been aligned, normalized, centered... and are ready to be subjected to univariate and multivariate data analysis (MVDA) (103).

Univariate methods analyze only one variable at a time and they include tests to compare different sets of samples such as  $t$  test (or its non-parametric analog Mann-Whitney test) for two-group problems or ANOVA (analysis of variance) for multiple-class problems. Multivariate methods use all variables simultaneously and deal with the relationship among variables. (121). The MVDA workflow typically involves two statistical approaches comprising unsupervised and supervised methods.

### Unsupervised multivariate data analysis

Unsupervised multivariate methods, in which no *a priori* knowledge about the samples is used by the employed algorithm, are usually performed in order to visualize the natural interrelationship among the different samples thus revealing groups, trends and outliers (122). Two of the most commonly used tools to performed unsupervised multivariate analysis in metabolomics studies are hierarchical cluster analysis (HCA) and principal component analysis (PCA).

In HCA, the multidimensional data obtained by untargeted metabolomics analysis is reduced to a correlation/distance matrix. Then, the samples are clustered together in a single dendrogram and the distances between the samples reflect the similarities and differences between their metabolomic patterns (123). Different distance measures (e.g. Euclidean, Pearson, Spearman) and clustering algorithms (e.g. average linkage, single linkage, complete linkage, ward, centroids) can be used in the development of HCA models (124).

PCA is a statistical method that reduces a great number of variables (usually correlated) into a smaller number of uncorrelated variables, which are called principal components (112, 122). This transformation is defined in such a way that the first principal component has the largest possible variance (that is, accounts for as much of the variability in the data as possible), and each succeeding component in turn has the highest variance possible under the constraint that it is orthogonal to (i.e., uncorrelated with) the preceding components. The goal of the exercise is dimensional reduction (usually to two or three components), while sacrificing as little accuracy as possible. The results of a PCA are usually discussed in terms of 'scores' that indicate the relationship between samples and 'loadings', which indicates the relationships (correlations) between the variables. The scores represent the original data in the new coordinate system and the loadings are the weights

## Introduction

---

applied to the original data during the projection process. Each point in the scores plot represents one sample and each point in the loading plot represents one feature. Sample points that cluster together have more similar metabolomic patterns (and hence more similar biochemical composition) than those that cluster apart (112, 122).

### Supervised multivariate data analysis

If the objective of data analysis is classification or regression, supervised predictive models have to be created. Several tools have been applied in metabolomics to achieve this purpose: random forests, artificial neural networks, support vector machine classification, discriminant analysis, SIMCA (soft independent modeling of class analogy)... However, partial least squares–discriminant analysis (PLS-DA) and orthogonal projection to latent structures–discriminant analysis (OPLS-DA) are the most popular ones (122, 125, 126). PLS-DA is a PLS-based model in which the dependent variable (Y block) represents class membership (127, 128). OPLS-DA is a variant of the PLS method in which the variation in X (in metabolomics it corresponds to the intensity of the detected features) is divided in two parts, one that is linearly related to Y and one that is unrelated (orthogonal) to Y (122, 129). PLS-DA and OPLS-DA are projection based methods, like PCA, however, they are preferred to PCA because the dimension reduction that PLS offers is guided explicitly by the among-groups variability, whereas PCA is only capable of identifying gross variability directions and is not designed to distinguish 'among-groups' and 'within-groups' variability (103, 128, 130). A common problem with PLS-DA is its propensity to data overfitting. This occurs when the algorithm appears to achieve good separation but has done so by picking up random noise rather than real signals (121, 131). This problem is addressed by using double cross validation (2CV) (132) in combination with permutation tests (133, 134).

In a 2CV procedure, the data are subdivided into two different subsets (the size depends on the times the validation loop is performed), one is used for model development and the other is reserved as a validation set. Within the first subset a second division into two different subsets is performed (the usual procedure at this stage is to develop the model with all the samples except one, that is used for model validation) in order to optimize model parameters such as the number of latent variables (LVs) employed to develop the model (132). The samples included in each of the subsets are interchanged until all the samples have been included in each one. The developed model is an average of all the generated during the cross validation (CV) strategy.

A permutation test involves randomly reassigning the class labels and performing PLS-DA on the newly relabeled data set. The process is repeated hundreds or thousands of times, and the performance measures are plotted on a histogram for visual assessment. From the resulting histogram, it is possible to determine whether the original class assignment is significantly different from, or a part of, the distribution based on the permuted class assignments (133).

### **1.7.5 State of the art in the application of metabolomics to hepatotoxicity prediction**

Metabolomics is increasingly being used in toxicological studies and is now recognized as a promising technology with potential application in different areas of toxicology such as screening of drug-candidates, identification of biomarkers of toxicity and elucidating mechanisms of toxicity (109, 112, 135). Several recent studies have highlighted the usefulness of metabolomics applied to the study of hepatotoxic effects, usually targeting body fluids such as urine and serum, using rodents as *in vivo* models (104, 136-140). However, the presence of metabolomic studies associated to hepatotoxicity in humans is scarce (141-143).

## Introduction

---

The application of metabolomics to cells in culture is an active field of research and several groups have put their efforts in the optimization of sample processing conditions applied to different types of cells and metabolomic applications (103). A number of cells including human fibroblasts (144, 145), human induced pluripotent stem cells (146), CHO cells (147, 148), primary-cultured human hepatocytes (149), cancer cells (150, 151), INS-1 cells (152, 153), HepaRG cells (154) and HepG2 cells (155, 156) have been used in metabolomic studies. In spite of the extensive available literature about the topic, there is no general consensus about the harvesting, extraction or analysis methods to be applied to mammalian cells in adherent culture. Therefore, optimization of sample processing and analysis conditions is a pre-requisite prior to the performance of metabolomic studies. Much more limited has been the application of metabolomics to cell culture systems for toxicity purposes and, in particular, for DILI studies. In contrast to transcriptomics or cytomics that have been widely applied to *in vitro* hepatotoxicity assessment, relatively few studies have used metabolomics (154, 156-158). Moreover, previously reported toxicometabolomic studies using liver-derived cell models (HepG2 cells, HepaRG cells and primary hepatocytes) were focused in the effects of a single hepatotoxin (or a very reduced number of them). Therefore, the potential utility of cell metabolomics to identify and classify drugs able to induce hepatotoxicity through different mechanisms has not been explored yet.

### 1.8 Hypothesis of work and objectives.

Based on the previous evidences our hypothesis stands that *in vitro* toxicometabolomics could be a valuable tool to study and decipher patterns associated to DILI. This approach may lead to high sensitive and specific predictions of hepatotoxicity risk to be used in drug development and pre-clinical safety studies as well as it could provide valuable information about candidate biomarkers, opening the possibility to discover generic and mechanism-specific biomarkers of hepatotoxicity.

We propose the following objectives:

1. Development of an analytical strategy for the LC-MS analysis of the metabolome: from sample processing and analysis to data analysis and biomarker validation.
2. Identification of biomarkers and metabolomic patterns associated to drug-induced hepatotoxicity using HepG2 as *in vitro* cellular model.
3. Extrapolation of *in vitro* biomarkers to *in vivo* medaka (*Oryzias latipes*) and rat models, and comparison of the molecular mechanisms among these models.





## **2. Methodology**

---



### 2.1 General procedures, equipment and reagents

All the LC solvents (i.e. water, methanol, acetonitrile and isopropanol) were of LC-MS grade and were purchased from Fisher Scientific (Loughborough, U.K.). All the LC-MS additives (i.e. formic acid and ammonium acetate) and the analytical standards (when available) were acquired from Sigma-Aldrich (Madrid, Spain). BA (deuterium labeled BA included) were obtained from Steraloids (Newport, USA). Peptides were acquired from Xaia Custom Peptides (Göteborg, Sweden) and Bachem (Bubendorf, Switzerland). The rest of deuterated internal standards (IS) were purchased from Cambridge Isotope Laboratories (Tewksbury, USA).

Protein determinations were performed using a 96-well adapted Lowry method (159, 160).

Tissue homogenizations were performed using a Precellys 24 dual system equipped with a Cryolys cooler (Precellys, Saint Quentin en Yvelines, France) in order to maintain the samples at a controlled temperature during the homogenization process (**Figure 2.1.A**).

Sample evaporations were performed using a Savant SPD 121P SpeeVac concentrator equipped with a refrigerated vapor trap (Thermo Fisher Scientific, Watham, USA) (**Figure 2.1.B**).



**Figure 2.1.** A) Precellys 24 Dual equipped with a Cryolys cooler. B) Savant SpeedVac connected to an oil-free vacuum pump and a refrigerated vapor trap.

## Methodology

---

### 2.2 Instrumentation used in MS-based metabolomics analysis

All the metabolomics analyses were performed using an LC-MS analytical platform. The LC separations were performed using a Waters Acquity UPLC system (Waters, UK), with regards to analytes detection two different mass spectrometers were employed: a Waters Synapt HDMS QToF mass spectrometer (Waters, UK) for untargeted metabolomics analysis and a Waters Xevo TQ-S mass spectrometer (Waters, UK) for targeted analysis (**Figure 2.2**).

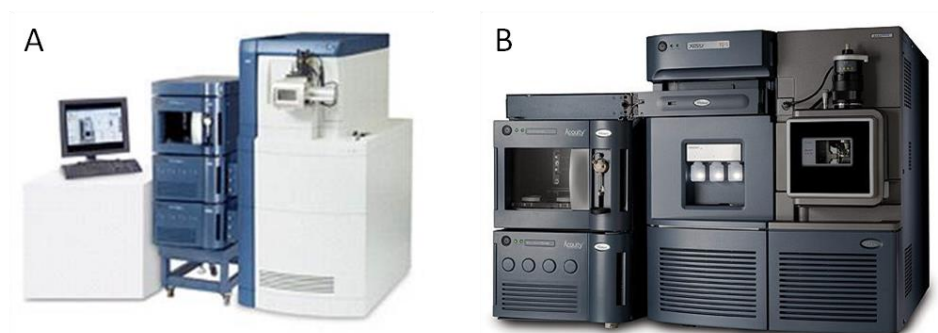


**Figure 2.2.** LC-MS metabolomic platforms employed. **A)** Instrument employed for untargeted metabolomic studies: a Waters Acquity UPLC system coupled to a Waters Synapt HDMS QToF mass spectrometer. **B)** Instrument employed for targeted metabolomic studies: a Waters Acquity UPLC system coupled to a Waters Xevo TQ-S mass spectrometer.

#### 2.2.1 Waters Acquity UPLC system

UPLC is a variant of high performance liquid chromatography (HPLC) that uses columns with a particle size below 2  $\mu\text{m}$  (typically 1.7-1.8  $\mu\text{m}$ ), which provides significant better separations than the traditional (3-5  $\mu\text{m}$ ) columns and enables much faster analysis. This technique allows the combination of columns with small particles and the use of higher flow

rates, thus obtaining an increased speed separation with superior resolution and sensitivity (161). This is achieved thanks to the high pressure (up to 15000 psi) that can be reached with the combined use of UPLC systems and sub 2  $\mu\text{m}$  particle size columns.

The Waters Acquity UPLC system employed to carry out the analysis is equipped with a binary solvent manager that enables to perform gradient elutions with a maximum of two eluents, a refrigerated sample manager that allows to keep the samples at low temperature to minimize sample degradation while waiting to be analyzed, and a thermostated column manager that allows to perform separations at a controlled temperature.

The system requires two elution solvents which are selected to achieve an appropriate chromatographic separation of the components present in a given sample and they are selected taking into account the chemistry of the employed chromatographic column. Additionally, two wash solvents that allow the cleaning of the injection system between injection cycles have to be selected: the weak needle wash (WNW) solvent and the strong needle wash (SNW) solvent. The WNW solvent has to be as close as possible to the initial conditions of the chromatographic separation. The SNW is aimed to clean the syringe in order to avoid inter-sample contamination.

Information about column temperature, flow rate, elution and wash solvents composition and gradient will be detailed for each of the used analytical methods.

### 2.2.2 Waters Synapt HDMS QToF mass spectrometer

Untargeted metabolomic studies were performed using a Waters Synapt HDMS QToF as mass spectrometer. This instrument enables the scan of a wide range of masses (50-1200 Da) with a high resolution ( $> 5000$  full width at half maximum (FWHM)) (see **Formula 2.1**) and high mass accuracy ( $< 5$  ppm) (see **Formula 2.2**).

## Methodology

---

$$\text{mass resolution (FWHM)} = \frac{\text{recorded ion mass}}{\text{mass peak width at half maximum}}$$

**Formula 2.1.** Expression to calculate mass resolution using the full width at half maximum (FWHM) approximation.

$$\text{mass error (ppm)} = 10^6 \times \frac{(\text{recorded ion mass} - \text{exact ion mass})}{\text{exact ion mass}}$$

**Formula 2.2.** Expression employed to calculate mass error in parts per million (ppm).

This mass spectrometer is equipped with an electro spray ionization (ESI) source and is able to operate in both positive and negative ionization modes. Moreover, mass acquisition can be recorded in MS and in MS/MS modes simultaneously, thus allowing to perform mass fragmentation to confirm identities of putative biomarkers. The data station operating software was Masslynx v4.1 (Waters, UK).

To ensure reliable mass measurements, the software requires mass axis calibration so that the  $m/z$  values for sample peaks can be accurately determined. Two different kinds of calibration procedures are performed before and during sample analysis, that is, off line and on line calibrations. The objective of off line calibration is to fix the relationship between the  $m/z$  and the time of flight of the ions inside the TOF tube, while on line calibration performs a real on time correction of that adjustment. Off line calibration is performed using a set of known reference peaks (i.e. via infusion of a solution containing 10% formic acid/0.1 M NaOH/acetonitrile (1:1/8)) so that the software determines the differences between the real mass of the reference peaks and the observed measurement of them along the mass axis. A calibration curve can then be generated allowing the accurate determination of masses included in the calibration mass range. On the other hand, on line calibration relies on the measurement of a single reference mass (i.e.

Leucine Enkephalin,  $m/z$  556.2771 or 554.2615, in ESI positive (+) and ESI negative (-), respectively, prepared at 50 pg/mL in acetonitrile/water (1:1) plus 0.1% formic acid) that is acquired during sample acquisition thanks to a dual electro spray ion source that allows the co-introduction of analyte and reference compounds directly into the ion source. The reference mass (also called lock mass) performs a real time correction of the calibration curve allowing to achieve a high accuracy in mass determination (< 5 ppm).

### 2.2.3 Waters Xevo TQ-S mass spectrometer

Targeted metabolomics analyses were performed using a Waters Xevo TQ-S mass spectrometer equipped with an ESI probe that allows the simultaneous acquisition in positive and negative ionization modes. The data station operating system was Masslynx v4.1 (Waters, UK). TQ mass spectrometers are designed for targeted analysis as they allow sensitive, selective and quantitative analysis of a known group of metabolites. The most common operational mode of TQ mass spectrometer is MRM. In TQ operating in MRM mode, the first quadrupole selects a parent ion that is fragmented in the collision cell to give specific fragments (daughter ions) that are selected in the second quadrupole before arriving to the detector. QuanOptimizer software (Waters, UK) was employed to optimize transitions (selection of parent and daughter ions), cone voltages and collision energies for each of the targeted metabolites.



## Methodology

---

### 2.3 Analytical conditions for LC-MS untargeted analysis

In all the cases the temperatures of the column and the autosampler were set at 40 °C and 4 °C, respectively. The sample injection volume was 5 µL and the flow rate was set at 0.4 mL/min. The ESI conditions were as follows: capillary was set at 3.2 kV and 2.8 kV in the positive and negative modes, respectively; cone voltage was set at 40 V; desolvation and source temperatures were set at 380 and 120 °C, respectively; the flow rates of cone and nebulization gases were set at 50 and 800 L/h, respectively. The same parameters were applied for simultaneous MS and MS/MS analysis, with a collision energy ramp from 5 to 60 eV in the MS/MS channel.

#### 2.3.1 Generic-RP untargeted analysis

LC-MS conditions for generic-RP untargeted analysis were adapted from reference (162). UPLC separation was performed using an Acquity UPLC HSST3 (1.7 µm, 2.1 × 100 mm; Waters) column. Eluent and washing solutions composition were: i) Solvent A: 0.1% formic acid in water; ii) Solvent B: 0.1% formic acid in acetonitrile; iii) WNW and seal wash (SW): water/acetonitrile (90:10, v/v); and iv) SNW: acetonitrile. A 26-min elution gradient was performed as follows: during the first 2 min, eluent composition was set at 99.9% A and 0.1% B, which was linearly changed to 75% A and 25% B in 4 min; then the proportion of B was increased to 80% in the next 4 min, followed by a further increase to 90% B reached at min 12 and 100% B at min 17 and kept for 5.5 min. Finally, the initial conditions were recovered and maintained for 2 min for column conditioning.

Mass detection was performed in the MS scan mode from 50 to 1000 Da with a scan time of 0.1 s.

### 2.3.2 Lipidomic-RP untargeted analysis

LC-MS conditions for lipidomic-RP untargeted analysis were adapted from reference (163). UPLC separation was performed using an Acquity UPLC BEH C18 (1.7  $\mu\text{m}$ , 2.1  $\times$  100 mm; Waters) column. Eluent and washing solutions composition were: i) Solvent A: 0.1% formic acid and 1% ammonium acetate 1M in water; ii) Solvent B: 0.1% formic acid and 1% ammonium acetate 1M in acetonitrile:isopropanol (5:2); iii) WNW and SW: water/acetonitrile (90:10, v/v); and iv) SNW: acetonitrile:isopropanol (5:2). Two different chromatographic separations were performed for ESI (+) and ESI (-) modes, respectively. In ESI (+) mode a 18-min elution gradient was performed as follows: initial eluent composition was set at 65 % A and 35% B, which was linearly changed to 20% A and 80% B in 2 min; then the proportion of B was increased to reach 100% at min 9 and kept for 7 min. Finally, the initial conditions were recovered and maintained for 2 min for column conditioning. In ESI (-) mode a 18-min elution gradient was performed as follows: initial eluent composition was set at 85% A and 15% B, which was linearly changed to 35% A and 65% B in 2 min; then the proportion of B was increased to reach 100% at min 11 and kept for 5 min. Finally, the initial conditions were recovered and maintained for 2 min for column conditioning.

Mass detection was performed in the MS scan mode from 200 to 1200 Da in ESI (+) and from 100 to 1200 Da in ESI (-), with a scan time of 0.1 s.

## Methodology

---

### 2.3.3 HILIC untargeted analysis

UPLC separation was performed using an Acquity UPLC BEH Amide (1.7  $\mu\text{m}$ , 2.1  $\times$  100 mm; Waters) column. Eluent and washing solutions composition were: i) Solvent A: acetonitrile; ii) Solvent B: 20 mM ammonium acetate pH 3 in water; iii) WNW: acetonitrile/water (90:10, v/v); and iv) SNW and SW: water/acetonitrile (90:10, v/v). A 18-min elution gradient was performed as follows: during the first 3 minutes eluent composition was set at 95% A and 5% B, which was linearly changed to 75% A and 25% B in 6 min; then the proportion of B was increased to reach 65% at min 13 and kept for 2 min. Finally, the initial conditions were recovered and maintained for 2.5 min for column conditioning.

Mass detection was performed in the MS scan mode from 50 to 1000 Da, with a scan time of 0.1 s.

### 2.4 Raw data processing and metabolite identification in untargeted metabolomic analysis

The main goal in data processing is to correctly arrange the huge amount of raw data generated by the MS files into a matrix data that eases later data handling as MVDA. Thus, data is arranged into a 2D matrix in which each row represent one sample (object) and each column one ion detected by the MS (variable). Variables (columns) are expressed by the combination of three characteristics, two that define the identity of the ion, that is  $m/z$  and RT, and the ion intensity measured for each sample (164).

Raw data was acquired using Masslynx v 4.1 software (Waters, UK) and was subsequently converted from \*.raw format to \*.cdf format using Data Bridge tool from Masslynx v4.1 software. Data processing was performed using the MZMine v.2.9.1 free software (165). The following steps were sequentially executed within the data processing (**Figure 2.3**): i) Peak picking/detection, it involves the detection of all signals above a given threshold, thus distinguishing true signals from noise; ii) Deconvolution of the detected signals in order to integrate mass and chromatographic information, as a result, the list of peaks (features) - characterized by RT,  $m/z$  and intensity for each sample - is obtained; iii) Alignment, in order to be able to compare among different samples, features must be matched and aligned across all the samples included in the sample set; iv) Gap filling, it involves gathering intensity information from peaks that were initially not detected in all the samples; v) Filtering, it consists in the elimination of those non informative features that are not present in a given number of samples, initial filtering was set to remove those features that are not present in at least 20% of the problem samples belonging to a common class or in 50% of a given type of quality control (QC) sample, once QC checking procedures have been performed, additional filters are applied and those features not present

## Methodology

in the problem samples or present in the blank QC samples are also removed (166, 167); vi) Normalization, different normalization approaches have been described in the bibliography (164, 168), however we decided to normalize data with respect the IS added to each sample during the homogenization and preparation processes (166, 167). As the response of the IS is affected by factors such as sample losses during preparation, volume of injection or mass detection, after IS normalization those confounding factors are corrected and removed from the data before further analysis steps. Additional normalization procedures for some types of samples - i.e. samples from HepG2 cultures and from liver tissue samples from medaka (*Oryzias latipes*) - include the normalization of the signal with respect the total amount of the biological sample, represented by the total amount of protein (103).

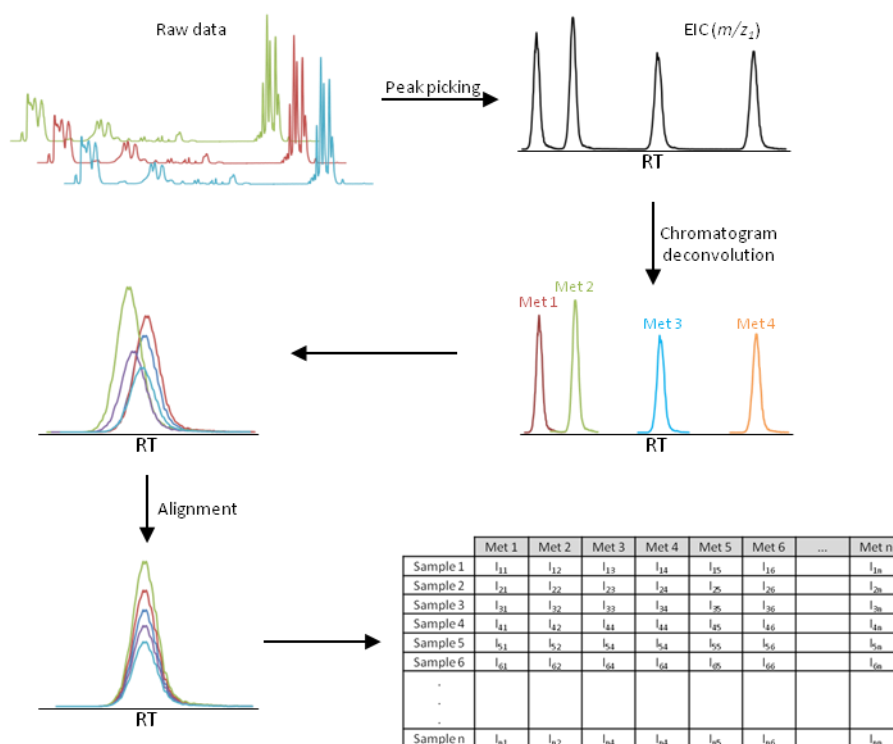


**Figure 2.3.** Schematic representation of the most important steps performed during data processing.

Finally, metabolite identification was performed by the query of the exact mass of the detected features against on line databases within a certain mass range ( $\pm 5$  ppm). The online databases employed to perform metabolite identification are: the Human Metabolome Database (HMDB) (110), the LIPID MAPS-Nature Lipidomics Gateway (169) and the Metlin database (170). The identity of metabolites of interest was confirmed by comparing the MS/MS spectra of the selected features with those of the proposed metabolites on the online databases HMDB (110), Metlin (170) and MassBank (171). The identities of the selected metabolites were further confirmed by the use of authentic standards when available.

## Methodology

### 2.5 Data analysis

All the univariate and multivariate statistical analysis as well as data plots were performed using R (172). The following packages were employed: 'pcaMethods' (173), 'mixOmics' (174), 'DiscriMiner' (175), 'gplots' (176), 'boot' (177), 'caret' (178), 'FactoMineR' (179), 'cvTools', 'pROC' (180), 'rgl' (181) and 'VennDiagram' (182). To perform data analysis, all the information for a given sample (i.e. the information provided by different analytical conditions) was joined into a single matrix comprising all the data available for each biological sample. The data analysis strategy is depicted in **Figure 2.4** (183)

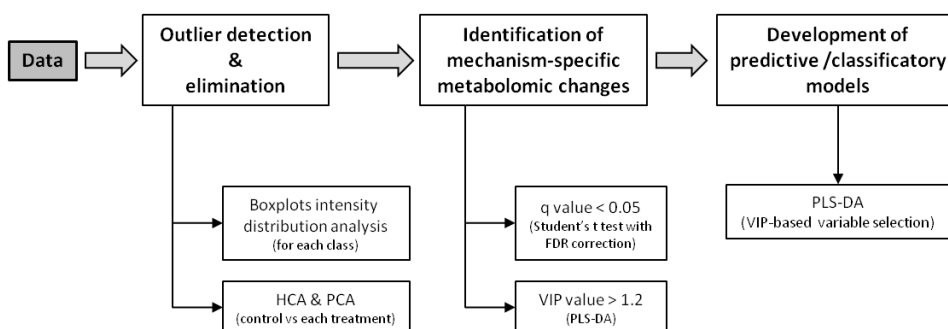


**Figure 2.4.** Workflow of data analysis strategy. Data analysis strategy is developed in three different stages. I) Outlier detection and elimination is performed based on the examination of the intensity distribution of the samples and non-supervised multivariate analysis such as hierarchical cluster analysis (HCA) and principal component analysis (PCA). II) In order to decipher those metabolomic patterns associated with specific mechanisms of toxicity, data is split in control vs one treatment datasets and those variables showing a  $q$  value  $< 0.05$  (based on a Student's  $t$  test with FDR correction for multiple testing) or a VIP (variable importance in the projection) value  $> 1.2$  (in PLS-DA models) are considered to be significantly different as a result of the mechanism of toxicity under study. III) Finally, predictive/classificatory models are developed based on PLS-DA modeling with a VIP-based selection criteria of discriminant variables.

### 2.5.1 Detection of outliers

The first step in data analysis is the detection of potential outliers. They are defined as those samples that show a behavior that stands out from the average one. Abnormal sample compositions can be due to sample degradation, instrumental errors, changes in measurement conditions or faults due to human errors (131). Two different strategies were implemented in order to perform an early detection of outliers in the data analysis process. First, density and box-and-whisker plots, in which all the information about the intensity distribution of all the features for a single sample is visualized using a single graphic, were drawn. Those samples whose distributions considerably differed with respect to the rest of samples belonging to their same class (i.e. control samples, steatosis samples...) were considered outliers and eliminated from the following steps. Then, unsupervised (that is, without using any *a priori* knowledge about the samples) multivariate analyses were performed in order to visualize the natural interrelationship among the different samples and to detect outliers that have not been previously detected and may interfere in the subsequent analysis. In the case of multiclass approaches (more than two groups) this was performed testing one treated group with respect to its control at the time (i.e. steatosis vs control, phospholipidosis vs control and so on). The tools employed to this end were HCA and PCA. In both approaches, samples that cluster together are considered to have more similar metabolomic patterns than those that cluster apart. Data sets were mean-centered and unit variance-scaled before performing HCA. Data sets were log-transformed, mean-centered and unit variance-scaled before carrying out the PCA. Samples whose position in the PCA scores plot is far from the rest of the samples of belonging to the same group (i.e. outside the Hotelling's  $T^2$  95% confidence ellipse (184)) may be considered outliers.



## Methodology

---

The process of outlier detection and elimination is exemplified in **Figure 2.5** using a simulated data set. The data set used in the example is composed of 100 variables and 20 observations, 10 belonging to group A and 10 belonging to group B. For group A the first 50 variables follow a normal distribution with mean 80 and standard deviation 15, the second 50 variables follow a normal distribution with mean 120 and standard deviation 15. For group B, the variables share the same characteristics but with the means inverted. For sample B5, a value of 160 is assigned for the mean of the first 50 variables. **Figure 2.5.A** shows that the mean value and the deviation of the intensity of the variables for sample B5 are greater than the ones obtained for the rest of samples. The PCA scores plot shows that sample B5 falls out of the Hotelling's  $T^2$  95% confidence ellipse obtained for group B (represented in red) (**Figure 2.5.B**). Finally, the dendrogram drawn at the top of the **Figure 2.5.C** shows that two clusters are obtained, corresponding to groups A and B, respectively. However, it can be seen that within the cluster corresponding to group B, sample B5 shows the greater distance with respect to the rest of the samples and is clustered apart of the rest samples of the group. Moreover, a close look at the heatmap reveals that the reason of this distance is an increase in the intensity in a group of variables with respect to the rest of the samples of the group. Then, sample B5 is identified as an outlier and the reason of its abnormal behavior with respect of the rest of samples of the group is evidenced.

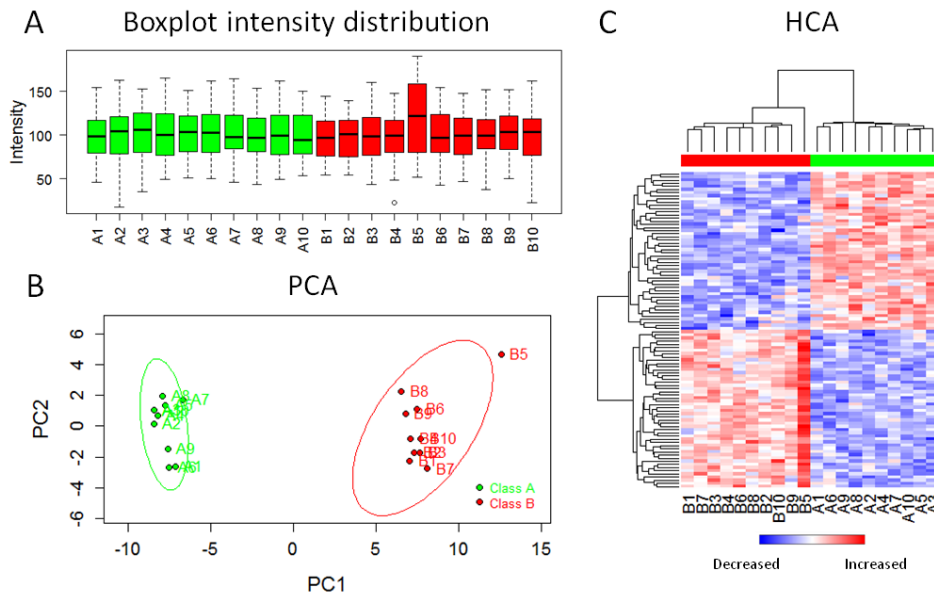


**Figure 2.5.** Simulated example of the application of boxplot of intensity distribution (A), PCA (B) and HCA (C) for the detection of outliers. **A)** The boxplot intensity distribution shows that sample B5 has a higher mean and a higher deviation compared to the rest of samples belonging to its same class (red color). Boxes denote interquartile ranges, lines denote medians, and whiskers denote the 10th and 90th percentiles. **B)** PCA scores plot. The Hotelling's  $T^2$  95% confidence ellipse is drawn for each group (green, class A, and red, class B). Sample B5 is out of the ellipse and far from the rest of samples of its same group. **C)** HCA, the dendrogram drawn at the top of the heatmap shows the big distance between sample B5 and the rest of the samples of the group, which are clustered together. Based on this information, sample B5 would be considered to be an outlier.

## Methodology

---

### 2.5.2 Identification of metabolomic alterations

In order to visualize the metabolomic changes provoked by each specific treatment with views to mechanistic elucidation, a  $t$  test with Benjamini-Hochberg (false discovery rate, FDR) correction for multiple testing was applied (185). Those variables with a  $q$  value  $< 0.05$  were considered to be significantly altered as a result of the treatment. As univariate tests do not reflect the multivariate nature of the data and the relationship among the different variables, PLS-DA models were built for each control-treatment case and those variables with a VIP (variable importance in the projection) value  $> 1.2$  were also considered to have a marked impact in discriminating between control and treatment groups. Based on those significantly altered metabolites, the pathway analysis tool of Metaboanalyst (186) and MBRole (187) were employed to map which pathways were significantly altered as a consequence of the toxic insult. Then, box-and-whisker plots of significantly altered metabolites/groups of metabolites/pathways were drawn to facilitate data visualization and interpretation.

To exemplify the proposed data analysis strategy with respect to detection of altered variables (metabolites) a simulated data set consisting of 100 variables and 30 samples, split in two groups of equal size, was created. The variables were generated following a normal distribution of mean 100 and standard deviation 15. Among the 100 variables, 10 variables were selected to have different mean between the two groups: V1 (A= 120, B= 100), V11 (A= 80, B= 100), V21 (A= 100, B=120), V31 (A= 100, B= 120), V41 (A= 140, B= 100), V51 (A= 60, B= 100), V61(A=100, B= 140), V71 (A= 100, B= 140), V81 (A= 120, B= 100), and V91(A= 100, B= 120). **Table 2.1** shows the results of selected variables using a simple  $t$  Student's test ( $p < 0.05$ ), a  $t$  Student's test with FDR correction ( $q < 0.05$ ) and using VIP value (VIP  $> 1.2$ ) as criteria. FDR was the most restrictive criteria, with only 8 selected variables, all of

them belonging to those made up to be altered between the two groups. Similar results were obtained with respect the total number and the identity of the variables selected with the  $p$  value and the VIP strategies. In both cases all the variables with a predefined difference in the mean between the two classes were selected, however, a number of variables that were not supposed to be different between the two groups were also included.

**Table 2.1.** Figures of the different strategies employed for variable selection over the simulated data described in Section 2.5.2.

Strategy	Number of selected variables	Number of really altered variables selected	Selected Variables
FDR	8	8	<i>V1, V31, V41, V51, V61, V71, V81, V91</i>
$p$ value	15	10	<i>V1, V4, V11, V21, V31, V36, V41, V42, V44, V51, V61, V71, V81, V90, V91</i>
VIP	16	10	<i>V1, V4, V11, V21, V31, V36, V41, V42, V44, V51, V61, V71, V75, V81, V90, V91</i>

FDR: variables with a  $q$  value  $< 0.05$ ;  $p$  value: variables with a  $t$  Student's  $p$  value  $< 0.05$ ; VIP: variables with VIP value  $> 1.2$ , VIP value corresponding to a PLS-DA model developed using 1 LV. Variables in italics represent variables with made up differences.

## Methodology

---

### 2.5.3 Predictive model development

The main aim in the development of predictive models is to use the model showing maximum parsimony, that is, the one that best fits with the minimum possible number of predictors. To this end, a PLS-DA analysis using VIP-based variable ranking and selection was performed.

#### *Model validation*

Two different strategies with respect to model validation were attempted: CV and permutation testing (132, 133). While the optimum way of validating any model is to use an external data set, the limitations in the number of samples and compounds tested drove us to use CV and permutation testing instead.

In a CV strategy the data is split in different subsets and depending on the way the CV is performed, some of the subsets are used to build the model and the rest are used to evaluate the capabilities of the model. Two different CV strategies were employed. For model development a 7-fold CV strategy was employed (**Figure 2.6.A**). Using this approximation, the data was split into 7 different subsets. In each round of the CV, 6 of the subsets were used to develop the model and the last one was used as test set to evaluate the capabilities of the model. The process was repeated until all the subsets were used as test set.

For model validation, two different parameters were employed: misclassification error and AUROC (area under the receiver operating characteristic curve), for multiclass problems the method developed by Hand and Till was employed (188). A randomized CV strategy was performed to estimate these parameters: 2/3 of the data were employed to develop the model and the rest 1/3 was used as test set (**Figure 2.6.B**). The partitions were repeated 100 times in a randomized manner.

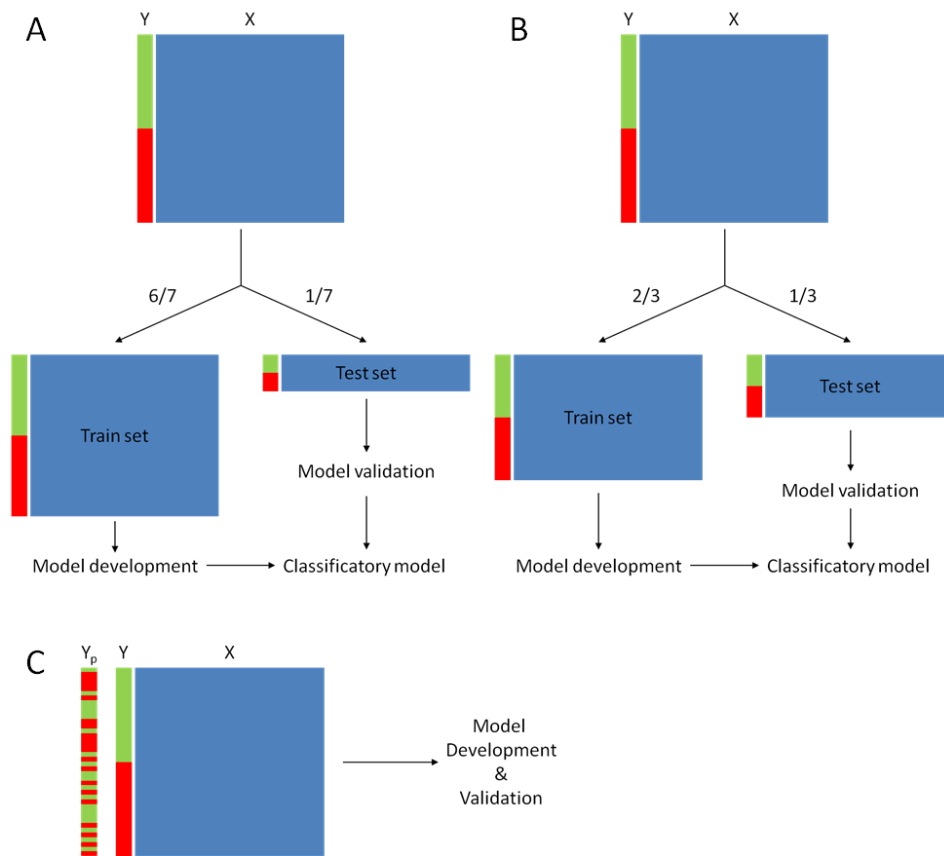


**Figure 2.6.** A) 7-fold CV, the data is split in 7 different subsets. 6 subsets are used as train set to build the model and the last one as test set to evaluate it. The process is repeated until all the subsets have been used as test set. B) The data is split in two subsets, 2/3 of the data are used as train set and the rest 1/3 as test set. The partitions are repeated 100 times randomly. C) In permutation testing the classes (Y) are randomly assigned (Y<sub>p</sub>) and the model is developed and validated using the permuted classes.

## Methodology

---

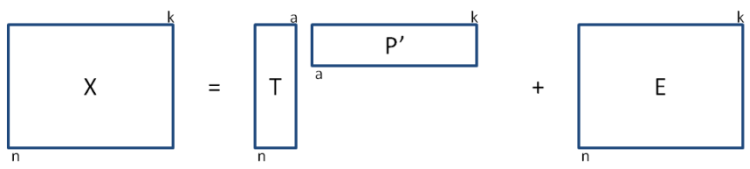
Finally, permutation testing was also employed as validation strategy. A permutation test involves the random reassignment of the class labels and the model development and evaluation based on the newly relabeled data set (**Figure 2.6.C**). Permutation testing compares the original model's goodness of fit with the values obtained after class randomization. The model performance figures of merit can be plotted on a histogram for visual assessment, making possible to determine whether the original class assignment is significantly different from, or a part of, the distribution based on the permuted class assignments. An empirical *p-value* can be calculated by determining the number of times the permuted data yielded a better result than the one using the original labels (133). The process was repeated 1000 times and the performance results were compared to those obtained with the real classes labelling (133).

### PLS-DA

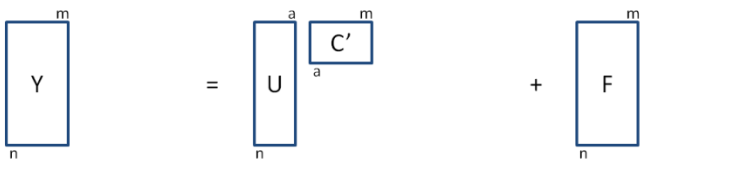
PLS-DA is a PLS-based model in which the dependent variable (Y block) represents class membership (127, 128). The whole objective in PLS-DA is to model the relationship between X (the MS data set) and Y (classes). The fundamental equations of PLS-DA (127) are written and graphically represented in **Figure 2.7**.

[eq 1] 
$$T = XW$$

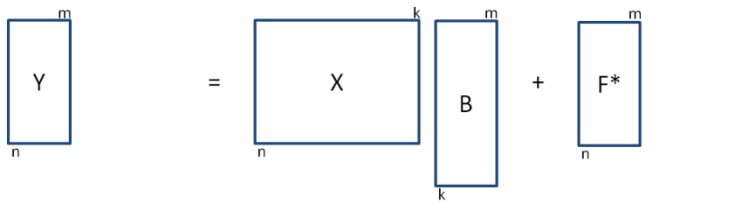
[eq 2] 
$$X = TP' + E$$



[eq 3] 
$$Y = UC' + F$$



[eq 4] 
$$Y = TC' + F^* = XWC' + F^* = XB + F^*$$



[eq 5] 
$$B = WC'$$

**Figure 2.7.** Fundamental equations of PLS-DA.  $n$  represents the number of observation,  $k$  the number of independent variables,  $m$  the number of classes in which the observations can be classified and  $a$  the number of LVs employed to develop the PLS-DA model.  $X$  is a  $n \times k$  matrix of predictors, and  $Y$  a  $n \times m$  matrix of responses.  $P$  ( $k \times a$ ) and  $C$  ( $m \times a$ ) are the matrix loadings of  $X$  and  $Y$ , respectively.  $T$  and  $U$  are  $n \times a$  scores matrices for  $X$  and  $Y$ , respectively.  $E$ ,  $F$  and  $F^*$  represent residual (i.e. error) matrices.  $W$  ( $k \times a$ ) represents the  $X$ -weight matrix and  $B$  ( $k \times a$ ) represents the matrix of regression coefficients for all  $Y$ s.  $X$  scores ( $T$ ) are calculated as a linear combination of the original predictors with the weights [eq 1].  $X$  and  $Y$  can be projected in the new  $a$  dimensional space [eq 2,3].  $Y$  can be predicted based on  $X$  scores ( $T$ ) [eq 4], which can be reformulated based on eq 1,5 to look as a multiple regression model in which the responses ( $Y$ ) can be predicted based on a series of predictors ( $X$ ) via the corresponding coefficients ( $B$ ). Equations 2, 3 and 4 are graphically represented.



## Methodology

---

Data sets were log-transformed, mean-centered and unit variance-scaled before carrying out the PLS-DA. The selection of the optimum number of LVs and the evaluation of the quality of the PLS-DA models was conducted by the typical CV procedure by leaving one-seventh of samples out of each round (**Figure 2.6.A**) (189). Different model parameters were used to evaluate model performance: i) total Y explained variance (i.e.,  $R^2$ ); ii) predictable Y variation (i.e.,  $Q^2$ ); iii) prediction accuracy, evaluated as misclassification error rate; and iv) AUROC. Different methods can be used in order to evaluate the importance of a variable in the output provided by a PLS-DA model (167), among them, we decided to employ the VIP value. The VIP score of a predictor summarizes the importance for the projections to find  $a$  LVs. Since the average of the squared VIP scores equals 1, the “greater than one” rule is generally used as a variable selection criterion (190). Therefore, an uninformative variable elimination process can be performed based on the VIP scores obtained (167). Such procedure not only improves model performance, but also achieves model simplification, a relevant issue concerning the further development of ‘target’ MS approaches to quantitatively determine biomarkers (167). As overfitting is a common problem associated with PLS-DA modeling (122, 189), a bootstrapping (191, 192) strategy coupled to VIP values determination was setup to select those metabolites that should be included in the final predictive model.

Bootstrapping is based on random resampling with replacement to estimate a statistic parameter. For each of the datasets used for PLS-DA model building, two hundred derived datasets were obtained by random sampling with replacement of the observations. A PLS-DA model was built for each of those derived datasets and the median VIP value for each predictor was calculated. PLS-DA models were built with decreasing number of variables according to their ranked median VIP value. For each model,  $R^2$ ,  $Q^2$  and prediction accuracy were recorded. The optimum

predictive model was selected as the one providing the highest accuracy with the lowest number of retained variables. To further assess model consistency and performance, a response permutation test ( $n = 1000$ ) based on  $R^2$ ,  $Q^2$ , prediction accuracy and AUROC was applied (133, 134).

In order to facilitate the understanding of the PLS-DA data analysis strategy, the whole process was applied over the simulated data described in **Section 2.5.2**. **Figure 2.8** shows the values of  $R^2$ ,  $Q^2$  and misclassification error obtained for PLS-DA models built using all the variables and a number of LVs varying from 1 to 3. From the obtained results it can be concluded that the optimum number of LVs to be used for PLS-DA model development is 1 as it provides the highest values of  $Q^2$ , which evaluates the predictive capabilities of the system, and accuracy.

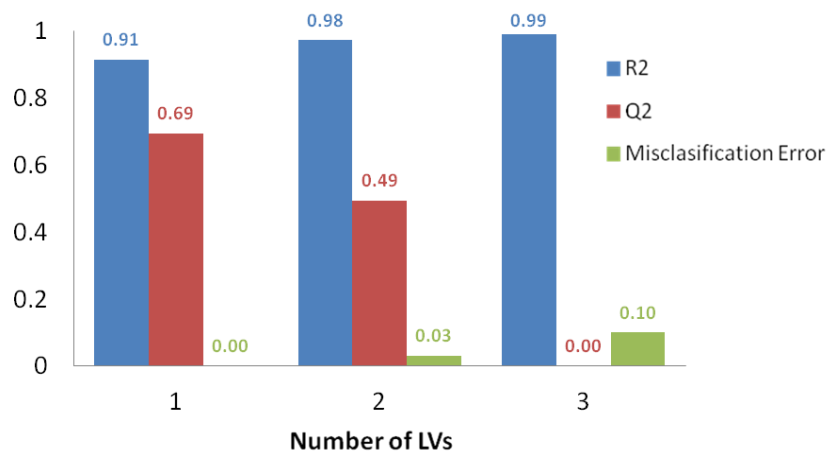


**Figure 2.8.** Values of  $R^2$ ,  $Q^2$  and misclassification error as a function of the number of LVs employed to build the PLS-DA model using the simulated data described in **Section 2.5.2**. The values obtained for each parameter and model are written over the corresponding bar.

## Methodology

---

After the determination of the optimum number of LVs, the next step is to determine the variables that should be included in the final predictive/classificatory model. To this end, PLS-DA models with an increasing number of variables, ranked according to the previously described strategy, were built and their performance was evaluated. Following the analysis of the example, all the variables with made up differences were within the top 15 ranked variables, furthermore the four variables with the highest simulated differences (i.e. V51, V61, V71 and V81) were the ones with the highest median VIP value. Moreover, **Figure 2.9**, shows that the model with the highest performance (i.e. AUROC = 1, misclassification error = 0) was achieved with only those four variables.

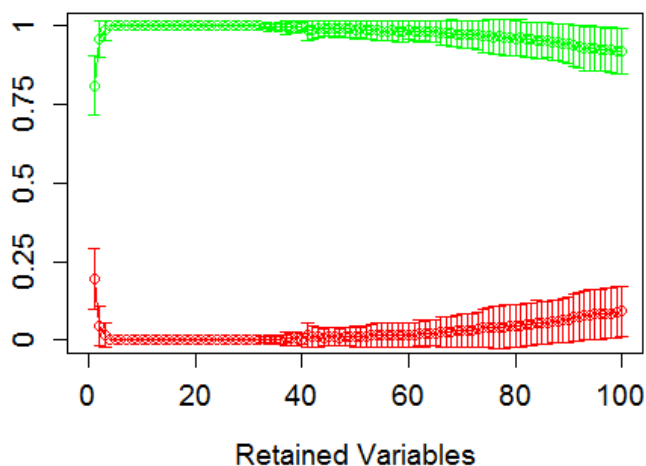


**Figure 2.9.** Values obtained for the AUROC (green) and misclassification error (red) versus the number of retained variables using the simulated data described in **Section 2.5.2** based on the bootstrapped resampling coupled to VIP ranking strategy. The data is expressed as mean  $\pm$  standard deviation. The minimum value for the misclassification error and the maximum value for the AUROC are obtained with the model developed using only the four top ranked variables.

The scores and loadings plots corresponding to the optimum PLS-DA model are represented in **Figure 2.10.A** and **Figure 2.10.B**, respectively. The position of a variable in the loadings plot is determined by its relation to other variables and to the class assignments. In the example represented in **Figure 2.10.B**, variables V41 and V71 are positively correlated to each other and to Class A, as represented by their close values obtained with respect to the first LV. The same conclusion can be obtained with respect to variables V51 and V61 and Class B.

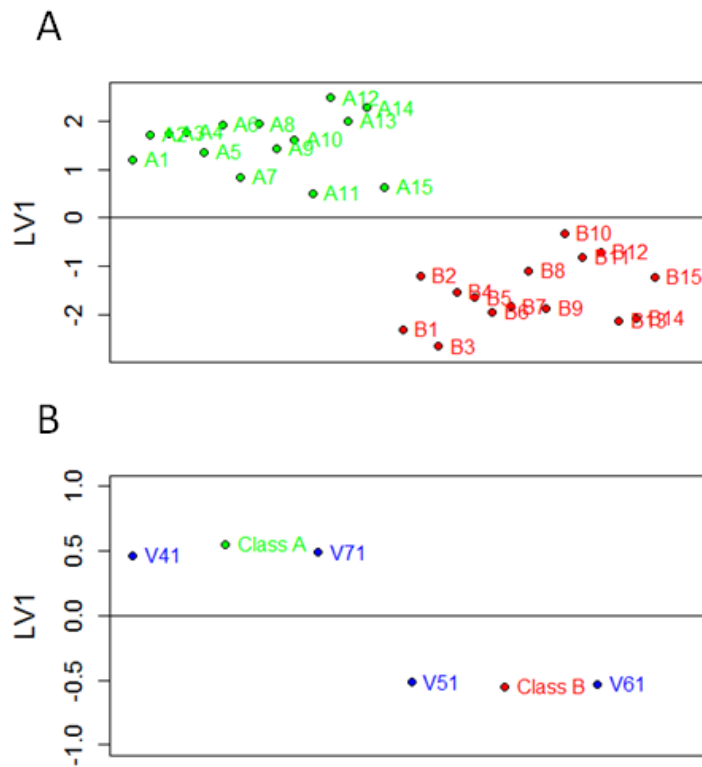


**Figure 2.10.** Scores (A) and loadings (B) plots corresponding to the PLS-DA model developed using the top 4 ranked variables and 1LV using the simulated data described in **Section 2.5.2** and a bootstrapping coupled to VIP-based ranking and variable selection strategy. Class A is represented in green, class B in red and variables in blue. X axis represents sample order.

## Methodology

Model validation was performed by using a permutation test. The results are shown in **Figure 2.11**. Four parameters were evaluated:  $R^2$ ,  $Q^2$ , misclassification error and AUROC. The histograms represent the distribution of values obtained for the permuted models and the value obtained with the real classes is represented by a red dot. For all the parameters it can be seen that the real value is outside the distribution of the values obtained with the permuted classes, as 1000 permutations have been performed, an experimental  $p$  value  $< 0.001$  can be assigned. These results indicate that the developed PLS-DA model is consistent and based on a real difference between the classes and does not reflect a chance correlation between them.

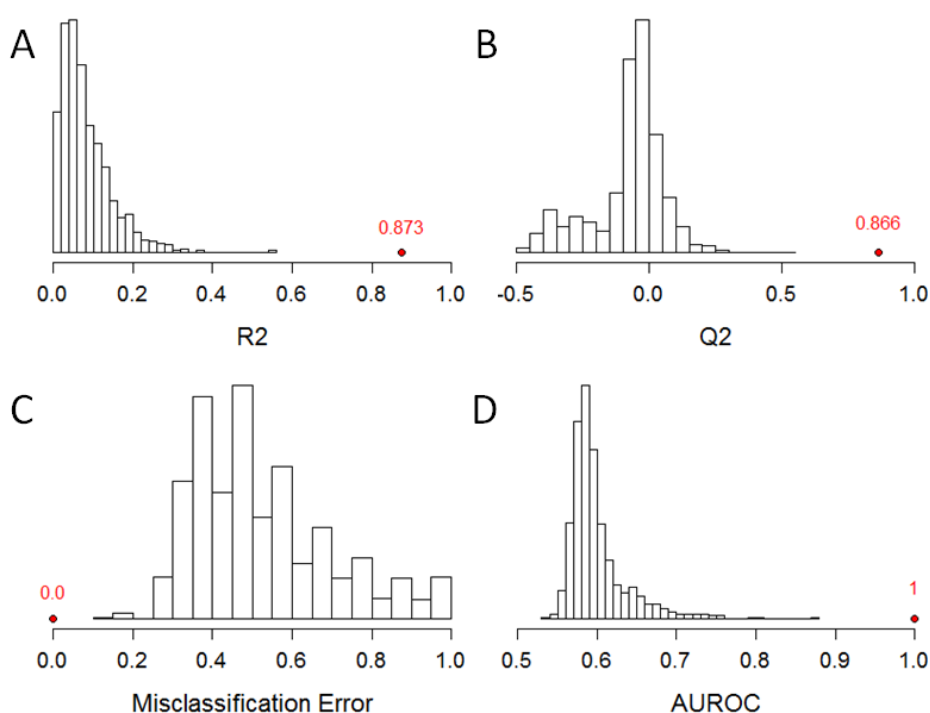


**Figure 2.11.** Permutations tests ( $n=1000$ ) for  $R^2$  (A),  $Q^2$  (B), misclassification error (C) and AUROC (D) corresponding to the PLS-DA model developed using the top 4 ranked variables and 1LV from the simulated data described in **Section 2.5.2** and a bootstrapping coupled to VIP-based ranking and variable selection strategy. Histograms represent the values provided by the PLS-DA models obtained using permuted classes. The red dots represent the value obtained for the PLS-DA model developed using the real classes, with the value written above it.

### 2.6 Culture and treatment of HepG2 cells with model hepatotoxic compounds

Human hepatoma HepG2 cell line (ECACC 85011430) was used for *in vitro* hepatotoxicity studies. HepG2 are adherent cells with a high proliferation rate. They are epithelial-like cells growing as monolayers and forming characteristic cell clusters or islands (**Figure 2.12**). HepG2 cells were routinely grown in culture grade flasks at 37 °C under a humidified atmosphere 5% CO<sub>2</sub> / 95% air in Ham's F-12 / Leibovitz L-15 (1:1, v/v) supplemented with 7% fetal bovine serum, 50 U/mL penicillin and 50 µg/mL streptomycin. Medium was renewed every 2 days. Cells reaching 70-80% confluence were ready to be used or passed. For subculturing purposes, cells were detached by treatment with 0.25% trypsin / 0.02% EDTA at 37 °C. A sample of the obtained cell suspension was used to determine cell viability (by the trypan blue exclusion test) and cell number (e.g., using a cell counter) (193). For metabolomic studies, cells were seeded at a density of 8×10<sup>4</sup> cells/cm<sup>2</sup> on 3.5 cm (for specific-conditions analysis and processing method optimization) or 6 cm culture dishes (for generic analysis in drug incubations).

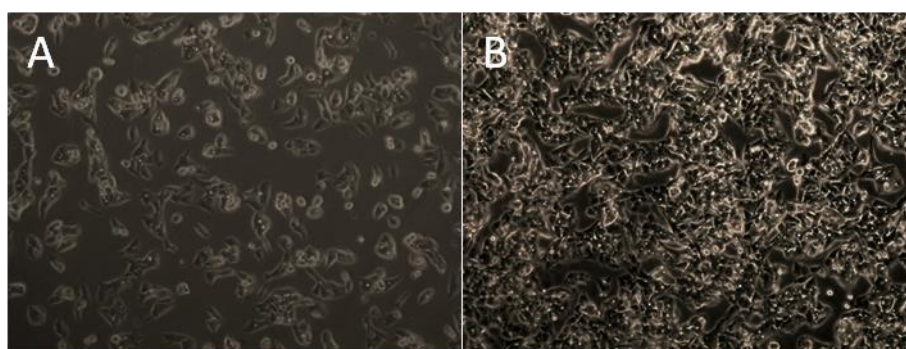


**Figure 2.12.** HepG2 cells cultured at low (panel A) and high (panel B) densities.

## Methodology

---

A total of 13 compounds were selected for the *in vitro* hepatotoxicity study based on data available in the literature (29, 69, 88, 89, 91, 92). Compounds with well-documented *in vivo* hepatotoxicity were classified according to the main mechanism involved in their toxicity (i.e. steatosis, phospholipidosis, cholestasis or OS) (**Table 2.2**) (29, 69, 88, 89, 91, 92). In addition, two compounds with no reports of hepatotoxic effects were used as negative controls (29). The stock solutions of the test compounds were prepared in DMSO and were freshly diluted in the culture medium to obtain the desired final concentration. Only sub-lethal concentrations of the compounds were used (**Table 2.2**) (29, 69, 88, 89, 91, 92). HepG2 cells (70-80% confluence) were treated for 24 h with the compounds. After incubation, cells were processed according to the procedures described below.

A specific additional culture design was applied to drugs causing steatosis and phospholipidosis in order to favor and accelerate the development of the hepatotoxic injury. Prior to being exposed to the model compounds, HepG2 cells were incubated for 14 h with a 62  $\mu$ M mixture of oleate and palmitate (2:1 ratio). Then, cells were incubated with the test compounds for 24 h in a FA free medium (32, 193).

**Table 2.2.** Model hepatotoxins included in the HepG2 cell studies classified by their mechanism of hepatotoxicity.

<b>Mechanism</b>	<b>Compound</b>	<b>Concentrations</b>
<b>Negative Control</b>	Culture medium	
	DMSO (Solvent)	0.5, 1.2%
	Citrate	500, 1000 $\mu\text{M}$
	Ketotifen	50, 100 $\mu\text{M}$
<b>Cholestasis</b>	Chlorpromazine	10, 20 $\mu\text{M}$
	Cyclosporine	10, 25, 50 $\mu\text{M}$
	Troglitazone	10, 20 $\mu\text{M}$
<b>Oxidative Stress</b>	Cumene Hydroperoxide	50, 100, 250 $\mu\text{M}$
	Tert-Butyl Hydroperoxide	50, 100, 250 $\mu\text{M}$
<b>Phospholipidosis</b>	Amiodarone	5, 10, 20 $\mu\text{M}$
	Clozapine	10, 20, 40 $\mu\text{M}$
	Fluoxetine	10, 20 $\mu\text{M}$
	Tilorone	5, 10, 20 $\mu\text{M}$
	Tamoxifen	15, 30 $\mu\text{M}$
<b>Steatosis</b>	Doxycycline	250, 500 $\mu\text{M}$
	Tetracycline	50, 100, 200, 400 $\mu\text{M}$
	Valproic acid	1, 2, 4, 8 mM



## Methodology

### 2.7 Sample processing and analysis optimization for HepG2 cells

Sample preparation is a crucial step in the onset of a metabolomic analysis involving mammalian cells in adherent culture. Different aspects regarding the untargeted analysis of the endometabolome of cultured HepG2 cells were evaluated: i) sample analysis; ii) metabolome extraction; and iii) sample harvesting and processing methodology (Figure 2.13).

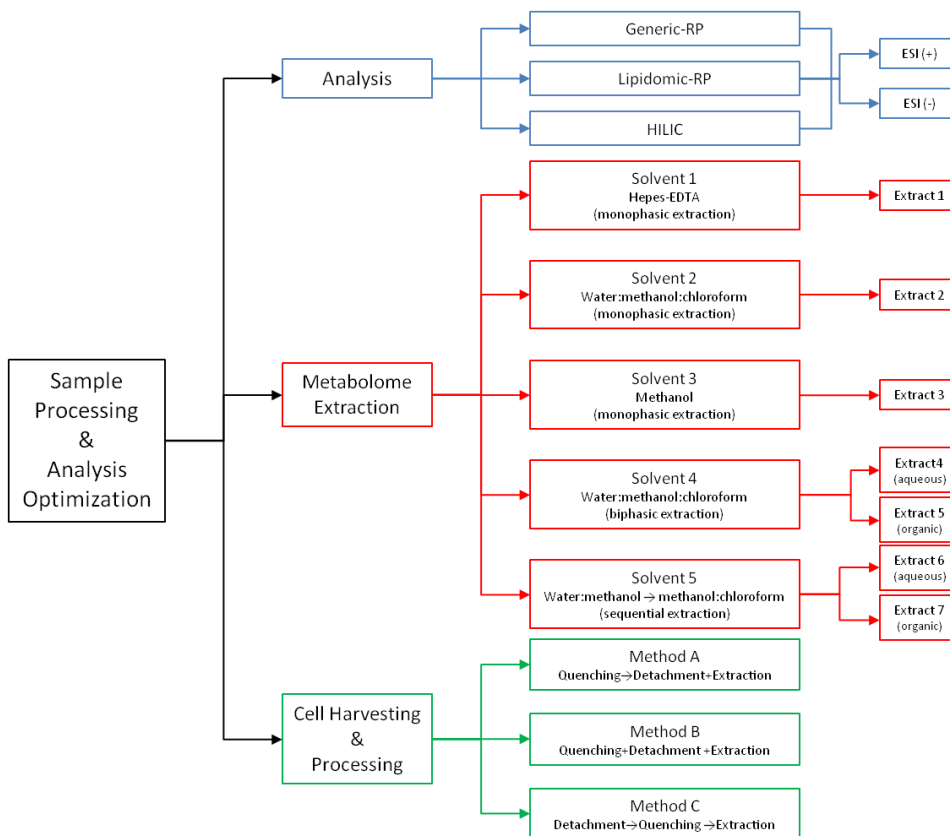


**Figure 2.13.** Schematic representation of the parameters evaluated during sample processing and analysis strategy optimization.

Each condition was tested using three biological replicates of HepG2 cells cultured in 3.5 cm plates. The optimum condition for each of the evaluated parameters was selected based on the number, nature and intensity of the detected features and metabolites.

In a first step, the extraction solvent and the different analytical conditions were tested and optimized in a combined manner. As a general procedure for sample processing of HepG2 cultures, the medium was removed and the cells were washed with phosphate buffer saline (PBS); then the cell monolayer was frozen using liquid N<sub>2</sub> to halt cellular metabolism and prevent metabolite degradation; finally, the cells were scrapped by using an organic solvent and submitted to three freeze/thaw cycles in order to increase cell lysis and metabolite extraction. In a second step, and based on the optimized extraction solvent and analysis strategy, the different sample harvesting and processing methods were evaluated.

### 2.7.1 Sample analysis

Three different LC conditions, each one using both ESI (+) and ESI (-) MS detection, were tested in order to optimize the untargeted metabolomic analysis: i) Generic-RP analysis; ii) Lipidomic-RP analysis; and iii) HILIC analysis (**Figure 2.13**).

#### *i). Generic-RP analysis*

The analytical conditions for the untargeted LC-MS analysis using a generic-RP chromatographic separation are detailed in **Section 2.3.1**.

For the analysis in ESI (+) mode, samples were resuspended in 75 µL of water:methanol (70:30) supplemented with the following IS:

- Paracetamol, C<sub>8</sub>H<sub>9</sub>NO<sub>2</sub>, *m/z* 152.0712, RT 4.75 min, 10 µg/mL.
- Caffeine, C<sub>8</sub>H<sub>10</sub>N<sub>4</sub>O<sub>2</sub>, *m/z* 195.0882, RT 6.74 min, 5 µg/mL.

## Methodology

---

- Sulfadimethoxine,  $C_{12}H_{14}N_4O_4S$ ,  $m/z$  311.0814, RT 8.11 min, 1  $\mu\text{g/mL}$ .
- Val-Tyr-Val,  $C_{19}H_{29}N_3O_5$ ,  $m/z$  380.2185, RT 6.93 min, 10  $\mu\text{g/mL}$ .
- Verapamil,  $C_{27}H_{38}N_2O_4$ ,  $m/z$  455.2910, RT 8.93 min, 0.5  $\mu\text{g/mL}$ .
- Terfenadine,  $C_{32}H_{41}NO_2$ ,  $m/z$  472.3216, RT 9.97 min, 5  $\mu\text{g/mL}$ .
- Reserpine,  $C_{33}H_{40}N_2O_9$ ,  $m/z$  609.2812, RT 9.27 min, 2.5  $\mu\text{g/mL}$ .

For the analysis in ESI (-) mode, samples were resuspended in 75  $\mu\text{L}$  of water:methanol (70:30) supplemented with the following IS:

- Lithocholic acid-2,2,4,4-D4 (LCA-D4),  $C_{24}H_{36}D_4O_3$ ,  $m/z$  379.3150, RT 10.50 min, 4  $\mu\text{g/mL}$ .
- Deoxycholic acid-2,2,4,4-D4 (DCA-D4),  $C_{24}H_{36}D_4O_4$ ,  $m/z$  395.3099, RT 9.46 min, 2  $\mu\text{g/mL}$ .
- Cholic acid-2,2,4,4-D4 (CA-D4),  $C_{24}H_{36}D_4O_5$ ,  $m/z$  411.3049, RT 8.53 min, 2  $\mu\text{g/mL}$ .
- Glycochenodeoxycholic acid-2,2,4,4-D4 (GCDCA-D4),  $C_{26}H_{39}D_4NO_5$ ,  $m/z$  452.3314, RT 7.98 min, 2  $\mu\text{g/mL}$ .
- Glycocholic acid-2,2,4,4-D4 (GCA-D4),  $C_{26}H_{39}D_4NO_6$ ,  $m/z$  468.3263, RT 7.59 min, 2  $\mu\text{g/mL}$ .
- Reserpine,  $C_{33}H_{40}N_2O_9$ ,  $m/z$  607.2656, RT 9.59 min, 2.5  $\mu\text{g/mL}$ .

### ii) Lipidomic-RP analysis

The analytical conditions for the untargeted LC-MS analysis using a lipidomic-RP chromatographic separation are detailed in **Section 2.3.2**.

For the analysis in ESI (+) mode, samples were resuspended in 75  $\mu\text{L}$  of methanol:chloroform (3:1) supplemented with the following IS:

- LysoPC(13:0),  $C_{21}H_{44}NO_7P$ ,  $m/z$  454.2934, RT 1.48 min, 25 ng/mL.
- Terfenadine,  $C_{32}H_{41}NO_2$ ,  $m/z$  472.3216, RT 1.89 min, 25 ng/mL.

For the analysis in ESI (-) mode, samples were resuspended in 75  $\mu$ L of methanol:chloroform (3:1) supplemented with the following IS:

- LCA-D4,  $C_{24}H_{36}D_4O_3$ ,  $m/z$  379.3150, RT 3.96 min, 4  $\mu$ g/mL.
- DCA-D4,  $C_{24}H_{36}D_4O_4$ ,  $m/z$  395.3099, RT 3.18 min, 2  $\mu$ g/mL.
- CA-D4,  $C_{24}H_{36}D_4O_5$ ,  $m/z$  411.3049, RT 2.61 min, 2  $\mu$ g/mL.
- GCDCA-D4,  $C_{26}H_{39}D_4NO_5$ ,  $m/z$  452.3314, RT 2.55 min, 2  $\mu$ g/mL.
- GCA-D4,  $C_{26}H_{39}D_4NO_6$ ,  $m/z$  468.3263, RT 2.23 min, 2  $\mu$ g/mL.

### iii) HILIC analysis

The analytical conditions for the untargeted LC-MS analysis using HILIC chromatographic separation are detailed in **Section 2.3.3**.

For the analysis in both ESI (+) and ESI (-) modes, samples were resuspended in 75  $\mu$ L of acetonitrile:water (70:30) supplemented with the following IS:

- Phenylalanine-D5 (Phe-D5),  $C_9H_6D_5NO_2$ ,  $m/z$  171.1182 / 169.1020, RT 7.10 min, 40  $\mu$ g/mL.
- Val-Tyr-Val,  $C_{19}H_{29}N_3O_5$ ,  $m/z$  380.2185 / 378.2029, RT 6.33 min, 10  $\mu$ g/mL.
- 8-BrAMP,  $C_{10}H_{13}BrN_5O_7P$ ,  $m/z$  425.9814 / 423.9658, RT 3.96 min, 20  $\mu$ g/mL.
- Leucine Enkephalin,  $C_{28}H_{37}N_5O_7$ ,  $m/z$  556.2771 / 554.2615, RT 6.45 min, 10  $\mu$ g/mL.

### 2.7.2 Metabolome extraction

Five different solvents, leading to seven different extracts, were tested: Solvent 1: 1mM Hepes, 1mM EDTA pH7.2 in water (monophasic extraction) (146), extract 1 (E1); Solvent 2: Water:methanol:chloroform (10:27:3) (monophasic extraction) (152), extract 2 (E2); Solvent 3: Methanol (monophasic extraction) (194), extract 3 (E3); Solvent 4:

## Methodology

---

Water:methanol:chloroform (1:1:1) (biphasic extraction) (195), extracts 4 (E4, aqueous) and 5 (E5, organic); and Solvent 5: Water:methanol (1:1), followed by methanol:chloroform (1:3) (sequential extraction) (162), extracts 6 (E6, aqueous) and 7 (E7, organic) (**Figure 2.13**).

The volumes and specific considerations derived from the nature of the different combination of solvents are described below. In all the cases after the crude extract was obtained, it was subjected to three freeze/thaw cycles in order to maximize cell lysis and metabolite extraction. The final step in all the cases and once the clean extracts were obtained was to evaporate them to dryness and resuspend them in the suitable solvent in concordance with the analytical condition to be employed

### 1. Monophasic extractions

This procedure was performed with solvents 1, 2 and 3. An initial volume of 750  $\mu\text{L}$  was used to scrap the cells, and a second volume of 250  $\mu\text{L}$  was employed (and pooled in the tube with the first one) to recover possible rests. After the freeze/thaw cycles, a 75  $\mu\text{L}$  aliquot of cell extract was taken and mixed with 75  $\mu\text{L}$  of 1 M NaOH to carry out protein quantification. Finally, the extracts were separated from the cell rests by centrifugation (10000 g, 10 min).

### 2. Biphasic extraction: solvent 4

Cells were scraped with 750  $\mu\text{L}$  of methanol:water (1:1) and an additional volume (250  $\mu\text{L}$ ) was used to recover possible rests (and pooled in the tube with the first one). After the freeze/thaw cycles, a 75  $\mu\text{L}$  aliquot was taken and mixed with 75  $\mu\text{L}$  of 1 M NaOH to carry out protein quantification. Then, 500  $\mu\text{L}$  of chloroform were added to the rest of the extract and the tube was vortexed (3 x 10 s). After vortexing,

samples were allowed to rest for 20 min at -20 °C and centrifuged (10000 g, 10 min). The upper aqueous phase and the lower organic phase were transferred to separate clean tubes.

### 3. Sequential extraction: solvent 5

750 µL of methanol:water (1:1) were used to scrap the cells, and a second volume of 250 µL was employed (and pooled in the tube with the first one) to recover possible rests. After the freeze/thaw cycles a 75 µL aliquot was taken and mixed with 75 µL of 1 M NaOH to carry out protein quantification. Then the samples were centrifuged (10000 g, 10 min) and the supernatants were transferred to clean tubes. The pellets were reextracted with 1 mL of methanol:chloroform (1:3). After centrifugation (10000 g, 10 min), the supernatants were transferred to clean tubes.

### **2.7.3 Sample processing strategy optimization**

Three key steps are involved in adherent cells processing with respect to the analysis of the endometabolome: i) metabolism quenching; ii) metabolite extraction and iii) cell detachment from the surface of the plate (103). Three different configurations were tested: Method A, quenching, followed by simultaneous detachment and extraction; Method B, simultaneous quenching, extraction and detachment; and Method C, detachment, followed by quenching, followed by extraction (**Figure 2.13, 2.14**).

To specifically evaluate these issues, the different cells harvesting and processing configurations were evaluated using the previously optimized sample analysis and extraction solvent conditions. In all the cases the first two steps regarding sample processing using HepG2 cells in culture consisted in the removal of the culture medium by aspiration and the washing of the cell monolayer with PBS. The final steps in all the cases

## Methodology

were to perform three freeze/thaw cycles in order to increase cell lysis and metabolites extraction, the separation of the cellular rests from the cellular extract and the evaporation to dryness of the clean extracts in order to be ready for resuspension in the suitable solvent for its analysis. The specific steps of each of the configurations are detailed below.

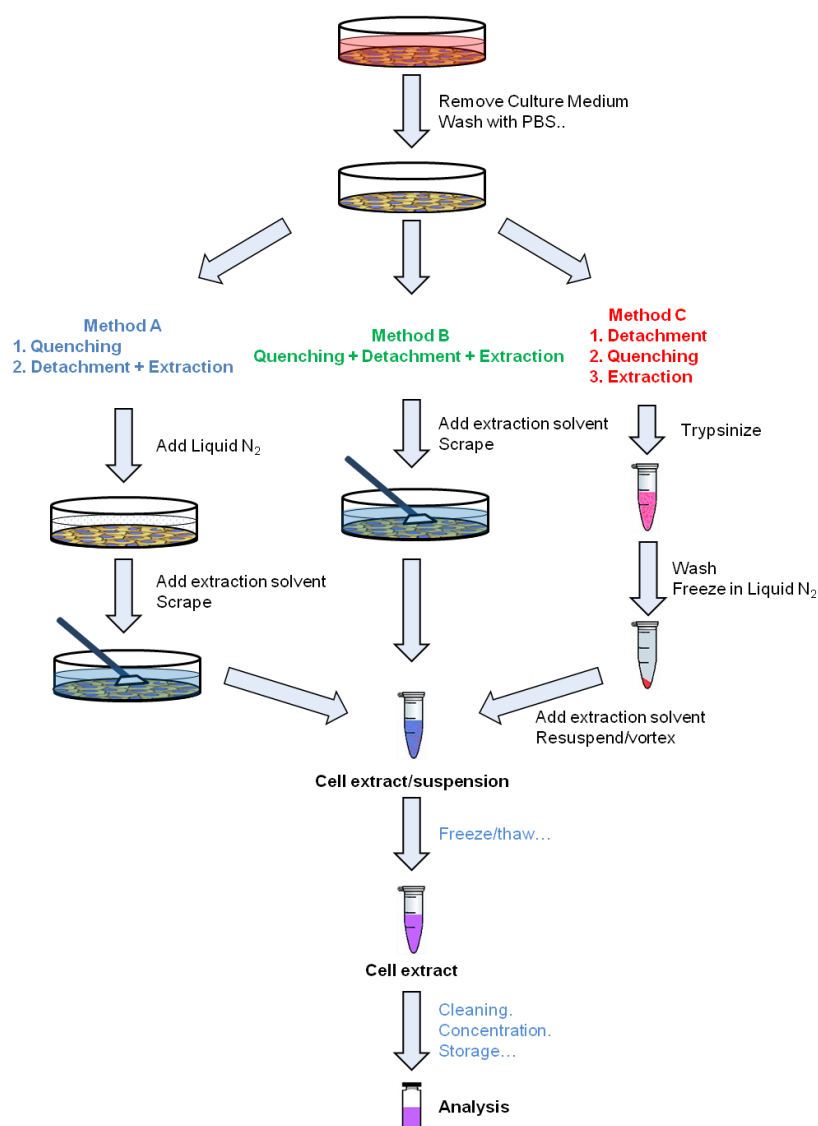


**Figure 2.14.** Sample processing strategies tested during the development and optimization phase. Figure adapted from reference (103).

### Method A

After washing, cell metabolism was immediately quenched by the addition of liquid N<sub>2</sub> over the cell monolayer. Frozen plates were stored at -80 °C until further processing. Simultaneous metabolite extraction and cell detachment were performed by the addition of the extraction solvent over the cell monolayer followed by cell detachment with a rubber cell scrapper.

### Method B

Simultaneous quenching, extraction and detachment were achieved by the addition of cold extraction solvent over the cell monolayer and the use of a rubber cell scrapper to detach the cells from the surface of the plate.

### Method C

Cells harvesting was performed by treatment with 0.25% trypsin / 0.02% EDTA at 37 °C. Thereafter, cells were recovered in 5% fetal bovine serum in PBS and transferred to a clean tube. After centrifugation (3000 g, 3 min), the supernatant was removed by aspiration and the cells were washed with PBS, thus repeating the centrifugation and the removal of the supernatant steps. The pellet was frozen in liquid N<sub>2</sub>, and stored at -80 °C until further processing. Metabolites were extracted by adding the extraction solvent to the cell pellet and vortexing until its complete resuspension.



## Methodology

---

### 2.8 Optimized sample extraction protocols for untargeted metabolomic analysis in HepG2 cells

#### 2.8.1 Generic protocol

Each experimental condition (test compound and concentration) was tested in triplicate using 6 cm diameter plates. After processing, each biological sample was split into four different fractions, one to perform protein quantification and three destined to be analyzed under four different conditions.

After removing the medium by aspiration and washing the monolayer with PBS, cells were frozen by the addition of liquid N<sub>2</sub>. At this point the plates were stored at -80 °C until further processing.

Metabolite extraction and cell detachment were performed by scrapping the cells with 800 µL of a water:methanol:chloroform (10:27:3) solution containing 0.375 µg/mL reserpine and 0.075 µg/mL sulfadimethoxine as IS. The cell extract/suspension was transferred to a clean 1.5 mL tube. The possible cellular rests present in the plate were recovered with 400 µL of the same extraction solution and pooled with the previous volume. The cellular extract/suspension was submitted to 3 freeze/thaw cycles (liquid N<sub>2</sub>, room temperature) in order to increase cell disruption and metabolite extraction. At this point three different aliquots were taken and processed independently.

A 50 µL aliquot was mixed with 100 µL of 0.66 N NaOH and used for protein determination.

A 600 µL aliquot was submitted to liquid-liquid extraction with chloroform. To this end, 300 µL of water and 450 µL of chloroform containing 0.01 µg/mL terfenadine as IS were added and the samples were vortexed (3 x 10 s) to put in contact both phases. Then, the samples were allowed to rest at -20 °C for 20 min and centrifuged (10 min, 10000 g, 4 °C). Each phase (the upper aqueous phase and the lower

organic phase) was transferred to a clean tube and evaporated to dryness. The organic phase was resuspended in 75  $\mu\text{L}$  of a methanol:chloroform (3:1) solution containing 0.5  $\mu\text{g}/\text{mL}$  verapamil as IS and analyzed using the lipidomic-RP ESI (+) approximation. The aqueous phase was resuspended in 75  $\mu\text{L}$  of acetonitrile:water (70:30) solution with IS (40  $\mu\text{g}/\text{mL}$  Phe-D5, 20  $\mu\text{g}/\text{mL}$  8-BrAMP and 10  $\mu\text{g}/\text{mL}$  Val-Tyr-Val) and analyzed using the HILIC approximation in both ESI (+) and ESI (-) modes.

Finally, the rest of the volume was centrifuged (10 min, 10000 g, 4  $^{\circ}\text{C}$ ) and the supernatant was transferred to a clean tube and evaporated to dryness. The residue was resuspended in 75  $\mu\text{L}$  of methanol:water (1:1) solution containing 4  $\mu\text{g}/\text{mL}$  LCA-D4 as IS and analyzed using the generic-RP ESI (-) approximation.

In all the cases the dry residue was stored at -80  $^{\circ}\text{C}$  until its analysis, and, once resuspended, it was centrifuged (10000 g, 10 min, 4  $^{\circ}\text{C}$ ) before transferring the clean supernatant to a 96-well plate for its LC-MS untargeted analysis.

### **2.8.2 Steatosis/Phospholipidosis specific protocol**

Each drug and concentration was tested by triplicate in 3.5 cm plates using a lipidomic-RP approximation adapted from reference (163). First of all, the medium was removed by aspiration, and the cell monolayer was washed once with PBS. Then the cell monolayer was frozen by the addition of liquid  $\text{N}_2$ . At this point the plates were stored at -80  $^{\circ}\text{C}$  until further processing.

The cells were scrapped using 400  $\mu\text{L}$  of cold PBS containing 0.375  $\mu\text{g}/\text{mL}$  reserpine as IS. The cell suspension/extract was transferred to a clean 2 mL tube. The possible cellular rests present in the plate were recovered with 200  $\mu\text{L}$  of the solution and pooled with the previous volume. The cellular extract/suspension was submitted to 3 freeze/thaw

## Methodology

---

cycles (liquid N<sub>2</sub>, room temperature) in order to increase cell disruption and metabolite extraction. An aliquot of 50 µL was mixed with 100 µL of 0.66 N NaOH and used for protein determination. The rest of the volume was mixed with 1100 µL of a methanol:chloroform (1:2) solution containing 0.01 µg/mL terfenadine as IS. After vortexing (3 x 10 s), the samples were allowed to rest at -20 °C for 20 min and centrifuged (10 min, 10000 g, 4 °C). The lower organic phase was transferred to a clean 2 mL tube and the aqueous phase was reextracted with 1100 µL of the methanol:chloroform (1:2) solution containing 0.01 µg/mL terfenadine as previously described. The second organic fraction was pooled with the first one. A 1 mL aliquot was taken and evaporated to dryness in a speedvac. The dry residue was stored at -80 °C until analysis. The residue was resuspended in 75 µL of a methanol:chloroform (3:1) solution containing 0.5 µg/mL verapamil and 4 µg/mL LCA-D4 as IS and analyzed using the lipidomic-RP approximation in both ESI (+) and ESI (-) modes (**Section 2.3.2**).

### 2.9 *In vivo* hepatotoxicity studies in medakafish (*Oryzias latipes*)

#### 2.9.1 Animal handling

Adult medaka (*Oryzias latipes*) CAB strain animals (**Figure 2.15**) (196) were kept in recirculating water 10 L aquaria at 28 °C on a 14 h light/10 h dark daily cycle. Daily, they were fed with *Artemia nauplii* twice and dry fed once (197).



**Figure 2.15.** Adult medaka (*Oryzias latipes*).

Animals were exposed to different hepatotoxic compounds classified according to their mechanism of toxicity (**Table 2.3**). Sub-lethal concentrations were used based on previous in house experimental data and bibliographic information (198-204). Stock solutions of the drugs were prepared in water or methanol (according to the manufacturer's instructions). For treatments, the fishes were transferred to 4L aquaria containing either drug at the specified concentration or 0.005% methanol as vehicle control (**Table 2.3**). After a 2h treatment, the fishes were returned to 10 L aquaria containing clean water. The treatment was repeated for 5 consecutive days and the fishes were sacrificed at the end of treatment.

## Methodology

---

**Table 2.3.** Model hepatotoxins included in the study using *Oryzias latipes*.

Mechanism	Compound	Concentration
Negative Control	Methanol (solvent)	0.005%
	17 $\alpha$ Ethynylestradiol	3 $\mu$ M
Cholestasis	Chlorpromazine	2 $\mu$ M
	Cyclosporine	2.5 $\mu$ M
Phospholipidosis	Amiodarone	2 $\mu$ M
	Tilorone	2 $\mu$ M
	Tamoxifen	2 $\mu$ M
Steatosis	Doxycycline	50 $\mu$ M
	Tetracycline	50 $\mu$ M
	Valproic acid	200 $\mu$ M

Individual adult medaka were anesthetized in cold PBS at 0 °C and immediately transferred to a dry plate and sacrificed by decapitation. The liver was extracted, placed in a tube, flash-frozen in liquid N<sub>2</sub>, and stored at -80 °C until further processing. All the experimental protocols were approved by the Institutional Animal Ethics Committee.

### 2.9.2 Sample processing and analysis

Frozen tissue samples (2 - 6 mg) were placed in 2 mL tubes containing CK14 ceramic beads and 650  $\mu$ L of methanol:water (3:1) containing the IS reserpine (0.375  $\mu$ g/mL) and sulfadimethoxine (0.075  $\mu$ g/mL) were added. Then, livers were homogenized twice for 25 s at 6,000 rpm at 4 °C in a Precellys 24 Dual system equipped with a Criolys cooler. Tubes were centrifuged at 3000 g for 5 min at 4°C, and the supernatants were transferred to clean tubes. A second extraction was performed with 350  $\mu$ L of the same solvent. Finally, the two extraction supernatants were pooled and stored at -80 °C until further processing.

An aliquot of 50  $\mu\text{L}$  was mixed with 100  $\mu\text{L}$  of 0.66N NaOH and used for protein determination.

A 600  $\mu\text{L}$  aliquot was transferred to a clean tube and evaporated to dryness. The dry residue was stored at  $-80\text{ }^{\circ}\text{C}$  until analysis. The residue was resuspended in 100  $\mu\text{L}$  of water:methanol (1:1) containing 0.5  $\mu\text{g}/\text{mL}$  verapamil and 4  $\mu\text{g}/\text{mL}$  LCA-D4 as IS. After centrifugation (10 min, 10000g,  $4\text{ }^{\circ}\text{C}$ ), the clean supernatant was transferred to a 96-well HPLC plate and analyzed using the generic-RP analysis conditions in ESI(-) mode (**Section 2.3.1**).

A 400  $\mu\text{L}$  aliquot was transferred to a clean tube and 200  $\mu\text{L}$  of chloroform containing 0.01  $\mu\text{g}/\text{mL}$  terfenadine as IS were added. After vortexing ( $3 \times 10\text{ s}$ ), samples were allowed to rest at  $-20\text{ }^{\circ}\text{C}$  for 20 min and centrifuged (10 min, 10000 g,  $4\text{ }^{\circ}\text{C}$ ). The upper aqueous phase and the lower organic phase were separately transferred to clean tubes and evaporated to dryness. The organic phase was resuspended in 100  $\mu\text{L}$  of methanol:chloroform (3:1) containing 0.5  $\mu\text{g}/\text{mL}$  verapamil as IS and analyzed using the lipidomic-RP approximation in ESI (+) mode (**Section 2.3.2**). The aqueous phase was resuspended in 100  $\mu\text{L}$  of acetonitrile:water (70:30) solution containing 40  $\mu\text{g}/\text{mL}$  Phe-D5, 20  $\mu\text{g}/\text{mL}$  8-BrAMP and 10  $\mu\text{g}/\text{mL}$  Val-Tyr-Val as IS and analyzed using the HILIC approximation in both ESI (+) and ESI (-) modes (**Section 2.3.3**).

## Methodology

---

### 2.10 *In vivo* hepatotoxicity studies in rats

#### 2.10.1 Animal handling

Six-week-old male OFA rats (200 – 240 g) were purchased from Charles River (Barcelona, Spain) and acclimatized to laboratory conditions for at least 7 days. Animals were housed in individual cages with woodchip bedding in a room maintained at 21 – 25 °C, 30 – 70% humidity and a 12 h light-dark cycle. Each animal was allowed free access to water and standard chow diet (Scientific Animal Food and Engineering, Augy, France).

Rats were divided into three different groups: i) Tetracycline (2 g/Kg/day); ii) Paracetamol (1 g/kg/day); and iii) Control. Drugs were administered orally at the indicated doses in a 0.5 % methylcellulose solution, control rats were administered vehicle (205). Treatments were repeated during 4 or 2 consecutive days for rats receiving the tetracycline or paracetamol treatment, respectively. The rats were sacrificed 24 h after the last administration.

Rats were anesthetized with sodium thiobarbital (0.1 g/kg). Blood was collected by cardiac puncture. After coagulation and centrifugation (1000 g for 10 min at 4 °C), serum samples were aliquoted and stored at -80 °C until their analysis by LC-MS. An aliquot was destined to perform serum biochemistry and enzymatic activities using standard laboratory procedures. Livers were removed, rinsed in PBS, divided into small portions, flash-frozen in liquid N<sub>2</sub>, and stored at -80 °C until the analysis. Serum and liver samples were obtained from the same animals. All the experimental protocols were approved by the Institutional Animal Ethics Committee.

### 2.10.2 Sample processing and untargeted LC-MS analysis

#### *Liver tissue samples*

Each frozen tissue sample (around 100 mg) was placed in a 2 mL tube containing CK14 ceramic beads and weighted. For each 100 mg of tissue, 650  $\mu\text{L}$  of methanol:water (3:1) containing the IS reserpine (0.375  $\mu\text{g}/\text{mL}$ ) and sulfadimethoxine (0.075  $\mu\text{g}/\text{mL}$ ) were added. Then, tissue was homogenized twice for 25 s at 6,000 rpm at 4  $^{\circ}\text{C}$  in a Precellys 24 Dual system. After centrifugation (3000 g, 5 min, 4 $^{\circ}\text{C}$ ), the supernatant was transferred to a clean tube. A second extraction was performed with 350  $\mu\text{L}$  per 100 mg of tissue of the solvent. Finally, the two extraction supernatants were pooled and stored at -80  $^{\circ}\text{C}$  until further processing.

A 100  $\mu\text{L}$  aliquot was transferred to a clean tube and evaporated to dryness using a speedvac. The dry residue was stored at -80  $^{\circ}\text{C}$  until analysis. The residue was resuspended in 100  $\mu\text{L}$  of water:methanol (1:1) containing 0.5  $\mu\text{g}/\text{mL}$  verapamil and 4  $\mu\text{g}/\text{mL}$  LCA-D4 as IS. After centrifugation (10 min, 10000g, 4  $^{\circ}\text{C}$ ), the clean supernatant was transferred to a 96-well HPLC plate and analyzed using the generic-RP analysis conditions in ESI (-) mode (**Section 2.3.1**).

A 200  $\mu\text{L}$  aliquot was transferred to a clean tube and 100  $\mu\text{L}$  of chloroform containing 0.01  $\mu\text{g}/\text{mL}$  terfenadine as IS were added. After vortexing (3 x 10 s), samples were allowed to rest at -20  $^{\circ}\text{C}$  for 20 min and centrifuged (10 min, 10000 g, 4  $^{\circ}\text{C}$ ). Each phase (the upper aqueous and the lower organic) was separately transferred to a clean tube and evaporated to dryness in a speedvac. The organic phase was resuspended in 100  $\mu\text{L}$  of methanol:chloroform (3:1) containing 0.5  $\mu\text{g}/\text{mL}$  verapamil as IS and analyzed using the lipidomic-RP approximation in ESI (+) mode (**Section 2.3.2**). The aqueous phase was resuspended in 100  $\mu\text{L}$  of acetonitrile:water (70:30) containing 40  $\mu\text{g}/\text{mL}$  Phe-D5, 20  $\mu\text{g}/\text{mL}$  8-BrAMP and 10  $\mu\text{g}/\text{mL}$  Val-Tyr-Val as IS and analyzed



## Methodology

---

using the HILIC approximation in both ESI (+) and ESI (-) modes (**Section 2.3.3**).

### Serum samples

For lipidomic-RP analysis, a 10  $\mu\text{L}$  aliquot was mixed with 40  $\mu\text{L}$  of PBS and 250  $\mu\text{L}$  of chloroform:methanol (2:1) containing 0.01  $\mu\text{g}/\text{mL}$  terfenadine as IS. After vortexing (3 x 10 s), samples were allowed to rest at -20  $^{\circ}\text{C}$  for 20 min and centrifuged (10 min, 10000 g, 4  $^{\circ}\text{C}$ ). A 100  $\mu\text{L}$  aliquot of the lower organic phase was transferred to a 96-well HPLC and 10  $\mu\text{L}$  of the IS verapamil (5.5  $\mu\text{g}/\text{mL}$  in methanol) were added. The analysis was performed using the lipidomic-RP approximation in ESI (+) mode (**Section 2.3.2**).

For generic-RP analysis, a 100  $\mu\text{L}$  aliquot was mixed with 300  $\mu\text{L}$  of cold methanol containing reserpine (0.375  $\mu\text{g}/\text{mL}$ ) and sulfadimethoxine (0.075  $\mu\text{g}/\text{mL}$ ) as IS. After vortexing (3 x 10 s), samples were allowed to rest at -20  $^{\circ}\text{C}$  for 30 min and centrifuged (10 min, 10000 g, 4  $^{\circ}\text{C}$ ). The clean supernatant was transferred to a clean tube and evaporated to dryness. The dry residue was stored at -80  $^{\circ}\text{C}$  until analysis. The residue was resuspended in 100  $\mu\text{L}$  of water:methanol (1:1) containing 0.5  $\mu\text{g}/\text{mL}$  verapamil and 4  $\mu\text{g}/\text{mL}$  LCA-D4 as IS. After centrifugation (10 min, 10000 g, 4  $^{\circ}\text{C}$ ), the clean supernatant was transferred to a 96-well HPLC plate and analyzed using the generic-RP analysis conditions in both ESI (+) and ESI (-) modes (**Section 2.3.1**).

### 2.11 Method validation for LC-MS/MS targeted analyses

The bioanalytical methods described in the following sections were developed and validated in terms of linearity, accuracy, and precision following the compliance criteria described by the FDA Guidance for industry: bioanalytical method validation (206).

The lower limit of quantification (LLOQ) was defined as the lowest concentration at which the analyte could be quantified with relative standard deviation (RSD) below 20% and below  $\pm 20\%$  deviation from the nominal value. The limit of detection (LOD) was determined as the lowest concentration at which the analyte response was at least three times the blank response. Calibration curves were generated by plotting the peak area ratio of the respective compound to the corresponding IS versus the nominal concentration. The line of best fit was determined by linear-weighted ( $1/x$ ) least-squares regression. The linearity acceptance criterion for the correlation coefficient was 0.99 or better. Each back calculated standard concentration should be within  $\pm 15\%$  deviation from the nominal value, except for the LLOQ, for which the maximum acceptable deviation was  $\pm 20\%$ .

## Methodology

---

### 2.12 Targeted analysis of bile acids

A targeted UPLC-MS MRM method for the simultaneous quantification of 31 BAs, including both major and minor non-conjugated or conjugated forms, was developed (207). It allows the comprehensive quantitative profiling of BAs in different biological matrices (i.e., serum, liver tissue, cultured cells) from different species (i.e., human, mouse and rat) (103, 207, 208).

#### 2.12.1 Bile acids included in the method

The following BAs were included in the analysis: lithocholic acid (LCA), murocholic acid (MuroCA), chenodeoxycholic acid (CDCA), deoxycholic acid (DCA), ursodeoxycholic acid (UDCA), hyodeoxycholic acid (HDCA), dehydrocholic acid (DHCA), cholic acid (CA),  $\alpha$ -muricholic acid ( $\alpha$ MCA),  $\beta$ -muricholic acid ( $\beta$ MCA),  $\omega$ -muricholic acid ( $\omega$ MCA), hyocholic acid (HCA), glycolithocholic acid (GLCA), glycochenodeoxycholic acid (GCDCA), glycodeoxycholic acid (GDCA), glyoursodeoxycholic acid (GUDCA), glycohyodeoxycholic acid (GHDCA), glycodehydrocholic acid (GDHCA), glycocholic acid (GCA), glycohyocholic acid (GHCA), tauroolithocholic acid (TLCA), taurochenodeoxycholic acid (TCDCA), taurodeoxycholic acid (TDCA), taoursodeoxycholic acid (TUDCA), taurohyodeoxycholic acid (THDCA), taurodehydrocholic acid (TDHCA), taurocholic acid (TCA), tauro- $\alpha$ -muricholic acid (T $\alpha$ MCA), tauro- $\beta$ -muricholic acid (T $\beta$ MCA), tauro- $\omega$ -muricholic acid (T $\omega$ MCA), taurohyocholic acid (THCA).

Deuterated IS: LCA-D4, DCA-D4, CA-D4) GCDCA-D4 and GCA-D4.

### 2.12.2 UPLC-MS analysis

UPLC separation was performed in an Acquity UPLC system (Waters, UK) equipped with an Acquity UPLC BEH C18 (1.7  $\mu\text{m}$ , 2.1  $\times$  100 mm; Waters) column. The temperatures of the column and the autosampler were set at 65  $^{\circ}\text{C}$  and 4  $^{\circ}\text{C}$ , respectively. The sample injection volume was 4  $\mu\text{L}$ . Eluent and washing solutions composition were: i) solvent A: 0.1% formic acid in water; ii) solvent B: 0.1% formic acid in acetonitrile; iii) WNW and SW: water:acetonitrile (90:10, v/v); and iv) SNW: acetonitrile. The flow rate was set at 0.5 ml/min. A 21-min elution gradient was performed as follows: during the first 0.5 min, eluent composition was set at 95% A and 5% B, which was linearly changed to 75% A and 25% B in 5 min; then the proportion of B was increased to 40% in the next 10.5 min, followed by a further increase to 95% B reached at min 17.5 and kept for 1.5 min. Finally, the initial conditions were recovered and maintained for 2 min for column conditioning.

The MS analysis was performed using a Waters Xevo TQ-S mass spectrometer equipped with an ESI source operating in the negative-ion mode working in the MRM mode. A capillary voltage of 2 kV, a source temperature of 120  $^{\circ}\text{C}$  and a desolvation temperature of 380  $^{\circ}\text{C}$  were used. Desolvation and cone gas flows were set as 800 L/h and 150 L/h, respectively, and the collision gas was 0.25 mL/min. Transitions, cone voltages, and collision energies were automatically tuned for each BA using the QuanOptimizer software (Waters, UK) (**Table 2.4**)

Standards calibration curves prepared in methanol:water (50:50, v/v) with concentrations in the 0.62 – 10000 nM range for each BA. IS concentrations were kept constant at all the calibration points at 1  $\mu\text{M}$  for LCA-D4 and at 0.5  $\mu\text{M}$  for CA-D4, DCA-D4, GCA-D4, and GCDCA-D4.

**Figure 2.16** shows the chromatograms obtained by injecting a mix standard solution at 300 nM (IS concentrations: 1  $\mu\text{M}$  for LCA-D4 and 0.5  $\mu\text{M}$  for CA-D4, DCA-D4, GCA-D4, and GCDCA-D4).

## Methodology

**Table 2.4.** Mass spectrometer setup for the quantification of selected bile acids.

Bile acid	Parent ion ( <i>m/z</i> )	Fragment ( <i>m/z</i> )	Cone (V)	Collision energy (eV)	Retention time (min)	Internal standard
LCA	375.3	375.3	90	10	17.74	LCA-D4
MuroCA	391.3	391.3	120	10	12.69	DCA-D4
CDCA	391.3	391.3	120	10	17.13	DCA-D4
DCA	391.3	391.3	120	10	17.22	DCA-D4
UDCA	391.3	391.3	120	10	14.00	DCA-D4
HDCA	391.3	391.3	120	10	14.41	DCA-D4
DHCA	401.2	401.2	90	10	9.14	CA-D4
CA	407.3	407.3	120	10	13.90	CA-D4
$\omega$ MCA	407.3	407.3	120	10	10.57	CA-D4
$\alpha$ MCA	407.3	407.3	120	10	10.92	CA-D4
$\beta$ MCA	407.3	407.3	120	10	11.30	CA-D4
HCA	407.3	407.3	120	10	12.71	CA-D4
GLCA	432.3	73.8	80	40	17.31	LCA-D4
GCDCA	448.3	73.8	80	40	14.61	GCDCA-D4
GDCA	448.3	73.8	80	40	15.32	GCDCA-D4
GUDCA	448.3	73.8	80	40	10.71	GCDCA-D4
GHDCA	448.3	73.8	80	40	10.97	GCDCA-D4
GDHCA	458.3	73.8	80	40	6.98	GCA-D4
GCA	464.3	73.8	80	40	11.08	GCA-D4
GHCA	464.3	73.8	80	40	9.71	GCA-D4
TLCA	482.3	80	130	60	16.17	LCA-D4
TCDCa	498.3	80	130	60	11.85	GCDCA-D4
TDCA	498.3	80	130	60	12.55	GCDCA-D4
TUDCA	498.3	80	130	60	8.61	GCDCA-D4
THDCA	498.3	80	130	60	8.71	GCDCA-D4
TDHCA	508.3	80	130	60	5.87	GCA-D4
TCA	514.3	80	130	60	9.10	GCA-D4
T $\omega$ MCA	514.3	80	130	60	6.59	GCA-D4
T $\alpha$ MCA	514.3	80	130	60	6.73	GCA-D4
T $\beta$ MCA	514.3	80	130	60	6.80	GCA-D4
THCA	514.3	80	130	60	7.80	GCA-D4
LCA-D4	379.3	379.3	90	10	17.74	
DCA-D4	395.3	395.3	120	10	17.22	
CA-D4	411.3	411.3	120	10	13.90	
GCDCA-D4	452.4	73.8	80	40	14.61	
GCA-D4	468.4	73.8	80	40	11.08	

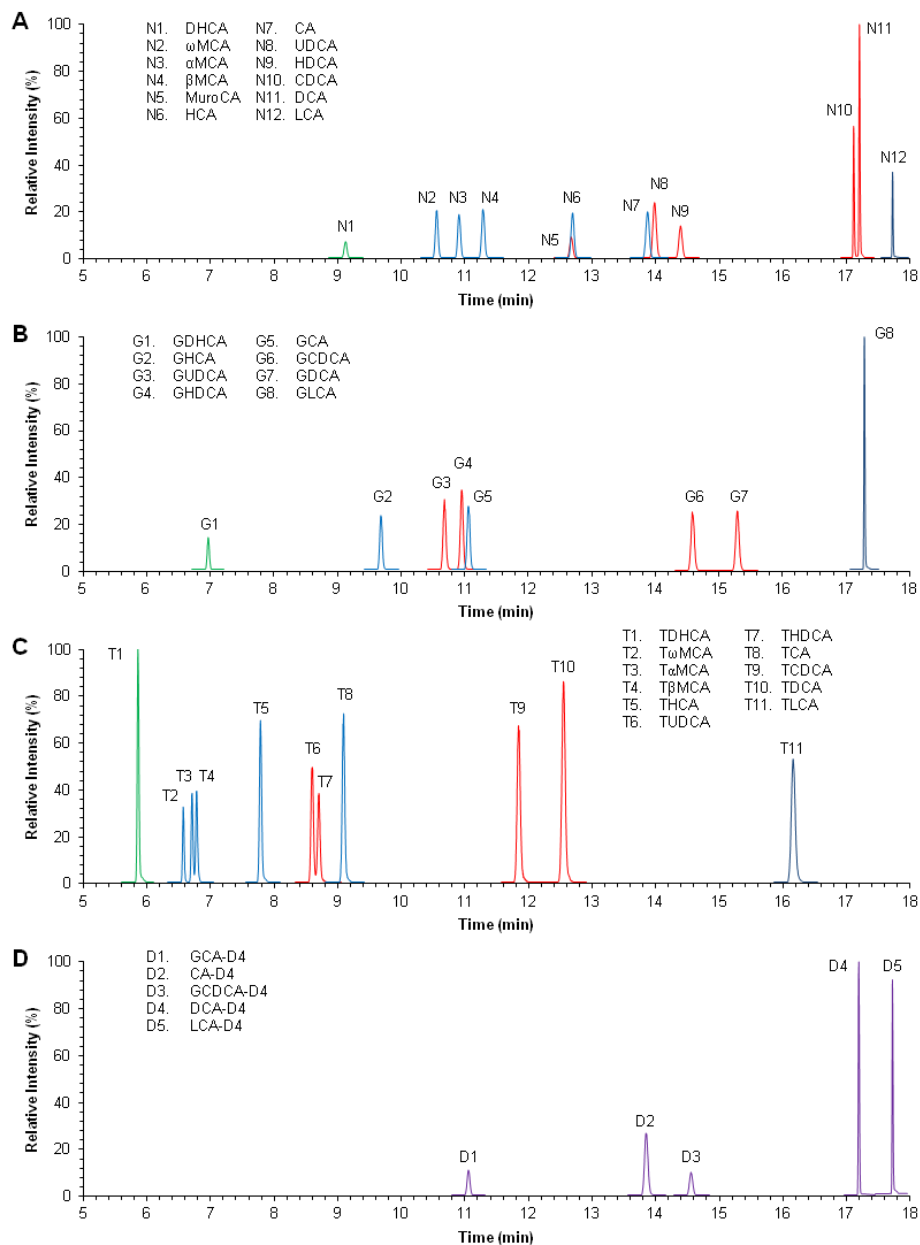


**Figure 2.16.** Chromatograms corresponding to the targeted LC-MS/MS analysis of BAs. **A)** Non-conjugated BAs. **B)** Glycine-conjugated BAs. **C)** Taurine-conjugated BAs. **D)** Deuterium-labeled IS. All the BAs were separated and detected in a single analytical run. Green: DHCA; blue: tri-hydroxylated BAs; red: di-hydroxylated BAs; dark blue: mono-hydroxylated BAs.

## Methodology

---

### 2.12.3 Sample processing

A mixed stock solution of all the IS was prepared in methanol:water (50:50, v/v) at a final concentration of 100  $\mu\text{M}$ , except LCA-D4, whose concentration was 200  $\mu\text{M}$ .

For serum samples, aliquots of 50  $\mu\text{L}$  were allowed to thaw on ice and were subsequently spiked with 25  $\mu\text{L}$  of a 1/100 dilution of the deuterated IS stock solution. Then, cold methanol (225  $\mu\text{L}$ ) was added for protein precipitation, and samples were vortexed ( $3 \times 10$  s) and allowed to rest at  $-20$   $^{\circ}\text{C}$  for 20 min. After centrifugation (10000 g, 10 min, 4  $^{\circ}\text{C}$ ), supernatants were transferred to clean tubes and evaporated to dryness. Samples were stored at  $-80$   $^{\circ}\text{C}$  until analysis.

Frozen hepatic tissue samples (5 – 100 mg) were placed in 2 mL tubes containing CK14 ceramic beads. For each 100 mg of tissue, 600  $\mu\text{L}$  of cold methanol and 200  $\mu\text{L}$  of a 1/100 dilution of the IS stock solution were added. Then, liver tissues were homogenized twice for 25 s at 6000 rpm at 4  $^{\circ}\text{C}$  in a Precellys 24 Dual system. After centrifugation (3000 g, 5 min, 4  $^{\circ}\text{C}$ ), supernatants were transferred to clean tubes. A second BA extraction was performed with 400  $\mu\text{L}$  of cold methanol. Finally, the two extraction supernatants were pooled and 150  $\mu\text{L}$  aliquots were evaporated to dryness and stored at  $-80$   $^{\circ}\text{C}$  until analysis.

For the LC-MS analysis, dry extracts (from serum or liver) were reconstituted in 50  $\mu\text{L}$  of methanol:water (50:50, v/v), centrifuged (1 min, 10000 g, 4  $^{\circ}\text{C}$ ), and transferred into 350  $\mu\text{L}$  volume 96-well plates for further analysis.

### 2.13 Targeted analysis of oxidative stress biomarkers

A targeted UPLC-MS MRM method was developed in our group in order to evaluate the oxidative stress damage induced to proteins, DNA and lipids in serum, tissue liver and cultured cells samples (209).

#### 2.13.1 OS markers included in the method

The markers included in the method are: GSH, oxidized glutathione (GSSG), ophthalmic acid, S-(5-adenosyl)-L-methionine (SAM), S-(5-adenosyl)-L-homocysteine (SAH), phenylalanine (Phe), tyrosines (3-iodo-L-tyrosine (I-Tyr), 3-nitro-tyrosine (N-Tyr), 3-chloro-L-tyrosine (Cl-Tyr), DL-o-tyrosine (o-Tyr), DL-m-tyrosine (m-Tyr), L-tyrosine (p-Tyr)), 8-hydroxy-2'-deoxyguanosine (8-OH-dG), 2-deoxyguanosine (2-dG) and malondialdehyde (MDA).

#### 2.13.2 UPLC-MS analysis

UPLC separation was performed in an Acquity UPLC system (Waters, UK) equipped with an Acquity UPLC HSST3 (1.8  $\mu\text{m}$ , 2.1  $\times$  100 mm; Waters) column. The temperatures of the column and the autosampler were set at 60 °C and 4 °C, respectively. The sample injection volume was 5  $\mu\text{L}$ . Eluent and washing solutions composition were: i) solvent A: 0.1% formic acid in water; ii) solvent B: 0.1% formic acid in acetonitrile; iii) WNW and SW: water:acetonitrile (90:10, v/v); and iv) SNW: water:acetonitrile (10:90, v/v). The flow rate was set at 0.3 mL/min. A 7-min elution gradient was performed as follows: during the first 2 min, eluent composition was set at 95% A and 5% B, which was linearly changed to 5% A and 95% B in 1.5 min and kept for 2 min. Finally, the initial conditions were recovered and maintained for 1 min for column conditioning.



## Methodology

The MS analysis was performed using a Waters Xevo TQ-S mass spectrometer (Waters) equipped with an ESI source operating in the positive-ion mode working in the MRM mode. A capillary voltage of 3 kV, a source temperature of 150 °C and a desolvation temperature of 380 °C were used. Desolvation and cone gas flows were set as 800 L/h and 150 L/h, respectively, and the collision gas was 0.25 mL/min. Transitions, cone voltages, and collision energies are shown in **Table 2.5**.

**Table 2.5.** Mass spectrometer setup for the quantification of selected oxidative stress markers.

Compound	Parent ion ( <i>m/z</i> )	Fragment ( <i>m/z</i> )	Cone (V)	Collision energy (eV)	Retention time (min)
GSSG	613.2	355.0	60	15	1.10
GSH <sup>a</sup>	433.1	201.0	20	20	3.32
SAM	398.9	136.0	22	17	0.74
SAHC	385.1	136.0	35	25	1.09
I-Tyr	308.1	291.0	40	15	3.33
Ophthalmic acid	290.2	161.1	15	15	1.16
8-OH-dG	284.0	168.0	30	15	2.16
2-dG	268.0	152.0	25	15	1.60
MDA <sup>b</sup>	235.0	159.0	30	30	4.08
N-Tyr	227.1	181.0	25	10	3.21
Cl-Tyr	216.0	170.0	30	15	2.37
o-Tyr	182.1	136.0	20	10	2.09
m-Tyr	182.1	136.0	20	10	1.52
p-Tyr	182.1	136.0	20	10	1.27
Phe	166.1	120.1	20	20	2.62
Phe-D5	171.1	125.1	20	20	2.62

<sup>a</sup> Compound quantified as the N-ethylmaleimide (NEM) derivative. <sup>b</sup> Compound derivatized with 2,4-dinitrophenylhydrazine (DNPH).

A derivatization step was required to avoid degradation of some labile analytes, thus improving compound stability, detection and quantification. Thereby, MDA and GSH were determined after reaction with 2, 4-dinitrophenylhydrazine (DNPH) (210-212) and N-ethylmaleimide (NEM) (213, 214), respectively.

Standards calibration curves were prepared in PBS (containing 0.5 mM DNPH and 5 mM NEM) in the concentration range from 1.25 µg/mL to 0.725 ng/mL for each compound. Phe-D5 (IS) concentration was kept constant at 0.2 µg/mL in all calibration points. **Figure 2.17** shows the chromatograms obtained by injecting a mix standard solution at a concentration of 1 µg/mL.

### 2.13.3 Sample processing

Biological samples were processed differently depending on their nature. Moreover, to allow optimal detection of all biomarkers in the different biological matrices, three different sample fractions were prepared : i) fraction I, obtained after a concentration step to determine low concentrated analytes; ii) fraction II, obtained after a dilution step to determine the high concentrated analytes ; and iii) fraction III, obtained after a basic hydrolysis and derivatization step (212), to determine MDA due to its instability.

Cell monolayers (previously washed and frozen in liquid N<sub>2</sub>) were scraped with 1 mL of 50 mM NEM in PBS and three freeze and thawing cycles were applied to ensure cell lysis. Frozen tissue samples (5–100 mg) were extracted using a Precellys 24 Dual system with a total of 1 mL of 50 mM NEM in PBS. Culture medium and serum samples were directly used to prepare the different fractions.

To obtain fraction I, 1200 µL or 600 µL of cold methanol were added to 400 µL of extract from cultured cells or 200 µL of liver tissue extract, respectively, and tubes were vortexed. For culture medium or serum

## Methodology

---

samples, 200  $\mu\text{L}$  of 10 mM NEM in PBS were added to 200  $\mu\text{L}$  of sample and, after vortexing, 1200  $\mu\text{L}$  of cold methanol were added. The obtained mix (from cultured cells, tissue, medium or serum) was allowed to rest for 20 min at  $-20\text{ }^{\circ}\text{C}$  and then centrifuged for 10 min at 10000 g at  $4\text{ }^{\circ}\text{C}$ . The clean supernatant was transferred to a clean tube and evaporated to dryness in a speedvac. The dry residue was reconstituted in 50  $\mu\text{L}$  of PBS containing 200 ng/mL Phe-D5, centrifuged (10 min, 10000 g,  $4^{\circ}\text{C}$ ), and the clean supernatant was transferred to a 96-well HPLC plate for its analysis.

To obtain fraction II, 115  $\mu\text{L}$  or 245  $\mu\text{L}$  of cold methanol were added to 10  $\mu\text{L}$  of cultured cell or 5  $\mu\text{L}$  of liver tissue extract. For culture medium or serum samples, 15  $\mu\text{L}$  of 10 mM NEM in PBS were added to 10  $\mu\text{L}$  of sample and, after vortexing, 100  $\mu\text{L}$  of cold methanol were added. Then the mix (from cultured cells, tissue, medium or serum) was allowed to rest for 20 min at  $-20\text{ }^{\circ}\text{C}$  and after centrifugation (10 min, 10000 g,  $4\text{ }^{\circ}\text{C}$ ), 50  $\mu\text{L}$  clean supernatant were transferred to 96-well HPLC plate and mixed with 50  $\mu\text{L}$  of PBS containing 400 ng/mL Phe-D5 for its analysis.

To obtain fraction III, 25  $\mu\text{L}$  of 6 N NaOH were added to 100  $\mu\text{L}$  of sample (cellular or tissue extract, medium or serum), and the mix was incubated at  $60\text{ }^{\circ}\text{C}$  for 30 min. Then, 60  $\mu\text{L}$  of 35% perchloric acid were added. The mix was centrifuged (10 min, 10000 g,  $4\text{ }^{\circ}\text{C}$ ). The clean supernatant was transferred to a clean tube and mixed with 15  $\mu\text{L}$  5 mM of DNPH, 2660 ng/mL Phe-D5 in PBS. The mix was incubated for 60 min at  $37\text{ }^{\circ}\text{C}$  and transferred to a 96-well HPLC plate.

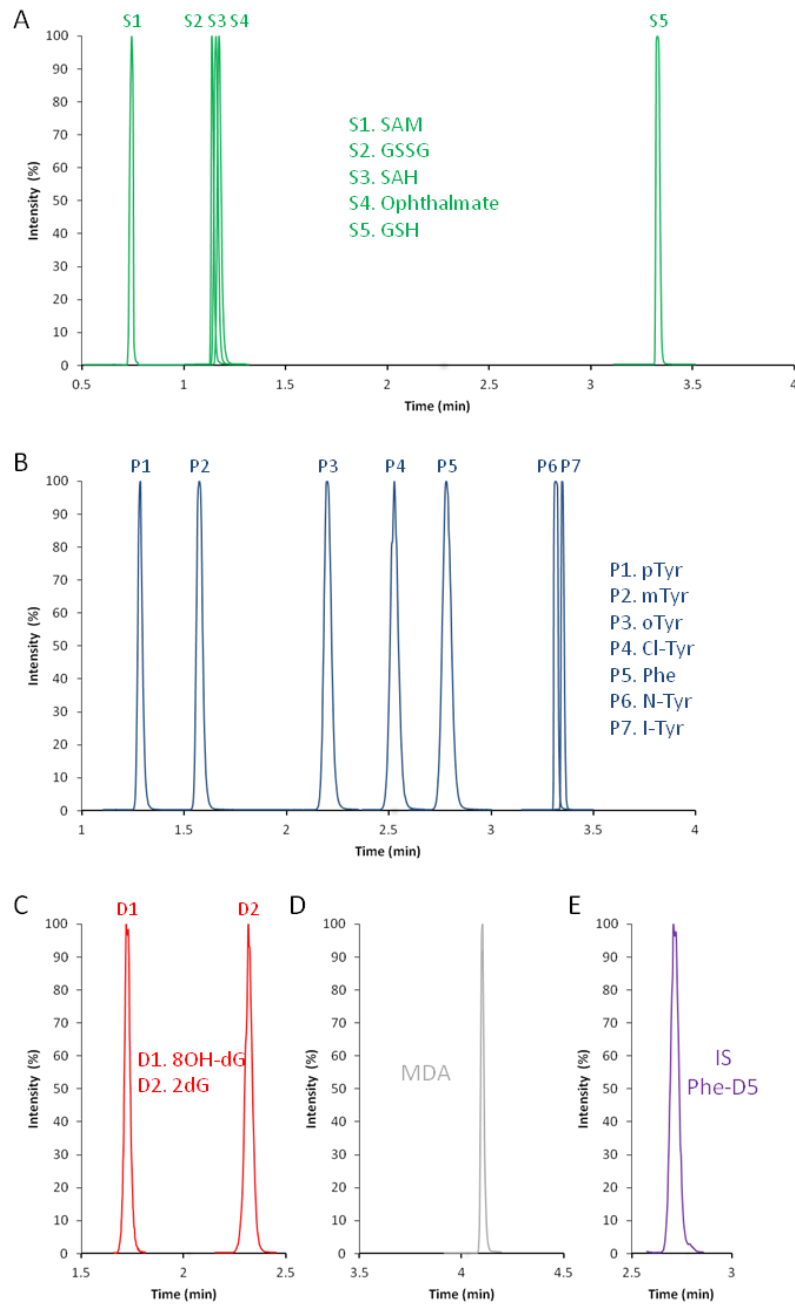


**Figure 2.17.** Chromatograms corresponding to the targeted LC-MS/MS analysis of OS markers and related compounds; **A)** Sulphur containing and related compounds; **B)** Markers of OS damage to proteins; **C)** Markers of OS damage to DNA; **D)** MDA; **E)** IS.

## Methodology

---

### 2.14 Targeted analysis of $\gamma$ -glutamyl dipeptides

A targeted HILIC-UPLC-MS MRM method for the simultaneous quantification of 32  $\gamma$ -glutamyl dipeptides and related metabolites was developed.

#### 2.14.1 Compounds included in the method

$\gamma$ -Glutamyl-dipeptides:  $\gamma$ -glutamyl-glycine,  $\gamma$ -glutamyl-alanine,  $\gamma$ -glutamyl-serine,  $\gamma$ -glutamyl-valine,  $\gamma$ -glutamyl-threonine,  $\gamma$ -glutamyl-homoserine,  $\gamma$ -glutamyl-aurine,  $\gamma$ -glutamyl-isoleucine,  $\gamma$ -glutamyl-leucine,  $\gamma$ -glutamyl-asparagine,  $\gamma$ -glutamyl-ornithine,  $\gamma$ -glutamyl-aspartate,  $\gamma$ -glutamyl-glutamine,  $\gamma$ -glutamyl-lysine,  $\gamma$ -glutamyl-glutamate,  $\gamma$ -glutamyl-methionine,  $\gamma$ -glutamyl-histidine,  $\gamma$ -glutamyl-phenylalanine,  $\gamma$ -glutamyl-arginine,  $\gamma$ -glutamyl-citrulline,  $\gamma$ -glutamyl-tyrosine,  $\gamma$ -glutamyl-triptophan,  $\gamma$ -glutamyl-cysteine,  $\gamma$ -glutamyl-homocysteine. Related compounds: pyroglutamic acid, glutamine, glutamic acid, GSSG, GSH, cysteinyl-glycine, bis-cysteinyl-glycine. Phe-D5 was used as IS.

#### 2.14.2 UPLC-MS analysis

UPLC separation was performed in an Acquity UPLC system (Waters, UK) equipped with an Acquity UPLC BEH Amide (1.7  $\mu$ m, 2.1  $\times$  100 mm; Waters) column. The temperatures of the column and the autosampler were set at 40  $^{\circ}$ C and 4  $^{\circ}$ C, respectively. The sample injection volume was 4  $\mu$ L. Eluent and washing solutions composition were: i) solvent A: acetonitrile; ii) solvent B: ammonium acetate pH3 200 mM in water; iii) WNW and SW: water:acetonitrile (10:90, v/v); and iv) SNW: water:acetonitrile (90:10, v/v). The flow rate was set at 0.3 mL/min.

A 12-min elution gradient was performed as follows: initial conditions were set at 85% A and 15% B and maintained for 1 min, the proportion of

B was increased to 35% in 5 min and then increased to 55% at min 9 and maintained for 0.5 min. Finally, the initial conditions were recovered and maintained for 2 min for column conditioning.

The MS analysis was performed using a Waters Xevo TQ-S mass spectrometer (Waters) equipped with an ESI source operating in the positive-ion mode working in the MRM mode. A capillary voltage of 3 kV, a source temperature of 120 °C and a desolvation temperature of 380 °C were used. Desolvation and cone gas flows were set as 800 L/h and 150 L/h, respectively, and the collision gas was 0.25 mL/min. Transitions, cone voltages, and collision energies were automatically tuned for each compound using the QuanOptimizer software (Waters, UK) (**Table 2.6**)

A derivatization step was required to avoid degradation of some labile analytes, thus improving compound stability, detection and quantification. Thereby, GSH,  $\gamma$ -glutamyl-cysteine,  $\gamma$ -glutamyl-homocysteine and cysteinyl-glycine were determined as NEM derivatives (213, 214).

Standard calibration curves (ranging 1.14 - 20000 nM for each compound) were prepared by serial half dilutions of a 100  $\mu$ M stock solution in acetonitrile:ammonium acetate pH3 100 mM in water (7:3). Phe-D5 (IS) concentration was kept constant at 1  $\mu$ M. **Figure 2.18** shows the chromatograms obtained by injecting a 625 nM mix standard solution.

## Methodology

**Table 2.6.** Mass spectrometer setup for the quantification of selected  $\gamma$ -glutamyl dipeptides and related compounds.

Compound	Retention time (min)	Parent ion ( $m/z$ )	Cone (V)	Fragment ( $m/z$ )	Ce (eV)
Pyroglutamate	3.94	130	30	84	20
Glutamine	5.77	147.1	40	84	15
Glutamate	6.17	148.1	40	84	15
$\gamma$ -Glu-Gly	7.03	205.1	40	84	10
$\gamma$ -Glu-Ala	6.59	219.1	40	90.1	10
$\gamma$ -Glu-Ser	7.35	235.1	40	106.1	10
$\gamma$ -Glu-Val	5.79	247.1	40	118.1	10
$\gamma$ -Glu-Thr	7.00	249.1	40	120.1	10
$\gamma$ -Glu-HomoSer	7.13	249.1	40	120.1	10
$\gamma$ -Glu-Tau	6.84	255.1	40	126	15
$\gamma$ -Glu-Leu	5.25	261.1	40	132.1	10
$\gamma$ -Glu-Ile	5.34	261.1	40	132.1	10
$\gamma$ -Glu-Asn	7.51	262.1	40	133.1	10
$\gamma$ -Glu-Orn	7.83	262.1	40	133.1	10
$\gamma$ -Glu-Asp	7.36	263.1	40	134	10
$\gamma$ -Glu-Gln	7.32	276.1	40	147.1	10
$\gamma$ -Glu-Lys	7.74	276.2	40	147.1	10
$\gamma$ -Glu-Glu	7.16	277.1	40	148.1	10
$\gamma$ -Glu-Met	5.81	279.1	40	150.1	10
$\gamma$ -Glu-His	7.65	285.1	40	156.1	10
Ophthalmic acid	6.47	290.1	40	161.1	10
$\gamma$ -Glu-Phe	5.34	295.1	50	166.1	10
Cys-Gly <sup>a</sup>	4.11	304.1	40	158	25
$\gamma$ -Glu-Arg	7.65	304.2	40	175.1	10
$\gamma$ -Glu-Citr	7.27	305.1	40	176.1	15
$\gamma$ -Glu-Tyr	5.99	311.1	50	182.1	10
$\gamma$ -Glu-Trp	5.22	334.1	50	205.1	15
(H-Cys-Gly-OH) <sub>2</sub>	8.32	355.1	50	177	20
$\gamma$ -Glu-Cys <sup>a</sup>	5.58	376.1	50	247.1	10
$\gamma$ -Glu-HomoCys <sup>a</sup>	5.29	390.1	60	261.1	10
GSH <sup>a</sup>	5.64	433.1	50	304.1	10
GSSG	8.64	613.2	60	484.1	15
Phe-D5 (IS)	3.34	171.1	40	125	20

<sup>a</sup> Compounds quantified as the N-ethylmaleimide (NEM) derivative.

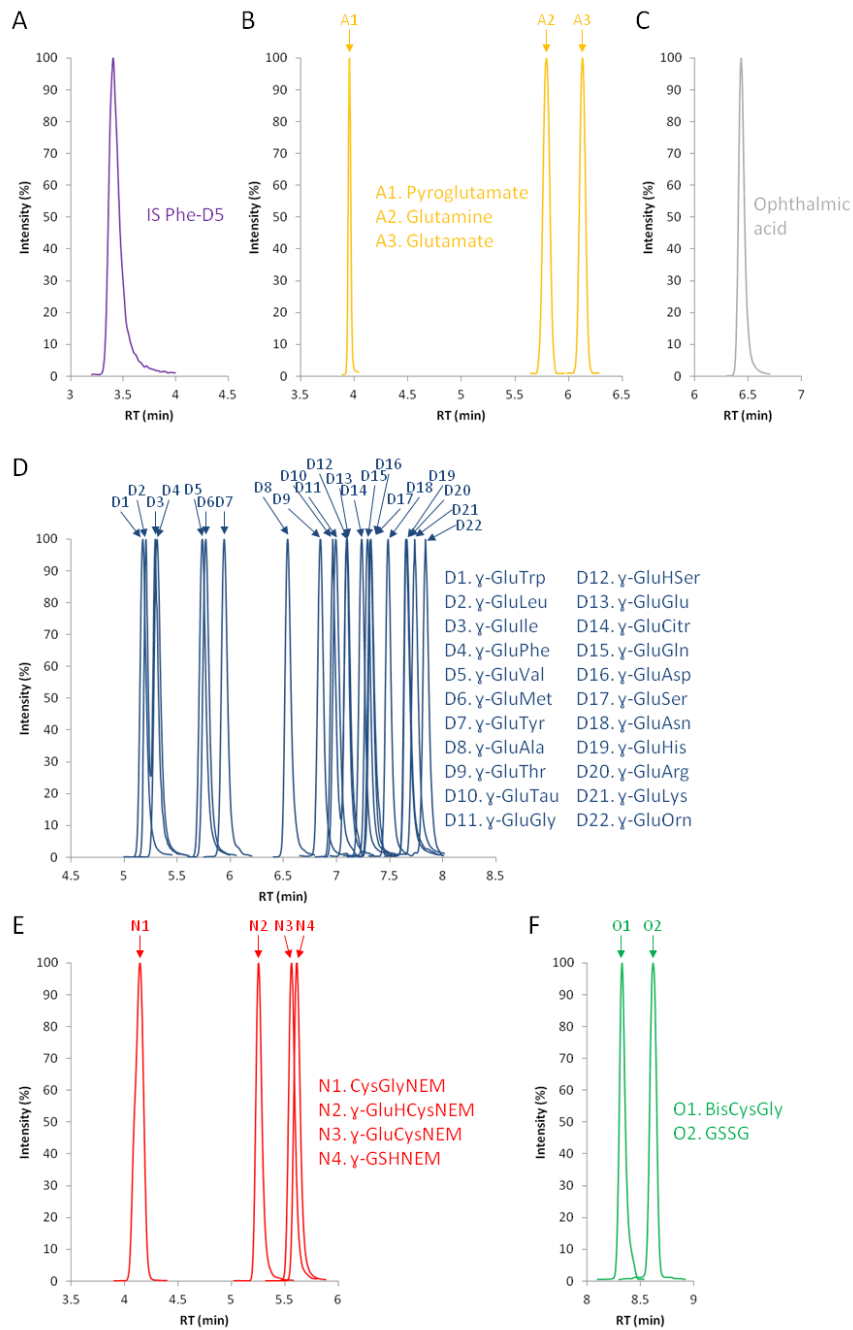


**Figure 2.18.** Chromatograms corresponding to the targeted LC-MS/MS analysis of  $\gamma$ -glutamyl dipeptides and related compounds. **A)** IS Phe-D5; **B)** Aminoacids; **C)** Ophthalmic acid; **D)**  $\gamma$ -Glutamyl dipeptides; **E)** Compounds detected as NEM derivatives; **F)** Oxidized compounds.



## Methodology

---

### 2.14.3 Sample processing

Biological samples were processed differently depending on their nature. Moreover, to allow optimal detection of all biomarkers in the different biological matrices, different dilutions and/or concentrations were used.

For hepatic tissue and cultured cells samples, the extracts were obtained as previously described in **Section 2.13.3**.

To obtain a 2x concentrated extract, 600  $\mu\text{L}$  of cold methanol were added to 200  $\mu\text{L}$  of extract. After vortexing, the mix was allowed to rest for 20 min at  $-20\text{ }^{\circ}\text{C}$ , centrifuged (10 min, 10000 g,  $4\text{ }^{\circ}\text{C}$ ) and the clean supernatant was transferred to a clean tube and evaporated to dryness in a speedvac. The dry residue was reconstituted in 100  $\mu\text{L}$  of acetonitrile:100 mM ammonium acetate pH3 in water (7:3) containing 1  $\mu\text{M}$  Phe-D5, centrifuged (10 min, 10000 g,  $4\text{ }^{\circ}\text{C}$ ) and the clean supernatant was transferred to a 96-well HPLC plate for its analysis.

To obtain 1/10 and 1/100 diluted samples, 120  $\mu\text{L}$  of cold methanol were added to 30  $\mu\text{L}$  of extract. After vortexing, the mix was allowed to rest for 20 min at  $-20\text{ }^{\circ}\text{C}$ . The extract was centrifuged (10 min, 10000 g,  $4\text{ }^{\circ}\text{C}$ ). To prepare a 1/10 dilution, 50  $\mu\text{L}$  clean supernatant were transferred to 96-well HPLC plate and mixed with 50  $\mu\text{L}$  of acetonitrile:100 mM ammonium acetate pH3 in water (7:3) containing Phe-D5 2  $\mu\text{M}$ . To prepare a 1/100 dilution, 5  $\mu\text{L}$  clean supernatant were transferred to 96-well HPLC plate and mixed with 95  $\mu\text{L}$  of acetonitrile:100 mM ammonium acetate pH3 in water (7:3) containing 1.05  $\mu\text{M}$  Phe-D5.

For serum samples, to obtain a non-diluted sample, 100  $\mu\text{L}$  of 50 mM NEM in were added to 100  $\mu\text{L}$  of serum. After vortexing, 600  $\mu\text{L}$  of cold methanol were added. The mix was vortexed, allowed to rest for 20 min at  $-20\text{ }^{\circ}\text{C}$ , centrifuged (10 min, 10000 g,  $4\text{ }^{\circ}\text{C}$ ) and the clean supernatant was transferred to a clean tube and evaporated to dryness in a speedvac.

## Methodology

---

The dry residue was reconstituted in 100  $\mu\text{L}$  of acetonitrile:100 mM ammonium acetate pH3 in water (7:3) containing 1  $\mu\text{M}$  Phe-D5, centrifuged (10 min, 10000 g, 4°C) and the clean supernatant was transferred to a 96-well HPLC plate for its analysis.

To obtain 1/16 and 1/80 dilutions, 30  $\mu\text{L}$  of 50 mM NEM were added to 30  $\mu\text{L}$  of serum. After vortexing, 240  $\mu\text{L}$  of cold methanol were added. After vortexing, the mix was allowed to rest for 20 min at -20 °C and centrifuged (10 min, 10000 g, 4 °C). To prepare a 1/16 dilution, 50  $\mu\text{L}$  clean supernatant were transferred to 96-well HPLC plate and mixed with 50  $\mu\text{L}$  of acetonitrile:100 mM ammonium acetate pH3 in water (7:3) containing 2  $\mu\text{M}$  Phe-D5. To prepare a 1/80 dilution, 10  $\mu\text{L}$  of clean supernatant were transferred to a 96-well HPLC plate and mixed with 90  $\mu\text{L}$  of acetonitrile:100 mM ammonium acetate pH3 in water (7:3) containing 1.11  $\mu\text{M}$  Phe-D5.



## 3. Results & Discussion



### 3.1 Quality assurance strategy in untargeted metabolomic analysis

The main premise in a metabolomics study is that the levels of the detected metabolites reflect the biological status of the system under study. Thus, a quality assurance strategy was implanted in sample preparation and analysis in order to ensure the quality of the results and to minimize and detect any sources of variation unrelated to the biological nature of the samples (166, 167). This was accomplished by the addition of IS to the problem samples, the inclusion of QC samples, a careful design of the sample acquisition process and a thorough equipment cleaning and maintenance before starting a batch analysis.

Different IS were incorporated to the samples at different steps of sample processing (i.e. sample homogenization and sample preparation for the LC-MS analysis). These IS have a dual function, on one hand the levels of the IS are used to evaluate the efficiency of the metabolome extraction along the different samples and to account for any possible sample loss; on the other hand, the IS also assists to monitor, within the problem samples, the robustness of the analysis regarding both chromatography (RT and peak shape) and detection (mass accuracy and peak area) aspects. Detailed information about the IS employed for each type of sample and analytical condition is provided in **Methodology**.

Here, different QC samples were used: i) Blank QC samples; ii) Pooled/commercially available QC samples; and iii) Class/treatment-specific pooled samples. Blank QC samples were processed like problem samples, but without the addition of the biological matrix; their purpose was to detect any contaminant ions coming from both sample processing and sample analysis. Pooled/commercially available samples QC were employed, when possible, to check the performance of the LC-MS analysis with samples of equal nature to the problem samples. In this sense, different QCs have been used: i) commercially available pooled

## Results & Discussion

---

serum (Sigma Aldrich, Spain); ii) a pool of liver tissue from Liver Bank at the Hospital La Fe (UHE-LAFE / CIBERehd, Valencia, Spain); and iii) pooled control samples from cellular cultures. These QC were spiked with different IS specifically selected to cover both a wide  $m/z$  and RT ranges for each analytical condition. Thus LC-MS performance was not only checked with respect to the metabolomic pattern, but also with respect to a few known peaks. Finally, class/treatment-specific pooled samples were also included in each batch analysis to perform simultaneous MS and MS/MS acquisition to facilitate feature identification.

The following considerations were taken into account with respect to each batch analysis or sample queue: i) As mass accuracy and response reproducibility may be compromised for long batch analysis times, total analysis time was limited to 48 h (215); ii) Pooled/commercially available QC sample was injected six times before starting the analysis of the problem samples, not only to condition the column but also to check system performance; iii) QC samples were alternated throughout the analysis batch sequence as follows: 1 pooled/commercially available QC every 15 problem samples and 1 blank QC every 10 problem samples; iv) Problem samples were analyzed in a random order but divided in representative blocks (e.g. blocks of the same number of samples belonging to different classes) (216); and v) Class/treatment-specific pooled samples were analyzed per triplicate at the end of the batch. The design of sample queue analysis is exemplified in **Figure 3.1**.

To test instrument's performance, the RSD of RT, peak area and mass accuracy of each IS was calculated for both problem samples and QCs. Acceptable RSD cutoffs for the peak area and RT were set at 15% and 1% respectively, while the threshold for mass error was set at 5 ppm. These figures were selected following the criteria described by the FDA Guidance for industry: bioanalytical method validation (206). Moreover, the analytical performance was evaluated with respect to the whole metabolomic pattern by using PCA. The relative position of a sample in

## Results & Discussion

the principal component scores plot is determined by the metabolomic pattern obtained, that is, the sum of its composition and the response obtained by the analytical platform. Samples that cluster together have a more similar metabolic pattern than those that cluster apart. Therefore, all the samples belonging to a given class (i.e. pooled QC, blank QC, problem samples...) are supposed to cluster together and apart from the samples belonging to a different class. Thus, a correct clustering of the samples is an indicative of a good performance of the UPLC-QToF system.

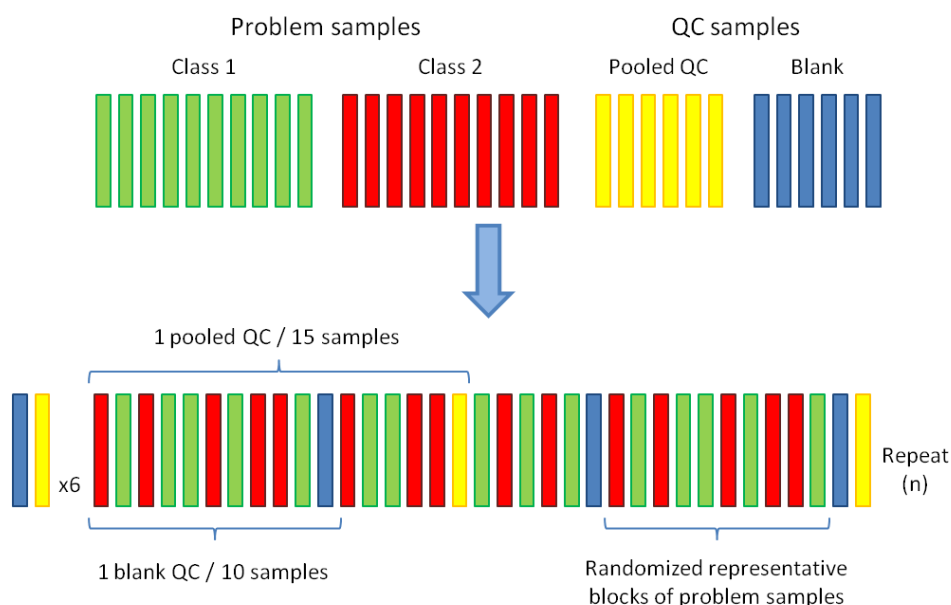


**Figure 3.1.** Analysis queue example in LC-MS untargeted metabolomic study. Problem samples are distributed in representative blocks and randomized within those blocks. Pooled quality control (QC) is injected 6 times before starting the analysis of problem samples in order to condition the column and to check system's performance. Blank QC is injected every 10 problem samples and pooled QC every 15 samples.

By way of example, **Figure 3.2** shows the values for area, mass accuracy and RT for the IS sulfadimethoxine and reserpine, under the generic RP in ESI (+) conditions, for all the samples included in the



## Results & Discussion

example study. **Figures 3.3-3.5** show the values for area, mass accuracy and RT for all the IS added to the pooled QC analyzed under the same conditions. All the recorded values, in both the QC and the samples, met the acceptance values.

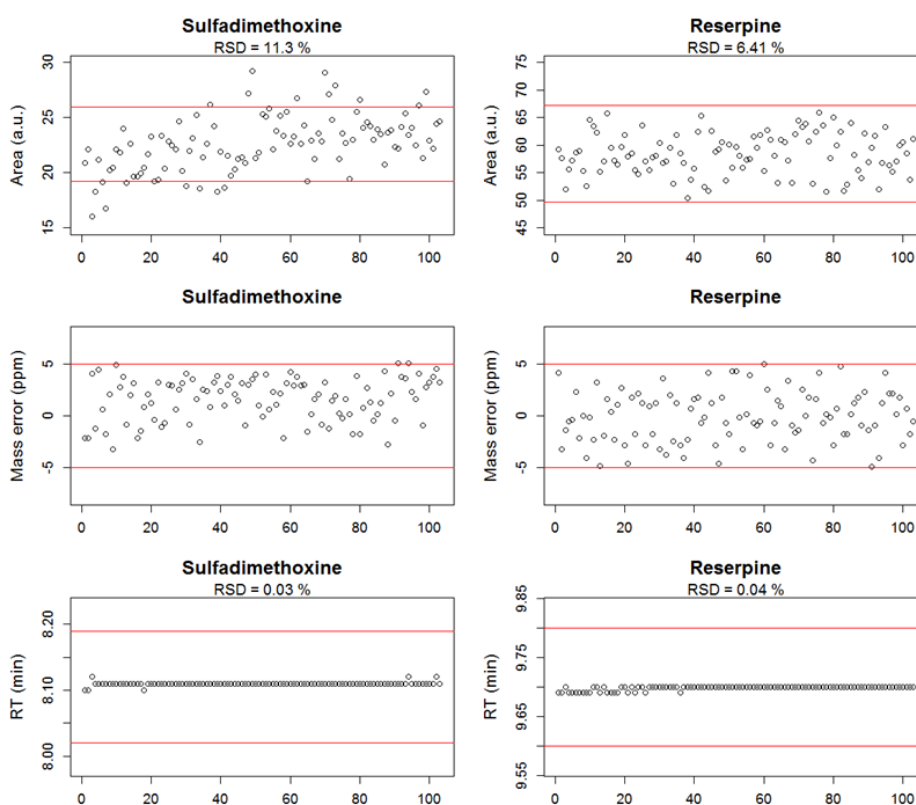


**Figure 3.2.** The peak area (upper panel), mass error (middle panel) and retention time (RT, lower panel) for the IS sulfadimethoxine and reserpine spiked in the problem samples. Each plot shows the values for all the problem samples analyzed under the generic-RP analysis in ESI (+) conditions. The red lines in the plots indicate the acceptance criterion for each parameter: 15% deviation for area, 1% deviation for RT and 5 ppm for mass error.

## Results & Discussion

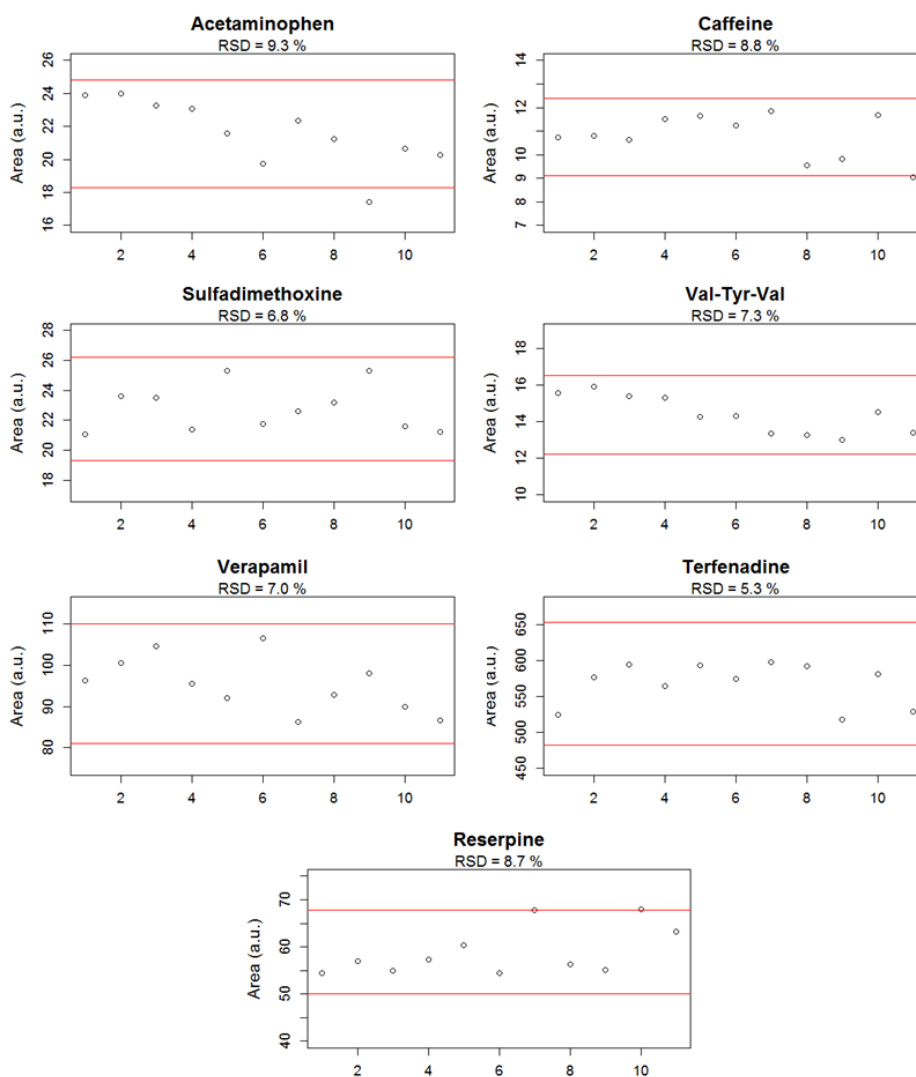


**Figure 3.3.** Peak area (arbitrary units) variation along sample batch analysis for the different IS spiked in the pooled QC. Each plot shows the values for the 11 analytical replicates of the pooled QC analyzed throughout the batch in the generic RP analysis in ESI (+) conditions. At the top of each plot, the relative standard deviation (RSD as a percentage) for the 11 measures is shown. The red lines indicate the  $\pm 15\%$  accepted deviation for the area.

## Results & Discussion

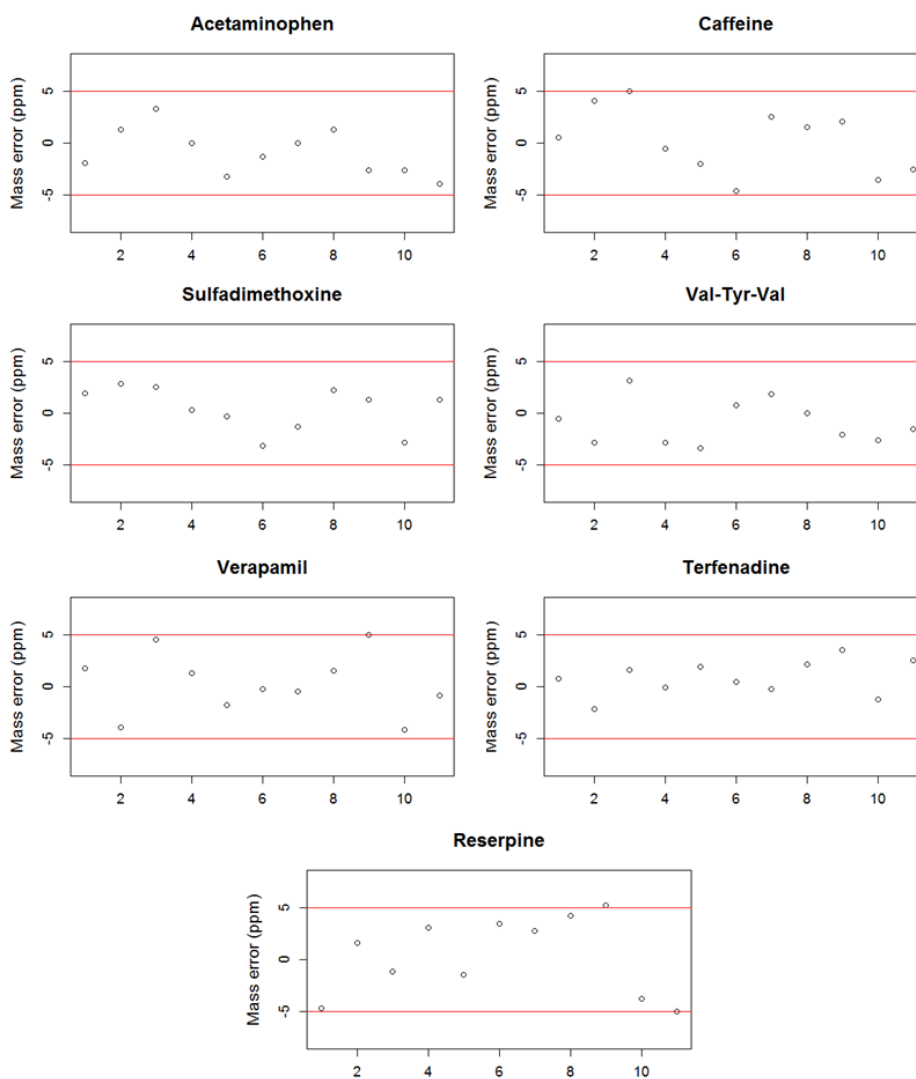


**Figure. 3.4.** Mass error (ppm) variation along sample batch analysis for the different IS spiked in the pooled QC. Each plot shows the values for the 11 analytical replicates of the pooled QC analyzed throughout the batch in the generic RP analysis in ESI (+) conditions. The red lines indicate the  $\pm 5$  ppm acceptance criterion as specified in the text.

## Results & Discussion

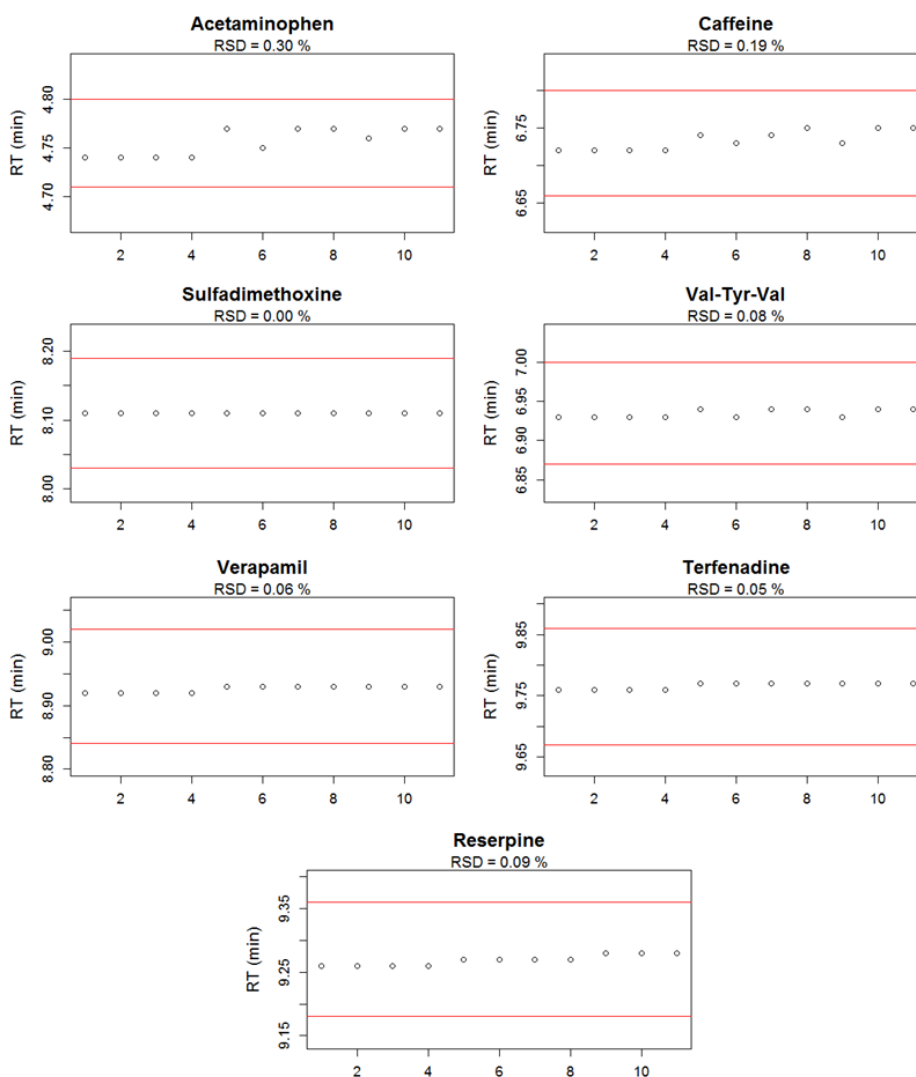


**Figure 3.5.** Retention time (RT, expressed in minutes) variation along sample batch analysis for the different IS spiked in the pooled QC. Each plot shows the values for the 11 analytical replicates of the pooled QC analyzed throughout the batch under the generic RP analysis in ESI (+) conditions. At the top of each plot, the relative standard deviation (RSD, percentage) for the 11 measures is shown. The red lines indicate the  $\pm 1\%$  accepted deviation for the RT.

## Results & Discussion

To investigate the natural sample relationship among the different QC and samples, a PCA was conducted (**Figure 3.6**). All the replicates of a given QC type were clustered together and separate from other QC samples or problem samples, thus indicating a good performance of the UPLC-QToF system throughout the batch analysis in terms of not only the targeted IS compounds, but the whole metabolomic profile.

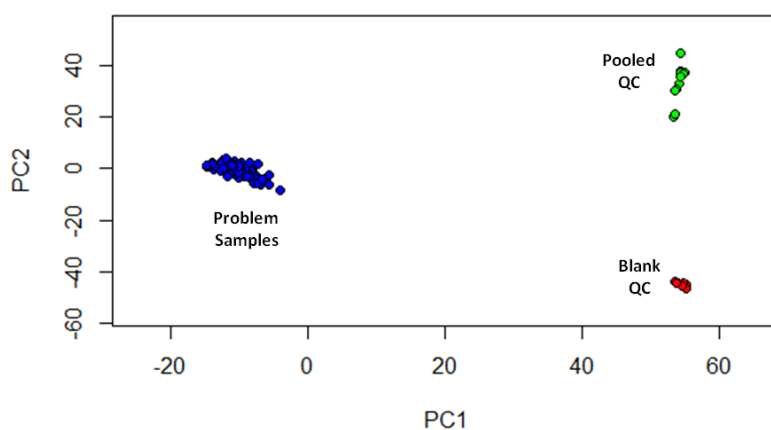


**Figure 3.6.** PCA scores plot showing the natural interrelationship among the different QC and problem samples included in the example study. Each point in the scores plot represents all the information provided by the generic-RP analysis in ESI (+) conditions for a given sample. Blue: problem samples; Green: Pooled QC; Red: Blank QC.

The present quality assurance strategy constitutes a straightforward method to evaluate system performance before, during and after problem samples acquisition. Pre-batch checks are designed to ensure that the system is in optimal conditions before starting the analysis, or before finishing the preparation of the problem samples. All the parameters (IS peak area, RT, peak symmetry, mass accuracy, QC global profile...) are checked during sample acquisition. Therefore, if a trouble is detected, the analysis can be halted and the samples can be stored (preventing sample injection or degradation). Finally, post-injection checks are the final evaluation previous to data analysis, thus preventing

## Results & Discussion

---

to waste time processing samples or batches that did not meet the quality standards. Moreover, the incorporation of analysis-specific IS is a helpful tool in the normalization data analysis stage as the IS levels reflect inter-samples differences in aspects such as injection volume, volume losses while preparing the sample, detection sensitivity...(133).

Recent publications have highlighted the importance of quality assurance strategy in metabolomic studies (133, 162, 215, 217). Common strategies to check systems performance in LC-MS based metabolomics include the use of QC samples and the addition of IS. However, previously reported strategies focused on checking the system performance before the start of the analysis and once it has finished. The strategy described here has the added value of carrying out live instrument performance checking as the parameters can be evaluated during the acquisition, what is especially important when the sample size is limited as it prevents samples to be injected (and consumed) or degraded while waiting or after being injected.

## Results & Discussion

---

### 3.2 Optimization of metabolome coverage for mammalian cells in adherent culture by using LC-MS

Untargeted metabolomics aims to detect the maximum possible number of metabolites in a given biological sample. In order to avoid metabolite degradation or alterations in their levels at the time of the sampling, sample processing has to allow the extraction of the metabolites of interest while providing a correct quenching of the cell metabolism. After the samples have been generated, they should be analyzed under the appropriate analytical conditions to achieve optimal chromatographic separation and detection of both polar and lipidic metabolites and maximize the information about their metabolomic profiles.

Several examples of the application of metabolomics to different cellular models are available in the literature (reviewed in reference (103)). However, there is no general consensus about the harvesting, extraction or analysis methods. Therefore, we evaluated different sample analysis and processing conditions in order to determine the best sample processing (including metabolism quenching, cell harvesting and metabolite extraction) and analysis protocol using HepG2 cells as cellular *in vitro* model (**Figure 2.13**).

#### 3.2.1 Optimization of endometabolome analysis by LC-MS

First, we evaluated the metabolome coverage offered by six different analytical conditions using three different chromatographic separations and each one tested in both ESI (+) and ESI (-) modes. Based on our previous experience in human liver tissue metabolomic profiling analysis (166), we decided to evaluate both HILIC and RP stationary phases. With respect to RP chromatography, two different approximations were used, one directed to detect the lipidome (lipidomic-RP) (163), and one

## Results & Discussion

---

intended to cover a wider set of metabolites from different polarities (generic-RP) (162). The seven HepG2 cells extracts (E1 to E7) obtained by the use of five different extraction solvents (solvent 1 to solvent 5) were analyzed by the six proposed analytical configurations (**Figure 2.13**). In all the cases the same cell harvesting and processing configuration (i.e. the way metabolism quenching, cell harvesting and metabolite extraction were applied) was performed based on a previously published one (152).

Results are summarized in **Table 3.1**, a detailed analysis of the figures revealed that a total of 103 polar and 492 lipidic unique metabolites were detected. As expected, no polar compounds were detected using the lipidomic-RP approximation, and no lipidic species were detected by using the HILIC conditions, however the generic-RP approximation was able to identify a range of polar and lipidic metabolites. Actually, polar metabolites could be detected using the lipidomic approximation and lipids using the HILIC one, however, the chromatographic signal, in terms of RT, peak shape and reproducibility, was not adequate and therefore those peaks were not considered for further analysis. As expected based on the characteristics (stationary and mobile phases) of the separation methods, lipidomic-RP approximation provided a broad coverage of lipidic species, with most of them being detected in ESI (+), although part of them were detected in ESI (-) mode as phosphatidylserine (PS), phosphatidylglycerol (PG), phosphatidic acid (PA)... On the other hand, although HILIC analysis did not provide a complete polar metabolite coverage, this approach rendered an acceptable number of polar compounds. Finally, the generic-RP approximation provided a complementary detection of both polar and non-polar compounds (i.e. FA and PL) thanks to the combined use of a RP column designed to enhance the retention of polar compounds and a chromatographic gradient set up to properly resolve both polar and lipidic metabolites.



## Results & Discussion

**Table 3.1.** Summary of the metabolites detected by each extract under the different analytical conditions.

		E1	E2	E3	E4	E5	E6	E7
Lipidomic-RP ESI(+)	ChE	10	11	16	0	17	4	15
	Cer	7	8	11	0	12	5	12
	DG	13	20	22	0	22	11	20
	FA	3	4	8	0	10	5	8
	LysoPC	11	12	16	0	18	9	18
	LysoPE	6	6	12	0	12	3	12
	PC	46	52	63	0	64	46	64
	PE	40	45	47	0	47	39	47
	PG	14	18	22	0	25	5	25
	PI	6	6	7	0	7	5	7
	PS	11	14	16	0	19	11	19
	SM	15	17	20	0	21	14	21
	TG	87	93	107	0	108	73	105
Lipidomic-RP ESI(-)	Cer	3	3	3	0	3	2	2
	FA	3	6	6	0	5	3	5
	LysoPE	5	11	12	0	12	9	10
	PC	3	9	8	0	9	7	8
	PE	17	18	17	0	17	17	15
	PG	3	11	11	0	11	9	9
	PS	4	8	10	0	10	7	8
Generic-RP ESI(+)	Polar	4	2	2	4	0	4	0
	DG	9	12	17	2	23	12	15
	LysoPC	1	7	7	0	8	4	5
	LysoPE	0	5	5	0	6	2	3
	MG	1	2	2	1	15	2	5
	PC	14	30	32	0	33	15	23
	PE	2	24	24	0	24	3	15
	PS	0	8	8	0	8	0	3
Generic-RP ESI(-)	SM	1	11	11	0	11	2	6
	Polar	12	21	16	21	0	21	0
	FA	5	12	11	7	15	13	11
	LysoPA	0	3	3	2	3	3	0
	LysoPE	0	7	7	0	7	2	1
	LysoPG	0	1	1	0	0	1	4
	LysoPI	0	2	2	0	0	1	0
	PG	0	9	9	0	9	2	4
HILIC ESI(+) HILIC ESI(-)	PI	0	12	12	0	12	1	7
	PS	0	5	5	0	5	1	3
	Polar	59	42	34	52	0	39	0
	Polar	44	34	25	41	0	37	0

E1-E7 refer to the different extracts obtained (see **Figure 2.13**). Color code refers to by-row centered and normalized mean intensity from the lower (blue) to higher (red) values. ChE: cholesterol ester, Cer: ceramides, DG: diacylglyceride, FA: free fatty acid, LysoPA: lysophosphatidic acid, LysoPC: lysophosphatidylcholine, LysoPE: lysophosphatidylethanolamine, LysoPG: lysophosphatidylglycerol, LysoPI: lysophosphatidylinositol, MG: monoacylglyceride, PC: phosphatidylcholine, PE: phosphatidylethanolamine, PG: phosphatidylglycerol, PI: phosphatidylinositol, Polar: polar metabolites, PS: phosphatidylserine, SM: sphingomieline, TG: triacylglyceride

## Results & Discussion

To graphically assess the relationship and the overlap between the metabolites extracted and detected by each analytical condition Venn diagrams were drawn (**Figure 3.7**).

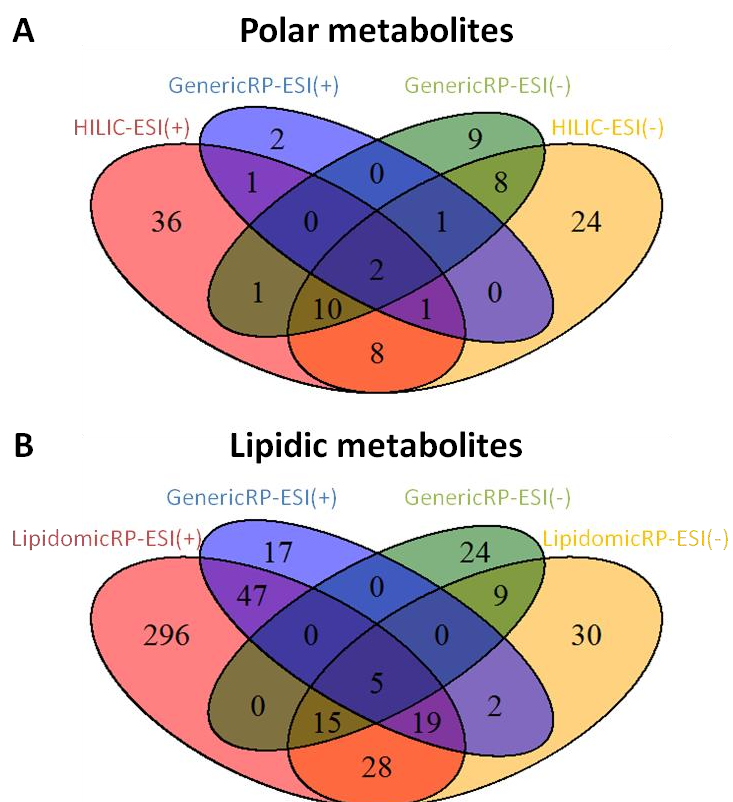


**Figure 3.7.** Venn diagrams showing the overlap between the different analytical conditions with respect to polar (**A**) and lipidic metabolites (**B**).

From the total 151 polar metabolites detected, the HILIC conditions provided the highest coverage detecting 113 species with 92 unique identifications. Generic-RP detected a total of 38 polar metabolites, 31 of them detected by using ESI (-), where 9 metabolites were not detected by any other analytical condition (**Figure 3.7.A**).

## Results & Discussion

---

With respect to the lipidome (**Figure 3.7.B**), a total of 661 lipids were detected. Generic-RP was able to achieve a good chromatographic separation of high to medium polar lipids as FA, PL, LysoPL... (**Table 3.1**), detecting a total of 143 metabolites with 138 unique metabolites. The lipidomic-RP approximation extended the coverage to highly apolar lipid species (e.g. TG and ChE) covering a total of 518 metabolites with 451 unique metabolites (**Figure 3.7.B**). Due to the diversity of the lipids, differences were obtained between ESI (+) and ESI (-) ionization modes that provided complementary information. Results showed that lipidomic-RP ESI (+) showed the highest lipidome coverage and no important complementary information was provided by generic-RP ESI (+), although using ESI (-) further information was obtained.

The overall analysis of the results revealed that using the combination of HILIC, lipidomic-RP with ESI (+) and generic-RP with ESI (-) the 90% of the total unique metabolites were covered.

LC-MS based metabolomics have been usually performed based on RP chromatography (107, 114, 115). However, the combination of HILIC and RP chromatographies has been satisfactorily employed by our group (166, 183) and others (218-220) as an analytical strategy suitable to expand the coverage of the metabolome. The added value of the strategy described herein resides not only in the combination of RP and HILIC stationary phases, but also in an experimental design that allows a comprehensive characterization of the entire lipidome. It has been recently suggested the use of HILIC chromatography to perform lipidomic analysis, mainly to cover highly to medium polar lipids such as PL, LysoPL and SM (221-223). Therefore, in our opinion, it is more appropriate to use a RP-based lipidomic as the one developed by the group of Professor Matej Oršic (163), whose usefulness and robustness have been extensively proven in many studies (224-226). Recently, *Fei et al* proposed an analytical strategy in which both polar and lipidic species were simultaneously analyzed using an HILIC-based chromatographic

## Results & Discussion

separation, thus reducing analysis time per sample (227). However, the usefulness of such approach might be limited by the fact that highly apolar lipids (i.e. FA, ChE, TG...) were not detected and the co-elution of polar and lipidic species, what could lead to ion suppression differences between samples and thus to misunderstanding of the results.

### 3.2.2 Optimization of endometabolome extraction

Five different extraction solvents that generated seven extracts were evaluated (Figure 2.13). Huge differences were obtained both in the nature, number and intensity of metabolites efficiently covered by each solvent combination (Table 3.1). A PCA analysis was performed in order to analyze the natural interrelationship between the different extracts (Figure 3.8).

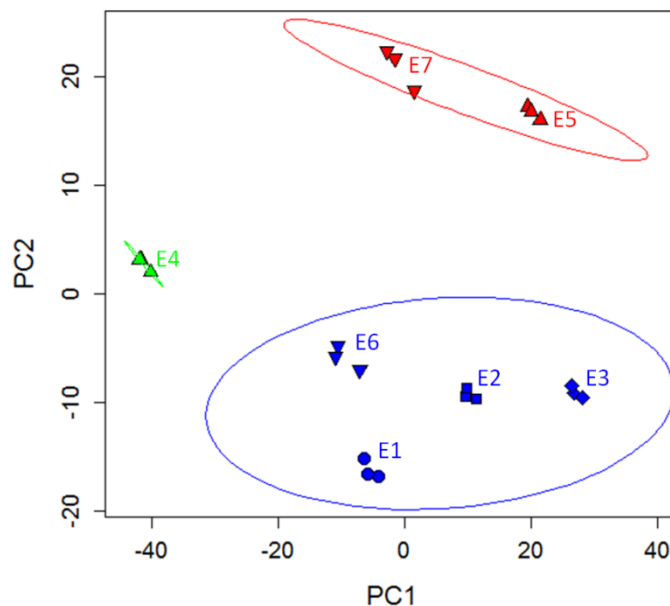


**Figure 3.8.** The PCA scores plot showing the natural interrelationship among the different extracts. Each cluster is represented by a different color and the lines denote 95 % confidence interval Hotelling's ellipse each one.

## Results & Discussion

---

Three different clusters were identified): i) E4, formed by extracts composed exclusively of polar metabolites; ii) E1, E2, E3 and E6, composed by extracts that achieved the extraction of both polar and lipidic compounds; and iii) E5 and E7, grouping extracts composed exclusively by lipidic metabolites. The direction along the first component is driven by an increased extraction of lipidic compounds, while the second component separated those extracts containing polar and/or lipidic compounds from those containing only lipidic metabolites (**Figure 3.8**).

With respect to the extraction of polar metabolites, extracts E1 and E4 provided the highest number and intensity of metabolites detected using HILIC conditions. With respect to lipids, extracts E3 and E5 were the ones providing the highest performance in lipidomic-RP ESI (+) conditions with a total of 367 and 382 detected compounds, respectively. However in general terms, and particularly for highly apolar lipids (i.e. ChE and TG), E5 provided higher extraction yields. Extracts E1, E2, E3 and E6 were able to extract both polar and lipidic metabolites. Among them, extract E1 was the one that achieved the best coverage of polar metabolites and E3 of lipids. However extract E2 was the one that provided the highest combined coverage of both polar and lipidic metabolites both in terms of detected metabolites (21 and 51, respectively in generic-RP ESI (-) conditions) and intensity (**Table 3.1**).

The overall review of these results showed that the combined analysis of E4 (HILIC), E5 (lipidomic-RP/ESI (+)), and E2 (generic-RP/ESI (-)), covered 90% of the metabolites comprised in the seven extracts.

Extraction with methanol alone or combined with other solvents (i.e. water or water and chloroform) is usually employed as a first approximation to metabolomic studies as a wide range of polar to medium apolar metabolites are extracted (103, 108). However, when the objective is to achieve a wider metabolome coverage and to exploit the capabilities of the analytical platform employed, different combinations

of extraction solvents can be tested. For example, with respect to the characterization of the lipidome, methanol extracts represent a good option to perform metabolomics studies covering the phospholipidome, while the addition of more apolar solvents (i.e. chloroform or dichloromethane) is needed when the focus is also put in highly apolar lipids such as TG or ChE (228). Our sample processing strategy, in which the combination of extraction solvents has been performed in a joint manner with respect the selection of the analytical conditions, allows to maximize the detection of metabolites of interest in each condition while minimizing the interferences provided by other groups of metabolites.

### 3.2.3 Optimization of cell harvesting and processing

Sample processing for adherent cells needs to overcome the following aspects: i) metabolism quenching; ii) cell detachment; and iii) metabolome extraction (103). These steps can be performed simultaneously or sequentially (103).

Three different approaches were tested to optimize cell harvesting and processing (**Figures 2.13, 2.14**). To focus on the influence of these specific factors on the metabolome coverage, the rest of operational variables were kept constant and all the samples were processed and analyzed based on the above mentioned results. All the methods showed similar figures in terms of the number of detected lipids (around 380 and 50 in lipidomic-RP ESI (+) and generic-RP ESI (-) conditions, respectively), although lower total intensities were obtained for method C with a mean decrease around 20% with respect to methods A and B (**Table 3.2**). An important decrease in both the intensity and number of identified polar metabolites was observed for method C: a total of 124 and 123 polar metabolites were identified using method A and B, respectively, while only 93 polar metabolites and a mean decrease in the total intensity near to 30% were detected using method C (**Table 3.2**).

## Results & Discussion

**Table 3.2.** Summary of the metabolites detected with each sample processing strategy under each analytical condition.

		Method A	Method B	Method C
<b>Lipidomic-RP ESI(+)</b>	ChE	17	15	16
	Cer	12	12	12
	DG	22	19	21
	FA	10	8	8
	LysoPC	18	17	17
	LysoPE	12	13	12
	PC	64	65	64
	PE	46	46	46
	PG	25	27	28
	PI	7	7	7
	PS	19	19	17
	SM	21	20	21
	TG	108	110	112
	Polar	21	18	13
<b>Generic-RP ESI(-)</b>	FA	12	13	11
	LysoPA	3	3	3
	LysoPE	7	7	7
	LysoPG	1	2	0
	LysoPI	2	2	2
	PG	9	7	9
	PI	12	11	12
	PS	5	5	5
<b>HILIC ESI(+)</b>	Polar	59	59	45
<b>HILIC ESI(-)</b>	Polar	44	46	36

Color code refers to fold of change with respect the mean value: blue = 0.5, white = 1, red = 2. ChE: cholesterol ester, Cer: ceramides, DG: diacylglyceride, FA: free fatty acid, LysoPA: lysophosphatidic acid, LysoPC: lysophosphatidylcholine, LysoPE: lysophosphatidylethanolamine, LysoPG: lysophosphatidylglycerol, LysoPI: lysophosphatidylinositol, MG: monoacylglyceride, PC: phosphatidylcholine, PE: phosphatidylethanolamine, PG: phosphatidylglycerol, PI: phosphatidylinositol, Polar: polar metabolites, PS: phosphatidylserine, SM: sphingomieline, TG: triacylglyceride.

Method C involves the use of trypsin to detach the cells from the plate surface and metabolism quenching is delayed with respect to the other two methods. It has been reported that trypsinization may compromise the cellular membrane integrity, leading to the loss of intracellular metabolites (150, 229, 230). Moreover, the delay in metabolism quenching may contribute to the enzymatic degradation of some metabolites (103). No significant differences were found with respect to methods A and B. However, from a practical point of view, an important

## Results & Discussion

---

advantage of method A is that several samples can be simultaneously generated and stored at -80 °C after metabolism quenching without the need of processing them just after their collection. This is especially useful when a high number of samples are generated at the same time, allowing to focus on time sensitive biological transformations, and when performing complex extraction procedures (152). Moreover, it has been previously shown an increased stability if the cells are stored previously to be extracted (as frozen plates), rather than the cellular extracts (152). Therefore, metabolism quenching with liquid N<sub>2</sub> followed by the simultaneous cells detachment and metabolite extraction was selected as the optimum strategy to perform sample processing when analyzing the endometabolome of cultured adherent cells.

### **3.2.4 Assembling an appropriate protocol for sample processing and analysis**

The optimized sample processing and analysis strategy is depicted in **Figure 3.9**. The first step in sample processing involves the removal of the culture medium followed by cell washing with PBS. Then, metabolism is quenched by the addition of liquid N<sub>2</sub> over the cell monolayer. At this step the cells can be stored at -80 °C, thus delaying the rest of sample processing steps. Cell detachment and metabolite extraction are performed simultaneously by scrapping the cells in water:methanol:chloroform (10:27:3) (152). The cell extract/suspension is submitted to three freeze/thaw cycles (liquid N<sub>2</sub>/room temperature) in order to increase cell disruption and metabolite extraction. The extract is then split in two different aliquots for untargeted metabolomic analysis plus an additional one for protein quantification. The first aliquot is destined to be analyzed using generic-RP ESI (-) conditions. The second aliquot is extracted with chloroform thus generating two different fractions: an aqueous fraction, that will be analyzed using HILIC



## Results & Discussion

separation coupled to both ESI (+) and ESI (-) detection, and an organic fraction, that will be analyzed using lipidomic-RP ESI (+) conditions. Then, three different aliquots are generated for each biological sample, which will be analyzed using four analytical conditions (**Figure 3.9**).

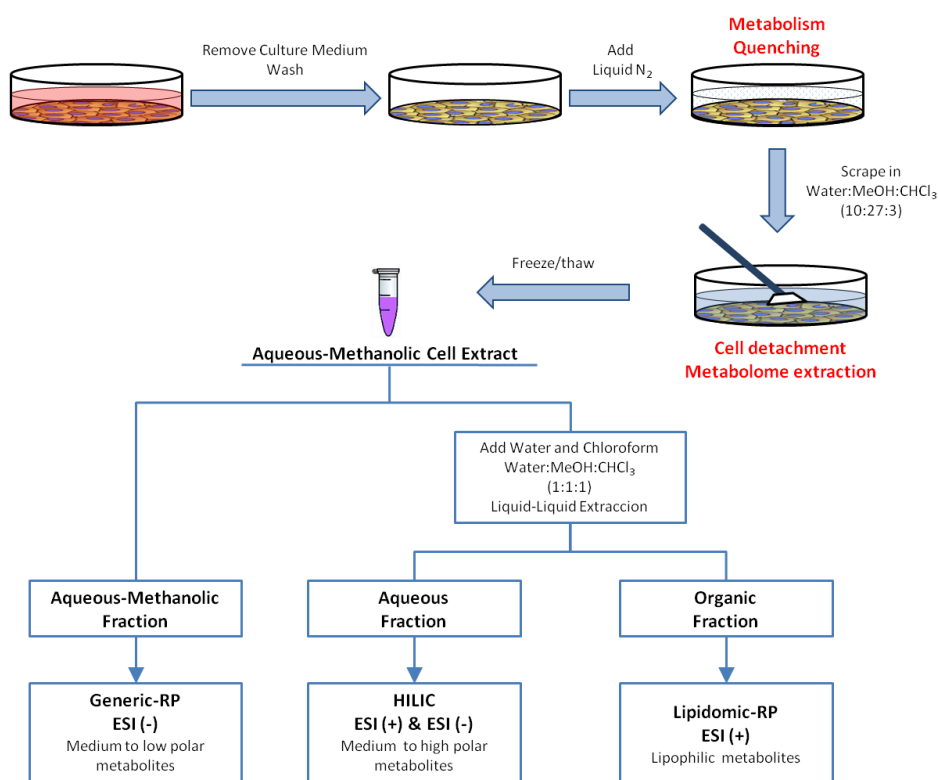


**Figure 3.9.** Workflow of the optimized sample processing and analysis strategy for the analysis of the endometabolome of HepG2 cells.

Few studies have evaluated different aspects of sample processing for mammalian adherent cell cultures (150-152, 227, 229, 231). These studies focused on the optimization of sample processing for a particular cell line, however, a series of conclusions can be extracted. Most of them focused on the detection of polar metabolites. The only study that evaluated some lipidic metabolites is the one performed by *Fei et al*

## Results & Discussion

---

(227). In all of them the decisions were taken on the basis of the levels of a set of metabolites and the total number/intensity of detected features. This strategy could lead to misunderstandings in results interpretation and decision making.

Our results agree with respect to the basic operational steps (i.e. metabolism quenching, cell detachment and cell disruption) described in the literature (103). It is not possible to compare our results with the previous ones in terms of metabolome extraction and analysis as our protocol aims to cover a wider range of metabolites, from highly polar (e.g. aminoacids, nucleotides, cofactors...) to lipidic (e.g. lysoPLs, PLs, TGs...) metabolites, compared to the previously mentioned studies. To analyze the extent of the improvement of metabolome coverage reached by each protocol modification, we decided to evaluate only those features that were matched with a known identity. This strategy allows a more accurate and reliable evaluation of the capabilities of the sample processing and analytical procedures.

The main strength of our study approach was the simultaneous optimization of sample processing and analysis, this allows to evaluate the capabilities of each analytical modification in combination with the extraction properties of each solvent mixture, thus maximizing the information that can be obtained from each biological sample. Our aim was to set up a sample processing and analysis strategy that allowed the determination of the widest possible number of metabolites. This approximation allows to get a more comprehensive information about the events that are occurring within the cell, which supposes a crucial advantage to the metabolic phenotyping of the cells and the possibility of the discovery of biomarkers. Moreover, as several different aliquots can be extracted from a single biological sample, it supposes an important saving of economic, biological and time resources. While the strategy described here provides a thorough mapping of the metabolome, it has some disadvantages. The proposed extraction

## Results & Discussion

---

method involves more complex sample manipulations compared to the extractions using aqueous:methanolic mixtures (103). Moreover, the analytical strategy involves the analysis of each biological sample under four different conditions. That supposes a considerable increase in the analysis time and the time and complexity of data analysis, and therefore a reduction in the efficiency compared to those methods that perform the analysis of the samples using a single analytical condition.

No comprehensive sample processing and analysis optimization has been previously performed using liver-derived cells although some metabolomic studies are available in the literature (154-157, 232). After the evaluation of several parameters regarding sample processing (i.e. metabolism quenching, cell harvesting and metabolome extraction) and analysis, we propose a strategy that allows a comprehensive coverage of the metabolome ranging from polar metabolites (e.g. aminoacids, nucleotides, cofactors, organic acids...) to the whole spectra of lipidic species (i.e. LysoPL, PL, FA, TG...). This strategy can be applied to any study involving the use of mammalian cells and mass spectrometry analysis.

### 3.3 Metabolomic analysis of HepG2 cells exposed to model hepatotoxic compounds

The main objective of the present thesis was the identification of mechanism-specific biomarkers, metabolomic patterns and altered pathways associated to drug-induced hepatotoxicity using HepG2 cells as *in vitro* model. HepG2 is the most commonly used and best characterized human liver-derived cell line. The main strengths associated to the use of HepG2 cells in pre-clinical testing are its human origin, unlimited availability, high reproducibility, easy culture and handle conditions, complete characterization and wide bibliographic documentation (5, 49). Their limited drug metabolizing and transport capabilities are the main drawbacks associated to their use.

The optimized analytical strategy described in **Section 3.2** was applied to unravel the metabolomic changes associated to hepatotoxicity in general and to specific mechanisms of hepatotoxicity in HepG2 cells. Model hepatotoxins and concentrations were selected based on previously published studies (**Table 2.2**) (29, 69, 88, 89, 91, 92). Four different mechanism of toxicity were tested: i) OS; ii) phospholipidosis; iii) steatosis and iv) cholestasis (29).

**Figure 3.10** shows the scores plots corresponding to the PCA analysis performed by comparing the metabolic profile of cells treated with control (i.e. non-hepatotoxic) compounds vs cells treated with compounds corresponding to each of the different mechanisms of hepatotoxicity included in the study.

## Results & Discussion

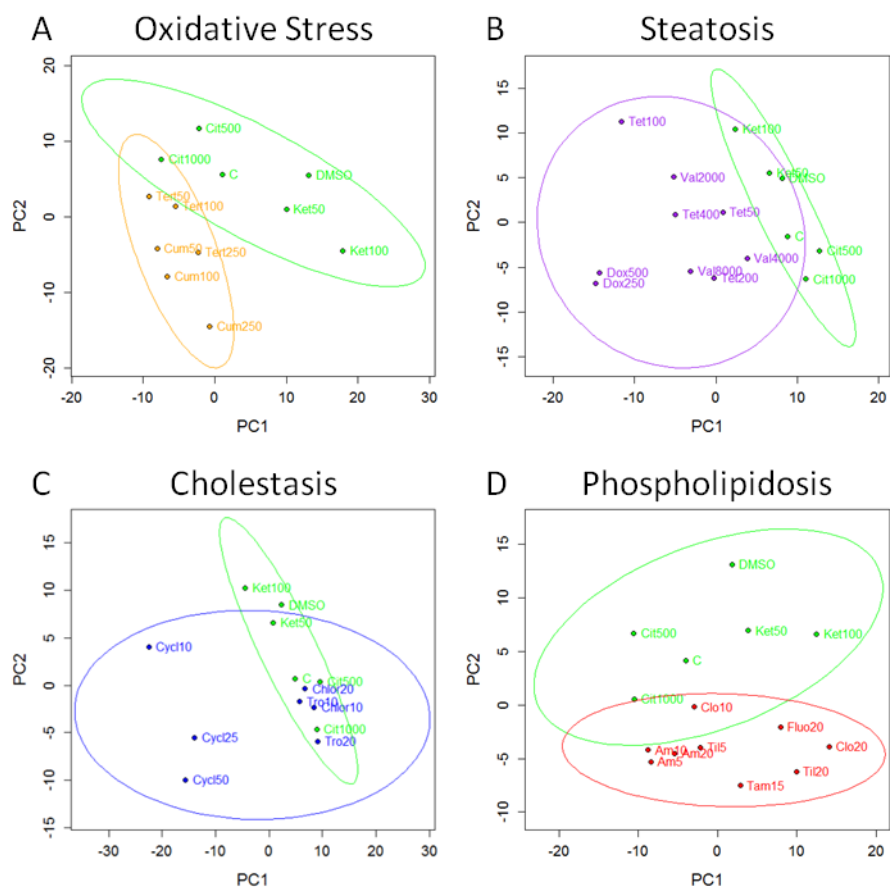


**Figure 3.10.** PCA scores plots corresponding to data obtained from HepG2 cells treated with hepatotoxins acting through different mechanisms of toxicity and analyzed using the generic metabolomic strategy. The lines denote 95 % confidence interval Hotelling's ellipse. PCA models were developed using two principal components. **A)** Control vs OS. **B)** Control vs Steatosis. **C)** Control vs Cholestasis. **D)** Control vs Phospholipidosis. Green: Control; Orange: OS; Purple: Steatosis; Blue: Cholestasis; Red: Phospholipidosis.

## Results & Discussion

---

The scores plots corresponding to the comparison of non-hepatotoxic compounds vs OS (**Figure 3.10.A**), steatosis (**Figure 3.10.B**) and phospholipidosis (**Figure 3.10.D**) show that the samples corresponding to cells treated with control compounds were clustered together and separated from those corresponding to hepatotoxic compounds. This trend indicates that the toxic insult induced changes in the metabolome that were detected by using our sample processing and analysis strategy. The PCA scores plot in **Figure 3.10.C** reveals that the changes induced in the metabolome by the three drugs from the cholestasis group were not homogeneous. While the samples corresponding to the treatment with cyclosporine were located far from the cluster of control samples in the scores plot, those corresponding to troglitazone and chlorpromazine were located within the 95% confidence interval Hotelling's ellipse corresponding to the control samples. This finding suggests no detectable changes in the HepG2 metabolome after treatment with troglitazone and chlorpromazine, at least at the concentrations and analytical conditions used in our study.

### 3.3.1 Identification of markers of hepatotoxicity

The PCA analyses shown in **Figure 3.10** revealed that the observed metabolome alterations were strong enough to be able to differentiate between control and hepatotoxic compounds using a non-supervised multivariate analysis. Thus, the next step in the data analysis workflow was to identify which metabolites and pathways were altered as a consequence of the different treatments. First, a general comparison between non-hepatotoxic and hepatotoxic compounds was performed in order to identify non-specific markers of hepatotoxicity. Then, the analysis was focused on the identification of specific markers and patterns associated to each of the studied mechanisms of toxicity. Two different strategies were performed to select those altered metabolites

## Results & Discussion

---

with the aim of capturing both the alterations reflecting uni- and multivariate dependencies (121). Those metabolites showing a  $q$  value  $< 0.05$  ( $p$  value using a Student's  $t$  test corrected using FDR) or a VIP value  $> 1.2$  (based on a PLS-DA model discriminating between control and the treatment of interest) were considered to be significantly altered as a result of the exposure to the toxicant.

### *Non-specific metabolome changes triggered by hepatotoxic compounds*

Those metabolites which were altered by all the hepatotoxic compounds may be considered as general biomarkers of toxicity. With respect to polar metabolites the most important changes were related to aminoacids (i.e. glutamine, histidine, methionine, phenylalanine, threonine, tyrosine, tryptophan, citrulline...), glycolysis (i.e. glucose-6-phosphate), OS markers (i.e. GSH/GSSG, cysteine-GSH disulfide (CSSG) and  $\gamma$ -glutamyl-glutamine), metabolism of purines (i.e. adenine and xanthine) and intermediates in PL metabolism (i.e. phosphocholine, glycerophosphocholine, LysoPL...). With respect to the lipidic species, several changes were observed in PL, FA, TG and acylcarnitines (**Figure 3.11**).

From a general point of view these results suggest that the hepatotoxic insult affected some of the most basic metabolic functions. Pathways such as glycolysis, urea cycle and metabolism of FA, aminoacids, nitrogen, purines and PL, that were revealed to be significantly altered using pathway enrichment analysis, are among the most important ones controlling energy production and maintaining cellular integrity and homeostasis. Moreover, the appearance of OS markers in conjunction with the alteration of metabolites related to the metabolism of FA suggests that the mitochondrion is a common target in hepatotoxic damage (34, 35).

## Results & Discussion

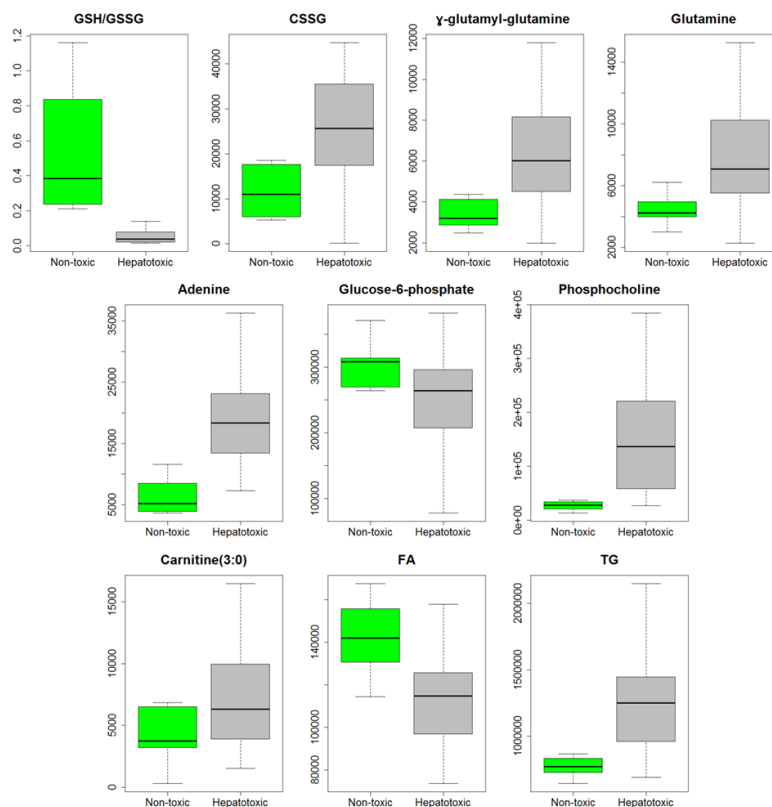


**Figure 3.11.** Boxplots showing the most important changes associated to generic hepatotoxicity in HepG2 cells analyzed following the generic untargeted metabolomic analysis strategy. Values are expressed as relative intensity. Boxes denote interquartile ranges, lines denote medians, and whiskers denote the 10th and 90th percentiles.

### Metabolomic changes provoked by OS inducers

Among the hepatotoxic compounds used in our study, cumene hydroperoxide and tert-butyl hydroperoxide were selected as pure OS inducers (**Table 2.2**). A total of 66 metabolites were significantly altered in HepG2 cells exposed to these model toxicants. A pathway enrichment analysis revealed that FA and TG metabolism, PL metabolism, glutamate and GSH metabolism, nitrogen and aminoacid metabolism and



## Results & Discussion

nucleobases metabolism were the pathways suffering the greatest impact. The most important metabolic changes are shown in **Figure 3.12**. As expected, a characteristic increase in well-known low-molecular-weight OS markers was found. Moreover, noteworthy changes in the lipidome, that can be interpreted as a secondary damage associated to the oxidative insult, were also observed (**Figure 3.12**).

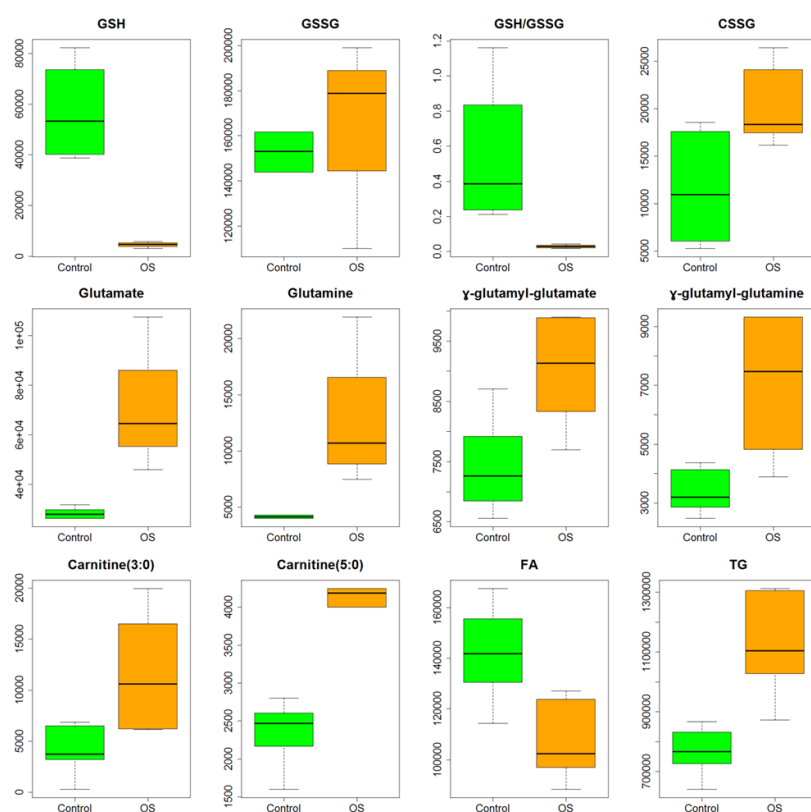


**Figure 3.12.** Boxplots showing the most important changes associated to OS treatment in HepG2 cells analyzed using the generic untargeted strategy. Values are expressed as relative intensity. Boxes denote interquartile ranges, lines denote medians, and whiskers denote the 10th and 90th percentiles.

## Results & Discussion

---

The most common change associated to OS damage is a decrease in the GSH/GSSG ratio. GSH is the predominant low-molecular-weight thiol (0.5 – 10 mmol/L) in animal cells, mainly located in the cytosol (85 – 90%), but also in many organelles (233, 234). Its high intracellular concentration, compared to other redox systems (i.e. NADP<sup>+</sup>/NADPH and thioredoxin (TrxSS/Trx(SH)<sub>2</sub>), makes the GSH/GSSG pool the principal redox buffer of the cell (50, 235). As seen in **Figure 3.12**, an important reduction in GSH levels and GSH/GSSG ratio was observed in HepG2 cells treated with OS-inducers, in agreement with previous *in vitro* studies in liver-based cellular models (236, 237). The shift of GSH/GSSG toward the oxidizing state activates several signaling pathways which, in conjunction with GSH efflux, has been associated to increased apoptosis in liver cells (234, 238, 239).

According to the observed changes in GSH and GSH/GSSG, increased levels of CSSG were also found (**Figure 3.12**). CSSG is a marker of oxidative damage to GSH (240). CSSG, usually assessed in serum, is the result of the reaction between cystine (the oxidized form of cysteine, which constitutes the major thiol pool in blood) and GSH, supplied from the cells to preserve the cysteine to cystine ratio (241). Nevertheless, CSSG is ubiquitously found in mammalian cells and under OS conditions its production is enhanced (240). Increased levels of CSSG have been reported in the liver of rats treated with paracetamol (140).

Tightly related, several compounds belonging to the  $\gamma$ -glutamyl cycle (i.e.  $\gamma$ -glutamyl-glutamine,  $\gamma$ -glutamyl-glutamate, glutamine and glutamate) showed altered levels as a result of the oxidative damage. The  $\gamma$ -glutamyl cycle (**Figure 3.13**) was postulated by Meister in the mid-seventies (242, 243) and accounts for the biosynthesis and degradation of GSH. GSH is synthesized from its constituent amino acids in two consecutive reactions (**Figure 3.13**) (233, 244). The first step, considered rate limiting, is catalyzed by glutamate cysteine ligase (GCL). GCL is specific for the glutamyl moiety and is regulated physiologically by

## Results & Discussion

inhibition by GSH and availability of its precursor, L-cysteine (243). The second step is catalyzed by GSH synthase (GS). In addition, the rate of GSH biosynthesis in the hepatocyte is balanced by its rate of export, mainly into plasma and bile (233, 244).

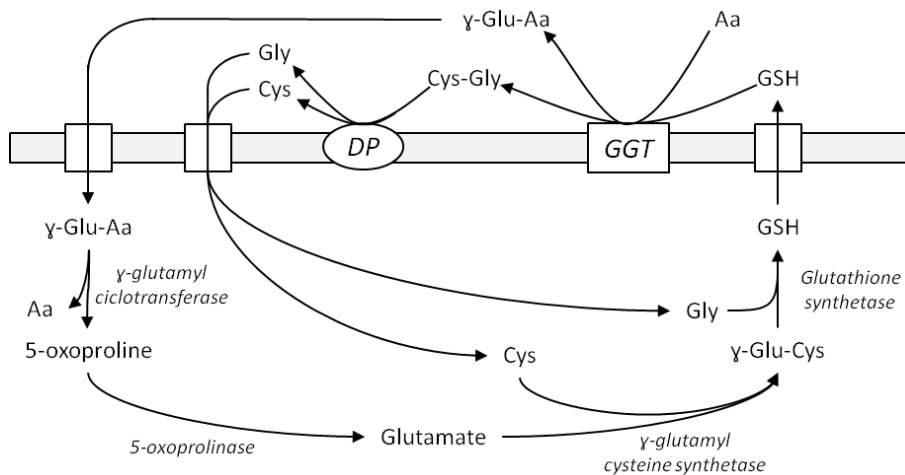


**Figure 3.13.**  $\gamma$ -glutamyl cycle. Enzymes are denoted in italics. Square boxes denote transmembrane transporters. GGT:  $\gamma$ -glutamyl transpeptidase. DP: dipeptidase. Figure adapted from references (233, 245).

Storage of cysteine is one of the most important functions of GSH because extracellular cysteine is extremely unstable and rapidly auto-oxidizes to cystine, in a process that produces potentially toxic oxygen free radicals (242). The  $\gamma$ -glutamyl cycle describes how GSH can be used as a continuous source of cysteine. GSH is released from the cell by carrier mediated transporter(s) and then  $\gamma$ -glutamyl transpeptidase (GGT) transfers the  $\gamma$ -glutamyl moiety of GSH to an amino acid, forming  $\gamma$ -glutamyl amino acid and cysteinylglycine which can be further metabolized to retrieve their constitutive amino acids. (233, 242, 244) (**Figure 3.13**).

## Results & Discussion

Two different theories can explain the appearance of  $\gamma$ -glutamyl dipeptides as a result of OS. *Soga et al* found increased serum levels of different  $\gamma$ -glutamyl dipeptides in different forms of liver disease (246). They hypothesized that  $\gamma$ -glutamyl dipeptides are synthesized via the ligation of glutamate with various amino acids and amines by GCS, and are indicative of the amount of GSH production (**Figure 3.14**) (246).

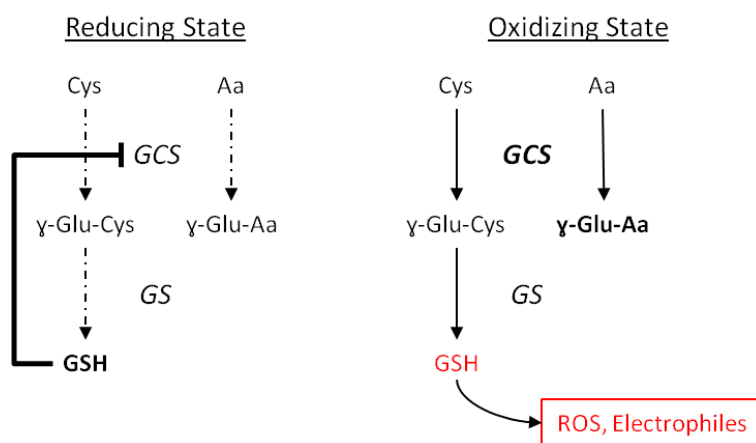


**Figure 3.14.** Hypothesis postulated by *Soga et al* (246) to explain the accumulation of  $\gamma$ -glutamyl dipeptides under OS conditions. Under reducing conditions, GCS is feedback inhibited by GSH and small amounts of  $\gamma$ -glutamyl dipeptides are synthesized (left panel). During OS, GSH is consumed, leading to GCS activation, which could result in biosynthesis of  $\gamma$ -glutamyl dipeptides. GCS:  $\gamma$ -glutamyl-cysteine synthetase; GS: glutathione synthetase. Figure adapted from reference (246).

However, not only  $\gamma$ -glutamyl dipeptides, but other components of the  $\gamma$ -glutamyl cycle were altered as a result of the oxidative damage. Under OS conditions, the flux of GSH to the  $\gamma$ -glutamyl cycle is enhanced to restore reduced thiol status of the cell (mainly as reduced cysteine) what could be an alternative theory to explain the observed metabolomic alterations (**Figures 3.12, 3.13**). Additional studies (measurement of enzyme activities and metabolic fluxes) would be required to clarify the

## Results & Discussion

---

contribution of each of the aforementioned pathways in the protection of the cell under OS conditions and the appearance of  $\gamma$ -glutamyl dipeptides.

With respect to the alterations in the lipidome, the most remarkable changes were a decrease in the levels of free FA and an increase in the levels of acylcarnitines and TG (**Figure 3.12**). Although the oxidative insult can induce damage in different molecules and cell organelles, the oxidative processes that take place in the mitochondria (along with the presence of an unprotected mtDNA) make them sensitive targets of oxidative damage (32-34). A consequence of mitochondrial damage is the inhibition of metabolic pathways in the mitochondria, including FA  $\beta$ -oxidation. This situation results in an accumulation of FA and intermediates of FA oxidation such as acylcarnitines. FA can either be esterified into TG or remain as a free form, this later reinforcing mitochondrial dysfunction and increasing OS (32-34, 247).

### Metabolomic alterations induced by steatogenic drugs

Three model drugs causing steatosis as main mechanism of toxicity were included in the study (**Table 2.2**): doxycycline, tetracycline and valproic acid. Drug-induced steatosis resulted in the alteration of 91 metabolites in HepG2 cells. A functional enrichment analysis revealed that FA and TG metabolism, aminoacid metabolism, urea cycle and nitrogen metabolism, PL metabolism and glutamate, cysteine and GSH metabolism were the most altered pathways.

The main alterations related to lipidic species were the increase in the levels of TG, DG, PL and LysoPL and the decrease in FA (**Figure 3.15**). With respect to polar metabolites, although several compounds were altered as a result of drug-induced steatosis, it is worthy to remark the changes in several OS markers (**Figure 3.15**).

## Results & Discussion

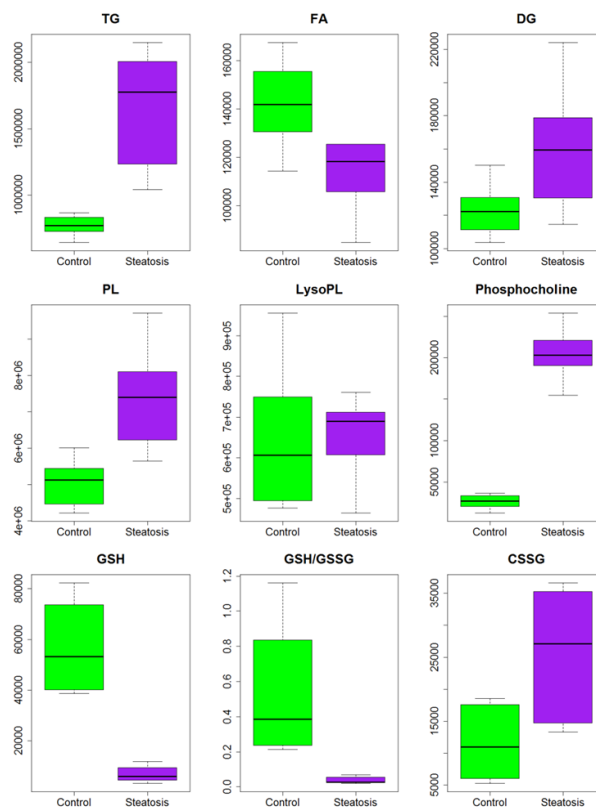


**Figure 3.15.** Boxplots showing the most important changes associated to steatosis treatment in HepG2 cells analyzed using the generic untargeted metabolomic analysis strategy. Values are expressed as relative intensity. Boxes denote interquartile ranges, lines denote medians, and whiskers denote the 10th and 90th percentiles.

The accumulation of TG inside the hepatic cells is the hallmark of hepatic steatosis. Increased TG deposits has been previously observed in the liver of patients suffering steatosis (106, 166, 248), in animal models of diet-induced (249-252) or drug-induced (253-255) steatosis and in cellular models of *in vitro* hepatosteatois (88, 154, 256). Different mechanisms leading to drug-induced hepatic steatosis have been identified (29, 32). Among them, impairment of FA  $\beta$ -oxidation due to mitochondrial disturbances is of special relevance (29, 32, 34, 35). There

## Results & Discussion

---

is substantial evidence that FA can directly cause toxicity by increasing OS and through the activation of inflammatory pathways (247); therefore, the accumulation of FA as TG is thought to be an adaptive and protective response of hepatocytes to excessive availability of free FA to the liver and its associated liver toxicity (257-259). Impairment of TG synthesis has been shown to improve of hepatic steatosis but increase cytotoxicity and liver damage (252, 260).

While TG are considered to be a non-lipotoxic counterpart in steatosis, the list of possible lipotoxic metabolites include FA, PA, LysoPA, LysoPC, ceramides, and DG (257, 259). Among them, the levels of LysoPL and DG were found to be elevated in cells treated with steatogenic drugs (**Figure 3.15**). The levels of LysoPL have been previously found to be elevated in liver biopsies and serum samples from patients suffering hepatic steatosis (166, 248, 261, 262), in palmitate-loaded HepaRG cells (154) and in mouse models of fatty liver disease and obesity (251, 263). LysoPL are generated through the action of phospholipases. LysoPC, produced by phospholipase A2 (PLA2), which catalyzes the hydrolysis of the fatty acyl ester bond at the sn-2 position of glycerophospholipids (**Figure 3.16**), have been implicated in several types of cell death (264-266). One recent study related elevated LysoPC content in the liver with the genesis and progression of necroinflammatory injury of hepatocytes (267). A direct role of LysoPC in lipotoxic liver injury was then demonstrated using human liver cell lines, mouse hepatocytes in primary culture, and in mice. Consistently, induction of phospholipase A2 genes has been found in non-alcoholic steatohepatitis (NASH) (106, 267).

## Results & Discussion

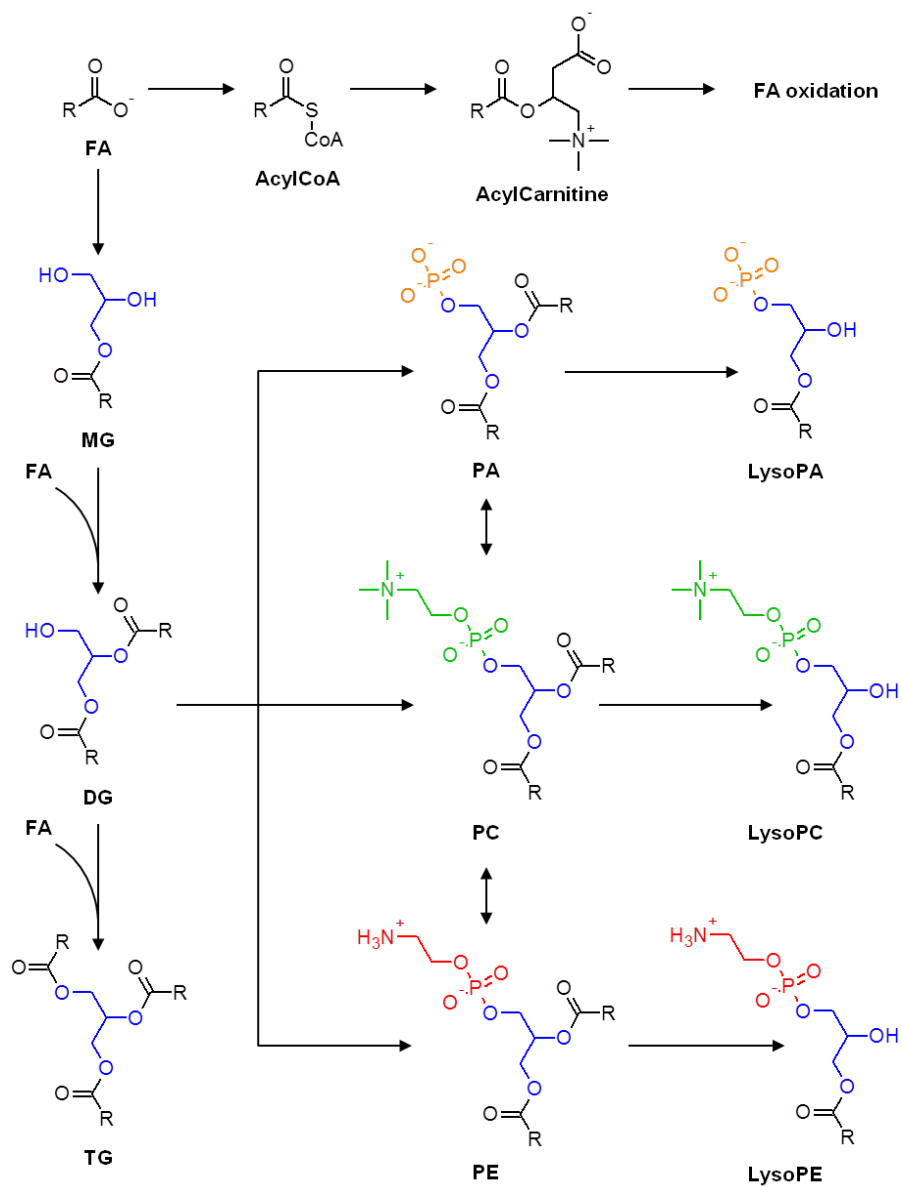


**Figure 3.16.** Main lipidic pathways showing alterations as a result of drug-induced steatosis. See the text for a detailed explanation of the consequences derived of the blockade and enhancement of specific routes. The glycerol backbone is highlighted in blue, the polar groups of the different PL are highlighted in different colors.



## Results & Discussion

---

Together with TG accumulation, increased levels of DG is the most common lipidomic pattern associated to hepatic steatosis and has been described in both liver (106, 248, 268) and serum (261, 262, 269) samples from patients with steatosis and in palmitate-loaded HepaRG cells (29). DG are intermediates in the synthesis of TG and their elevated levels may be a consequence of the elevated traffic of FA from its free form to MG, DG and finally TG (**Figure 3.16**). However, DG species are well-known activating ligands of most protein kinase C (PKC) isoforms and increases in DG species have been suspected as a major contributor to hepatic lipotoxicity (259). Moreover, DG signaling through PKC has been shown to be an important event in cancer progression (270, 271) and specific DG transferases have been implicated in the progression of non-alcoholic fatty liver disease (NAFLD) and liver fibrosis (272, 273). The increased levels of DG in combination with the increased levels of phosphocholine could lead to higher rates of PC biosynthesis via the CDP-choline pathway (i.e. Kennedy pathway) (274, 275), thus resulting in increased levels of PL as observed (**Figures 3.15, 3.16**).

Impairment of FA  $\beta$ -oxidation by steatogenic drugs can lead to an enhancement of extramitochondrial FA oxidation, thus promoting higher rates of ROS production and lipid peroxidation (276). Accordingly, a decrease in GSH levels and GSH/GSSG ratio, and an increase of CSSG levels were observed in HepG2 cells exposed to steatosis-inducing drugs (**Figure 3.15**). GSH depletion and oxidative damage to macromolecules have been reported in liver biopsies from patients with steatosis (166, 268). Increased ROS levels have also been described in palmitate-loaded HepaRG (154) and H4IIEC3 (277) cells and in primary cultured human hepatocytes and HepG2 cells treated with steatogenic drugs (88, 92).

## Results & Discussion

---

### Metabolomics changes associated to cholestatic damage

Chlorpromazine, cyclosporine and troglitazone, three compounds reported to induce cholestasis, were included in the study (**Table 2.2**). The PCA scores plot shown in **Figure 3.10.C** revealed that chlorpromazine and troglitazone did not induce any detectable changes at the employed concentrations. Therefore, we decided to exclude those samples from the data analysis and focused on the alterations induced in HepG2 cells as a consequence of the incubation with cyclosporine.

A total of 92 metabolites were altered in cyclosporine-treated cells. Aminoacid metabolism, urea cycle and nitrogen metabolism, FA and TG metabolism, PL metabolism and glutamate and GSH metabolism were revealed as the most affected pathways using enrichment analysis. The altered metabolites and pathways did not suggest an obvious relation to the expected mechanism of toxicity through a cholestatic effect. However, the results suggest that cyclosporine was able to induce changes that were consistent with OS and steatosis mechanisms of hepatotoxicity. **Figure 3.17** shows increased levels of GSSG, CSSG and  $\gamma$ -glutamyl-glutamine and a decreased GSH/GSSG ratio as previously observed for OS (**Figure 3.12**). On the other hand, the increase in acylcarnitines, DG, TG, phosphocholine and PL (**Figure 3.17**) is similar to the pattern previously observed for steatosis-inducing compounds (**Figure 3.15**). Cyclosporine is not only a cholestasis-inducing drug, but has also been reported as being able to induce OS and lipid accumulation (89, 92, 278, 279) and inhibit  $\beta$  oxidation of FA, thus resulting in the accumulation of FA and TG (280, 281). Cyclosporine is an immunosuppressant drug widely used in organ transplantation to prevent rejection, accumulation of free FA has been described in post-transplant recipients after the treatment with cyclosporine (282). Moreover, a recent study comparing the effect of steatotic compounds in the expression profile of 47 transcription factors revealed that the

## Results & Discussion

pattern induced by cyclosporine was similar to the obtained with a set of well-defined statotoxic drugs (69).

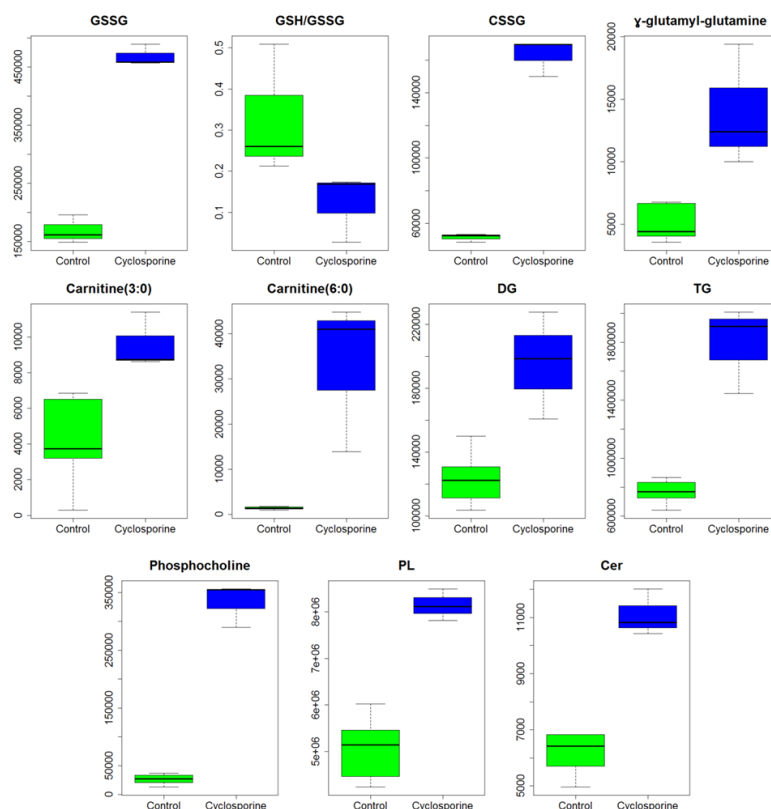


**Figure 3.17.** Boxplots showing the most important changes associated to HepG2 cells exposed to cyclosporine A and analyzed using the generic untargeted metabolomic strategy. Values are expressed as relative intensity. Boxes denote interquartile ranges, lines denote medians, and whiskers denote the 10th and 90th percentiles.

The development of drug-induced cholestasis is based on the direct or indirect effect that the drugs induces in the function of BA transporters such as the basolateral uptake transporters (NTCP and OATPs), the canalicular efflux transporters (BSEP, MRP2, and MDR3), and the basolateral efflux transporters (MRP3 and MRP4) (38, 45, 48). Therefore,

## Results & Discussion

---

the study of cholestasis requires the choice of an experimental model in which those transporters are active and correctly located. Unfortunately the loss of native cell polarization in HepG2 cells affects the correct expression, location and activity of transporters (49). *Hilgendorf et al* compared the expression profile of 36 transporters (related or relevant for drug transport) in HepG2 and human liver and both qualitative and quantitative differences were found (283). A study performed by *Ulvestad et al* revealed decreased levels of mRNA for BSEP, MDR1, NTCP and OATP1B1 in HepG2 cells and other hepatocellular models with respect to the levels observed in primary cultured human hepatocytes (284). Moreover, OATP1B1 and NTCP showed low levels of activity in HepG2 cells that were correlated with a cytoplasmic localization instead of a membrane localization of the transporters (284).

In contrast to HepG2 cells, hepatocytes cultured in a collagen sandwich configuration reestablish cell polarity and tight junctional complexes, leading to the formation of sealed bile canaliculi (285, 286). Therefore, sandwich-cultured hepatocytes are the most commonly used cellular model for BA uptake and efflux studies and to identify hepatotoxicity associated to drugs that cause iatrogenic cholestasis (287, 288). As an alternative to the use of primary cultured hepatocytes, HepaRG cell line has shown its potential in the study of the mechanisms involved in the development of drug-induced cholestasis (289-291). However, although no consistent results were obtained with the selected drugs and no characteristic pattern associated to cholestasis in HepG2 cells was defined, our analytical conditions were able to identify metabolomic alterations besides the ones directly associated to cholestatic injury and consistent with the information available in the literature.

## Results & Discussion

### Metabolomic changes associated to phospholipidogenic insult

Five model hepatotoxic drugs causing phospholipidosis as main mechanism of toxicity were used in the study (**Table 2.2**): amiodarone, clozapine, fluoxetine, tilorone and tamoxifen. Phospholipidogenic drugs induced changes in 65 identified metabolites. A pathway enrichment analysis showed that PL metabolism, unsaturated FA metabolism, urea cycle, aminoacid metabolism and glutamate and GSH metabolism were the most affected pathways as a result of the treatment with phospholipidogenic drugs (**Figure 3.18**).

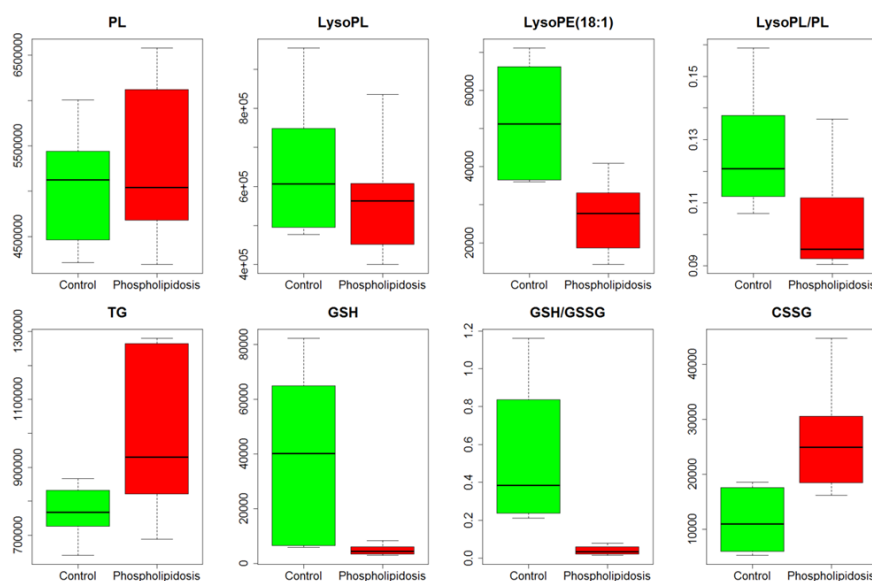


**Figure 3.18.** Boxplots showing the most important changes associated to HepG2 cells treated with phospholipidogenic drugs and analyzed following the untargeted metabolomic strategy. Values are expressed as relative intensity. Boxes denote interquartile ranges, lines denote medians, and whiskers denote the 10th and 90th percentiles.

## Results & Discussion

---

A slight increase in the PL levels and a slight decrease in the LysoPL levels in the phospholipidosis group were observed. However, it is noteworthy to point out the decrease in the most abundant LysoPE, LysoPE(18:1), and the decrease in the LysoPL/PL ratio. Moreover, a slight increase in the amount of TG was also detected (**Figure 3.18**). With respect to polar metabolites, the most remarkable changes were associated with the appearance of OS markers (i.e. increased levels of CSSG and decreased levels of GSH and the ratio GSH/GSSG) (**Figure 3.18**).

The most characteristic alteration associated to phospholipidosis is an excessive accumulation of PL; however, such hallmark was not reproduced under our experimental conditions (24h incubation with sub-lethal concentrations of the drugs) and only slight but non-significant increases in PL were observed in HepG2 cells. Phospholipidosis is a chronic process and PL accumulation in the liver is only observed after long-term/repeated treatments with the drug (32). The observed decrease in LysoPL and in the LysoPL/PL ratio can be interpreted as an inhibition of the degradation of PL that ultimately would lead to their excessive accumulation (**Figure 3.16**). It is well known that drugs inducing phospholipidosis, especially CADs, inhibit lysosomal phospholipase activity (292, 293). Indeed, inhibition of phospholipases A1, A2 and C by CADs has been observed both *in vitro* and *in vivo* (294, 295) and a dose dependent inhibition has been reported in the case of amiodarone (296, 297). The mechanism responsible of this inhibition is unknown. It has been suggested that the drug can bind to PL, thus resulting in the formation of complexes that are either resistant to breakdown or can act as enzyme (phospholipase) inhibitors (294). As an alternative mechanism, the accumulation of phospholipidosis-inducing drugs (usually cations) can neutralize the anionic surface charge in lysosomal lipid bilayers required by phospholipase activity (298). Besides this simple and attractive view of the problem, recent studies have suggested that not only impaired phospholipase activity, but also

## Results & Discussion

---

alterations in lysosomal enzyme transport and PL or cholesterol biosynthesis are mechanisms likely involved in the development of drug-induced phospholipidosis (71).

Besides the alterations in PL and LysoPL levels, increases in TG and OS markers were also observed in HepG2 cells treated with phospholipidosis-inducing drugs (**Figure 3.18**). It is known that some drugs that cause phospholipidosis (especially CADs) can also induce mitochondria damage and steatosis (299, 300) and manifestations such as impaired lysosomal protein degradation, decreased pinocytosis and endocytosis, and increased free radical formation have also been reported in studies using *in vitro* models (37, 301, 302). *Alakoskela et al* suggested that drug (CAD)-lipid interactions may lead to changes in lipid-dependent protein activities not only in lysosomes, but also in other cellular compartments (303). In particular, the complex structure and physicochemical characteristics of mitochondria (e.g., double membrane, mitochondrial membrane potential) facilitate the progressive accumulation of CADs, thus damaging their function (32, 303).

### **3.3.2 Development of a metabolomic approximation focused on the detection of lipidomic alterations induced by steatogenic and phospholipidogenic drugs**

Our general untargeted metabolomic analysis strategy allowed us to detect metabolic alterations in HepG2 cells treated with drugs inducing steatosis or phospholipidosis (**Figures 3.15, 3.18**). These results showed that although the drugs induced important alterations in the metabolome which can be directly associated to a particular mechanism of toxicity, only early markers of toxicity were detected. For example, in the case of phospholipidosis a decrease in the LysoPL/PL ratio (**Figure 3.18**) was observed, which can be directly related to the mechanism of

## Results & Discussion

---

toxicity, however, no significant increases in the total content of PL, or particular classes of PL, were detected.

Steatosis and phospholipidosis-inducing drugs usually require chronic treatments to show their characteristic clinical manifestations (32). Therefore, we decided to apply a new experimental design that favored a faster development of the toxic events associated to phospholipidosis and steatosis. *Gomez-Lechón et al* studied the fat accumulation dynamics in HepG2 cells as a function of the concentration and composition of free FAs in the culture medium (193). *Donato et al* adapted this strategy to develop an experimental design in which a low concentration of free FAs is provided to cultured cells to serve as an external source of FA that facilitates and accelerates the evolution of the toxic insult (88). Palmitic (FA(16:0)) and oleic (FA(18:1)) acids are the most abundant free FAs in the liver in both normal subjects and patients with NAFLD (268). Thus, HepG2 cells were pre-incubated for 14 h with a mixture of FA (62  $\mu$ M 2:1 ratio of oleate and palmitate) before being exposed to drugs (88). As the main alterations associated to phospholipidosis and steatosis were found in the lipidome (**Figures 3.15, 3.18**), our new analytical strategy was focused on the analysis of lipidic species (see **Section 2.8.2** for detailed information).

**Figure 3.19.A-B** show the scores plots corresponding to the PCA analysis performed by comparing the lipidomic profiles of HepG2 cells treated with control compounds vs HepG2 cells treated with phospholipidogenic or steatogenic drugs, respectively. The clear separation in the PCA scores plots between control and treated cells suggests that the experimental design and analytical strategy were appropriate for the detection of phospholipidosis and steatosis-induced alterations. Moreover, **Figure 3.19.C** shows the PCA scores plot corresponding to the three groups included in the study. Three different clusters are observed, one corresponding to each different class (i.e. control, phospholipidosis and steatosis). The first component seems to



## Results & Discussion

be describing the differences caused by steatogenic drugs, while the second component describes the separation of the phospholipidogenic ones. Therefore, the proposed experimental design seems to be suitable to differentiate not only between control and treated samples, but even a non-supervised analysis such a PCA was able to detect that steatosis and phospholipidosis-inducing drugs provoked different alterations in the lipidome of HepG2 cells previously incubated with a mixture of free FAs.

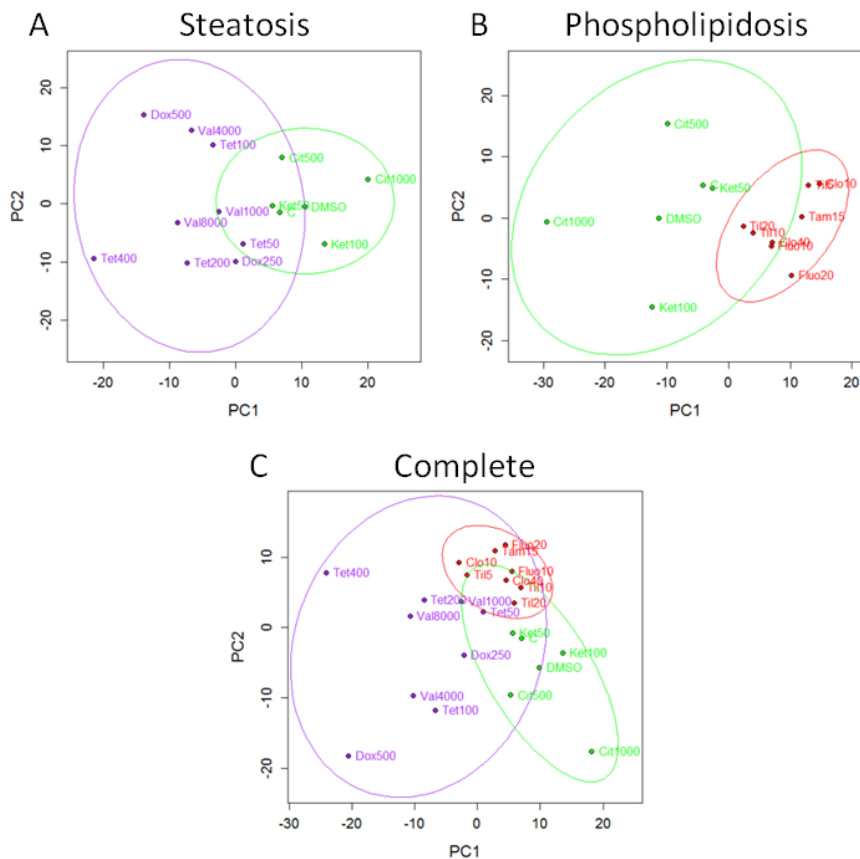


**Figure 3.19.** PCA scores plots corresponding to the lipidomic analysis of HepG2 cells preloaded with a mixture of free FAs and treated with phospholipidogenic and steatogenic compounds. **A)** Control (green) vs phospholipidosis (red). **B)** Control (green) vs steatosis (purple). **C)** All groups together. All the PCA analysis were performed using only two PCs. The lines denote 95 % confidence interval Hotelling's ellipse..

## Results & Discussion

---

### Alterations in the lipidome

The new experimental conditions (cells pre-incubated with a FA mixture) reproduced all the changes previously observed in the lipidome of cells treated with the drugs in absence of an external source of FAs (**Figures 3.15, 3.18**), but additional metabolite alterations were observed (**Figures 3.20, 3.21**). In general, the differences found in cells cultured in standard medium (without FA) were subtle and indicative of a very early stage of hepatotoxicity, whereas the changes observed in cells pre-incubated with FA were more extensive and indicative of a more advanced damage.

The supplementation of culture medium with FA facilitated PL accumulation (the hallmark of phospholipidosis) in HepG2 cells treated with phospholipidosis-inducing drugs. Increased levels of PC, PE and PS were observed as well as a subtle increase in the levels of PI and PG (**Figure 3.20**). The decrease in LysoPL content was more evident with lowered levels of both LysoPC and LysoPE, thus resulting in a decrease in the LysoPC/PC and LysoPE/PE ratios. Besides these changes in the phospholipidome, increases in TG, ceramides and SM levels were also produced (**Figure 3.21**). The increased levels of different lipids, and PL in particular, are in agreement with previous reports found in the literature. *Baronas et al* found several types of PL altered in urine from rats treated with different compounds inducing phospholipidosis (304). Notable increase in PC and PE, primary substrates for PLA2, as well as PS were described in MDCK cells treated with amiodarone or D-threo-1-phenyl-2-decanoylamino-3-morpholino-propanol, whereas no changes in PI levels were found (297). These changes were consistent with the known substrate specificity of PLA2 (297). Our results showing decreased levels of LysoPC, LysoPE, LysoPC/PC and LysoPE/PE (**Figure 3.20**) are also in concordance with a diminished hydrolytic activity of PLA2, although other potential mechanism explaining PL over accumulation cannot be

## Results & Discussion

discarded (32, 37). Finally, a previous study in HepaRG cells exposed to amiodarone for 2 weeks showed strong increases in PE and PC levels and moderate increases in SM, PI, PS and TG (107). Interestingly, by using our experimental strategy a similar pattern of PL alterations was detected in HepG2 cells shortly exposed to amiodarone and other phospholipidosis inducers (**Figures 3.20, 3.21**), evidencing the utility of this approach to the study the early stages of drug-induced phospholipidosis.

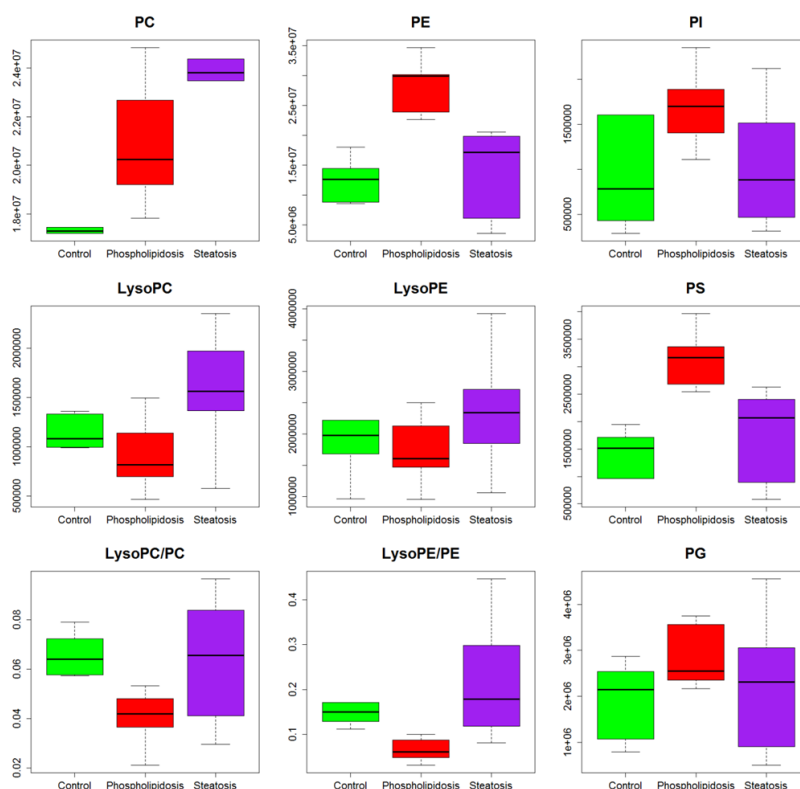


**Figure 3.20.** Boxplots showing the changes induced in the levels of PLs and LysoPLs as a result of the treatment with steatosis and phospholipidosis-inducing drugs in HepG2 cells previously incubated with a mixture of free FAs. Values are expressed as relative intensity. Boxes denote interquartile ranges, lines denote medians, and whiskers denote the 10th and 90th percentiles. Green: control; Red: phospholipidosis; Purple: steatosis.

## Results & Discussion

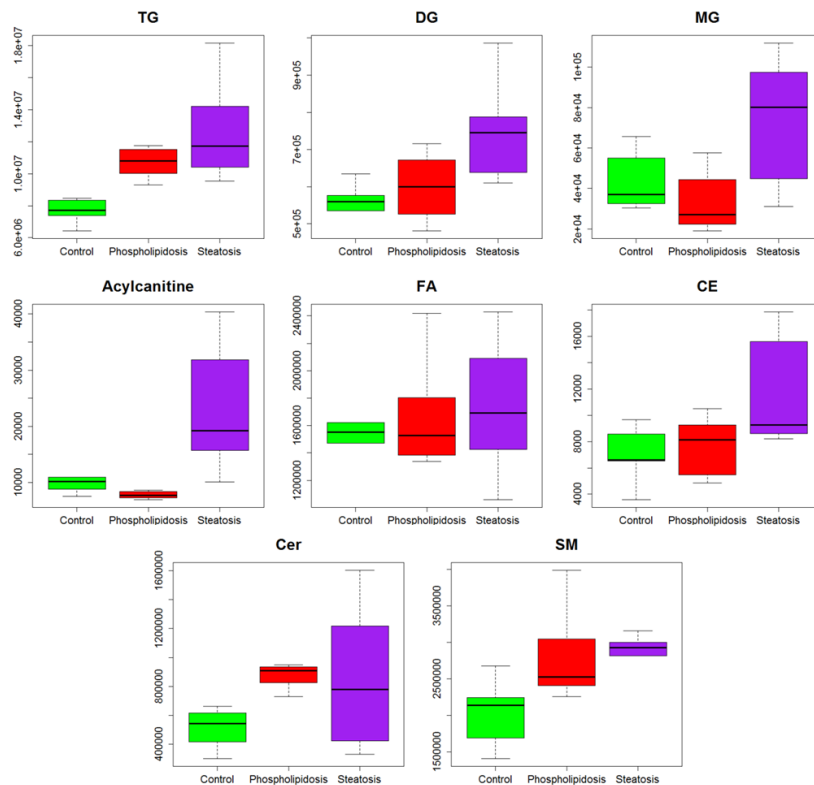


**Figure 3.21.** Boxplots showing the changes induced in the lipidome (except phospholipids) as a result of the treatment with steatosis and phospholipidosis-inducing drugs in HepG2 cells previously incubated with a mixture of FA. Values are expressed as relative intensity. Boxes denote interquartile ranges, lines denote medians, and whiskers denote the 10th and 90th percentiles. Green: control; Red: phospholipidosis; Purple: steatosis.

In relation to steatogenic drugs, the presence of an external source of free FA in combination with a lipidomic focused analysis allowed the detection of changes not previously observed in the generic analysis (cells cultured in absence of FA supplement). Thus, besides the increase in TG and DG, an increase in the levels of MG, acylcarnitines, ChE, ceramides and SM was also observed (**Figure 3.21**). A detailed analysis of the phospholipidome revealed that only the levels of PC (the most abundant PL inside the cells) were increased by steatosis inducers, while

## Results & Discussion

---

the levels of the rest of PL did not show any significant change (**Figure 3.20**). This suggests a contribution of *de novo* synthesis of PC via the CDP-choline pathway as a result of the elevated levels of DG and phosphocholine (274, 275) (**Figures 3.15, 3.16**). A higher increase in the levels of both LysoPC and LysoPE was also found (**Figure 3.20**). Drug-induced steatosis is characterized by TG accumulation, mainly, but not exclusively, due to FA oxidation impairment as a result of mitochondrial disturbances (29, 32, 34, 35). The result of this situation is the accumulation of both intermediates of FA oxidation, such as acylcarnitines, and of TG synthesis, such as MG, and DG (**Figures 3.16, 3.21**). Similar results have been previously reported in humans, animal and cell-based models of steatosis (106, 154, 248, 250, 268). Besides the expected alterations related to FA metabolism and TG synthesis, increased levels of ceramides and SM were also observed (**Figure 3.21**). Ceramides are complex lipids composed of sphingosine and a FA. Ceramides further combine with phosphocholine forming SM, the major sphingophospholipid in humans. Ceramides can also be rapidly generated from SM by sphingomyelinase induced hydrolysis (305, 306). Previous reports have found elevated hepatic levels of ceramides in fatty liver disease (248, 307, 308) and increased levels of sphingosine, the precursor in ceramide synthesis, in FA overloaded HepaRG cells (154).

It is well described that the degree of saturation of free FAs has a strong effect on the tendency of the cells to store them as TG, while unsaturated FAs are more likely incorporated into TG, their saturated counterparts are channeled towards other cellular fates (258). Thus steatosis- and cytotoxicity-inducing properties of palmitic and oleic acids are different, while the steatogenic capacity of oleic acid is higher, palmitic acid induces a higher cytotoxicity as it remains as a free FA (193). Our results showed that when HepG2 cells pre-treated with the oleic and palmitic acids mixture were exposed to model steatogenic drugs, there was an intracellular accumulation of palmitic acid (FA(16:0)),

## Results & Discussion

whereas a decrease in the levels of oleic acid (FA(18:1)) was observed (**Figure 3.22**). Accordingly, the levels of SM and TG containing only FA(16:0) and FA(18:1) moieties showed a higher increase for those species incorporating a higher proportion of oleate (**Figure 3.22**). Thus, the fold of change for SM follows the tendency  $SM(d36:2) > SM(d34:1) > SM(d32:0)$ . With respect to TG, the same tendency was observed:  $TG(54:3) > TG(52:2) > TG(50:1) > TG(48:0)$  (**Figure 3.22**).

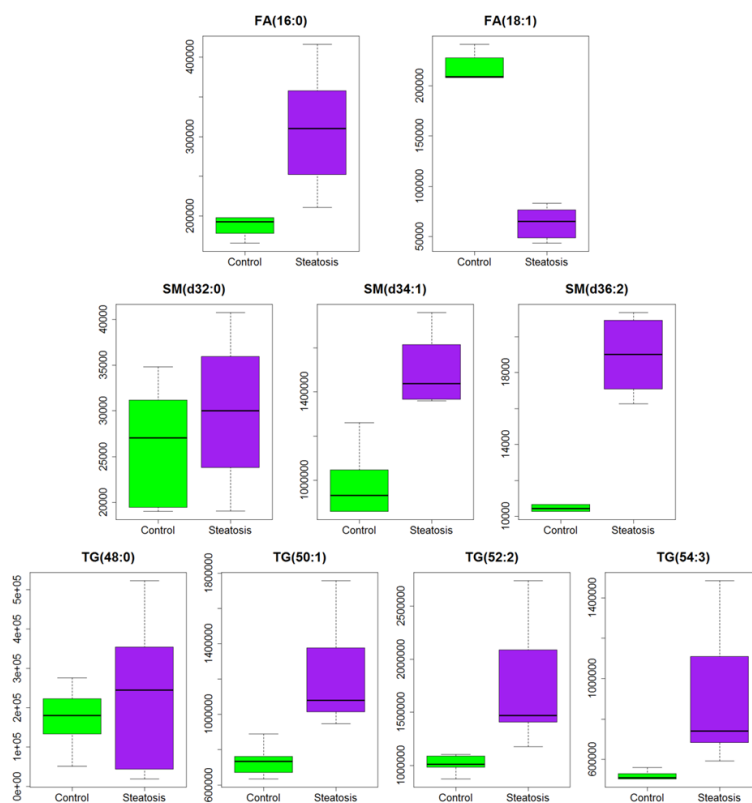


**Figure 3.22.** Boxplots showing the differences in palmitic and oleic acid distribution in lipidic species as a result of drug-induced steatosis in HepG2 cells pre-incubated with a mix of palmitic and oleic acids and analyzed using a lipidomic strategy. Boxes denote interquartile ranges, lines denote medians, and whiskers denote the 10th and 90th percentiles. Green: control; Purple: steatosis.

## Results & Discussion

---

The combined use of a lipidomic-specific chromatographic separation in combination with high mass-resolution MS allowed us to describe not only changes in the total amount of lipids or TG, as is the case of enzymatic- or fluorescence-based methods, but to provide a more detailed description and a deeper understanding of the changes induced in specific species of lipids.

### *Alterations in the levels of lipidic species containing only FA(16:0) and/or FA(18:1) moieties*

The follow up of the compounds provided to the cells represents an appealing option to the development of target analyses to evaluate the evolution of the hepatotoxic damage. Palmitic and oleic acids can be directed to different cell metabolic pathways. They can be converted into other FA by desaturases and elongases (248, 269) or can be incorporated into the different lipid classes that compose the lipidome (**Figure 3.16**). This information could be obtained by deuterium-labeled FA incubations or acyl-CoA desaturase/elongase activity measurement. We propose a simpler approximation based on the comparative analysis of the different types of lipids containing only palmitic or oleic acid moieties. **Table 3.3** shows a good concordance between the changes in the total levels of each of the lipidic species detected and the changes observed for those species containing only palmitic and oleic acid moieties. While the fold of change for specific species (i.e. those containing only palmitic or only oleic acid as moieties) might differ, the average value for all the species containing only palmitic and/or oleic acid as components provided similar results than the average of all the different combinations of FA for a given lipid class. Therefore, the evaluation of those lipidic species containing only palmitic and/or oleic acid as moieties constitutes a good option for the development of targeted analysis that would result in the generation of quantitative results and

## Results & Discussion

the save of both time and economical resources, while providing a representative snapshot of the alterations produced in the lipidome.

**Table 3.3.** Values of fold of change for control vs treated cells for each of the lipid classes and treatments indicated. The values correspond to the lipidomic analysis of HepG2 treated either with steatogenic or phospholipidogenic compounds in the presence of an external source of FA. 16:0 column corresponds to lipidic species containing only the FA(16:0). 18:1 column corresponds to lipidic species containing only the FA(18:1). Mean column correspond to the mean value obtained for those lipidic species containing only FA(16:0) and/or FA(18:1) moieties. Total corresponds to the mean value obtained for all the species of a given class.

	Phospholipidosis				Steatosis			
	16:0	18:1	Mean	Total	16:0	18:1	Mean	Total
Acylcarnitine	0.99	0.95	0.97	0.86	2.70*	2.69*	2.7*	2.45*
ChE	1.03	1.1	1.08	1.1	2.08**	1.99*	2.03**	1.64*
Cer	n.d.	0.89	2.09***	1.75***	n.d.	3.74***	2.28*	1.15*
DG	1.24	1.47	1.31	1.11	1.40*	1.38*	1.33*	1.3**
FA	1.46**	0.33***	0.88	1.05	1.56**	0.31***	0.92	1.08
LysoPC	0.73*	0.82	0.77*	0.80*	1.45*	1.43*	1.44*	1.56*
LysoPE	1.18	1.02	1.07	0.93	1.54	1.25	1.33	1.23
MG	0.65*	0.79	0.74	0.77	1.57*	1.69*	1.65*	1.96*
PC	1.85**	1.19*	1.25**	1.20**	1.7*	1.42**	1.54**	1.28**
PE	2.38***	2.78***	2.59***	2.25***	1.1	1.2	1.16	0.64
PG	1.99***	2.12*	1.9*	1.83*	1.57	0.87	1.11	0.79
PI	n.d.	2.53**	2.45**	1.14	n.d.	0.81	0.9	0.66
PS	n.d.	2.52***	2.52***	2.17***	n.d.	1.28	1.28	0.73
SM	1.1	1.17	1.42*	1.35*	1.13	1.94***	1.73***	1.26**
TG	1.69	1.28**	1.31**	1.40***	1.31	1.76**	1.67*	1.45**

Comparisons between control and each treatment were performed using a Student t test. \*: p value < 0.05; \*\* p value < 0.01; \*\*\* p value < 0.001.



## Results & Discussion

---

### 3.3.3 Targeted analysis of OS markers

The untargeted analysis of HepG2 exposed to hepatotoxic compounds (**Section 3.3.1**) revealed that the presence of OS markers is a common hepatotoxicity event, even in the case of hepatotoxins whose primary mechanism of toxicity is not directly related to OS (29, 88, 89, 92). In order to achieve a deeper insight in the involvement of OS in hepatotoxicity, a quantitative targeted analytical method aimed to determine a set of well-known OS biomarkers was developed in our laboratory (209). The markers included in the method are: i) sulfur-containing substances, as GSH, GSSG, SAM and SAH (214, 309); ii) phenylalanine (310) and tyrosines I-Tyr, N-Tyr, Cl-Tyr, o-Tyr, m-Tyr and p-Tyr as markers of oxidative protein damage (311, 312); iii) 8-OH-dG and 2-dG, which indicate DNA damage (313), iv) MDA, which indicate peroxidation (314); and v) ophthalmic acid, that indicates GSH consumption (138).

The targeted analysis was applied to a set of four compounds that induce hepatotoxicity through different mechanism (tert-butyl hydroperoxide (OS), amiodarone (phospholipidosis), tetracycline (steatosis) and cyclosporine (cholestasis)) and with previous reports of OS and mitochondrial impairment (29, 88, 89, 91, 92, 291). Among the OS markers analyzed, GSH/GSSG ratio, ophthalmic acid and MDA were significantly altered following a dose-dependent tendency **Figure 3.23**.

## Results & Discussion

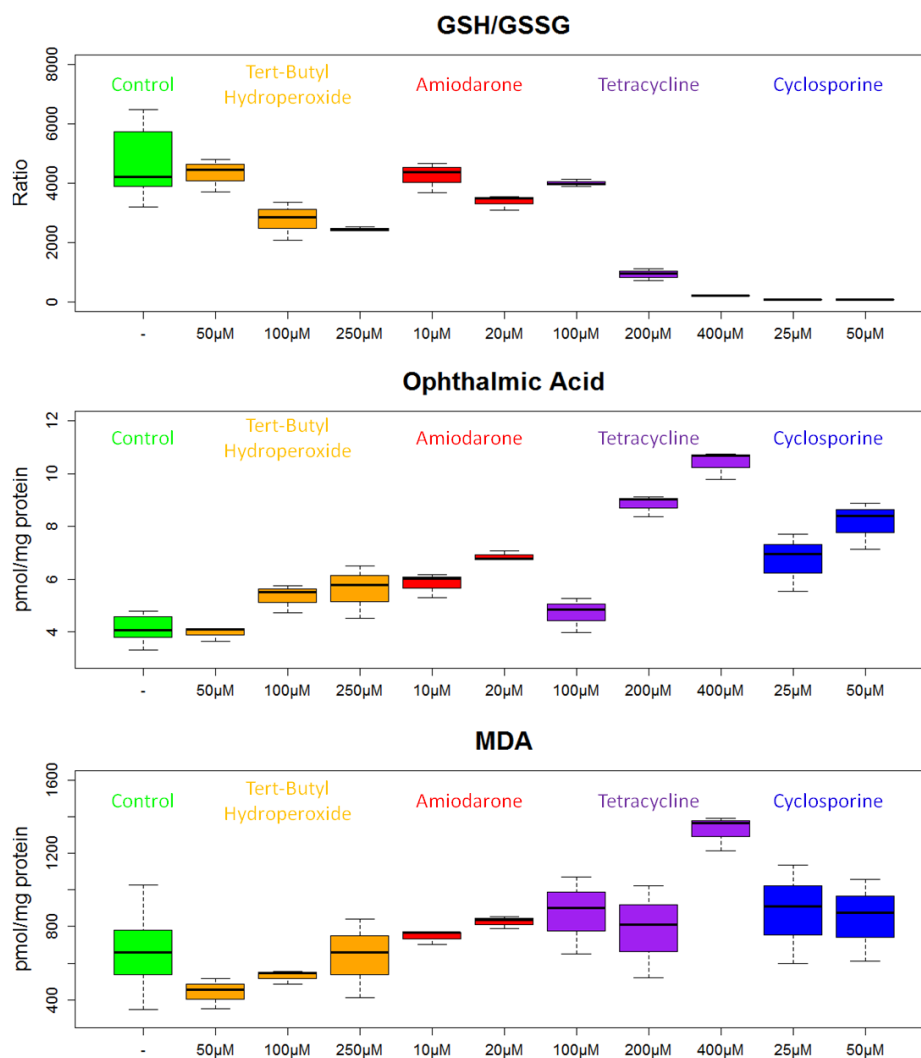


**Figure 3.23.** Boxplots showing the results obtained with the targeted analysis of OS markers (GSH/GSSG, upper panel; ophthalmic acid, middle panel; and MDA, lower panel) for HepG2 cells treated with control compounds (green), tert-butyl hydroperoxide (orange), amiodarone (red), tetracycline (purple) and cyclosporine (blue). Boxes denote interquartile ranges, lines denote medians, and whiskers denote the 10th and 90th percentiles. The value in the x-axis denotes the concentration at which the indicated compound has been employed.

## Results & Discussion

---

As expected, all compounds induced a concentration-dependent decrease in the GSH/GSSG ratio (**Figure 3.23**). These results confirm the tendency of a decreased GSH/GSSG ratio observed in the untargeted analysis (**Figures 3.12, 3.15, 3.17, 3.18**) and are in agreement with those previously reported for both OS as a primary (209, 236, 237) and secondary (88, 140, 279, 315) hepatotoxic damage both *in vivo* and in liver-based cellular models.

An increase in the levels of ophthalmic, in parallel to the decrease in the GSH/GSSG ratio, was also observed for the four compounds (**Figure 3.23**). Ophthalmic acid was not detected using the untargeted analysis strategy, however the increased sensitivity provided by the UPLC/MS-MS targeted method allowed its detection and quantification. Ophthalmic acid ( $\gamma$ -glutamyl-2-aminobutyrate-glycine) is a nonsulfur-containing analog of GSH in which the cysteine moiety has been substituted by 2-aminobutyric acid. It shares the same biosynthetic pathway than GSH: the first step in the synthesis of ophthalmic acid is the linking of 2-aminobutyrate to glutamate, a step catalyzed by GCS; subsequently, glycine is linked to this dipeptide via GS (138, 316, 317) (**Figure 3.13, 3.14**). Under OS conditions, the activity of the enzyme GCS is enhanced thus leading to an increased synthesis of ophthalmic acid (**Figure 3.14**). However, due to the lack of a thiol group, ophthalmic acid is not further metabolized under OS conditions and thus accumulates (138). Ophthalmic acid was first proposed as a marker of OS and GSH depletion by *Soga et al* (138). They found increased levels of ophthalmic acid in the liver and serum of mice treated with acetaminophen following a pattern that correlated with GSH depletion (138). Increased levels of ophthalmic acid have also been reported in THLE-2E1 cells and in the liver of rats treated with acetaminophen (140, 318). More recently, we have reported increased levels of ophthalmic acid in primary-cultured rat hepatocytes incubated for 24 h with 500  $\mu$ M cumene hydroperoxide and in the serum of patients suffering non-alcoholic steatohepatitis (209). It is not clear

## Results & Discussion

---

whether ophthalmic acid has any meaningful physiological role or it is simply a byproduct associated to GCS activation during OS (138, 316). Nevertheless, it has been shown that ophthalmic acid is able to competitively inhibit and trans-stimulate GSH transport in liver canalicular membranes (319), which can be interpreted as an adaptive mechanism to minimize GSH efflux during OS. Therefore, it has been hypothesized that it can act as a GSH analog for functions that do not require the presence of the thiol group (138).

Increased levels of MDA, a marker of lipid peroxidation, were observed in HepG2 cells treated with amiodarone, tetracycline or cyclosporine but not with tert-butyl hydroperoxide (**Figure 3.23**). Increased MDA levels have been reported in hepG2 cells shortly (3 h) treated with tert-butyl-hydroperoxide and hydrogen peroxide (211) but not after longer incubation (24 h) with the OS inducer cumene hydroperoxide (209). High MDA levels have been previously reported in HepG2 cells exposed to amiodarone (320), in the liver of rats administered cyclosporine (321, 322) and in the liver of patients with steatosis (209, 268). Moreover, increased lipid peroxidation has been previously described in liver mitochondria of rats previously administered amiodarone (315). Interestingly, amiodarone, tetracycline and cyclosporine have been previously described to induce mitochondrial impairment while tert-butyl hydroperoxide is considered a pure OS inducer (32, 88, 92). Amiodarone inhibits  $\beta$ -oxidation of FA (30, 323-325), inhibits complexes I, II, and III in the respiratory chain (315, 325, 326), uncouples oxidative phosphorylation (324, 327) and decreases mitochondrial membrane potential (325, 328). Tetracycline has been reported to inhibit  $\beta$ -oxidation (323, 329, 330) and cyclosporine inhibits  $\beta$ -oxidation (280, 281) and complexes I and II (331). Therefore, the oxidative damage produced by amiodarone, tetracycline or cyclosporine is secondary to other hepatotoxic effects, thus resulting in a delayed appearance of the OS markers and a situation that is more likely to become chronic and

## Results & Discussion

---

amplified. In contrast, tert-butyl hydroperoxide is able to induce OS by itself and its effects are detected shortly after exposure (209).

### 3.3.4 Development of predictive/classificatory models of hepatotoxicity

One of our goals was to develop a model able to predict and classify the potential hepatotoxicity of new drug candidates. Thus, firstly, we considered the development of a model aimed to discriminate between non-toxic and hepatotoxic compounds. Secondly, we tried to develop a more sophisticated model aimed to discriminate among the different mechanisms of toxicity included in our study. Cholestasis was not considered to develop the model and finally four different classes (i.e. control, OS, phospholipidosis and steatosis) were used.

Predictive models were built using PLS-DA and a bootstrapped strategy coupled to VIP ranking to order and select variables according to their importance in the model, fitting and predictive (predictability) capacity. The optimum number of variables was selected as the one that provided the highest figures of merit (accuracy and AUROC).

#### Predictive model for the discrimination between non-toxic and hepatotoxic compounds

Here the objective was to develop a mathematical model able to classify between non-toxic and hepatotoxic compounds. CV was used to select the optimum number of LVs in the PLS-DA model. Based on the values of  $R^2$ ,  $Q^2$  and misclassification error, two LVs were selected (**Figure 3.24.A**). After fixing the number of LVs, the variables were ranked according to their importance in the model. The results of model performance (evaluated based on AUROC and misclassification error) vs

## Results & Discussion

the number of retained variables included in the model are shown in the **Figure 3.24.B**.

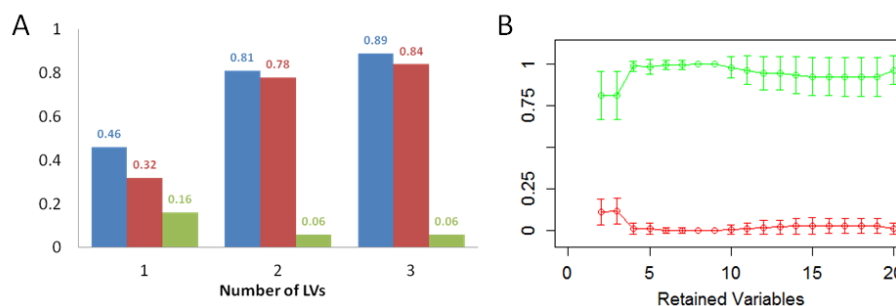


**Figure 3.24.** **A)** Values of  $R^2$  (blue),  $Q^2$  (red) and misclassification error (green) as a function of the number of LVs employed to build the PLS-DA model using all the variables from the data obtained with the generic untargeted metabolomic analysis of HepG2 treated with either non-toxic or hepatotoxic compounds. The values obtained for each parameter and model are written over the corresponding bar. **B)** Values obtained for the AUROC (green) and misclassification error (red) vs the number of retained variables for the top-20 ranked variables using PLS-DA models with two LVs. The data is expressed as mean  $\pm$  standard deviation.

A perfect classification (AUROC = 1, misclassification error = 0) was obtained using only 8 variables (i.e. adenine, FA(20:4), LysoPC(18:2), FA(22:6), phosphocholine, GMP, FA(20:3) and LysoPE(24:1)). The PLS-DA scores and loadings plot corresponding to the model developed using 2LV and 8 retained variables are shown in **Figure 3.25**. A clear separation was observed between non-toxic and hepatotoxic compounds, with no overlap between the 95 % confidence interval Hotelling's ellipse drawn for each of the classes (**Figure 3.25.A**). The loadings plot revealed that only 2 of the 8 variables included in the final model showed a positive correlation with the onset of hepatotoxicity (i.e. adenine and phosphocholine) (**Figure 3.25.B**), whereas the remaining 6 variables correlated with the assignment to the non-toxic group. The model retrieved good figures of performance based on CV:  $R^2 = 0.82$ ,  $Q^2$

## Results & Discussion

= 0.81, misclassification error = 0.00 and AUROC = 1. Moreover, a permutation test was also performed in order to further validate model consistency and performance (133). No overlap was obtained between the actual figures estimated using CV and the distribution of values calculated for the permuted models (**Figure 3.25.C-D**).

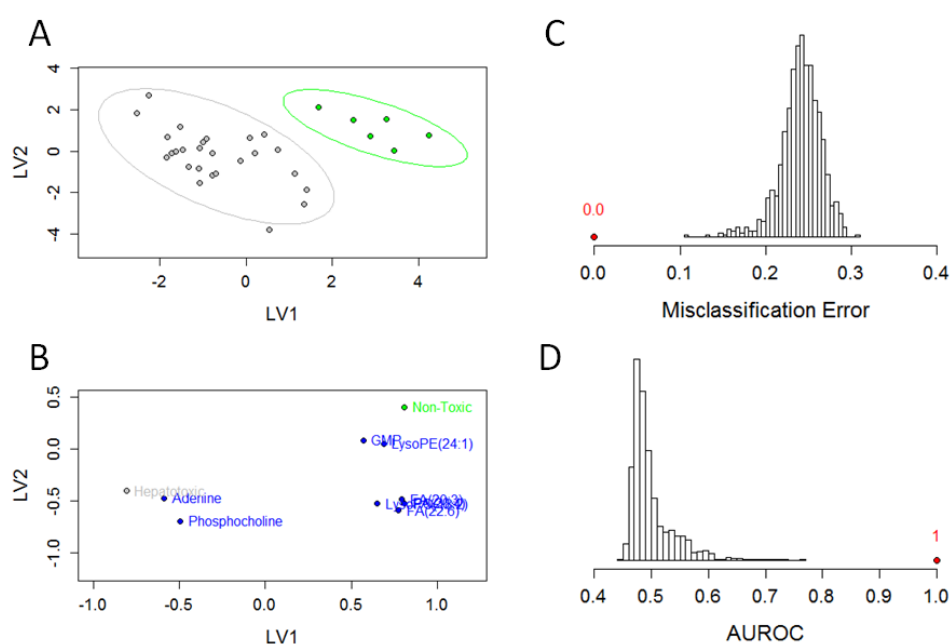


**Figure 3.25.** Summary of the results provided by the PLS-DA model built using 2 LVs and the top-ranked 8 variables based on the data obtained with the generic untargeted metabolomic analysis of HepG2 treated with either non-toxic or hepatotoxic compounds. **A)** Scores plot. The lines denote 95 % confidence interval Hotelling's ellipse for each class. Green: non-toxic; Grey: hepatotoxic **B)** Loadings plot. Green: non-toxic; Grey: hepatotoxic; Blue: metabolites. **C)** Permutation test for the misclassification error. **D)** Permutation test for the AUROC. In both cases the histograms represent the values obtained using the permuted classes. The actual value obtained with the real classes is indicated by the red dot and the value written above it.

## Results & Discussion

---

The results obtained for the PLS-DA model suggest that our experimental and data analysis strategies represent a good option to discriminate hepatotoxic and non-hepatotoxic drugs. However, the validation methods were based only on CV and permutation testing and only a limited number of model hepatotoxins were included in the study, what would result in overoptimistic results.

The present model, constitute the first metabolomic-based strategy to discriminate hepatotoxic compounds in human hepatic cells in culture. Several examples of the development of predictive models of hepatotoxicity are available in the literature. Both *in vivo* and *in vitro* assays based on the analysis of traditional cytotoxicity end points (e.g. ATP content, lactate dehydrogenase (LDH) release, urea syntesis...) (332), transcriptomics/gene expression (64, 333, 334), proteomics (62, 78, 335) and HCS (52, 87, 90, 93, 336, 337) have been proposed. Among them, the combined used of *in vitro* liver-based cellular models and HCS is the most popular strategy. HCS assays are usually performed in 96-well or 386-well formats, what allows for high throughput analyses and, therefore, large lists of compounds have been tested. Cell count, ROS generation, mitochondrial damage, lipid accumulation and intracellular calcium are the most commonly parameters analyzed by HCS assays (338). With respect to their predictive capabilities, high specificity values (~90%) but sensitivity values ranging from 50 to 90% have been reported (338). This low sensitivity, specially associated to drugs that do not induce cell death or even in the case of non-proliferative cellular models, constitute an important drawback (338).

An important advantage of metabolomics, compared to other screening methods, is the detection of early metabolic alterations that occur in absence of cell death. However, to be competitive with respect to techniques such as HCS a higher number of hepatotoxins must be tested in order to identify a set of highly reliable markers of toxicity. Then, the development of quantitative targeted analysis of selected



## Results & Discussion

markers would considerably increase sample throughput and minimize sample requirements.

### Predictive model for the discrimination of specific mechanisms of hepatotoxicity

After the development of a classificatory model to discriminate between hepatotoxic and non-hepatotoxic compounds, our next goal was to develop a model able to discriminate among the different mechanism of toxicity. Using a CV strategy the optimum number of LV to develop the PLS-DA model was set to three (**Figure 3.26.A**). Then the model performance (evaluated based on AUROC and misclassification error) vs the number of retained variables included in the model was assessed (**Figure 3.26.B**).

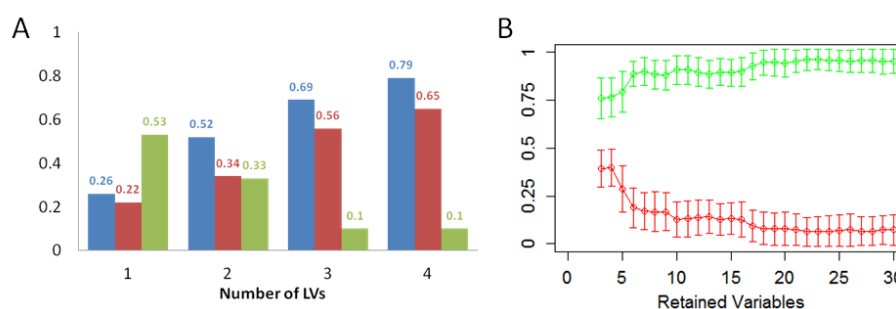


**Figure 3.26. A** Values of R<sup>2</sup> (blue), Q<sup>2</sup> (red) and misclassification error (green) as a function of the number of LVs employed to build the PLS-DA model using all the variables from the data obtained with the generic untargeted metabolomic analysis of HepG2 treated with either non-toxic or hepatotoxic compounds acting through different mechanism of hepatotoxicity (i.e. OS, phospholipidosis and steatosis). The values obtained for each parameter and model are written over the corresponding bar. **B** Values obtained for the AUROC (green) and misclassification error (red) calculated using CV vs the number of retained variables for the top-30 ranked variables using PLS-DA models with three LVs. The data is expressed as mean  $\pm$  standard deviation.

## Results & Discussion

The maximum value of AUROC and minimum value of misclassification error were obtained using the top 22 ranked variables (i.e. adenine, GSH, LysoPC(20:0), GSH/GSSG, LysoPC(18:2), phosphocholine,  $\gamma$ -glutamyl-glutamine, LysoPC(22:1), LysoPC(20:1), LysoPC(24:0), SM(d44:2), LysoPC(24:1), LysoPC(22:6), PC(44:11), LysoPC(26:1), FA(20:4), aspartic acid, carnitine(5:0), SM(d32:2), LysoPC(18:1), TG(60:8), and AMP). The final PLS-DA model rendered the following figures using CV:  $R^2 = 0.73$ ,  $Q^2 = 0.72$ , misclassification error =  $0.06 \pm 0.08$ , AUROC =  $0.96 \pm 0.05$ . The good values obtained with respect the AUROC and the misclassification error represent good indicators of the capabilities of the PLS-DA model.

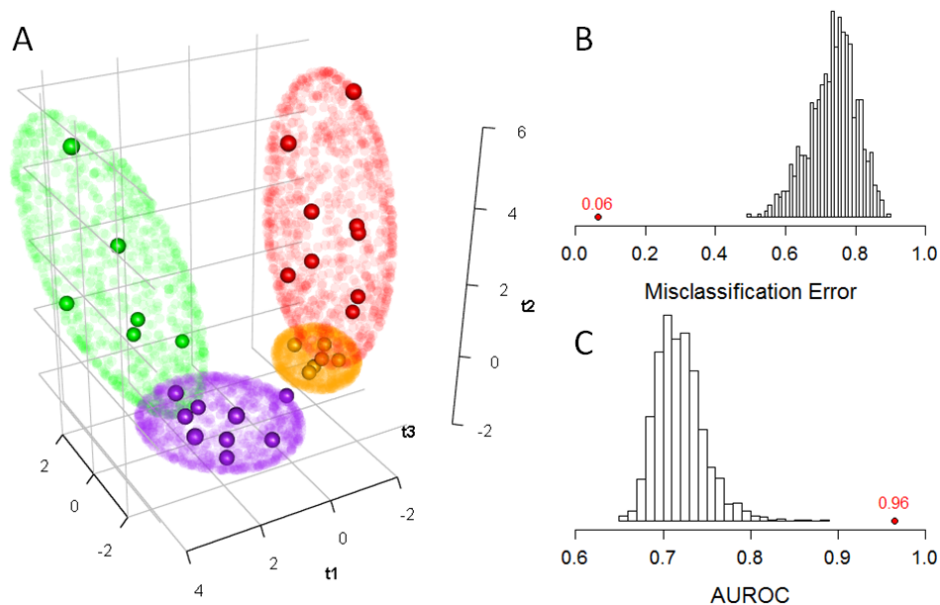


**Figure 3.27.** Summary of the results provided by the PLS-DA model built using 3 LVs and the top-22 ranked variables based on the data obtained with the generic untargeted metabolomic analysis of HepG2 treated with either non-toxic or hepatotoxic compounds acting through different mechanism of hepatotoxicity (i.e. OS, phospholipidosis and steatosis). **A)** Scores plot. The lines denote 95 % confidence interval Hotelling's ellipse for each class. Green: non-toxic; orange: OS; red: phospholipidosis; purple; steatosis. **B)** Permutation test for the misclassification error. **C)** Permutation test for the multiclass AUROC. In both cases the histograms represent the values obtained using the permuted classes. The actual value obtained with the real classes is indicated by the red dot and the value written above it.

## Results & Discussion

---

A good separation between the different groups is observed in the PLS-DA scores plot (**Figure 3.27. A**), and there is almost no overlap between the 95 % confidence interval Hotelling's ellipses drawn for each class. The model was further validated using a permutation test strategy with excellent results, as no overlap was obtained for values obtained using the permuted classes and the real values obtained with the actual PLS-DA for the misclassification error (**Figure 3.27. B**) and the AUROC (**Figure 3.27. C**)

As previously discussed for the model aimed at the discrimination between non-hepatotoxic and hepatotoxic compounds, although the results obtained for the present PLS-DA model were very encouraging, they must be carefully analyzed as only a limited number of compounds were evaluated and no external validation was performed.

Only a few studies aimed at the classification/prediction of different mechanisms of toxicity have been reported in the literature (92, 332). The HCS-based assay developed by *Tolosa et al* aimed to screen and classify drugs according to their hepatotoxicity mechanism (apoptosis, genotoxicity, OS, mitochondrial damage and bioactivation) (92). To this end, cell viability, morphological nuclear changes, mitochondrial membrane potential, intracellular calcium concentration and OS were measured in HepG2 cells and a mean sensitivity of 90 % was obtained when evaluating the different mechanisms of toxicity (92). On the other hand, *Germano et al* employed sandwich-cultured rat hepatocytes and a combination of different techniques in order to distinguish between steatosis, phospholipidosis and cholestasis. The assay included biochemical assays (i.e. ATP content, LDH release, urea synthesis and albumin secretion), HCS (i.e. Mrp-2 mediated transport, neutral lipid accumulation and PL accumulation) and gene expression quantification (i.e. nuclear receptors, transporters and CYPs). Their results suggested that the strategy might be a suitable tool for the evaluation of phospholipidosis and cholestasis but not for steatosis (332).

## Results & Discussion

---

Our method was able to distinguish between non-toxic compounds and compounds inducing OS, steatosis and phospholipidosis. However, it failed in the evaluation of cholestatic drugs. As indicated above, identification of drug-induced cholestasis would require the use of liver-based cellular models that correctly express the transporters of interest (i.e. HepaRG or sandwich-cultured hepatocytes). However, and besides its limitations, our method supposes a valuable alternative to detect mechanism-specific alterations at subcytotoxic concentrations. Moreover, while the number of parameters evaluated simultaneously using other strategies such as HCS is highly limited (338), untargeted metabolomics allows to measure hundreds of signals that could be later ranked and selected. Similarly, targeted analysis allows the simultaneous quantification of dozens up to hundreds of compounds (103, 108). Finally, the applicability of the present strategy to routine toxicological evaluation and compound screening would be conditioned to the definition of set of reliable mechanism-specific markers to be quantified by the use of a LC-MS/MS targeted method.

### *Predictive model for steatosis and phospholipidosis based on lipidic species containing only FA(16:0) and/or FA(18:1) moieties*

As seen above, the changes induced in lipidic species containing only FA(16:0) and/or FA(18:1) were representative of the general changes induced in the lipidome by treatment with drugs inducing either phospholipidosis or steatosis (**Table 3.3**). Then, we decided to develop a predictive/classificatory model based on those lipidic species composed only by FA(16:0) and/or FA(18:1) moieties.

Using a CV strategy, the optimum number of LV to develop the PLS-DA model was set to two based on the values of  $R^2$ ,  $Q^2$  and misclassification error (**Figure 3.28.A**). The results of model performance (evaluated based on multiclass AUROC and misclassification error) vs the number of

## Results & Discussion

retained variables included in the model retrieved a maximum value of AUROC and minimum value of misclassification error for the model built using the top 8 ranked variables (i.e. Cer(d36:2), FA(18:1), SM(d36:2), LysoPC(16:0), PE(32:0), PE(36:2), PC(36:2), PC(34:1)) (**Figure 3.28.B**).

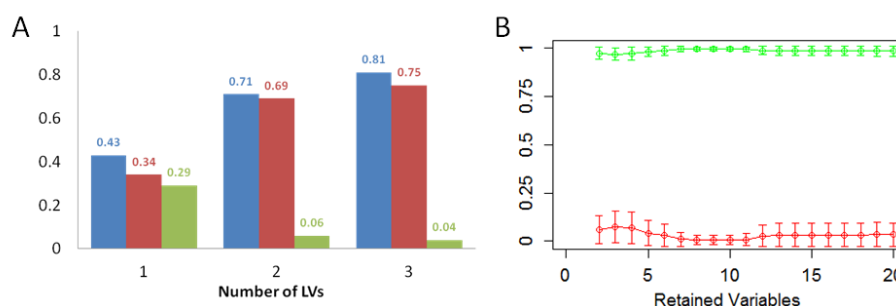


**Figure 3.28.** A) Values of R<sup>2</sup> (blue), Q<sup>2</sup> (red) and misclassification error (green) as a function of the number of LVs employed to build the PLS-DA model using all the variables from the data obtained with the lipidomic analysis of HepG2 treated with either non-toxic or hepatotoxic compounds inducing steatosis or phospholipidosis in the presence of an external source of FA, and using those lipidic compounds containing only FA(16:0) and/or FA(18:1) moieties. The values obtained for each parameter and model are written over the corresponding bar. B) Values obtained for the AUROC (green) and misclassification error (red) calculated using CV vs. the number of retained variables for the top-20 ranked variables using PLS-DA models with two LVs. The data is expressed as mean  $\pm$  standard deviation.

The final PLS-DA model rendered the following figures using CV: R<sup>2</sup> = 0.76, Q<sup>2</sup> = 0.73, misclassification error = 0.03  $\pm$  0.08, AUROC = 0.98  $\pm$  0.03. A good separation between the different groups was observed in the PLS-DA scores plot (**Figure 3.29.A**), with only a few overlap between the 95 % confidence interval Hotelling's ellipses drawn for steatosis and phospholipidosis. The first component was driven by the differences induced by steatogenic compounds and the second component described the separation between non-toxic and hepatotoxic compounds (in particular between phospholipidosis and control samples). The contribution of each of the variables included in the final model can be evaluated by their position in the loadings plot (**Figure 3.29.B**). FA(18:1)

## Results & Discussion

was associated to the assignment to control class, PE(32:0) and PE(36:2) to phospholipidosis, LysoPC(16:0), SM(d36:2) and Cer(d36:2) to steatosis and PC(34:1) and PC(36:2) to both steatosis and phospholipidosis. These results are in concordance with the alterations shown in **Table 3.3**. The model was further validated using permutation testing (**Figure 3.29.C-D**). No overlap was obtained between the values obtained using the permuted classes and the real values obtained with the actual PLS-DA for the misclassification error (**Figure 3.29.C**) and the AUROC (**Figure 3.29.D**) thus pointing the excellent consistency of the developed model.

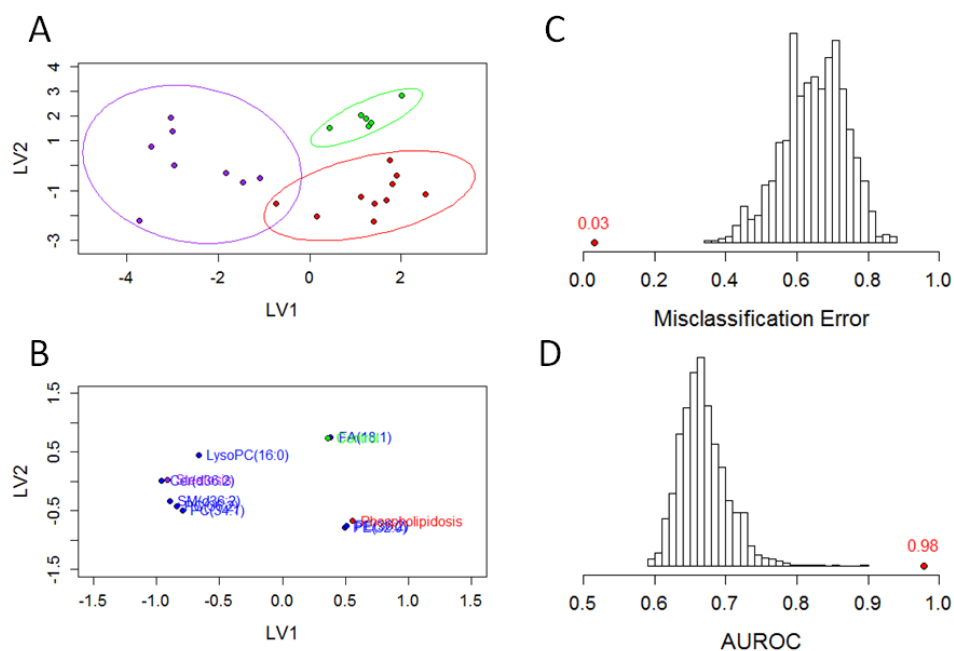


**Figure 3.29.** Summary of the results provided by the PLS-DA model built using 2 LVs and the top-ranked 8 variables based on the data obtained with the lipidomic analysis of HepG2 treated with either non-toxic or hepatotoxic compounds inducing steatosis or phospholipidosis in the presence of an external source of FA. **A)** Scores plot. The lines denote 95 % confidence interval Hotelling's ellipse for each class. Green: control; Red: phospholipidosis; Purple: steatosis. **B)** Loadings plot. Green: control; Red: phospholipidosis; Purple: steatosis; Blue: metabolites. **C)** Permutation test for the misclassification error. **D)** Permutation test for the AUROC. In both cases the histograms represent the values obtained using the permuted classes. The actual value obtained with the real classes is indicated by the red dot and the value written above it.

## Results & Discussion

---

The results reinforce the idea that the development of a targeted quantitative analysis of those species containing only palmitic and oleic acids as moieties (in cells pre-incubated with a palmitate/oleate mixture) might constitute a straightforward strategy for the prediction of drug-induced phospholipidosis and steatosis.

Different examples are available in the literature with respect to the prediction of drug-induced steatosis (69, 88, 89), phospholipidosis (71, 339-341) or both simultaneously (300, 332).

Two different approximations have been applied to the study of drug-induced steatosis in cultured cells, *Donato et al* performed an HCS analysis using HepG2 cells as model (88, 89). Among the different evaluated parameters, the combination of lipid accumulation (measured using BODIPY) and ROS generation was the one that provided the best performance (88, 89). On the other hand, *Benet et al* identified a series of transcription factors (i.e. FOXA, HEX and SBREP1C) whose expression levels in HepG2 cells might be used to predict drug-induced steatosis (69).

The gold standard confirmatory method for the detection of phospholipidosis is electron microscopy (342). However, the method is expensive, time consuming, and not dedicated to medium and high-throughput screenings. In addition, drug-induced phospholipidosis detected by electron microscopy could be discovered only after subchronic/chronic intake of compounds (343). Two alternative techniques, feasible to be adapted to high throughput, have arisen as an alternative: HCS and gene expression. HCS methods are usually based on the incorporation of fluorescent PL analog or a lipid-specific fluorescent dye (i.e. NBD-PE, NBD-PE, LipidTox, Nile red...) (339-341, 344, 345). Gene expression methods (71, 339, 341, 343) are based on the measure of the expression of 17 genes associated to phospholipidosis and previously identified by *Sawada et al* (71). Both methods provided high values of sensitivity and specificity (~90 %), however, it has been

## Results & Discussion

---

reported that HCS based assays allow multiplexing and a higher throughput (341).

The few studies that simultaneously evaluated steatosis and phospholipidosis (300, 332) reported unsatisfactory results with respect their capabilities to accurately classify steatogenic drugs.

In summary, our strategy based on the pre-incubation of the cells with a mixture of free FA achieved to accelerate the development of the hepatotoxic damage. Moreover the metabolomic analysis of the lipidomic alterations was able to detect events that occur in early stages of the toxic insult thus being able to differentiate between control, steatogenic and phospholipidogenic drugs. This fact represents an advantage with respect the methods available in the literature and after the suitable validation and development of a targeted quantitative analysis might represent a real alternative to the established methods.



## Results & Discussion

---

### 3.4 Extrapolation of *in vitro* results to *in vivo* models

After exploring the capabilities of HepG2 cells coupled to MS-based metabolomics to predict DILI, we decided to test whether the results obtained using a simple *in vitro* model could be extrapolated to *in vivo* models. First we evaluated the usefulness of medaka fish (*Oryzias latipes*) to predict human hepatotoxicity using a study design comparable to that performed in HepG2. Then, the changes were compared with those obtained using rats, an *in vivo* animal model widely used in hepatotoxicity studies (137, 140, 205, 304). Finally, the rat model was used to search for non-invasive serum markers of hepatotoxicity.

#### 3.4.1 Differential metabolomic profiling analysis of medaka

Medaka fish (*Oryzias latipes*) allows to use a high number of individuals with minimum requirements and provides information of relevance to human metabolism. The main advantages of medaka are its high reproductive rate, rapid maturation, and little cost in terms of rearing space and daily maintenance owing to their small size (203, 346). Moreover, the use of small fishes like medaka is in line with the 3R's (reduce, refine, and replace) approach of animal use for scientific purposes by replacing higher order animals with lower order ones (347).

Physiologically, medaka are omnivores and metabolize sugars and lipids in a manner analogous to that of mammals (348, 349). With the exception of some structural and anatomical differences, the general cellular composition and function of a healthy medaka liver is virtually the same as in mammals (350). It is worthy to mention that significant differences exist in the lipid composition between medaka and human liver. The most abundant FA in healthy human liver are palmitate (FA(16:0), 28%) and oleate (FA(18:1), 35%), and polyunsaturated FA

## Results & Discussion

---

represent around 19% of the total (106, 268, 351). The most abundant FA in medaka liver are palmitate (FA (16:0), 27% ), oleate (FA(18:1), 16%) and docosahexaenoate (FA(22:6), 24%), with a 39% of the FA being polyunsaturated (352, 353). With respect to xenobiotic metabolism, medaka metabolize drugs using similar pathways as humans as they possess a wide range of CYPs, enabling metabolic reactions including hydroxylation, conjugation, oxidation, demethylation and de-ethylation (202, 203, 354, 355).

Small fish models (mainly medaka and zebrafish) are being increasingly used as an *in vivo* model system for the evaluation of novel drug candidates for efficacy and safety testing (201, 203, 356) and recent literature has confirmed that mammalian and small fish toxicity profiles are strikingly similar (203, 357, 358). It is worthy to mention the contribution of small fish models in the understanding of diet-induced steatosis and steatohepatitis development (346, 359).

The hepatic metabolomic profiles of medaka fish treated with model hepatotoxic compounds were compared with those obtained using HepG2 cells and with the data available in the literature regarding toxicity in humans and other animal models. The compounds were administered once a day for five consecutive days. This dosing protocol is closer to drug dosage in humans than treatment protocols in *in vitro* experiments in which the cells are exposed uninterruptedly to the drug for a given period of time (e.g., 24 h).

The analytical strategy was equivalent to that applied to unravel the metabolomic changes in HepG2 cells. **Figure 3.30** shows the scores plots corresponding to the PCA analysis comparing the hepatic metabolic profile of medaka exposed to vehicle vs medaka treated with compounds inducing cholestasis, phospholipidosis or steatosis. Samples from control group clustered together and separated from those corresponding to hepatotoxic compounds. These results suggest that the treatments induced marked changes in the hepatic metabolome.

## Results & Discussion

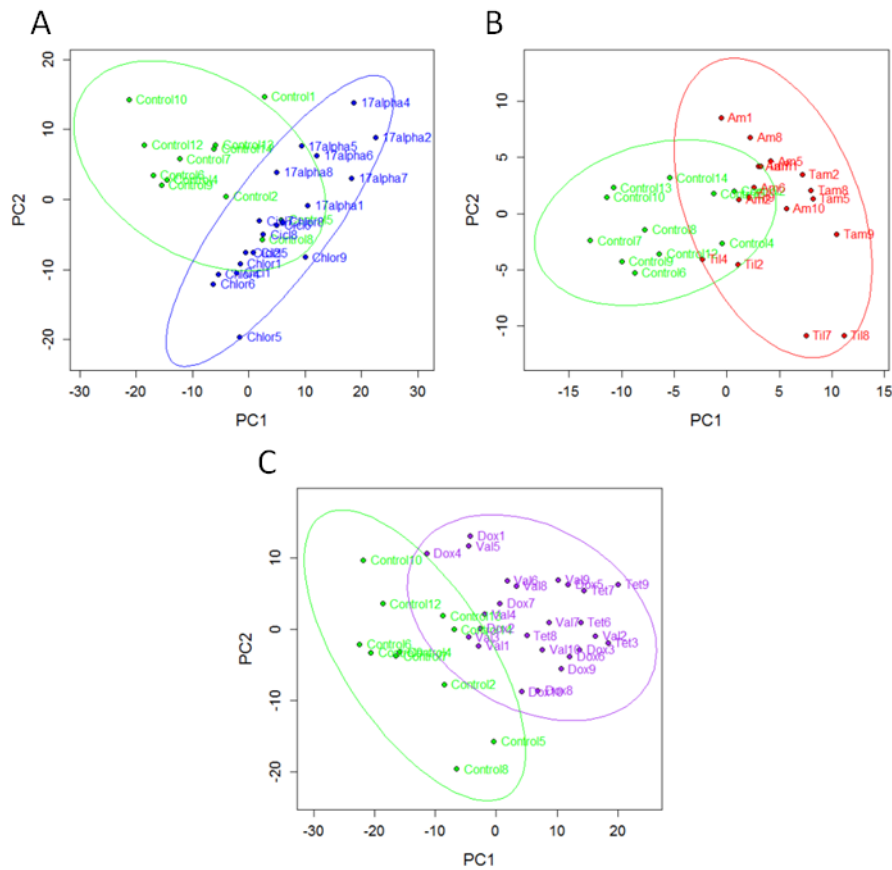


**Figure 3.30.** Scores plots corresponding to the PCA performed using the data obtained from the metabolomic analysis of liver of medaka treated either with control (i.e. non-toxic) or hepatotoxic compounds acting through different mechanisms of toxicity (i.e. cholestasis, phospholipidosis and steatosis). The lines denote 95 % confidence interval Hotelling's ellipse drawn for each class. PCA models were developed using two principal components. **A)** Control vs cholestasis. **B)** Control vs Phospholipidosis. **C)** Control vs Steatosis. Green: Control; Blue: Cholestasis; Red: Phospholipidosis; Purple: Steatosis.

## Results & Discussion

---

### *Identification of markers of hepatotoxicity*

First, a general comparison between untreated medaka (control group) and those treated with hepatotoxic compounds was performed in order to identify non-specific markers of hepatotoxicity. Then, the analysis was focused on the identification of specific markers and patterns associated to each of the studied mechanisms of hepatotoxicity.

A total of 9 compounds acting through different mechanism of toxicity were included in the study (**Table 2.3**). The generic changes observed in medaka were comparable to those observed for HepG2 cells (**Figure 3.11**). With respect to the lipidic species, several changes were observed in PLs, FAs, TG and acylcarnititines. With respect to polar metabolites the most important changes were related to glycolysis (i.e. glucose-6-phosphate), pentose phosphate pathway (i.e. ribose-5-phosphate), OS markers (i.e. GSH/GSSG and ophthalmic acid) and intermediates in PL metabolism (i.e. choline and glycerophosphoethanolamine) (**Figure 3.31**). Besides the similarities between HepG2 and medaka models, some differences were also observed as no relevant changes were detected in the metabolism of purines or aminoacids in the case of medaka. A main reason for these differences could be the proliferative nature of HepG2 cells compared to the normal non-proliferative state of hepatocytes (5).

From the detected alterations it can be concluded that the generic changes induced by hepatotoxic insults in medaka are directed to key aspects of lipid metabolism (i.e. PL, TG, FA and TG) and that mitochondrial damage is likely to be implied as suggested by the altered energetic metabolism and the appearance of markers of OS (34, 35).

## Results & Discussion

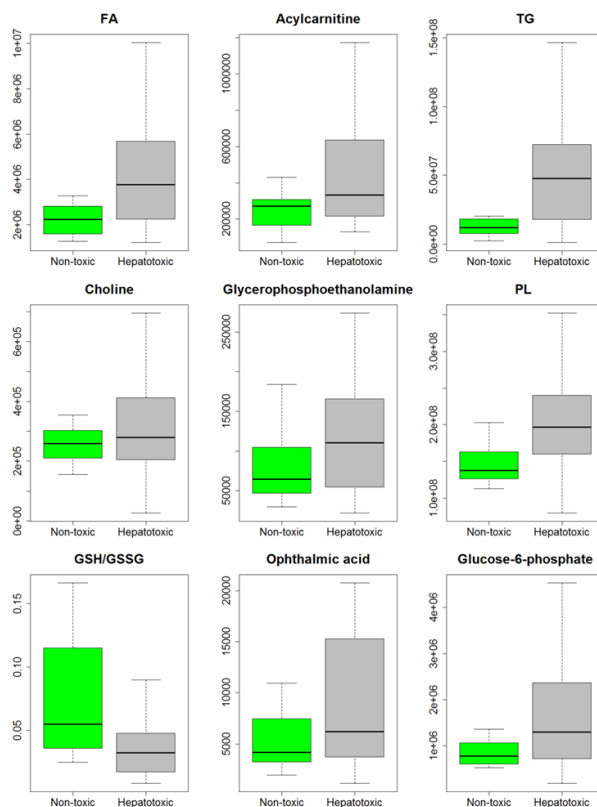


**Figure 3.31.** Boxplots showing the most important changes associated to generic hepatotoxicity in the liver of medaka analyzed following the generic untargeted metabolomic analysis strategy. Values are expressed as relative intensity. Boxes denote interquartile ranges, lines denote medians, and whiskers denote the 10th and 90th percentiles.

### Liver's metabolome changes triggered by cholestatic drugs

Three compounds classified as cholestatic were included in the study (**Table 2.3**): 17 $\alpha$ -ethynylestradiol, chlorpromazine and cyclosporine. Up to 197 metabolites were altered in the liver of medaka treated with cholestatic drugs, with impact on FA, TG and PL, urea cycle, nitrogen metabolism, aminoacid metabolism, and glutamate and GSH metabolism revealed by pathway enrichment analysis (**Figure 3.32**).

## Results & Discussion

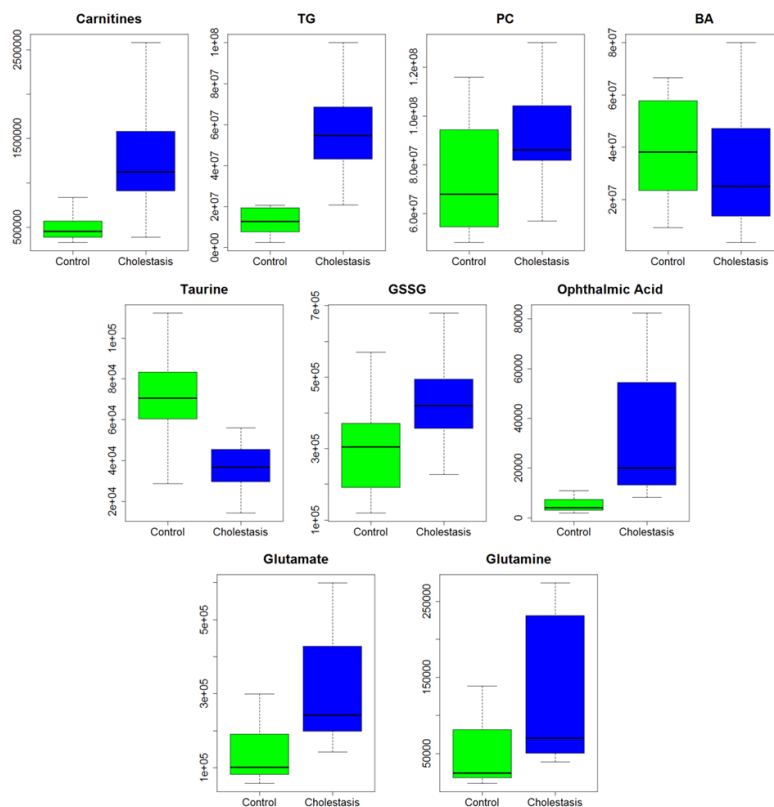


**Figure 3.32.** Boxplots showing the most important changes associated to cholestasis treatment in the liver of medaka analyzed following a generic untargeted analysis strategy. Values are expressed as relative intensity. Boxes denote interquartile ranges, lines denote medians, and whiskers denote the 10th and 90th percentiles.

The altered pathways and metabolites (**Figure 3.32**) were similar to those obtained as a result of drug-induced OS in HepG2 cells (**Figure 3.12**) with no characteristic alterations indicative of a specific cholestasis hepatotoxicity mechanism. Our results are in agreement with the reported ability of these compounds to induce OS and mitochondrial impairment both *in vitro* and *in vivo* (29, 89, 91, 92).

Five different species of BAs were found in the liver of medaka: trihydroxycholic acid, tauro-trihydroxycholic acid, tauro-dihydroxycholic

## Results & Discussion

---

acid, trihydroxycholestanic acid and tauro-trihydroxycholestanic acid. These results are in concordance with the data available in the literature (360-362). No significant differences were found in the levels of total or a particular BA in the liver of medaka treated with cholestatic drugs. These results are in agreement with previous studies in medaka and zebrafish. *Driessen et al* compared the changes in gene expression induced in zebrafish embryos incubated with hepatotoxicants, including three cholestatic drugs (cyclosporine, 17 $\alpha$ -ethynylestradiol and chlorpromazine) (200). Their results showed alterations in genes and pathways that could be related to hepatotoxic responses in general, but not specifically to cholestasis (200). Similar results were obtained in a study that compared the changes in gene expression in zebrafish embryos treated with cyclosporine with those occurring in other models (i.e. HepaRG and mouse liver) (357). In a study of  $\alpha$ -naphthylisothiocyanate-induced hepatobiliary toxicity in medaka, a similar response at both cellular and systemic levels was obtained in comparison with previous studies in rodents, however, no alterations to bile transport were found (363).

The alterations observed are consistent with an OS damage due to mitochondrial impairment, although a diminished canalicular efflux may play a role. The main alterations in the lipidome include increased levels of acylcarnitines, TG and PC (**Figure 3.32**). With respect to polar metabolites, it is worthy to highlight the appearance of OS markers related to GSH metabolism: increase in the levels of GSSG, ophthalmic acid, glutamate and glutamine and decreased levels of taurine. Interestingly, the increases in GSSG and ophthalmic acid are not accompanied by a decrease in the levels of GSH or GSH/GSSG ratio (**Figure 3.32**). This could be due to a diminished canalicular efflux of GSH by an inhibition of the corresponding transporters by the cholestatic drugs. Accordingly, PC, that are usually released into bile, showed

## Results & Discussion

---

increased levels and it cannot be discarded a contribution of decreased canalicular efflux to explain it.

As previously discussed, mitochondrial impairment may result in decreased FA oxidation thus leading to the over accumulation of FA oxidation intermediates as acylcarnitines, and ultimately of TG as a protective response to prevent free FA accumulation (34, 259) (**Figure 3.16**). The mitochondrial impairment exacerbates the production of ROS that may be accompanied with other mechanisms of ROS production and/or GSH depletion, thus leading to OS. As previously discussed, increased levels of some OS markers such as GSSG, glutamate, glutamine and ophthalmic acid (**Figure 3.32**) can be related to GSH oxidation, synthesis and recycling (**Figures 3.13, 3.14**). The observed decrease in taurine levels could also be due to an oxidative insult. Previous studies have reported decreased levels of taurine associated to oxidative damage and GSH depletion (138, 140), suggesting that under that circumstances cysteine is shunted to GSH production at the expense of taurine biosynthesis (140).

### Hepatic metabolic alterations induced by phospholipidogenic drugs

Amiodarone, tilorone and tamoxifen were studied as model phospholipidosis inducers (**Table 2.3**). 117 metabolites showed significant changes in the liver of medaka fish treated with these drugs. The alterations were mainly focused in PL, glutamate and GSH metabolism (**Figure 3.33**).



## Results & Discussion

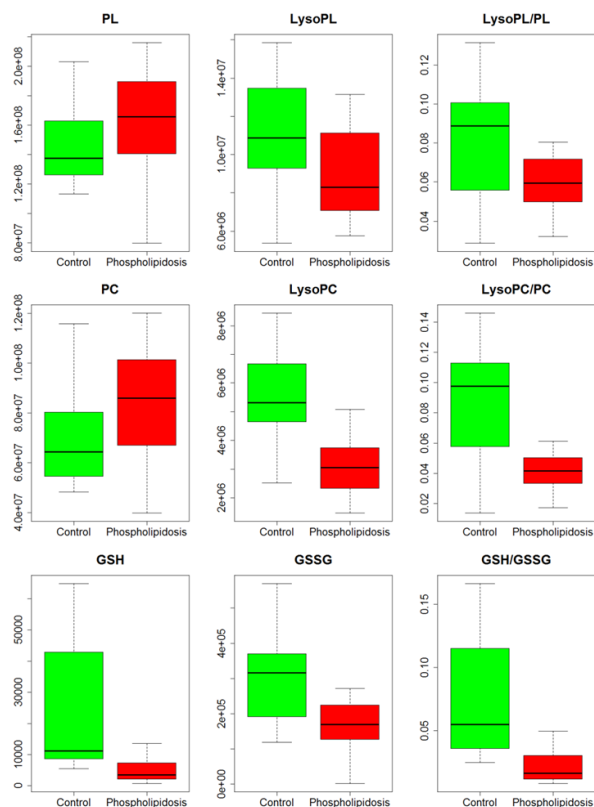


**Figure 3.33.** Boxplots showing the most important changes associated to phospholipidosis treatment in the liver of medaka analyzed following a generic untargeted analysis strategy. Values are expressed as relative intensity. Boxes denote interquartile ranges, lines denote medians, and whiskers denote the 10th and 90th percentiles.

These metabolic changes showed a great concordance with those obtained in HepG2 cells (**Figure 3.18**). As observed in HepG2, only a discrete (non-significant) increase in the levels of PL was obtained. This feature was accompanied by a decrease in the levels of LysoPL thus resulting in a lower LysoPL/PL ratio suggestive of a reduction in PL degradation (292, 293). An increase in the GSSG levels and a decrease in the GSH levels and GSH/GSSG ratio were also observed, indicative of OS damage, as previously found for HepG2 cells (**Figures 3.18, 3.33**).

## Results & Discussion

### Hepatic metabolomic markers of drug-induced steatosis

Three compounds classified as steatotic were included in the study (Table 2.3): doxycycline, tetracycline and valproic acid. A total of 295 metabolites were altered as a consequence of drug-induced steatosis, thus impacting several metabolic pathways: metabolism of unsaturated FA, PL metabolism, FA and TG metabolism, pentose phosphate pathway, glutamate and GSH metabolism and BA metabolism as revealed by pathway enrichment analysis (Figure 3.34).

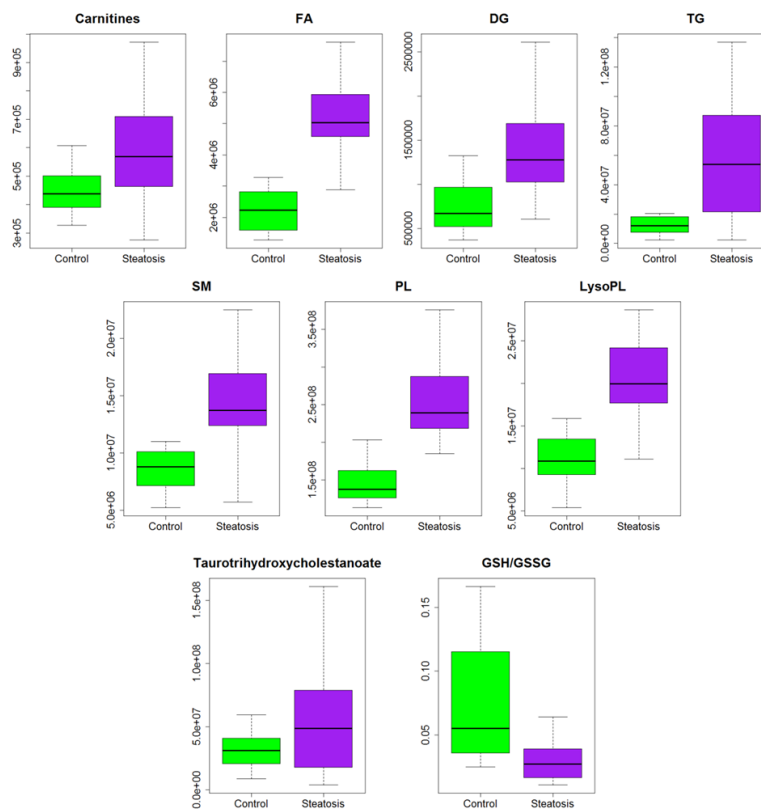


**Figure 3.34.** Boxplots showing the most important changes associated to steatosis treatment in the liver of medaka analyzed following a generic untargeted analysis strategy. Values are expressed as relative intensity. Boxes denote interquartile ranges, lines denote medians, and whiskers denote the 10th and 90th percentiles.

## Results & Discussion

---

The main changes in the lipidome included increased levels of acylcarnitines, FA, DG, TG, SM, PL, LysoPL and taurotrihydroxycholestanoic acid (the main BA in the liver of medaka fish). With respect to polar metabolites, the most remarkable alteration was the decrease in the GSH/GSSG ratio (**Figure 3.34**). These changes were more similar to those observed in lipid-loaded HepG2 cells (**Figures 3.20, 3.21**) than those obtained without an external source of free FA in the medium (**Figure 3.15**).

In mammals, short-chain FA (SCFA) and medium-chain FA (MCFA) absorbed by intestinal epithelial cells are released directly into the portal vein without esterification, while most LCFA form TG and are released into lymph ducts as chylomicron particles (4, 346). In fish, a two-step absorption model for dietary lipids has been proposed. Immediately after feeding, a fraction of dietary FA are found in the plasma, either as unbound FA (SCFA) or bound to carrier proteins (LCFA) and only later LCFA are resynthesized as TG and released as chylomicron particles into the blood thus performing an inter-organ transport of lipids that resembles the one occurring in mammals (346, 348, 352). The way the free FA are delivered into the liver from the intestine is similar to the phenomena that takes place in steatotic patients in which an exacerbated flux of free FA from adipose tissue to liver occurs (31, 259, 276, 364, 365). This may be the cause why NAFLD and NASH are developed more easily in medaka than in other animal models of high fat diet-induced steatosis (346, 366) and the reason of the fast development of NAFLD in our experimental conditions compared to HepG2. As observed for HepG2, the impairment in FA  $\beta$ -oxidation induced by the steatotic drugs resulted in the alteration of the levels of lipidic species not only directly related to TG and FA metabolism, but also to PL and SM metabolism (**Figures 3.20, 3.21, 3.34**). Moreover an induction of OS, represented by the decrease in the GSH/GSSG ratio, was also observed (**Figure 3.34**), in

## Results & Discussion

---

concordance with previous results and the known hepatotoxic mechanism of action of the employed molecules.

Finally, an increase in the intrahepatic levels of taurotrihydroxycholestanic acid was observed after treatment with steatogenic drugs (**Figure 3.34**). This finding, not observed in the HepG2 model, has been reported in the literature as a consequence of diet or drug-induced steatosis either in humans or in animal models (140, 166).

### *Development of predictive/classificatory models of hepatotoxicity based on medaka metabolite profiling*

After the identification of generic and mechanism-specific markers of hepatotoxicity, the next step was the development of predictive/classificatory models of hepatotoxicity.

As an initial approximation, a predictive model centered only in the discrimination of hepatotoxic compounds was developed. Using a CV strategy the optimum number of LV to develop the PLS-DA model was set to two based on the values of  $R^2$ ,  $Q^2$  and misclassification error (**Figure 3.35.A**). Once the number of LVs was set, the number of variables to be included in the final model was selected based on model performance (**Figure 3.35.B**). The lowest value of misclassification error and the highest value of AUROC were obtained with the model developed using only the top ranked 6 variables (i.e. PE(40:0), DG(34:3), DG(38:7), PC(42:2), TG(46:4), PC(40:1))

## Results & Discussion

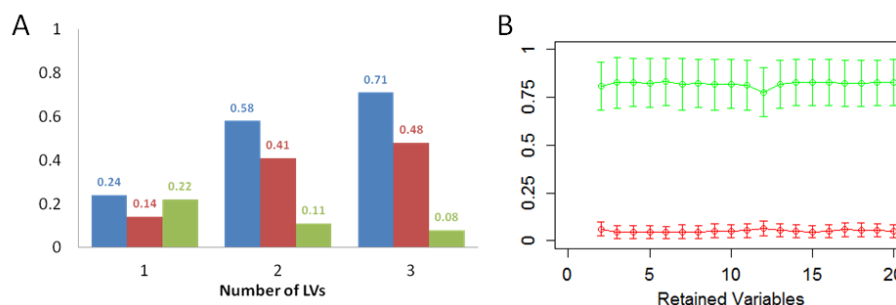


**Figure 3.35.** A) Values of  $R^2$  (blue),  $Q^2$  (red) and misclassification error (green) as a function of the number of LVs employed to build the PLS-DA model using the data obtained with the generic untargeted metabolomic analysis of the liver of medaka treated with either non-toxic or hepatotoxic compounds. B) Values obtained for the AUROC (green) and misclassification error (red) calculated using CV vs. the number of retained variables for the top-20 ranked variables using PLS-DA models with two LVs. The data is expressed as mean  $\pm$  standard deviation.

The PLS-DA scores and loadings plot corresponding to the model developed using 2LV and 6 retained variables are shown in **Figure 3.36**. Some overlap can be observed between 95 % confidence interval Hotelling's ellipse drawn for each of the classes (**Figure 3.36.A**). The poor separation between the classes was also confirmed by the bad results obtained for performance parameters of the model:  $R^2 = 0.61$ ,  $Q^2 = 0.60$ , misclassification error =  $0.05 \pm 0.03$  and AUROC =  $0.81 \pm 0.14$ . Although the permutation testing rendered good results (**Figure 3.36.C-D**), the information provided by the parameters evaluated by CV and the PLS-DA scores plot pointed the limited utility of the developed model. The results provided by the PCA scores plot suggested that the pattern generated by hepatotoxins acting through a specific mechanism can be distinguished independently from the control samples (**Figure 3.30**). Therefore, it can be concluded that no useful common pattern can be deduced with classificatory or predictive perspectives and each mechanism of toxicity has to be evaluated as an independent entity.

## Results & Discussion

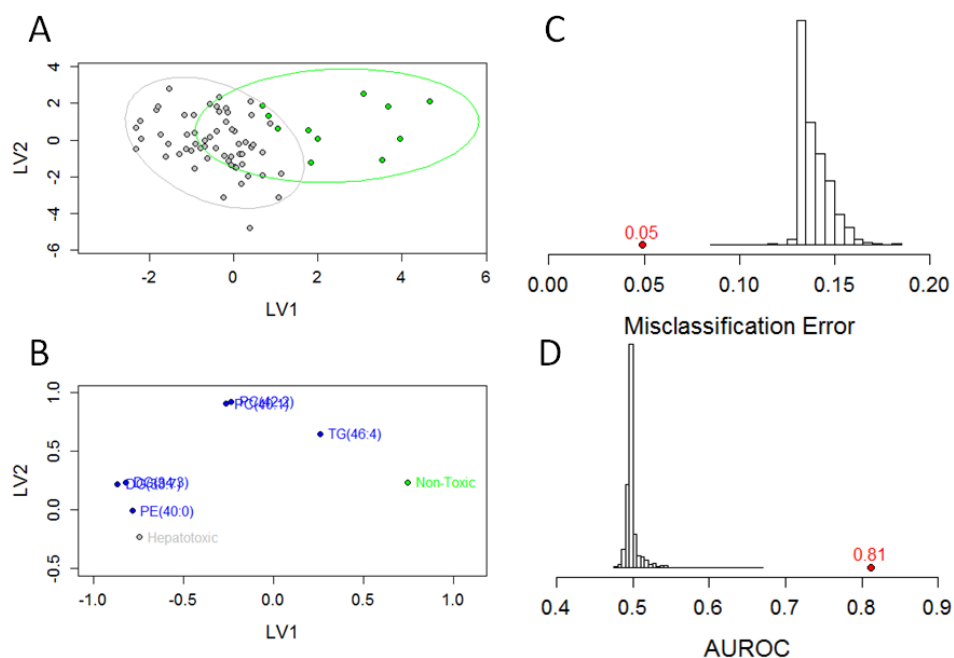


**Figure 3.36.** Summary of the results provided by the PLS-DA model built using 2 LVs and the top-ranked 6 variables based on the data obtained with the generic untargeted metabolomic analysis of livers from medaka treated with either non-toxic or hepatotoxic compounds. **A)** Scores plot. The lines denote 95 % confidence interval Hotelling's ellipse for each class. Green: non-toxic; Grey: hepatotoxic. **B)** Loadings plot. Green: non-toxic; Grey: hepatotoxic; Blue: metabolites. **C)** Permutation test for the misclassification error. **D)** Permutation test for the AUROC. In both cases the histograms represent the values obtained using the permuted classes. The actual value obtained with the real classes is indicated by the red dot and the value written above it.

Following the data analysis workflow, the next step was to develop a model focused on the discrimination between specific mechanisms of toxicity (i.e. non-toxic, cholestasis/OS, phospholipidosis and steatosis). Using a CV strategy the optimum number of LV to develop the PLS-DA model was set to three (**Figure 3.37.A**). The maximum value of AUROC and minimum value of misclassification error were obtained for the model built using the top 23 ranked variables (i.e. glycerophosphoethanolamine, PE(36:0), PE(44:5), PE(44:6), PC(44:12),

## Results & Discussion

LysoPA(18:2), LysoPC(20:1), LysoPE(20:4), PE(42:4), PE(44:8), cytidine, LysoPC(20:0), ophthalmic acid, carnitine(18:1), FA(20:2), PE(40:0), GSH, DG(38:7), carnitine(18:2), DG(40:8), methylhistidine, carnitine(4:0) and FA(20:4) (**Figure 3.37.B**).

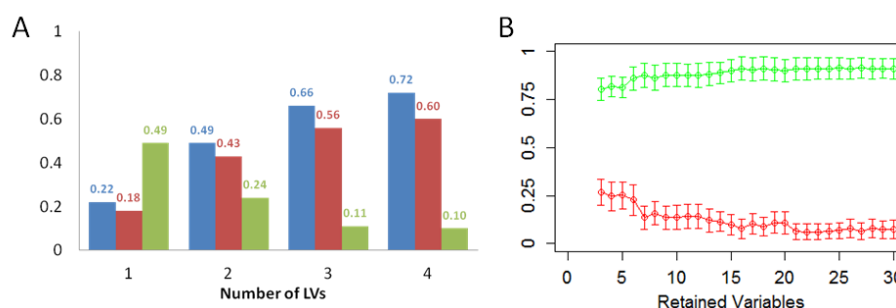


**Figure 3.37.** **A**) Values of R<sup>2</sup> (blue), Q<sup>2</sup> (red) and misclassification error (green) as a function of the number of LVs employed to build the PLS-DA model using the data obtained with the generic untargeted metabolomic analysis of liver from medaka treated with either non-toxic or hepatotoxic compounds acting through different mechanism of hepatotoxicity (i.e. cholestasis, phospholipidosis and steatosis). **B**) Values obtained for the AUROC (green) and misclassification error (red) calculated using CV vs. the number of retained variables for the top-30 ranked variables using PLS-DA models with three LVs using. The data is expressed as mean  $\pm$  standard deviation.

The final PLS-DA model provided the following figures: R<sup>2</sup> = 0.69, Q<sup>2</sup> = 0.65, misclassification error = 0.05  $\pm$  0.04, AUROC = 0.92  $\pm$  0.07. A good separation between the different groups is observed in the PLS-DA scores plot (**Figure 3.38.A**), with low overlap between the 95 % confidence interval Hotelling's ellipses drawn for each class. The model was further validated using a permutation test strategy with excellent results, as no overlap was obtained for values obtained using the permuted classes and the real values obtained with the actual PLS-DA for the misclassification error (**Figure 3.38.B**) and the AUROC (**Figure 3.38.C**).

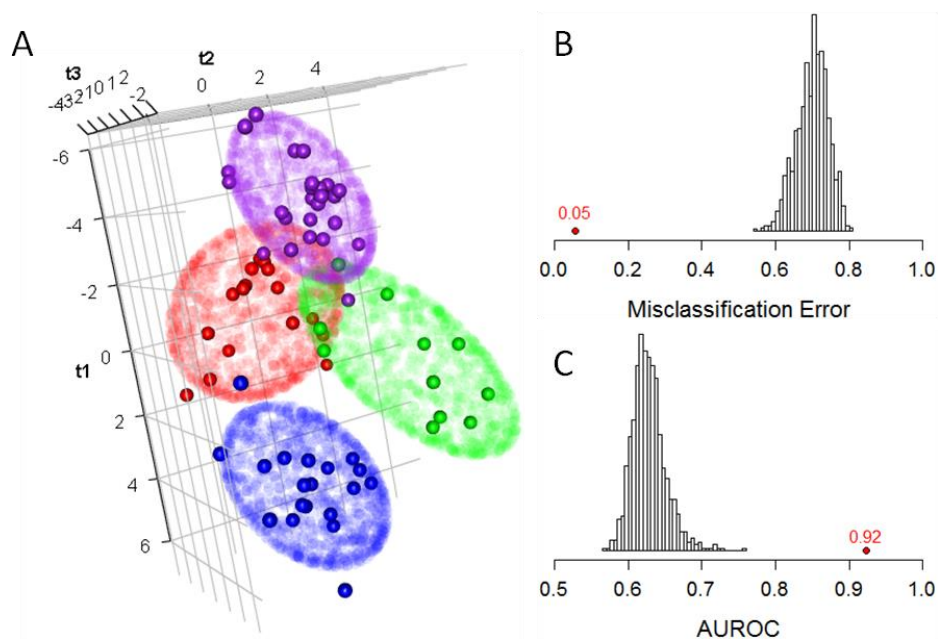


**Figure 3.38.** Summary of the results provided by the PLS-DA model built using 3 LVs and the top-23 ranked variables based on the data obtained with the generic untargeted metabolomic analysis of livers of medaka treated with either non-toxic or hepatotoxic compounds acting through different mechanism of hepatotoxicity. **A)** Scores plot. The lines denote 95 % confidence interval Hotelling's ellipse for each class. Green: non-toxic; blue: cholestasis; red: phospholipidosis; purple: steatosis. **B)** Permutation test for the misclassification error. **C)** Permutation test for the multiclass AUROC. In both cases the histograms represent the values obtained using the permuted classes. The actual value obtained with the real classes is indicated by the red dot.

In summary, although the application of our experimental and analytical design to medaka was of limited utility in predicting hepatotoxicity in a generic sense, the good results provided by the model computing the different mechanisms of hepatotoxicity corroborate the trend obtained by the non-supervised analysis (**Figure 3.30**). In a general sense, the results provided by the experiments performed in medaka were comparable both in terms of hepatotoxicity markers and predictive capabilities with those obtained *in vitro* using HepG2 cells, and represent an additional evidence to highlight the usefulness of medaka as animal model for the study of hepatotoxicity.



## Results & Discussion

### 3.4.2 Differential metabolomic analysis of rats exposed to tetracycline and paracetamol

As a final approximation to predict human hepatotoxicity, our metabolomic strategy was applied to the analysis of metabolomic changes in serum and liver tissue of rats exposed to hepatotoxic drugs. The main drawback of this experimental model is its limitation in the number of animals per study due to ethical, economical, space and handling restrictions. Therefore only two model hepatotoxins (tetracycline, representative of steatosis, and paracetamol, representative of OS) were selected as proof of principle of our analytical strategy. First, untargeted metabolomic analyses were performed using both liver and serum samples and finally targeted analyses of serum hepatotoxicity markers were performed.

The clinical chemistry data obtained in rats treated with paracetamol and tetracycline are shown in **Table 3.4**. Both drugs induced the increase of total bilirubin in serum, indicative of hepatobiliary damage. On the other hand paracetamol, but not tetracycline provoked an increase in alanine aminotransferase (ALT).

**Table 3.4.** Clinical laboratory analysis of serum samples from rats treated with hepatotoxic compounds.

Parameter	Control	Paracetamol	Tetracycline
Glucose (mg/dL)	110 ± 40	n.d.	180 ± 60*
TG (mg/dL)	65 ± 19	n.d.	40 ± 30
Total cholesterol (mg/dL)	82 ± 11	n.d.	90 ± 40
HDL cholesterol (mg/dL)	45 ± 9	n.d.	58 ± 18
Total bilirubin (mg/dL)	0.15 ± 0.03	0.24 ± 0.03 ***	0.4 ± 0.2 **
ALT (U/L)	53 ± 12	76 ± 11 **	50 ± 20
AST (U/L)	200 ± 80	260 ± 70	190 ± 50

Data expressed as mean ± standard deviation. Comparisons performed using a Student *t* test. \*: *p* value < 0.05; \*\*: *p* value < 0.01; \*\*\*: *p* value < 0.001. ALT: alanine aminotransferase; AST: aspartate aminotransferase; HDL: High density lipoprotein.

## Results & Discussion

### Untargeted metabolomic analysis

First of all, the serum and liver samples from rats administered either vehicle, paracetamol or tetracycline were analyzed using an untargeted metabolomic strategy. The corresponding PCA scores plots are shown in **Figure 3.39**. In all the cases the non-supervised analysis was able to distinguish between samples from rats administered vehicle or hepatotoxic compounds. Therefore, following our pre-established data analysis workflow, the metabolomic data were explored in order to look for the alterations induced in the metabolome by each of the treatments.

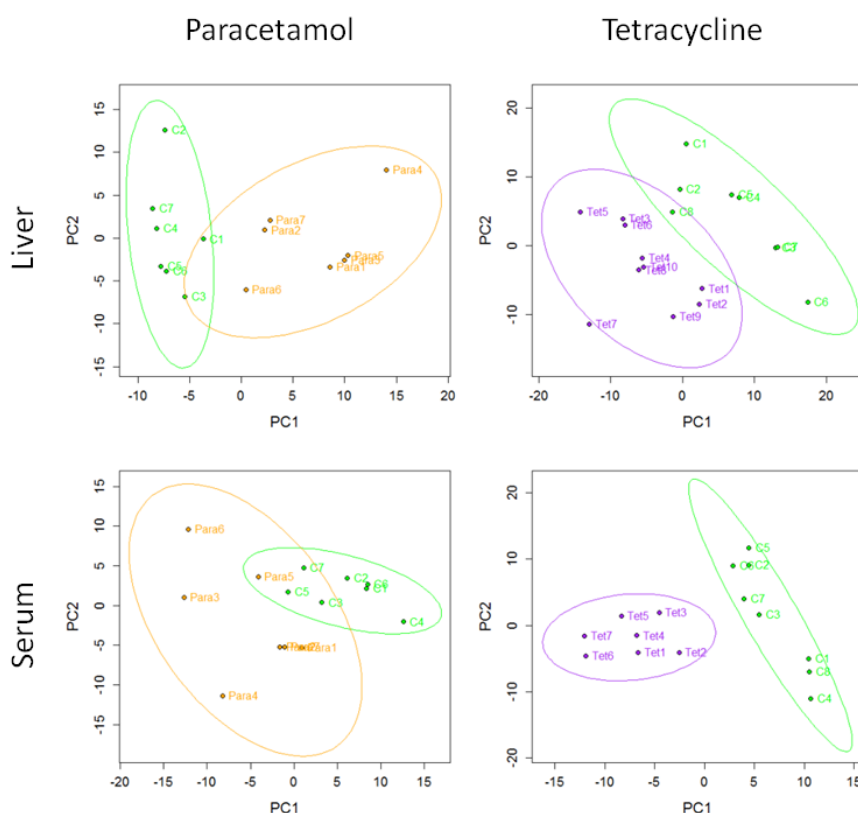


**Figure 3.39.** Scores plots corresponding to the PCA performed using the data obtained from the metabolomic analysis of liver (upper panels) and serum (lower panels) of rats dosed either vehicle (i.e. control, green) or model hepatotoxins (i.e. paracetamol, left panels, orange, and tetracycline, right panels, purple). The lines denote 95 % confidence interval Hotelling's ellipse drawn for each class. PCA models were developed using two principal components.

## Results & Discussion

---

### Metabolomic changes associated to the treatment with tetracycline

As previously observed using HepG2 cells and medaka, steatosis was the main mechanism involved in tetracycline hepatotoxicity. Although tetracycline treatment induced no or a very subtle hepatic damage (**Table 3.4**), the PCA analysis showed a clear separation between tetracycline and vehicle-treated rats (**Figure 3.39**).

As expected for a steatogenic drug, and following the tendency observed for the two experimental models used previously, the treatment with tetracycline induced an increase in the levels of hepatic TG and a decrease of FAs (**Figure 3.40**). These changes suggest an increased flux of FA to TG synthesis (**Figure 3.40**). However, the increase in intrahepatic levels of TG was not accompanied by TG increase in serum (**Table 3.4**), what can be related to a reduction in lipid export by the inhibition of microsomal TG transfer protein activity. Both mechanisms of steatosis have been previously associated to tetracycline (32, 88). Although the total amount of FA was diminished in the liver, increased levels of hydroxylated FA (i.e. FA(14:0)(OH) and FA(16:0)(OH)) were observed. Tetracycline is known to inhibit  $\beta$ -oxidation of FA (32, 88), thus leading to extramitochondrial FA oxidation resulting in higher rates of ROS production and lipid peroxidation. Increased levels of 3-hydroxyadipic acid (3-hydroxyhexanedioic acid) were also observed (**Figure 3.42**). This metabolite is derived from the  $\omega$ -oxidation of 3-hydroxy FA and the subsequent  $\beta$ -oxidation of longer chain 3-hydroxy dicarboxylic acids (367), which is consistent with the increased levels of FA(14:0)(OH) and FA(16:0)(OH) detected in the liver of rats administered tetracycline. Moreover, increased urinary levels of 3-hydroxyadipic acid and other 3-hydroxy-dicarboxylic acids have been also previously reported as a result of inhibition of FA oxidation (367).

## Results & Discussion

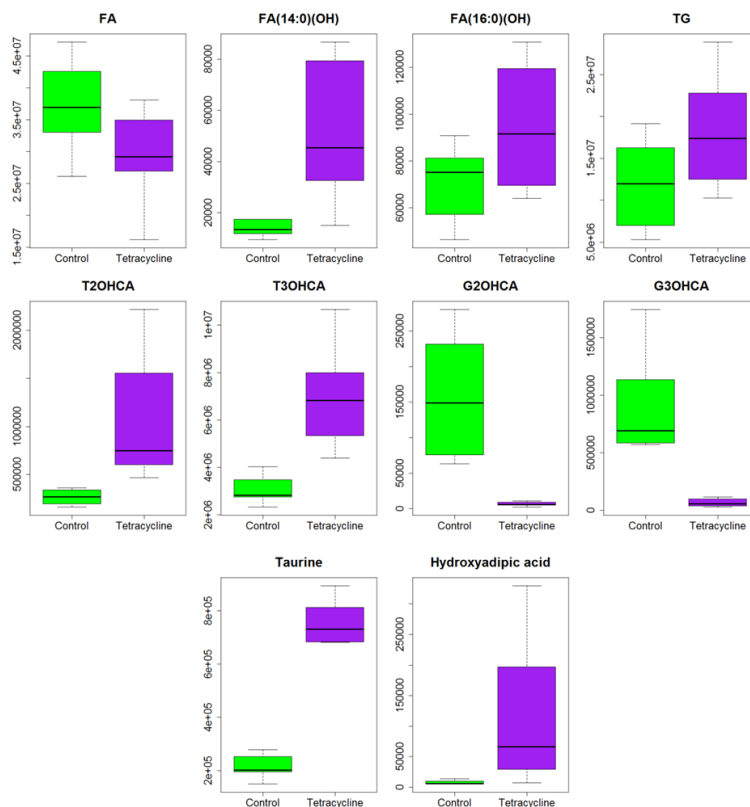


**Figure 3.40.** Boxplots showing the most important changes associated to tetracycline treatment in the liver of rats. Analysis performed following a generic untargeted metabolomics analysis strategy. Values are expressed as relative intensity. Boxes denote interquartile ranges, lines denote medians, and whiskers denote the 10th and 90th percentiles.

Several changes in the levels of intrahepatic BA were also detected (**Figure 3.40**). Tetracycline-treatment induced an increase in taurine-conjugated BAs (the main class of BAs in rat liver (207)), accompanied by increased levels of taurine, and a decrease in the levels of glycine-conjugated BAs (a minor class in rat liver (207)). Interestingly, altered levels of BA were also detected in the serum of rats treated with tetracycline (**Figure 3.41**), with decreased levels of non-conjugated and glycine conjugated BAs and increased levels of taurine-conjugated BAs.

## Results & Discussion

Previous reports have pointed out that rats administered tetracycline showed alterations in the BA pool in different samples (i.e. liver, serum and urine) (137, 140, 368).

Increased levels of total acylcarnitines were also found (**Figure 3.41**). Similar results have been reported in the serum of rats treated with tetracycline (140) and in the serum of patients with steatosis (369). These data are coherent with the previously described inhibition of  $\beta$ -oxidation of FA by tetracycline (32, 88).

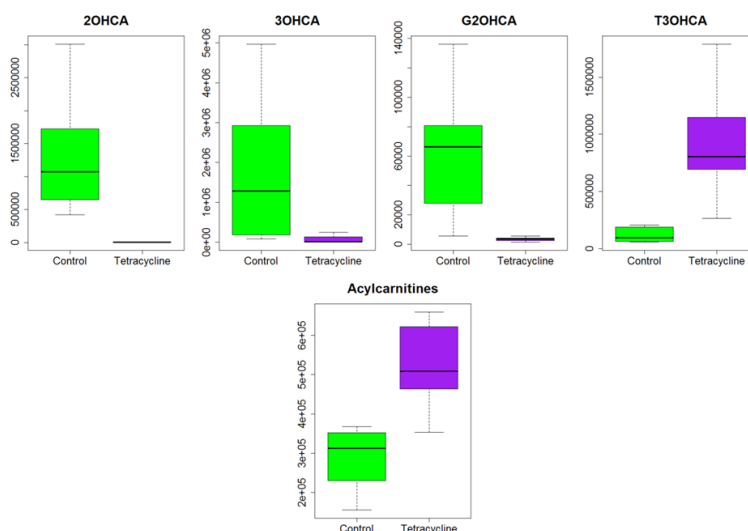


**Figure 3.41.** Boxplots showing the most important changes associated to tetracycline treatment in the serum of rats. Analysis performed following a generic untargeted metabolomics analysis strategy. Values are expressed as relative intensity. Boxes denote interquartile ranges, lines denote medians, and whiskers denote the 10th and 90th percentiles.

## Results & Discussion

---

### Metabolomic changes associated to the treatment with paracetamol

Paracetamol is normally detoxified by sulfation or glucuronidation (370). When administered at high doses, it is metabolized by different CYPs (i.e. CYP1A2, CYP2A6, CYP2E1 and CYP3A4) to generate the reactive intermediate N-acetyl-p-benzoquinone imine (NAPQI) (371), which is further inactivated by conjugation with GSH before excretion. In absence of sufficient GSH, the reactive NAPQI can cause toxic and covalent protein modifications that lead to cell death and tissue injury (372). Proteomic and transcriptomic studies have shown that paracetamol can cause numerous changes in pathways related to cellular stress response, mitochondrial function, and metabolism, as well as in cell cycle, structural, signaling, and apoptotic proteins (373, 374).

Paracetamol administration induced several changes in the hepatic metabolome of rats. The most altered pathways were related to FA oxidation, PL metabolism, OS and BA metabolism. Paracetamol treatment resulted in the alteration of several species of PL and intermediates in PL biosynthesis and degradation, such as choline, phosphocholine and glycerophosphoethanolamine (**Figure 3.42**), what can be related to NAPQI-mediated damage to intracellular membranes. More interesting is the detection of alterations that can be related to the  $\beta$ -oxidation of FA such a decrease in the levels of FA and an increase in the levels of acylcarnitines (**Figure 3.42**). These results are in concordance with a previous metabolomic study in the serum of paracetamol-treated Cyp2e1-null mice which revealed that the CYP2E1-mediated metabolic activation and OS following paracetamol treatment can cause irreversible inhibition of FA oxidation, potentially through suppression of PPAR $\alpha$ -regulated pathways (220).

## Results & Discussion

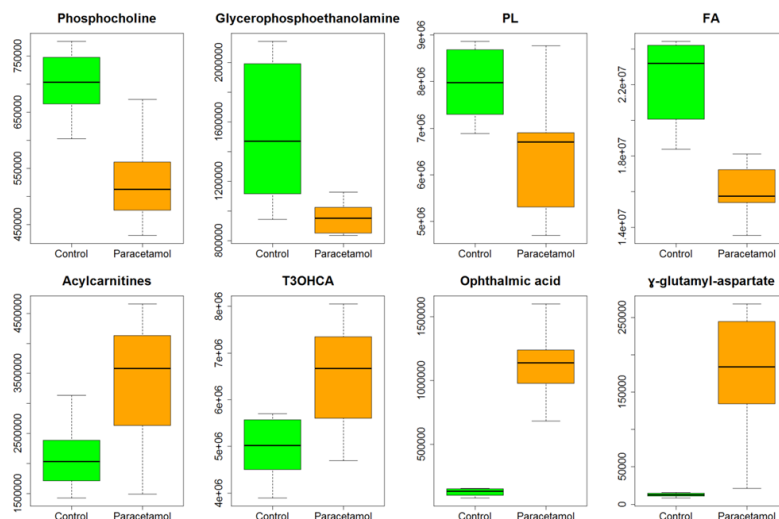


**Figure 3.42.** Boxplots showing the most important changes associated with paracetamol treatment in the liver of rats. Analysis performed following a generic untargeted metabolomics analysis strategy. Values are expressed as relative intensity. Boxes denote interquartile ranges, lines denote medians, and whiskers denote the 10th and 90th percentiles.

Directly related to the oxidative insult and the GSH consumption provoked by NAPQI was the appearance of alterations of metabolites related to GSH metabolism and  $\gamma$ -glutamyl cycle (**Figures 3.13, 3.14**) such as ophthalmic acid and  $\gamma$ -glutamyl-aspartate (**Figure 3.42**). Besides these alterations, no changes in the levels of GSH, GSSG or GSH/GSSG were observed. In a previous study the kinetics of GSH and ophthalmic acid were analyzed in paracetamol-overdosed mice (138). The appearance of ophthalmic acid is an early event related to GSH decrease and, whereas the intrahepatic levels of GSH are rapidly recovered after the administration, the levels of ophthalmic acid require longer times to recover the pre-dose status (138). Alterations in the intrahepatic levels of  $\gamma$ -glutamyl-dipeptides and related compounds have been previously described as a result of paracetamol overdose in rat (140). Finally, it is interesting to point out that alterations in the levels of BAs were also

observed (**Figure 3.42**). Alterations in the hepatic BA pool as a result of paracetamol treatment have been previously described (140).

The main alterations in the serum metabolome of rats administered paracetamol were related to BAs and  $\gamma$ -glutamyl-dipeptides and related compounds (see next section for detailed information).

### **3.4.3 Targeted analysis of non-invasive serum markers of hepatotoxicity in rats**

As shown in the previous section, the untargeted metabolomic analysis of liver and serum samples from rats treated with either tetracycline or paracetamol revealed BAs and  $\gamma$ -glutamyl-dipeptides and related compounds as the most promising biomarker candidates. *Yamazaki et al* (140) analyzed the serum and hepatic metabolome of rats treated with different model hepatotoxins, including paracetamol and tetracycline, and pointed out that perturbation of BA homeostasis and OS are early events of DILI in rats. Moreover, a recent study concluded that drugs that impaired both mitochondrial energetics and BSEP functional activity produced more severe manifestations of DILI than drugs that only have a single liability factor (375).

Based on these evidences we decided to develop targeted analysis methods for the evaluation of the serum levels of BAs and  $\gamma$ -glutamyl-dipeptides and related compounds.

#### Targeted analysis of BA

BAs are major components of bile formed from cholesterol through various enzymatic reactions in hepatocytes. Before being excreted into bile canaliculi, primary BAs synthesized in the liver (i.e., CA and CDCA in humans plus  $\alpha$ MCA and  $\beta$ MCA in rodents) (41, 42, 376-380) are mainly conjugated with taurine or glycine amino acids through the terminal



## Results & Discussion

---

side-chain carboxylic group present in the BA structure (42). BAs are transported across the canalicular membrane of the hepatocytes into the bile and stored in the gallbladder before being released into the intestinal tract (381). In the intestine, primary BAs are deconjugated and converted into secondary BAs by microbiota through dehydroxylation and epimerization reactions (39, 42, 377, 382). Then, most BAs are reabsorbed back to the liver, conjugated by hepatocytes, and re-excreted into bile to complete enterohepatic circulation (41, 42, 381) (**Figure 3.43**).

In the past, BAs were considered to be mere detergents required for the solubilization and absorption of dietary fats. However, BAs are now recognized as regulatory molecules capable of activating specific receptors. BAs are physiological ligands for the farnesoid X receptor (FXR), an intracellular BA sensor that controls the expression of the genes involved in BA synthesis, metabolism, and transport in order to minimize the deleterious effects of their accumulation (39, 42). BAs are also able to bind other nuclear receptors (e.g. PXR or VDR) and the G-protein coupled receptor TGR5 and can activate several cell signaling pathways (i.e., JNK, ERK, or AKT) (39, 40, 43, 44). By activating these receptors and signaling cascades, BAs regulate not only their own homeostasis but also FA, lipoprotein, glucose, and energy metabolism (39-41). The primary signaling function of BAs seems to be the regulation of metabolic flux in the liver and the gastrointestinal tract during the feed/fast cycle; however, they are also involved in the control of cell proliferation and inflammatory processes (39, 41). Alterations in the levels of BAs have been described in a series of pathological situations including hepatobiliary or drug-induced liver injury (140, 166, 183, 368, 383).

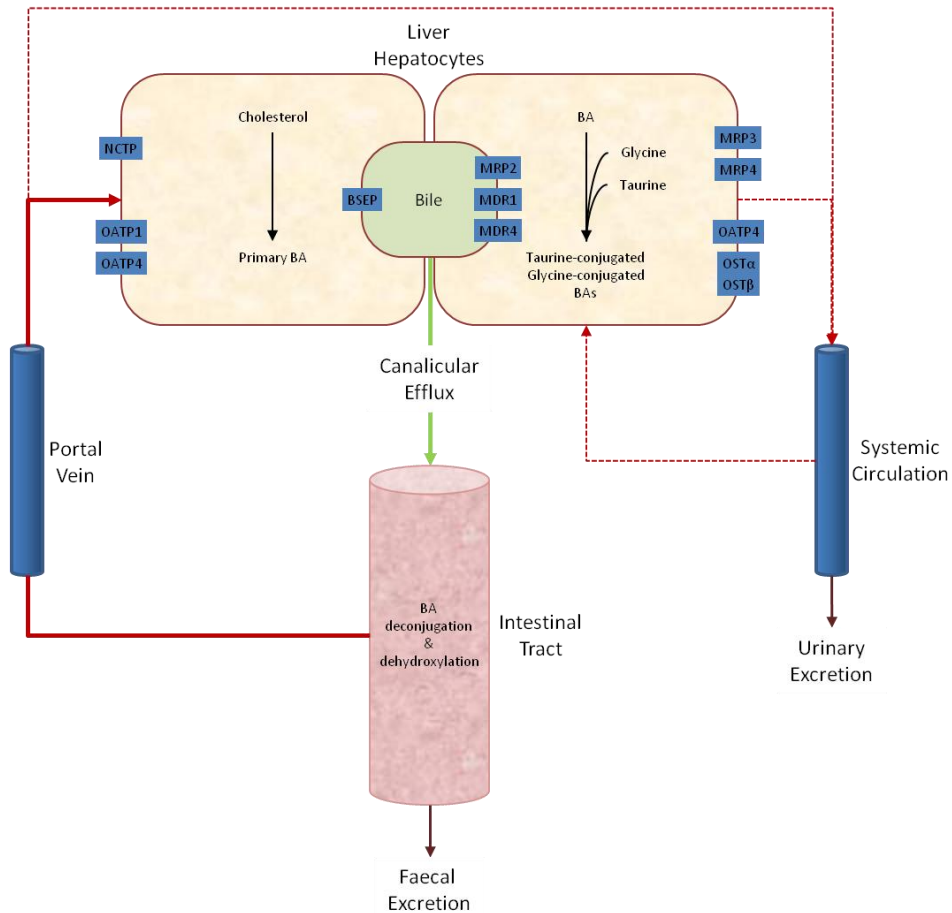


**Figure 3.43.** Summary of BA metabolism and transport processes. Primary BAs are synthesized in the hepatocytes from cholesterol through various enzymatic reactions. BAs are mainly conjugated with taurine and glycine before being excreted into the bile canaliculi. In the intestine, primary BAs are deconjugated and converted into secondary BAs by microbiota. Most BAs are reabsorbed back to the liver to complete enterohepatic circulation. Although BAs recycling is a very efficient process, a little amount is excreted in the faeces. Moreover, a low percentage of reabsorbed BAs escape hepatic uptake and enter into the systemic circulation. Under cholestatic conditions urinary excretion might occur. At the basolateral membrane of hepatocytes, BA efflux is an important spillover route for BA and bilirubin (bili) that has accumulated during BA overload under cholestatic conditions.

## Results & Discussion

BAs targeted analysis was performed using a validated LC-MS/MS method that allowed the simultaneous quantification of 31BAs including non-conjugated, taurine-conjugated and glycine-conjugated major and minor species (207, 384). The results are shown in **Table 3.5** and **Figure 3.44**.

**Table 3.5.** BA concentration (expressed as nM) in the serum of rats as a result of the indicated treatments.

Bile Acid	Control	Paracetamol	Tetracycline
CDCA	2100 ± 1500	2400 ± 1600	50 ± 50 **
DCA	900 ± 1000	2100 ± 900 *	1.6 ± 1.5 *
UDCA	180 ± 120	220 ± 120	7 ± 5 **
HDCA	2000 ± 2000	1100 ± 500	35 ± 7 *
CA	9000 ± 6000	28000 ± 7000 ***	160 ± 150 **
ωMCA	3000 ± 4000	15000 ± 9000 **	17 ± 17 *
αMCA	3000 ± 2000	8000 ± 5000 *	16 ± 18 *
βMCA	1800 ± 1800	9000 ± 4000 ***	30 ± 30 *
HCA	400 ± 500	1800 ± 1500 **	n.d.
GCDCA	70 ± 70	90 ± 70	n.q.
GDCA	200 ± 200	500 ± 600	n.q.
GHDCA	100 ± 100	40 ± 30	n.d.
GCA	700 ± 700	2800 ± 1700 **	36 ± 19 *
GHCA	10 ± 10	20 ± 20	n.d.
TCDC	45 ± 17	60 ± 40	140 ± 70 ***
TDCA	60 ± 60	160 ± 60 **	8 ± 4 *
TUDCA	5 ± 2	10 ± 4	5 ± 3
THDCA	170 ± 140	50 ± 30	3 ± 3 **
TCA	280 ± 130	2100 ± 1000 ***	1300 ± 600 ***
TωMCA	40 ± 30	80 ± 40 *	16 ± 3
TαMCA	190 ± 130	380 ± 130 *	330 ± 180 *
TβMCA	80 ± 40	200 ± 200 *	170 ± 90 **
Non-conjugated	23000 ± 15000	70000 ± 30000 ***	300 ± 300 **
Glycine-conjugated	1100 ± 900	3000 ± 2000 **	40 ± 20 **
Taurine-conjugated	900 ± 300	3100 ± 1200 ***	2000 ± 900 **
Total	25000 ± 16000	70000 ± 30000 ***	2400 ± 800 **

Data expressed as mean ± standard deviation. Comparisons between control and each treatment were performed using a Student t test, p values were adjusted for multiple comparisons using false discovery rate method. \*: p value < 0.05; \*\* p value < 0.01; \*\*\* p value < 0.001. n.d. not detected; n.q. not quantified

## Results & Discussion

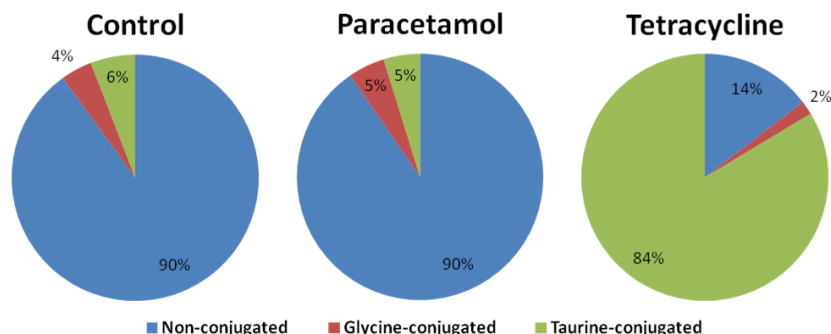


**Figure 3.44.** BA composition in the serum of rats as a result of the indicated treatments. Results expressed as percentage of the indicated group of BA (non-conjugated, glycine-conjugated and taurine-conjugated) with respect the total pool of BA.

With respect to tetracycline, a generic reduction in the levels of all the individual species was observed except for those taurine-conjugated species of primary BAs (i.e. TCA, TCDCA, T $\alpha$ MCA and T $\beta$ MCA). Similar results have been reported by *Yamazaki et al* (140). Under normal circumstances the serum BA pool is dominated by non-conjugated BA (**Table 3.5, Figure 3.44**) (207). The changes induced by tetracycline result in a decrease of both non-conjugated and glycine-conjugated BAs, what, besides the increase in taurine-conjugated BAs, leads to a decrease in the total amount of BAs in the serum. Moreover, **Figure 3.44** shows how the circulating BA pool of tetracycline-dosed rats is dominated by taurine-conjugated BAs. Tetracycline is a broad-spectrum antibiotic which can induce severe alterations in the microbiota, which in the end may be responsible of the changes observed in the BA pool (**Figure 3.43**). Therefore rather than a specific pattern of hepatic damage, changes in the BA pool might be the consequence of the damages in the gastrointestinal microbiota. Furthermore, these alterations in the BA pool can have severe consequences in the hepatic FA, lipoprotein, glucose and energy metabolism (39-42).

## Results & Discussion

---

With respect to paracetamol, the induced changes in the serum levels of BAs were more quantitative than qualitative. While the proportion between non-conjugated, taurine-conjugated and glycine-conjugated BAs was maintained (**Figure 3.44**), the total amount of each group species was increased around 3-fold with contribution of both primary and secondary BAs (**Table 3.5**).

These results, in conjunction with the extensive available literature of BAs alterations in hepatobiliary diseases and DILI (137, 140, 166, 183, 368), reinforce the usefulness of BA profiling for the discovery of biomarkers of disease and toxicity (207, 384).

### Targeted analysis of $\gamma$ -glutamyl dipeptides and related compounds

$\gamma$ -glutamyl dipeptides and ophthalmic acid have been previously described as markers of OS both as a result of different hepatobiliary diseases (246, 369) and as a result of DILI (138, 140).  $\gamma$ -glutamyl dipeptides can be synthesized in the liver via two different mechanisms (**Figures 3.13, 3.14**): i) via the ligation of glutamate with various amino acids and amines by GCS (246); ii) via the action of GGT over GSH. In both cases their appearance can be related to a (temporary or permanent) decrease in the intrahepatic levels of GSH due to an oxidative insult. Given the utility of  $\gamma$ -glutamyl dipeptides and related compounds (i.e. ophthalmic acid, GSH, GSSG, cysteinyl-glycine,...) as OS markers, a LC-MS/MS targeted analytical method was developed (**Section 2.14**).

The targeted analysis of serum samples revealed that, as expected, several compounds were altered in paracetamol overdosed rats, while no significant alterations were produced as a result of the administration of tetracycline (**Table 3.6**).

## Results & Discussion

**Table 3.6.**  $\gamma$ -Glutamyl dipeptides and related compounds concentration (expressed as nM) in the serum of rats as a result of the indicated treatments.

Compound	Control	Paracetamol	Tetracycline
Pyroglutamate	8400 ± 1900	10600 ± 400	5700 ± 800
Glutamine	360000 ± 60000	400000 ± 30000	330000 ± 70000
Glutamate	123000 ± 16000	117000 ± 5000	110000 ± 10000
$\gamma$ -Glutamyl-Glycine	12000 ± 4000	13000 ± 1000	9000 ± 3000
$\gamma$ -Glutamyl-Alanine	3900 ± 1400	6500 ± 1700 *	4400 ± 800
$\gamma$ -Glutamyl- Serine	8000 ± 2000	13300 ± 1900 **	7000 ± 2000
$\gamma$ -Glutamyl-Valine	1000 ± 300	1400 ± 300	900 ± 400
$\gamma$ -Glutamyl-Threonine	7100 ± 800	12000 ± 2000 ***	6000 ± 2000
$\gamma$ -Glutamyl-Taurine	1600 ± 400	1700 ± 300	1400 ± 100
$\gamma$ -Glutamyl-Leucine	2400 ± 700	3100 ± 400	1900 ± 500
$\gamma$ -Glutamyl-Isoleucine	290 ± 140	380 ± 140	180 ± 120
$\gamma$ -Glutamyl-Asparagine	2300 ± 700	3300 ± 300	2400 ± 600
$\gamma$ -Glutamyl-Glutamine	48000 ± 14000	55000 ± 19000	42000 ± 13000
$\gamma$ -Glutamyl-Lysine	11000 ± 5000	14000 ± 5000	10000 ± 2000
$\gamma$ -Glutamyl-Glutamate	1500 ± 500	3000 ± 500 **	1170 ± 190
$\gamma$ -Glutamyl-Metthionine	1300 ± 400	1900 ± 1100	1280 ± 170
$\gamma$ -Glutamyl-Histidine	1700 ± 600	2700 ± 500 *	1900 ± 500
Ophthalmate	1200 ± 600	10000 ± 4000 ***	1200 ± 300
$\gamma$ -Glutamyl-Phenylalanine	900 ± 300	1800 ± 300 **	1200 ± 400
$\gamma$ -Glutamyl-Arginine	5900 ± 1400	10000 ± 2000 **	4500 ± 1300
$\gamma$ -Glutamyl-Citrulline	4100 ± 1500	5000 ± 2000	1400 ± 400 *
$\gamma$ -Glutamyl-Tyrosine	2000 ± 400	3400 ± 700 **	1500 ± 400
$\gamma$ -Glutamyl-Triptophan	270 ± 70	530 ± 150 **	270 ± 50
$\gamma$ -Glutamyl-Cysteine	900 ± 400	1500 ± 600	700 ± 300
GSH	2700 ± 1600	6000 ± 6000	2800 ± 1400
GSSG	8000 ± 2000	16100 ± 1700 ***	8800 ± 1900

Data expressed as mean ± standard deviation. Comparisons between control and each treatment were performed using a Student t test, p values were adjusted for multiple comparisons using false discovery rate method. \*: p value < 0.05; \*\* p value < 0.01; \*\*\* p value < 0.001.

We have previously observed alterations in the levels of ophthalmic acid in HepG2 cells treated with tetracycline (**Figure 3.26**), thus indicating that OS was a mechanism involved in the hepatotoxic effect. In contrast, no alterations in the levels of OS markers were detected in the serum of tetracycline-dosed rats. Similar results have been previously

## Results & Discussion

---

reported by *Yamazaki et al* (140). Tetracycline can induce OS damage as a result of the mitochondrial disturbances induced by the inhibition of  $\beta$ -oxidation of FA and their extramitochondrial catabolism (32, 88, 276). HepG2 cells are less efficient in preventing oxidative damage than hepatocytes within the physiological environment provided by the liver (5), which may explain the higher oxidative damage in HepG2 cells compared to the in the *in vivo* model. Moreover, OS markers (a decrease in the GSH/GSSG ratio) were also detected in the liver of medaka administered steatogenic drugs (**Figure 3.40**). As previously discussed, lipid metabolism in medaka favors the development of the drug-induced steatosis insult to an extent comparable to that observed in NASH, a clinical situation in which OS play an essential role (31, 246, 276, 369).

Several metabolites related to GSH metabolism were altered in the serum of rats overdosed paracetamol (**Table 3.6**). These finding are in agreement with GSH depletion induced by NAPQI which results in increased GSH recycling via the  $\gamma$ -glutamyl cycle and GSH synthesis via the consecutive action of GCS and GS. No significant alterations in the levels of GSH were observed. These results are in concordance with a previously published study showing a rapid recovery of GSH levels after the oxidative insult (138). Upon OS, GSH/GSSG pair shift toward the oxidized state and then GSSG may either recycle to GSH or exit from the cells to prevent its intracellular accumulation (385). This could explain the high GSSG levels detected in the serum of rats overdosed paracetamol (**Table 3.6**). Overall, the increased levels of  $\gamma$ -glutamyl dipeptides were indicative of an OS state; however, the identification of specific patterns of altered  $\gamma$ -glutamyl and its potential utility to identify the mechanisms responsible of OS remain to be investigated.

## 4. Conclusions & Outlook





### 4.1. Conclusions

The work presented in this thesis can be divided into two different stages. First, our efforts were devoted to the development of the suitable protocols to apply LC-MS-based metabolomics to mammalian cells in culture. And in the second stage the developed protocols were applied to the metabolic profiling of different *in vitro* and *in vivo* models. Based on the work described in the present thesis, the following conclusions can be drawn:

1. The use of IS and QC samples in conjunction with a carefully designed sample analysis define a quality assurance framework that allows to monitor the performance of the analytical platform before, during and after sample analysis.
  2. The combined use of uni- and multivariate data analyses represent a straightforward strategy for the identification of metabolomic alterations and the development of predictive/classificatory models.
  3. The use of bespoke metabolome extraction and analysis protocols based on the chemical properties of each metabolite class allows to expand the endometabolome coverage of HepG2 cells.
  4. The application of metabolomics to the study of DILI using HepG2 represents a suitable tool to detect pre-lethal alterations associated to hepatotoxicity and thus it may be implemented as a sensitive tool in pre-clinical testing.
- 4.1 Metabolomics revealed generic and mechanism-specific sensitive pre-lethal markers of hepatotoxicity in HepG2 cells that were coherent with the known *in vivo* alterations.

## Conclusions & Outlook

---

- 4.2 Predictive models aimed to distinguish between non-hepatotoxic and hepatotoxic compounds or between non-hepatotoxic compounds and those acting through specific mechanisms of hepatotoxicity (i.e. oxidative stress, steatosis and phospholipidosis) were satisfactorily developed.
5. The combination of a lipid-focused metabolomics analysis in conjunction with HepG2 cells pre-loaded with fatty acids constitutes a suitable strategy for the fast development of drug-induced phospholipidosis and steatosis, the detection of sensitive mechanism-specific lipid markers and the development of predictive/classificatory models.
6. Oxidative insult was revealed as a common event associated to hepatotoxicity and the development of a specific targeted analysis method allowed to quantify different markers of oxidative stress in HepG2 cells.
7. Metabolomic alterations in medaka (*Oryzias latipes*) are in agreement with those observed in HepG2 cells and suggest this *in vivo* model as a suitable alternative for high throughput hepatotoxicity testing.
8. Experiments in rats revealed that BAs and  $\gamma$ -glutamyl dipeptides are common serum markers associated to hepatotoxicity and could be good candidates as biomarkers of DILI in pre-clinical and clinical testing.

### 4.2. Outlook

The first aim achieved within the framework herein defined was the development of a global sample preparation and analysis strategy for the determination of HepG2's endometabolome. While the methodology developed here expands the metabolome coverage, it presents some limitations that are intrinsic to the employed analytical platform (i.e. LC-MS). Thus, we are planning to evaluate whether the incorporation of GC-MS into our analytical workflow could suppose a significant improvement in the detection and characterization of any group of metabolites of interest.

The results obtained in the development of this thesis have allowed us to identify metabolomic alterations associated to specific mechanisms of hepatotoxicity using HepG2 cells as *in vitro* model. However, HepG2 cells present some limitations such as low biotransformation capabilities, low expression and activity of transporters relevant to hepatotoxicity and the lack of a cell polarity that resembles the *in vivo* phenotype. Different alternatives are available to circumvent these limitations, and among them, HepaRG cells are the most promising one. Moreover, we plan to evaluate a higher number of model hepatotoxins in order to select a well defined set of biomarkers with respect to the development of LC-MS/MS targeted quantitative analyses.

The *in vivo* experiments in rats, allowed us to identify BAs and  $\gamma$ -glutamyl dipeptides and related compounds as promising serum biomarkers of hepatotoxicity. Moreover, the development of targeted LC-MS/MS analyses allowed us their quantification in a highly sensitive and specific way. Two different lines of experimentation could arise from these observations. On one hand, the increase in the number of model hepatotoxins tested in rodent models would allow us to identify patterns of BAs and  $\gamma$ -glutamyl dipeptides associated to hepatotoxicity in general or to specific mechanism of hepatotoxicity. On the other hand, the

## Conclusions & Outlook

---

analysis of serum samples from patients who have suffered a DILI event would allow us to determine whether those alterations and biomarkers identified in rodents are applicable to human hepatotoxicity.

### RESUMEN EN CASTELLANO

El hígado es un órgano especialmente susceptible a sufrir toxicidad debido a su particular localización anatómica y a su papel en el metabolismo y detoxificación de xenobióticos en general y fármacos en particular. Múltiples mecanismos están implicados en el daño que un fármaco o sus metabolitos pueden producir en los hepatocitos. El modo en que los orgánulos, macromoléculas y/o funciones se ven afectadas define el patrón del daño hepático. En base a la manifestación clínica inicial provocada a raíz del daño hepático, cuatro mecanismos de toxicidad diferentes pueden tener lugar: i) Esteatosis, caracterizada por la acumulación de lípidos, principalmente triglicéridos, en el interior de los hepatocitos; ii) Fosfolipidosis, caracterizada por la excesiva acumulación de fosfolípidos en el interior de las células; iii) Colestasis, producida a raíz de una disminución en el flujo biliar que conduce a la acumulación de sales biliares con los consecuentes daños para el hepatocito; y iv) Estrés oxidativo, producido cuando la generación de especies oxidantes sobrepasa la capacidad antioxidante de las células.

El daño hepático causado por fármacos es un problema de gran relevancia a nivel sanitario y económico y la hepatotoxicidad es la principal causa de finalización de ensayos clínicos y de retirada de fármacos tras su comercialización. Uno de los principales problemas asociados a la hepatotoxicidad es el fallo a la hora de detectar fármacos potencialmente hepatotóxicos durante el proceso de desarrollo de nuevos fármacos. Los ensayos pre-clínicos deberían ser capaces de detectar posibles hepatotoxinas en etapas tempranas del proceso de desarrollo con el fin de minimizar los riesgos sanitarios y las pérdidas económicas. Múltiples modelos celulares hepáticos *in vitro* han sido desarrollados para su uso en la investigación toxicológica con el fin de conseguir una mayor comprensión de los mecanismos de hepatotoxicidad y detectar el potencial de nuevas entidades químicas de

## Resumen en Castellano

---

producir toxicidad a nivel hepático. Aunque no consiguen reproducir fielmente la fisiología de un organismo completo o la complejidad del hígado, su bajo coste, alta reproducibilidad y la posibilidad de disponer de modelos de origen humano hacen de ellas un buen complemento para los tradicionales estudios *in vivo* y especialmente útiles para la predicción de fenómenos tóxicos en etapas tempranas del desarrollo de fármacos.

Los estudios toxicológicos basados en modelos celulares *in vitro* se han llevado a cabo tradicionalmente usando ensayos de citotoxicidad, basados en la estimación de la viabilidad celular y/o el estado metabólico o funcional de las células previamente expuestas al tóxico en estudio. No obstante, la utilidad de este tipo de estudios es limitada ya que monitorizan eventos que tienen lugar en etapas avanzadas del daño celular, cuando las células se encuentran cercanas a la muerte, y por tanto no se puede extraer información mecanística alguna. La aplicación de las nuevas tecnologías "ómicas" (transcriptómica, proteómica, citómica y metabonómica) permite la determinación simultánea de múltiples parámetros en una misma muestra biológica y representa una herramienta más sensible y potente para el estudio de eventos relacionados con la hepatotoxicidad. Entre ellas la metabonómica se dedica al estudio de los productos finales de la "cascada ómica" proporcionando de este modo una información que no está accesible a través de otras "ómicas", lo que representa una mayor proximidad al fenotipo que el estudio de los genes, los transcritos o las proteínas.

En base a estas evidencias, decidimos evaluar si la metabonómica en combinación con modelos celulares *in vitro* y con modelos animales *in vivo* puede representar una alternativa útil para el estudio de mecanismos de hepatotoxicidad y el reconocimiento de patrones característicos asociados a estos. Los siguientes objetivos fueron definidos dentro del marco de trabajo de la presente tesis: 1) Puesta a punto de una estrategia analítica basada en LC-MS para el estudio del

metaboloma: desde el procesamiento y análisis de las muestras hasta el análisis de los datos y la validación de biomarcadores; 2) Identificación de biomarcadores y patrones metabonómicos específicos asociados a mecanismos de hepatotoxicidad usando HepG2 como modelo celular *in vitro*; 3) Comparación de los resultados obtenidos *in vitro* con modelos animales *in vivo*.

En primer lugar definimos un marco de trabajo adecuado que, gracias a la combinación de un cuidadoso diseño del análisis de las muestras, en conjunción con la incorporación de diferentes patrones internos y controles de calidad, nos permitió llevar a cabo los análisis metabonómicos en un ambiente que aseguraba la calidad de los resultados obtenidos.

A continuación optimizamos una estrategia de procesamiento y análisis de las muestras de interés que nos permitió la extracción y análisis diferenciado de un gran rango de metabolitos, desde altamente polares hasta muy apolares, lo que nos permitió maximizar la cobertura del metaboloma. Con respecto a la extracción del metaboloma esto se consiguió gracias a una extracción en múltiples pasos en la que la combinación de solventes con diferentes características hizo posible la extracción diferencial de los metabolitos en base a sus propiedades químicas. Con respecto al análisis, se consiguió gracias a la combinación de cromatografía en fase reversa e HILIC, lo que permite la separación y detección de las diferentes clases de metabolitos en condiciones óptimas, maximizando la cobertura y minimizando las interferencias.

La aplicación de las herramientas previamente desarrolladas a células HepG2 previamente tratadas con hepatotoxinas modelo que actúan a través de diferentes mecanismos de hepatotoxicidad nos permitió la identificación de patrones metabonómicos específicos asociados a cada uno de los mecanismos de interés. Además, los metabolitos y rutas metabólicas alteradas fueron coherentes con los mecanismos de hepatotoxicidad previamente descritos en humanos. En base a los



## Resumen en Castellano

---

resultados obtenidos, experimentos adicionales fueron llevados a cabo para lograr una mejor caracterización de las alteraciones provocadas a consecuencia de daños por estrés oxidativo o desórdenes relacionados con lípidos como son la esteatosis y la fosfolipidosis.

La utilidad de la estrategia analítica fue confirmada mediante su aplicación a estudios *in vivo* con medaka (*Oryzias latipes*) y rata como modelos animales. Los resultados *in vivo* mostraron una gran concordancia con los obtenidos *in vitro* usando HepG2 como modelo. Además, el uso de rata como modelo animal nos permitió identificar marcadores comunes de hepatotoxicidad en sangre que podrían ser usados como marcadores en estudios preclínicos o incluso extrapolados a humanos.

En base al trabajo presentado en esta tesis, las siguientes conclusiones pueden ser extraídas:

1. El uso de patrones internos y muestras de control de calidad en conjunción con un cuidadoso diseño del análisis de las muestras supone un marco adecuado de control de calidad para la monitorización del funcionamiento de la plataforma analítica antes, durante y después del análisis de las muestras.
2. El uso combinado de técnicas de análisis uni- y multivariante representa una estrategia adecuada de análisis de datos para la identificación de alteraciones metabolómicas y el desarrollo de modelos clasificatorios/predictivos.
3. El uso de un protocolo de extracción y análisis del metabonoma adaptado a las propiedades químicas de las clases de metabolitos permite expandir la cobertura del endometaboloma en células HepG2.

4. La aplicación de la metabonomía al estudio del daño hepático inducido por fármacos en HepG2 representa una herramienta adecuada para la detección de alteraciones pre-letales asociadas a hepatotoxicidad y por tanto puede ser implementada como una herramienta sensible en ensayos preclínicos.
  - 4.1 Los estudios metabólicos revelaron marcadores asociados con hepatotoxicidad genérica y asociada a mecanismos específicos de hepatotoxicidad en células HepG2 que además eran coherentes con las alteraciones *in vivo* previamente descritas.
  - 4.2 Se desarrollaron modelos predictivos dirigidos a la discriminación entre compuestos no tóxicos y compuestos hepatotóxicos y entre compuestos no tóxicos y compuestos que actúan a través de mecanismos de hepatotoxicidad específicos: estrés oxidativo, esteatosis y fosfolipidosis.
5. La combinación de una aproximación lipidómica en conjunción con HepG2 precargadas con ácidos grasos representa una estrategia adecuada para el rápido desarrollo de esteatosis y fosfolipidosis inducidos por fármacos, la detección de marcadores lipídicos asociados a dichos mecanismos y el desarrollo de modelos clasificatorios/predictivos.
6. El daño oxidativo fue revelado como un evento común asociado a hepatotoxicidad, el desarrollo de un análisis dirigido permitió la cuantificación de diferentes marcadores de estrés oxidativo en células HepG2.
7. Las alteraciones metabólicas detectadas en medaka (*Oryzias latipes*) fueron coherentes con las observadas en HepG2 lo que sugiere que medaka representa una alternativa válida como modelo *in vivo* de alto rendimiento para la predicción de hepatotoxicidad.

## Resumen en Castellano

---

8. Experimentos en rata revelaron que las sales biliares y los  $\gamma$ -glutamil dipeptidos son marcadores séricos comunes asociados a hepatotoxicidad y pueden ser buenos candidatos a biomarcadores de daño hepático inducido por fármacos en ensayos tanto pre-clínicos como clínicos.

### REFERENCES

1. Renato P, Correa AV, Nathanson MH: Functional organization of the liver. In: Rodés J, Benhamou J-P, Blei AT, Reichen JR, Manocchia M, eds. Textbook of hepatology: from basic science to clinical practice. 3rd edition ed: Malden: Wiley-Blackwell Publishing., 2007.
2. Grisham JW: Organizational Principles of the Liver. In: Arias IM, Alter HJ, Boyer JL, Cohen DE, Fausto N, Shafritz DA, Wolkoff AW, eds. The Liver: Biology and Pathobiology 5th Edition ed: John Wiley & Sons, Ltd, 2009.
3. Bioulac-Sage P, Le Bail B, Balabaud C: Liver and biliary tract histology. In: Rodés J, Benhamou JP, Blei AT, Reichen JR, Manocchia M, eds. Textbook of hepatology: from basic science to clinical practice. 3rd edition ed: Malden: Wiley-Blackwell Publishing., 2007.
4. Frayn KN. Metabolic Regulation : A Human Perspective. 3rd Edition ed: Wiley-Blackwell, 2010.
5. LeCluyse EL, Witek RP, Andersen ME, Powers MJ. Organotypic liver culture models: meeting current challenges in toxicity testing. *Crit Rev Toxicol* 2012;42:501-548.
6. Rappaport AM. Microcirculatory units in the mammalian liver. Their arterial and portal components. *Bibl Anat* 1977:116-120.
7. Frevert U, Engelmann S, Zougbede S, Stange J, Ng B, Matuschewski K, Liebes L, et al. Intravital observation of Plasmodium berghei sporozoite infection of the liver. *PLoS Biol* 2005;3:e192.
8. Kmiec Z. Cooperation of liver cells in health and disease. *Adv Anat Embryol Cell Biol* 2001;161:III-XIII, 1-151.
9. Mehal WZ: Intrahepatic lymphocytes. In: Rodés J, Benhamou JP, Blei AT, Reichen JR, Manocchia M, eds. Textbook of hepatology: from basic science to clinical practice. 3rd edition ed: Malden: Wiley-Blackwell Publishing., 2007.
10. Semela D, Shah VH: Liver sinusoidal endothelial cells. In: Rodés J, Benhamou JP, Blei AT, Reichen JR, Manocchia M, eds. Textbook of hepatology: from basic science to clinical practice. 3rd edition ed: Malden: Wiley-Blackwell Publishing., 2007.
11. Godoy P, Hewitt NJ, Albrecht U, Andersen ME, Ansari N, Bhattacharya S, Bode JG, et al. Recent advances in 2D and 3D in vitro systems using primary hepatocytes, alternative hepatocyte sources and non-parenchymal liver cells and their use in investigating mechanisms of hepatotoxicity, cell signaling and ADME. *Arch Toxicol* 2013;87:1315-1530.
12. Cullen JM. Mechanistic classification of liver injury. *Toxicol Pathol* 2005;33:6-8.
13. Lee WM. Drug-induced hepatotoxicity. *N Engl J Med* 2003;349:474-485.

## References

---

14. Russmann S, Kullak-Ublick GA, Grattagliano I. Current concepts of mechanisms in drug-induced hepatotoxicity. *Curr Med Chem* 2009;16:3041-3053.
15. Liddle C, Stedman CA: Hepatic metabolism of drugs. In: Rodés J, Benhamou J-P, Blei AT, Reichen JR, Manocchia M, eds. *Textbook of hepatology: from basic science to clinical practice*. 3rd edition ed: Malden: Wiley-Blackwell Publishing., 2007.
16. Holt M, Ju C. Drug-induced liver injury. *Handb Exp Pharmacol* 2010;3-27.
17. Kaplowitz N. Drug-induced liver injury. *Clin Infect Dis* 2004;38 Suppl 2:S44-48.
18. Holt MP, Ju C. Mechanisms of drug-induced liver injury. *AAPS J* 2006;8:E48-54.
19. Watkins PB, Seeff LB. Drug-induced liver injury: summary of a single topic clinical research conference. *Hepatology* 2006;43:618-631.
20. Kaplowitz N. Drug-induced liver disorders: implications for drug development and regulation. *Drug Saf* 2001;24:483-490.
21. Sgro C, Clinard F, Ouazir K, Chanay H, Allard C, Guilleminet C, Lenoir C, et al. Incidence of drug-induced hepatic injuries: a French population-based study. *Hepatology* 2002;36:451-455.
22. Andrade RJ, Camargo R, Lucena MI, Gonzalez-Grande R. Causality assessment in drug-induced hepatotoxicity. *Expert Opin Drug Saf* 2004;3:329-344.
23. Russo MW, Galanko JA, Shrestha R, Fried MW, Watkins P. Liver transplantation for acute liver failure from drug induced liver injury in the United States. *Liver Transpl* 2004;10:1018-1023.
24. Kaplowitz N: Drug-Induced Liver Injury. In: Kaplowitz N, DeLeve LD, eds. *Drug-induced liver disease*. 3rd edition ed: Academic Press, 2013.
25. Zimmerman HJ. *Hepatotoxicity: the adverse effects of drugs and other chemicals on the liver*: Lippincott Williams & Wilkins, 1999.
26. Grattagliano I, Bonfrate L, Diogo CV, Wang HH, Wang DQ, Portincasa P. Biochemical mechanisms in drug-induced liver injury: certainties and doubts. *World J Gastroenterol* 2009;15:4865-4876.
27. Greer ML, Barber J, Eakins J, Kenna JG. Cell based approaches for evaluation of drug-induced liver injury. *Toxicology* 2010;268:125-131.
28. Tujios S, Fontana RJ. Mechanisms of drug-induced liver injury: from bedside to bench. *Nat Rev Gastroenterol Hepatol* 2011;8:202-211.
29. Gomez-Lechon MJ, Tolosa L, Castell JV, Donato MT. Mechanism-based selection of compounds for the development of innovative in vitro approaches to hepatotoxicity studies in the LIINTOP project. *Toxicol In Vitro* 2010;24:1879-1889.
30. Jaeschke H, Gores GJ, Cederbaum AI, Hinson JA, Pessayre D, Lemasters JJ. Mechanisms of hepatotoxicity. *Toxicol Sci* 2002;65:166-176.

## References

---

31. Portincasa P, Grattagliano I, Palmieri VO, Palasciano G. Nonalcoholic steatohepatitis: recent advances from experimental models to clinical management. *Clin Biochem* 2005;38:203-217.
32. Donato MT, Gomez-Lechon MJ. Drug-induced liver steatosis and phospholipidosis: cell-based assays for early screening of drug candidates. *Curr Drug Metab* 2012;13:1160-1173.
33. Labbe G, Pessayre D, Fromenty B. Drug-induced liver injury through mitochondrial dysfunction: mechanisms and detection during preclinical safety studies. *Fundam Clin Pharmacol* 2008;22:335-353.
34. Begriche K, Massart J, Robin MA, Borgne-Sanchez A, Fromenty B. Drug-induced toxicity on mitochondria and lipid metabolism: mechanistic diversity and deleterious consequences for the liver. *J Hepatol* 2011;54:773-794.
35. Pessayre D, Mansouri A, Berson A, Fromenty B. Mitochondrial involvement in drug-induced liver injury. *Handb Exp Pharmacol* 2010:311-365.
36. Reasor MJ, Hastings KL, Ulrich RG. Drug-induced phospholipidosis: issues and future directions. *Expert Opin Drug Saf* 2006;5:567-583.
37. Reasor MJ, Kacew S. Drug-induced phospholipidosis: are there functional consequences? *Exp Biol Med (Maywood)* 2001;226:825-830.
38. Yang K, Kock K, Sedykh A, Tropsha A, Brouwer KL. An updated review on drug-induced cholestasis: mechanisms and investigation of physicochemical properties and pharmacokinetic parameters. *J Pharm Sci* 2013;102:3037-3057.
39. Hylemon PB, Zhou H, Pandak WM, Ren S, Gil G, Dent P. Bile acids as regulatory molecules. *J Lipid Res* 2009;50:1509-1520.
40. Pols TW, Noriega LG, Nomura M, Auwerx J, Schoonjans K. The bile acid membrane receptor TGR5 as an emerging target in metabolism and inflammation. *J Hepatol* 2011;54:1263-1272.
41. Thomas C, Pellicciari R, Pruzanski M, Auwerx J, Schoonjans K. Targeting bile-acid signalling for metabolic diseases. *Nat Rev Drug Discov* 2008;7:678-693.
42. Chiang JY. Bile acids: regulation of synthesis. *J Lipid Res* 2009;50:1955-1966.
43. Khan AA, Chow EC, Porte RJ, Pang KS, Groothuis GM. The role of lithocholic acid in the regulation of bile acid detoxication, synthesis, and transport proteins in rat and human intestine and liver slices. *Toxicol In Vitro* 2011;25:80-90.
44. Reschly EJ, Krasowski MD. Evolution and function of the NR1I nuclear hormone receptor subfamily (VDR, PXR, and CAR) with respect to metabolism of xenobiotics and endogenous compounds. *Curr Drug Metab* 2006;7:349-365.
45. Padda MS, Sanchez M, Akhtar AJ, Boyer JL. Drug-induced cholestasis. *Hepatology* 2011;53:1377-1387.

## References

---

46. Palmeira CM, Rolo AP. Mitochondrially-mediated toxicity of bile acids. *Toxicology* 2004;203:1-15.
47. Trottier J, Bialek A, Caron P, Straka RJ, Heathcote J, Milkiewicz P, Barbier O. Metabolomic profiling of 17 bile acids in serum from patients with primary biliary cirrhosis and primary sclerosing cholangitis: a pilot study. *Dig Liver Dis* 2012;44:303-310.
48. Pauli-Magnus C, Meier PJ. Hepatobiliary transporters and drug-induced cholestasis. *Hepatology* 2006;44:778-787.
49. Gomez-Lechon MJ, Lahoz A, Gombau L, Castell JV, Donato MT. In vitro evaluation of potential hepatotoxicity induced by drugs. *Curr Pharm Des* 2010;16:1963-1977.
50. Yuan L, Kaplowitz N. Glutathione in liver diseases and hepatotoxicity. *Mol Aspects Med* 2009;30:29-41.
51. Jaeschke H, McGill MR, Ramachandran A. Oxidant stress, mitochondria, and cell death mechanisms in drug-induced liver injury: lessons learned from acetaminophen hepatotoxicity. *Drug Metab Rev* 2012;44:88-106.
52. O'Brien PJ, Irwin W, Diaz D, Howard-Cofield E, Krejsa CM, Slaughter MR, Gao B, et al. High concordance of drug-induced human hepatotoxicity with in vitro cytotoxicity measured in a novel cell-based model using high content screening. *Arch Toxicol* 2006;80:580-604.
53. Olson H, Betton G, Robinson D, Thomas K, Monro A, Kolaja G, Lilly P, et al. Concordance of the toxicity of pharmaceuticals in humans and in animals. *Regul Toxicol Pharmacol* 2000;32:56-67.
54. Kia R, Sison RL, Heslop J, Kitteringham NR, Hanley N, Mills JS, Park BK, et al. Stem cell-derived hepatocytes as a predictive model for drug-induced liver injury: are we there yet? *Br J Clin Pharmacol* 2013;75:885-896.
55. Hewitt NJ, Lechon MJ, Houston JB, Hallifax D, Brown HS, Maurel P, Kenna JG, et al. Primary hepatocytes: current understanding of the regulation of metabolic enzymes and transporter proteins, and pharmaceutical practice for the use of hepatocytes in metabolism, enzyme induction, transporter, clearance, and hepatotoxicity studies. *Drug Metab Rev* 2007;39:159-234.
56. Forte TM, McCall MR, Knowles BB, Shore VG. Isolation and characterization of lipoproteins produced by human hepatoma-derived cell lines other than HepG2. *J Lipid Res* 1989;30:817-829.
57. Javitt NB. Hep G2 cells as a resource for metabolic studies: lipoprotein, cholesterol, and bile acids. *FASEB J* 1990;4:161-168.
58. Knowles BB, Howe CC, Aden DP. Human hepatocellular carcinoma cell lines secrete the major plasma proteins and hepatitis B surface antigen. *Science* 1980;209:497-499.
59. Donato MT, Jover R, Gomez-Lechon MJ. Hepatic cell lines for drug hepatotoxicity testing: limitations and strategies to upgrade their

## References

---

- metabolic competence by gene engineering. *Curr Drug Metab* 2013;14:946-968.
60. Schoonen WG, Westerink WM, de Roos JA, Debiton E. Cytotoxic effects of 100 reference compounds on Hep G2 and HeLa cells and of 60 compounds on ECC-1 and CHO cells. I mechanistic assays on ROS, glutathione depletion and calcein uptake. *Toxicol In Vitro* 2005;19:505-516.
  61. Schoonen WG, Stevenson JC, Westerink WM, Horbach GJ. Cytotoxic effects of 109 reference compounds on rat H4IIE and human HepG2 hepatocytes. III: Mechanistic assays on oxygen consumption with MitoXpress and NAD(P)H production with Alamar Blue. *Toxicol In Vitro* 2012;26:511-525.
  62. Van Summeren A, Renes J, Bouwman FG, Noben JP, van Delft JH, Kleinjans JC, Mariman EC. Proteomics investigations of drug-induced hepatotoxicity in HepG2 cells. *Toxicol Sci* 2011;120:109-122.
  63. Jetten MJ, Kleinjans JC, Claessen SM, Chesne C, van Delft JH. Baseline and genotoxic compound induced gene expression profiles in HepG2 and HepaRG compared to primary human hepatocytes. *Toxicol In Vitro* 2013;27:2031-2040.
  64. Van den Hof WF, Coonen ML, van Herwijnen M, Brauers K, Wodzig WK, van Delft JH, Kleinjans JC. Classification of hepatotoxicants using HepG2 cells: A proof of principle study. *Chem Res Toxicol* 2014;27:433-442.
  65. Xu JJ, Diaz D, O'Brien PJ. Applications of cytotoxicity assays and pre-lethal mechanistic assays for assessment of human hepatotoxicity potential. *Chem Biol Interact* 2004;150:115-128.
  66. Wang Z, Gerstein M, Snyder M. RNA-Seq: a revolutionary tool for transcriptomics. *Nat Rev Genet* 2009;10:57-63.
  67. Waring JF, Ciurlionis R, Jolly RA, Heindel M, Ulrich RG. Microarray analysis of hepatotoxins in vitro reveals a correlation between gene expression profiles and mechanisms of toxicity. *Toxicol Lett* 2001;120:359-368.
  68. Li HH, Aubrecht J, Fornace AJ, Jr. Toxicogenomics: overview and potential applications for the study of non-covalent DNA interacting chemicals. *Mutat Res* 2007;623:98-108.
  69. Benet M, Moya M, Donato MT, Lahoz A, Hervas D, Guzman C, Gomez-Lechon MJ, et al. A simple transcriptomic signature able to predict drug-induced hepatic steatosis. *Arch Toxicol* 2014;88:967-982.
  70. Blomme EA, Yang Y, Waring JF. Use of toxicogenomics to understand mechanisms of drug-induced hepatotoxicity during drug discovery and development. *Toxicol Lett* 2009;186:22-31.
  71. Sawada H, Takami K, Asahi S. A toxicogenomic approach to drug-induced phospholipidosis: analysis of its induction mechanism and



## References

---

- establishment of a novel in vitro screening system. *Toxicol Sci* 2005;83:282-292.
72. Cui Y, Paules RS. Use of transcriptomics in understanding mechanisms of drug-induced toxicity. *Pharmacogenomics* 2010;11:573-585.
  73. Wilkins MR, Pasquali C, Appel RD, Ou K, Golaz O, Sanchez JC, Yan JX, et al. From proteins to proteomes: large scale protein identification by two-dimensional electrophoresis and amino acid analysis. *Biotechnology (N Y)* 1996;14:61-65.
  74. Anderson NL, Anderson NG. Proteome and proteomics: new technologies, new concepts, and new words. *Electrophoresis* 1998;19:1853-1861.
  75. Blackstock WP, Weir MP. Proteomics: quantitative and physical mapping of cellular proteins. *Trends Biotechnol* 1999;17:121-127.
  76. Anderson L, Seilhamer J. A comparison of selected mRNA and protein abundances in human liver. *Electrophoresis* 1997;18:533-537.
  77. Kennedy S. The role of proteomics in toxicology: identification of biomarkers of toxicity by protein expression analysis. *Biomarkers* 2002;7:269-290.
  78. Van Summeren A, Renes J, Lizarraga D, Bouwman FG, Noben JP, van Delft JH, Kleinjans JC, et al. Screening for drug-induced hepatotoxicity in primary mouse hepatocytes using acetaminophen, amiodarone, and cyclosporin a as model compounds: an omics-guided approach. *OMICS* 2013;17:71-83.
  79. Van Summeren A, Renes J, van Delft JH, Kleinjans JC, Mariman EC. Proteomics in the search for mechanisms and biomarkers of drug-induced hepatotoxicity. *Toxicol In Vitro* 2012;26:373-385.
  80. Bouhifd M, Hartung T, Hogberg HT, Kleensang A, Zhao L. Review: toxicometabolomics. *J Appl Toxicol* 2013;33:1365-1383.
  81. Goodacre R, Vaidyanathan S, Dunn WB, Harrigan GG, Kell DB. Metabolomics by numbers: acquiring and understanding global metabolite data. *Trends Biotechnol* 2004;22:245-252.
  82. Garbis S, Lubec G, Fountoulakis M. Limitations of current proteomics technologies. *J Chromatogr A* 2005;1077:1-18.
  83. Bernas T, Gregori G, Asem EK, Robinson JP. Integrating cytomics and proteomics. *Mol Cell Proteomics* 2006;5:2-13.
  84. Herrera G, Diaz L, Martinez-Romero A, Gomes A, Villamon E, Callaghan RC, O'Connor JE. Cytomics: A multiparametric, dynamic approach to cell research. *Toxicol In Vitro* 2007;21:176-182.
  85. Gomase VS, Tagore S. Cytomics. *Curr Drug Metab* 2008;9:263-266.
  86. Gough AH, Johnston PA. Requirements, features, and performance of high content screening platforms. *Methods Mol Biol* 2007;356:41-61.
  87. Abraham VC, Towne DL, Waring JF, Warrior U, Burns DJ. Application of a high-content multiparameter cytotoxicity assay to prioritize

## References

---

- compounds based on toxicity potential in humans. *J Biomol Screen* 2008;13:527-537.
88. Donato MT, Martinez-Romero A, Jimenez N, Negro A, Herrera G, Castell JV, O'Connor JE, et al. Cytometric analysis for drug-induced steatosis in HepG2 cells. *Chem Biol Interact* 2009;181:417-423.
  89. Donato MT, Tolosa L, Jimenez N, Castell JV, Gomez-Lechon MJ. High-content imaging technology for the evaluation of drug-induced steatosis using a multiparametric cell-based assay. *J Biomol Screen* 2012;17:394-400.
  90. Garside H, Marcoe KF, Chesnut-Speelman J, Foster AJ, Muthas D, Kenna JG, Warrior U, et al. Evaluation of the use of imaging parameters for the detection of compound-induced hepatotoxicity in 384-well cultures of HepG2 cells and cryopreserved primary human hepatocytes. *Toxicol In Vitro* 2014;28:171-181.
  91. Tolosa L, Gomez-Lechon MJ, Perez-Cataldo G, Castell JV, Donato MT. HepG2 cells simultaneously expressing five P450 enzymes for the screening of hepatotoxicity: identification of bioactivable drugs and the potential mechanism of toxicity involved. *Arch Toxicol* 2013;87:1115-1127.
  92. Tolosa L, Pinto S, Donato MT, Lahoz A, Castell JV, O'Connor JE, Gomez-Lechon MJ. Development of a multiparametric cell-based protocol to screen and classify the hepatotoxicity potential of drugs. *Toxicol Sci* 2012;127:187-198.
  93. Xu JJ, Henstock PV, Dunn MC, Smith AR, Chabot JR, de Graaf D. Cellular imaging predictions of clinical drug-induced liver injury. *Toxicol Sci* 2008;105:97-105.
  94. Oliver SG, Winson MK, Kell DB, Baganz F. Systematic functional analysis of the yeast genome. *Trends Biotechnol* 1998;16:373-378.
  95. Tweeddale H, Notley-McRobb L, Ferenci T. Effect of slow growth on metabolism of *Escherichia coli*, as revealed by global metabolite pool ("metabolome") analysis. *J Bacteriol* 1998;180:5109-5116.
  96. Nicholson JK. Global systems biology, personalized medicine and molecular epidemiology. *Mol Syst Biol* 2006;2:52.
  97. Fiehn O. Metabolomics--the link between genotypes and phenotypes. *Plant Mol Biol* 2002;48:155-171.
  98. Nicholson JK, Lindon JC, Holmes E. 'Metabonomics': understanding the metabolic responses of living systems to pathophysiological stimuli via multivariate statistical analysis of biological NMR spectroscopic data. *Xenobiotica* 1999;29:1181-1189.
  99. Lindon JC, Holmes E, Bollard ME, Stanley EG, Nicholson JK. Metabonomics technologies and their applications in physiological monitoring, drug safety assessment and disease diagnosis. *Biomarkers* 2004;9:1-31.
  100. Nicholson JK, Lindon JC. Systems biology: Metabonomics. *Nature* 2008;455:1054-1056.

## References

---

101. Cortes M, Pareja E, Castell JV, Moya A, Mir J, Lahoz A. Exploring mass spectrometry suitability to examine human liver graft metabonomic profiles. *Transplant Proc* 2010;42:2953-2958.
102. Folger O, Jerby L, Frezza C, Gottlieb E, Ruppin E, Shlomi T. Predicting selective drug targets in cancer through metabolic networks. *Mol Syst Biol* 2011;7:501.
103. Leon Z, Garcia-Canaveras JC, Donato MT, Lahoz A. Mammalian cell metabolomics: experimental design and sample preparation. *Electrophoresis* 2013;34:2762-2775.
104. Masson P, Spagou K, Nicholson JK, Want EJ. Technical and biological variation in UPLC-MS-based untargeted metabolic profiling of liver extracts: application in an experimental toxicity study on galactosamine. *Anal Chem* 2011;83:1116-1123.
105. Patterson AD, Maurhofer O, Beyoglu D, Lanz C, Krausz KW, Pabst T, Gonzalez FJ, et al. Aberrant lipid metabolism in hepatocellular carcinoma revealed by plasma metabolomics and lipid profiling. *Cancer Res* 2011;71:6590-6600.
106. Puri P, Baillie RA, Wiest MM, Mirshahi F, Choudhury J, Cheung O, Sargeant C, et al. A lipidomic analysis of nonalcoholic fatty liver disease. *Hepatology* 2007;46:1081-1090.
107. Dettmer K, Aronov PA, Hammock BD. Mass spectrometry-based metabolomics. *Mass Spectrom Rev* 2007;26:51-78.
108. Villas-Boas SG, Mas S, Akesson M, Smedsgaard J, Nielsen J. Mass spectrometry in metabolome analysis. *Mass Spectrom Rev* 2005;24:613-646.
109. Nicholson JK, Connelly J, Lindon JC, Holmes E. Metabonomics: a platform for studying drug toxicity and gene function. *Nat Rev Drug Discov* 2002;1:153-161.
110. Wishart DS, Jewison T, Guo AC, Wilson M, Knox C, Liu Y, Djoumbou Y, et al. HMDB 3.0--The Human Metabolome Database in 2013. *Nucleic Acids Res* 2013;41:D801-807.
111. Beecher CW: The human metabolome. In: Garrigan GG, Goodacre R, eds. *Metabolic profiling: Its role in biomarker discovery and gene function analysis*: Springer, 2003; 311-319.
112. Robertson DG. Metabonomics in toxicology: a review. *Toxicol Sci* 2005;85:809-822.
113. Clarke CJ, Haselden JN. Metabolic profiling as a tool for understanding mechanisms of toxicity. *Toxicol Pathol* 2008;36:140-147.
114. Lenz EM, Wilson ID. Analytical strategies in metabonomics. *J Proteome Res* 2007;6:443-458.
115. Wilson ID, Plumb R, Granger J, Major H, Williams R, Lenz EM. HPLC-MS-based methods for the study of metabonomics. *J Chromatogr B Analyt Technol Biomed Life Sci* 2005;817:67-76.

## References

---

116. Alpert AJ. Hydrophilic-interaction chromatography for the separation of peptides, nucleic acids and other polar compounds. *Journal of Chromatography A* 1990;499:177-196.
117. Buszewski B, Noga S. Hydrophilic interaction liquid chromatography (HILIC)--a powerful separation technique. *Anal Bioanal Chem* 2012;402:231-247.
118. Hemström P, Irgum K. Hydrophilic interaction chromatography. *J Sep Sci* 2006;29:1784-1821.
119. Spagou K, Tsoukali H, Raikos N, Gika H, Wilson ID, Theodoridis G. Hydrophilic interaction chromatography coupled to MS for metabonomic/metabolomic studies. *J Sep Sci* 2010;33:716-727.
120. Lu W, Bennett BD, Rabinowitz JD. Analytical strategies for LC-MS-based targeted metabolomics. *J Chromatogr B Analyt Technol Biomed Life Sci* 2008;871:236-242.
121. Saccenti E, Hoefsloot HC, Smilde AK, Westerhuis JA, Hendriks MM. Reflections on univariate and multivariate analysis of metabolomics data. *Metabolomics* 2013:1-14.
122. Trygg J, Holmes E, Lundstedt T. Chemometrics in metabonomics. *J Proteome Res* 2007;6:469-479.
123. Eisen MB, Spellman PT, Brown PO, Botstein D. Cluster analysis and display of genome-wide expression patterns. *Proc Natl Acad Sci U S A* 1998;95:14863-14868.
124. Xia J, Wishart DS. Metabolomic data processing, analysis, and interpretation using MetaboAnalyst. *Curr Protoc Bioinformatics* 2011;Chapter 14:Unit 14 10.
125. Hendriks MM, Eeuwijk FAv, Jellema RH, Westerhuis JA, Reijmers TH, Hoefsloot HC, Smilde AK. Data-processing strategies for metabolomics studies. *TrAC Trends in Analytical Chemistry* 2011;30:1685-1698.
126. Kaddurah-Daouk R, Kristal BS, Weinshilboum RM. Metabolomics: a global biochemical approach to drug response and disease. *Annu Rev Pharmacol Toxicol* 2008;48:653-683.
127. Wold S, Sjöström M, Eriksson L. PLS-regression: a basic tool of chemometrics. *Chemometrics and intelligent laboratory systems* 2001;58:109-130.
128. Barker M, Rayens W. Partial least squares for discrimination. *Journal of chemometrics* 2003;17:166-173.
129. Trygg J, Wold S. Orthogonal projections to latent structures (O-PLS). *Journal of chemometrics* 2002;16:119-128.
130. Brereton R. *Chemometrics for pattern recognition*: John Wiley & Sons, 2009.
131. Xia J, Wishart DS. Web-based inference of biological patterns, functions and pathways from metabolomic data using MetaboAnalyst. *Nat Protoc* 2011;6:743-760.

## References

---

132. Martens HA, Dardenne P. Validation and verification of regression in small data sets. *Chemometrics and intelligent laboratory systems* 1998;44:99-121.
133. Bijlsma S, Bobeldijk I, Verheij ER, Ramaker R, Kochhar S, Macdonald IA, van Ommen B, et al. Large-scale human metabolomics studies: a strategy for data (pre-) processing and validation. *Anal Chem* 2006;78:567-574.
134. Lindgren F, Hansen B, Karcher W, Sjöström M, Eriksson L. Model validation by permutation tests: Applications to variable selection. *Journal of chemometrics* 1996;10:521-532.
135. Lindon JC, Holmes E, Nicholson JK. Metabonomics in pharmaceutical R&D. *FEBS J* 2007;274:1140-1151.
136. Chen C, Krausz KW, Idle JR, Gonzalez FJ. Identification of novel toxicity-associated metabolites by metabolomics and mass isotopomer analysis of acetaminophen metabolism in wild-type and Cyp2e1-null mice. *J Biol Chem* 2008;283:4543-4559.
137. Kumar BS, Chung BC, Kwon OS, Jung BH. Discovery of common urinary biomarkers for hepatotoxicity induced by carbon tetrachloride, acetaminophen and methotrexate by mass spectrometry-based metabolomics. *J Appl Toxicol* 2012;32:505-520.
138. Soga T, Baran R, Suematsu M, Ueno Y, Ikeda S, Sakurakawa T, Kakazu Y, et al. Differential metabolomics reveals ophthalmic acid as an oxidative stress biomarker indicating hepatic glutathione consumption. *J Biol Chem* 2006;281:16768-16776.
139. Spagou K, Wilson ID, Masson P, Theodoridis G, Raikos N, Coen M, Holmes E, et al. HILIC-UPLC-MS for exploratory urinary metabolic profiling in toxicological studies. *Anal Chem* 2011;83:382-390.
140. Yamazaki M, Miyake M, Sato H, Masutomi N, Tsutsui N, Adam K-P, Alexander DC, et al. Perturbation of bile acid homeostasis is an early pathogenesis event of drug induced liver injury in rats. *Toxicol Appl Pharmacol* 2013;268:79-89.
141. Clayton TA, Lindon JC, Cloarec O, Antti H, Charuel C, Hanton G, Provost JP, et al. Pharmacometabonomic phenotyping and personalized drug treatment. *Nature* 2006;440:1073-1077.
142. Fannin RD, Russo M, O'Connell TM, Gerrish K, Winnike JH, Macdonald J, Newton J, et al. Acetaminophen dosing of humans results in blood transcriptome and metabolome changes consistent with impaired oxidative phosphorylation. *Hepatology* 2010;51:227-236.
143. Jetten MJ, Gaj S, Ruiz-Aracama A, de Kok TM, van Delft JH, Lommen A, van Someren EP, et al. 'Omics analysis of low dose acetaminophen intake demonstrates novel response pathways in humans. *Toxicol Appl Pharmacol* 2012;259:320-328.

## References

---

144. Bennett BD, Yuan J, Kimball EH, Rabinowitz JD. Absolute quantitation of intracellular metabolite concentrations by an isotope ratio-based approach. *Nat Protoc* 2008;3:1299-1311.
145. Yuan J, Bennett BD, Rabinowitz JD. Kinetic flux profiling for quantitation of cellular metabolic fluxes. *Nature protocols* 2008;3:1328-1340.
146. Panopoulos AD, Yanes O, Ruiz S, Kida YS, Diep D, Tautenhahn R, Herrerias A, et al. The metabolome of induced pluripotent stem cells reveals metabolic changes occurring in somatic cell reprogramming. *Cell Res* 2012;22:168-177.
147. Chong WP, Thng SH, Hiu AP, Lee DY, Chan EC, Ho YS. LC-MS-based metabolic characterization of high monoclonal antibody-producing Chinese hamster ovary cells. *Biotechnol Bioeng* 2012;109:3103-3111.
148. Sellick CA, Hansen R, Maqsood AR, Dunn WB, Stephens GM, Goodacre R, Dickson AJ. Effective quenching processes for physiologically valid metabolite profiling of suspension cultured mammalian cells. *Anal Chem* 2008;81:174-183.
149. Croixmarie V, Umbdenstock T, Cloarec O, Moreau A, Pascussi JM, Parmentier Y, Boursier-Neyret C, et al. Metabonomic studies on human hepatocyte in primary culture. *Methods Mol Biol* 2010;640:355-374.
150. Dettmer K, Nurnberger N, Kaspar H, Gruber MA, Almstetter MF, Oefner PJ. Metabolite extraction from adherently growing mammalian cells for metabolomics studies: optimization of harvesting and extraction protocols. *Anal Bioanal Chem* 2011;399:1127-1139.
151. Sheikh KD, Khanna S, Byers SW, Fornace A, Jr., Cheema AK. Small molecule metabolite extraction strategy for improving LC/MS detection of cancer cell metabolome. *J Biomol Tech* 2011;22:1-4.
152. Lorenz MA, Burant CF, Kennedy RT. Reducing time and increasing sensitivity in sample preparation for adherent mammalian cell metabolomics. *Anal Chem* 2011;83:3406-3414.
153. Fernandez C, Fransson U, Hallgard E, Spegel P, Holm C, Krogh M, Warell K, et al. Metabolomic and proteomic analysis of a clonal insulin-producing beta-cell line (INS-1 832/13). *J Proteome Res* 2008;7:400-411.
154. Brown MV, Compton SA, Milburn MV, Lawton KA, Cheatham B. Metabolomic signatures in lipid-loaded HepaRGs reveal pathways involved in steatotic progression. *Obesity (Silver Spring)* 2013;21:E561-570.
155. Bai J, Wang MX, Chowbay B, Ching CB, Chen WN. Metabolic profiling of HepG2 cells incubated with S(-) and R(+) enantiomers of anti-coagulating drug warfarin. *Metabolomics* 2011;7:353-362.
156. Ruiz-Aracama A, Peijnenburg A, Kleinjans J, Jennen D, van Delft J, Hellfrisch C, Lommen A. An untargeted multi-technique

## References

---

- metabolomics approach to studying intracellular metabolites of HepG2 cells exposed to 2,3,7,8-tetrachlorodibenzo-p-dioxin. *BMC Genomics* 2011;12:251.
157. Croixmarie V, Umbdenstock T, Cloarec O, Moreau A, Pascussi JM, Boursier-Neyret C, Walther B. Integrated comparison of drug-related and drug-induced ultra performance liquid chromatography/mass spectrometry metabonomic profiles using human hepatocyte cultures. *Anal Chem* 2009;81:6061-6069.
  158. Marion TL, Perry CH, St Claire RL, 3rd, Brouwer KL. Endogenous bile acid disposition in rat and human sandwich-cultured hepatocytes. *Toxicol Appl Pharmacol* 2012;261:1-9.
  159. Gomez-Lechon MJ, Ponsoda X, O'Connor E, Donato T, Jover R, Castell JV. Diclofenac induces apoptosis in hepatocytes. *Toxicol In Vitro* 2003;17:675-680.
  160. Lowry OH, Rosebrough NJ, Farr AL, Randall RJ. Protein measurement with the Folin phenol reagent. *J Biol Chem* 1951;193:265-275.
  161. Swartz ME. UPLC™: an introduction and review. *Journal of Liquid Chromatography & Related Technologies* 2005;28:1253-1263.
  162. Want EJ, Masson P, Michopoulos F, Wilson ID, Theodoridis G, Plumb RS, Shockcor J, et al. Global metabolic profiling of animal and human tissues via UPLC-MS. *Nat Protoc* 2013;8:17-32.
  163. Nygren H, Seppanen-Laakso T, Castillo S, Hyotylainen T, Oresic M. Liquid chromatography-mass spectrometry (LC-MS)-based lipidomics for studies of body fluids and tissues. *Methods Mol Biol* 2011;708:247-257.
  164. Katajamaa M, Oresic M. Data processing for mass spectrometry-based metabolomics. *J Chromatogr A* 2007;1158:318-328.
  165. Pluskal T, Castillo S, Villar-Briones A, Oresic M. MZmine 2: modular framework for processing, visualizing, and analyzing mass spectrometry-based molecular profile data. *BMC Bioinformatics* 2010;11:395.
  166. Garcia-Cañaveras JC, Donato MT, Castell JV, Lahoz A. A comprehensive untargeted metabonomic analysis of human steatotic liver tissue by RP and HILIC chromatography coupled to mass spectrometry reveals important metabolic alterations. *J Proteome Res* 2011;10:4825-4834.
  167. Quintás G, Portillo N, García-Cañaveras JC, Castell JV, Ferrer A, Lahoz A. Chemometric approaches to improve PLS-DA model outcome for predicting human non-alcoholic fatty liver disease using UPLC-MS as a metabolic profiling tool. *Metabolomics* 2012;8:86-98.
  168. Want E, Masson P. Processing and analysis of GC/LC-MS-based metabolomics data. *Methods Mol Biol* 2011;708:277-298.
  169. Fahy E, Sud M, Cotter D, Subramaniam S. LIPID MAPS online tools for lipid research. *Nucleic Acids Res* 2007;35:W606-612.

## References

---

170. Smith CA, O'Maille G, Want EJ, Qin C, Trauger SA, Brandon TR, Custodio DE, et al. METLIN: a metabolite mass spectral database. *Ther Drug Monit* 2005;27:747-751.
171. Horai H, Arita M, Kanaya S, Nihei Y, Ikeda T, Suwa K, Ojima Y, et al. MassBank: a public repository for sharing mass spectral data for life sciences. *J Mass Spectrom* 2010;45:703-714.
172. R Core Team. R: A Language and Environment for Statistical Computing. In: Vienna, Austria: R Foundation for Statistical Computing; 2014.
173. Stacklies W, Redestig H, Scholz M, Walther D, Selbig J. *pcaMethods*—a bioconductor package providing PCA methods for incomplete data. *Bioinformatics* 2007;23:1164-1167.
174. González I, Lê Cao K, Déjean S. *MixOmics*: Omics data integration project. In: R package version 5.0-1; 2013.
175. Sanchez G. *Discriminer*: Tools of the Trade for Discriminant Analysis. In: R package version 0.1-29; 2013.
176. Warnes GR, Bolker B, Bonebakker L, Gentleman R, Liaw WHA, Lumley T, Maechler M, et al. *gplots*: Various R programming tools for plotting data. In: R package version 2.13.0; 2014.
177. Canty A, Ripley B. *boot*: Bootstrap R (S-Plus) Functions. R package version 1.3-11 2014.
178. Kuhn M. *caret*: Classification and Regression Training. R package version 6.0-30 2014.
179. Husson F, Josse J, Le S, Mazet J. *FactoMineR*: Multivariate Exploratory Data Analysis and Data Mining with R. R package version 1.26 2014.
180. Robin X, Turck N, Hainard A, Tiberti N, Lisacek F, Sanchez JC, Muller M. *pROC*: an open-source package for R and S+ to analyze and compare ROC curves. *BMC Bioinformatics* 2011;12:77.
181. Adler D, Murdoch D. *rgl*: 3D visualization device system (OpenGL). R package version 0.92 2012;798.
182. Chen H, Boutros PC. *VennDiagram*: a package for the generation of highly-customizable Venn and Euler diagrams in R. *BMC Bioinformatics* 2011;12:35.
183. Cortes M, Pareja E, García-Cañaveras JC, Donato MT, Montero S, Mir J, Castell JV, et al. Metabolomics discloses donor liver biomarkers associated with early allograft dysfunction. *J Hepatol* 2014;61:564-574.
184. Hotelling H. The generalization of Student's ratio. *Ann Math Stat* 1931;2:360-378.
185. Benjamini Y, Hochberg Y. Controlling the false discovery rate: a practical and powerful approach to multiple testing. *Journal of the Royal Statistical Society. Series B (Methodological)* 1995:289-300.
186. Xia J, Mandal R, Sinelnikov IV, Broadhurst D, Wishart DS. *MetaboAnalyst 2.0*--a comprehensive server for metabolomic data analysis. *Nucleic Acids Res* 2012;40:W127-133.



## References

---

187. Chagoyen M, Pazos F. MBRole: enrichment analysis of metabolomic data. *Bioinformatics* 2011;27:730-731.
188. Hand DJ, Till RJ. A simple generalisation of the area under the ROC curve for multiple class classification problems. *Machine learning* 2001;45:171-186.
189. Westerhuis JA, Hoefsloot HC, Smit S, Vis DJ, Smilde AK, van Velzen EJ, van Duijnhoven JP, et al. Assessment of PLS-DA cross validation. *Metabolomics* 2008;4:81-89.
190. Chong I-G, Jun C-H. Performance of some variable selection methods when multicollinearity is present. *Chemometrics and intelligent laboratory systems* 2005;78:103-112.
191. Efron B. Bootstrap methods: another look at the jackknife. *The annals of Statistics* 1979:1-26.
192. Efron B, Tibshirani RJ. *An introduction to the bootstrap*: CRC press, 1994.
193. Gomez-Lechon MJ, Donato MT, Martinez-Romero A, Jimenez N, Castell JV, O'Connor JE. A human hepatocellular in vitro model to investigate steatosis. *Chem Biol Interact* 2007;165:106-116.
194. Cao B, Aa J, Wang G, Wu X, Liu L, Li M, Shi J, et al. GC-TOFMS analysis of metabolites in adherent MDCK cells and a novel strategy for identifying intracellular metabolic markers for use as cell amount indicators in data normalization. *Anal Bioanal Chem* 2011;400:2983-2993.
195. Wu H, Southam AD, Hines A, Viant MR. High-throughput tissue extraction protocol for NMR- and MS-based metabolomics. *Anal Biochem* 2008;372:204-212.
196. Yamamoto T. *Medaka (killifish): biology and strains*: Yugen-sha, 1975.
197. Kinoshita M, Murata K, Naruse K, Tanaka M. *Medaka: biology, management, and experimental protocols*: John Wiley & Sons, 2009.
198. Bando K, Kunimatsu T, Sakai J, Kimura J, Funabashi H, Seki T, Bamba T, et al. GC-MS-based metabolomics reveals mechanism of action for hydrazine induced hepatotoxicity in rats. *J Appl Toxicol* 2011;31:524-535.
199. Chen YH, Lee HC, Hsu RJ, Chen TY, Huang YK, Lo HC, Hu SC, et al. The toxic effect of Amiodarone on valve formation in the developing heart of zebrafish embryos. *Reprod Toxicol* 2012;33:233-244.
200. Driessen M, Kienhuis AS, Pennings JL, Pronk TE, van de Brandhof E-J, Roodbergen M, Spaik HP, et al. Exploring the zebrafish embryo as an alternative model for the evaluation of liver toxicity by histopathology and expression profiling. *Arch Toxicol* 2013;87:807-823.
201. He JH, Guo SY, Zhu F, Zhu JJ, Chen YX, Huang CJ, Gao JM, et al. A zebrafish phenotypic assay for assessing drug-induced hepatotoxicity. *J Pharmacol Toxicol Methods* 2013;67:25-32.

## References

---

202. Hill A, Mesens N, Steemans M, Xu JJ, Aleo MD. Comparisons between in vitro whole cell imaging and in vivo zebrafish-based approaches for identifying potential human hepatotoxicants earlier in pharmaceutical development. *Drug Metab Rev* 2012;44:127-140.
203. McGrath P, Li CQ. Zebrafish: a predictive model for assessing drug-induced toxicity. *Drug Discov Today* 2008;13:394-401.
204. Sun L, Shao X, Chi J, Hu X, Jin Y, Fu Z. Transcriptional responses in the brain, liver and gonad of Japanese ricefish (*Oryzias latipes*) exposed to two anti-estrogens. *Comp Biochem Physiol C Toxicol Pharmacol* 2011;153:392-401.
205. Kikkawa R, Fujikawa M, Yamamoto T, Hamada Y, Yamada H, Horii I. In vivo hepatotoxicity study of rats in comparison with in vitro hepatotoxicity screening system. *J Toxicol Sci* 2006;31:23-34.
206. FDA C. Guidance for industry: bioanalytical method validation. US Department of Health and Human Services. Food and Drug Administration, Center for Drug Evaluation and Research (CDER), Center for Veterinary Medicine (CV) 2001.
207. García-Cañaveras JC, Donato MT, Castell JV, Lahoz A. Targeted profiling of circulating and hepatic bile acids in human, mouse, and rat using a UPLC-MRM-MS-validated method. *J Lipid Res* 2012;53:2231-2241.
208. García-Cañaveras JC, Donato MT, Lahoz A: Ultra-Performance Liquid Chromatography Mass Spectrometry Targeted Profiling of Bile Acids: Application to Serum, Liver Tissue and Cultured Cells of Different Species. In: Raftert D, ed. *Mass Spectrometry in Metabolomics*: Humana Press, 2014.
209. Carretero A, León Z, García-Cañaveras JC, Zaragoza Á, Gómez-Lechón MJ, Donato MT, Lahoz A. In vitro/in vivo screening of oxidative homeostasis and damage to DNA, protein, and lipids using UPLC/MS-MS. *Anal Bioanal Chem* 2014;406:5465-5476.
210. Korchazhkina O, Exley C, Andrew Spencer S. Measurement by reversed-phase high-performance liquid chromatography of malondialdehyde in normal human urine following derivatisation with 2,4-dinitrophenylhydrazine. *J Chromatogr B Analyt Technol Biomed Life Sci* 2003;794:353-362.
211. Mateos R, Goya L, Bravo L. Determination of malondialdehyde by liquid chromatography as the 2,4-dinitrophenylhydrazone derivative: a marker for oxidative stress in cell cultures of human hepatoma HepG2. *J Chromatogr B Analyt Technol Biomed Life Sci* 2004;805:33-39.
212. Mateos R, Lecumberri E, Ramos S, Goya L, Bravo L. Determination of malondialdehyde (MDA) by high-performance liquid chromatography in serum and liver as a biomarker for oxidative stress. Application to a rat model for hypercholesterolemia and evaluation of the effect of diets rich in phenolic antioxidants from

## References

---

- fruits. *J Chromatogr B Analyt Technol Biomed Life Sci* 2005;827:76-82.
213. Camera E, Rinaldi M, Briganti S, Picardo M, Fanali S. Simultaneous determination of reduced and oxidized glutathione in peripheral blood mononuclear cells by liquid chromatography-electrospray mass spectrometry. *J Chromatogr B Biomed Sci Appl* 2001;757:69-78.
214. Rossi R, Dalle-Donne I, Milzani A, Giustarini D. Oxidized forms of glutathione in peripheral blood as biomarkers of oxidative stress. *Clin Chem* 2006;52:1406-1414.
215. Zelena E, Dunn WB, Broadhurst D, Francis-McIntyre S, Carroll KM, Begley P, O'Hagan S, et al. Development of a robust and repeatable UPLC-MS method for the long-term metabolomic study of human serum. *Anal Chem* 2009;81:1357-1364.
216. Want EJ, Wilson ID, Gika H, Theodoridis G, Plumb RS, Shockcor J, Holmes E, et al. Global metabolic profiling procedures for urine using UPLC-MS. *Nat Protoc* 2010;5:1005-1018.
217. Naz S, Vallejo M, García A, Barbas C. Method validation strategies involved in non-targeted metabolomics. *Journal of Chromatography A* 2014.
218. Ivanisevic J, Zhu ZJ, Plate L, Tautenhahn R, Chen S, O'Brien PJ, Johnson CH, et al. Toward 'omic scale metabolite profiling: a dual separation-mass spectrometry approach for coverage of lipid and central carbon metabolism. *Anal Chem* 2013;85:6876-6884.
219. Dunn WB, Broadhurst D, Begley P, Zelena E, Francis-McIntyre S, Anderson N, Brown M, et al. Procedures for large-scale metabolic profiling of serum and plasma using gas chromatography and liquid chromatography coupled to mass spectrometry. *Nat Protoc* 2011;6:1060-1083.
220. Chen C, Krausz KW, Shah YM, Idle JR, Gonzalez FJ. Serum metabolomics reveals irreversible inhibition of fatty acid beta-oxidation through the suppression of PPARalpha activation as a contributing mechanism of acetaminophen-induced hepatotoxicity. *Chem Res Toxicol* 2009;22:699-707.
221. Cifkova E, Holcapek M, Lisa M, Ovcacikova M, Lycka A, Lynen F, Sandra P. Nontargeted quantitation of lipid classes using hydrophilic interaction liquid chromatography-electrospray ionization mass spectrometry with single internal standard and response factor approach. *Anal Chem* 2012;84:10064-10070.
222. Schwalbe-Herrmann M, Willmann J, Leibfritz D. Separation of phospholipid classes by hydrophilic interaction chromatography detected by electrospray ionization mass spectrometry. *J Chromatogr A* 2010;1217:5179-5183.
223. Tang DQ, Zou L, Yin XX, Ong CN. HILIC-MS for metabolomics: An attractive and complementary approach to RPLC-MS. *Mass Spectrom Rev* 2014.

## References

---

224. Hogg K-LN, Craig MN, Uy CE, Nygren H, Asadi A, Speck M, Fraser JD, et al. Overexpression of PPAR $\gamma$  Specifically in Pancreatic  $\beta$ -Cells Exacerbates Obesity-Induced Glucose Intolerance, Reduces  $\beta$ -Cell Mass, and Alters Islet Lipid Metabolism in Male Mice. *Endocrinology* 2014;155:3843-3852.
225. Orešič M, Hyötyläinen T, Kotronen A, Gopalacharyulu P, Nygren H, Arola J, Castillo S, et al. Prediction of non-alcoholic fatty-liver disease and liver fat content by serum molecular lipids. *Diabetologia* 2013;56:2266-2274.
226. Pietiläinen KH, Sysi-Aho M, Rissanen A, Seppänen-Laakso T, Yki-Jarvinen H, Kaprio J, Oresic M. Acquired obesity is associated with changes in the serum lipidomic profile independent of genetic effects--a monozygotic twin study. *PLoS One* 2007;2:e218.
227. Fei F, Bowdish DM, McCarry BE. Comprehensive and simultaneous coverage of lipid and polar metabolites for endogenous cellular metabolomics using HILIC-TOF-MS. *Anal Bioanal Chem* 2014;406:3723-3733.
228. Seppänen-Laakso T, Oresic M. How to study lipidomes. *J Mol Endocrinol* 2009;42:185-190.
229. Bi H, Krausz KW, Manna SK, Li F, Johnson CH, Gonzalez FJ. Optimization of harvesting, extraction, and analytical protocols for UPLC-ESI-MS-based metabolomic analysis of adherent mammalian cancer cells. *Anal Bioanal Chem* 2013;405:5279-5289.
230. Teng Q, Huang W, Collette TW, Ekman DR, Tan C. A direct cell quenching method for cell-culture based metabolomics. *Metabolomics* 2009;5:199-208.
231. Ritter JB, Genzel Y, Reichl U. Simultaneous extraction of several metabolites of energy metabolism and related substances in mammalian cells: optimization using experimental design. *Analytical biochemistry* 2008;373:349-369.
232. Jennen D, Ruiz-Aracama A, Magkoufopoulou C, Peijnenburg A, Lommen A, van Delft J, Kleinjans J. Integrating transcriptomics and metabolomics to unravel modes-of-action of 2,3,7,8-tetrachlorodibenzo-p-dioxin (TCDD) in HepG2 cells. *BMC Syst Biol* 2011;5:139.
233. Lu SC. Regulation of glutathione synthesis. *Mol Aspects Med* 2009;30:42-59.
234. Wu G, Fang YZ, Yang S, Lupton JR, Turner ND. Glutathione metabolism and its implications for health. *J Nutr* 2004;134:489-492.
235. Hansen JM, Go YM, Jones DP. Nuclear and mitochondrial compartmentation of oxidative stress and redox signaling. *Annu Rev Pharmacol Toxicol* 2006;46:215-234.
236. Cervinkova Z, Krivakova P, Labajova A, Rousar T, Lotkova H, Kucera O, Endlicher R, et al. Mechanisms participating in oxidative damage of isolated rat hepatocytes. *Arch Toxicol* 2009;83:363-372.

## References

---

237. Lotkova H, Cervinkova Z, Kucera O, Krivakova P, Kand'ar R. Protective effect of S-adenosylmethionine on cellular and mitochondrial membranes of rat hepatocytes against tert-butylhydroperoxide-induced injury in primary culture. *Chem Biol Interact* 2005;156:13-23.
238. Ghibelli L, Fanelli C, Rotilio G, Lafavia E, Coppola S, Colussi C, Civitareale P, et al. Rescue of cells from apoptosis by inhibition of active GSH extrusion. *FASEB J* 1998;12:479-486.
239. Hammond CL, Madejczyk MS, Ballatori N. Activation of plasma membrane reduced glutathione transport in death receptor apoptosis of HepG2 cells. *Toxicol Appl Pharmacol* 2004;195:12-22.
240. Yuan W, Edwards JL. Thiol metabolomics of endothelial cells using capillary liquid chromatography mass spectrometry with isotope coded affinity tags. *J Chromatogr A* 2011;1218:2561-2568.
241. Jones DP, Carlson JL, Mody VC, Cai J, Lynn MJ, Sternberg P. Redox state of glutathione in human plasma. *Free Radic Biol Med* 2000;28:625-635.
242. Meister A. On the enzymology of amino acid transport. *Science* 1973;180:33-39.
243. Meister A, Anderson ME. Glutathione. *Annu Rev Biochem* 1983;52:711-760.
244. Lu SC. Regulation of hepatic glutathione synthesis: current concepts and controversies. *FASEB J* 1999;13:1169-1183.
245. Sastre J, Pallardo F, Viña J: Glutathione. In: Grune T, ed. *Reactions, Processes*. Volume 20: Springer Berlin Heidelberg, 2005; 91-108.
246. Soga T, Sugimoto M, Honma M, Mori M, Igarashi K, Kashikura K, Ikeda S, et al. Serum metabolomics reveals gamma-glutamyl dipeptides as biomarkers for discrimination among different forms of liver disease. *J Hepatol* 2011;55:896-905.
247. Feldstein AE, Werneburg NW, Canbay A, Guicciardi ME, Bronk SF, Rydzewski R, Burgart LJ, et al. Free fatty acids promote hepatic lipotoxicity by stimulating TNF-alpha expression via a lysosomal pathway. *Hepatology* 2004;40:185-194.
248. Kotronen A, Seppanen-Laakso T, Westerbacka J, Kiviluoto T, Arola J, Ruskeepaa AL, Oresic M, et al. Hepatic stearoyl-CoA desaturase (SCD)-1 activity and diacylglycerol but not ceramide concentrations are increased in the nonalcoholic human fatty liver. *Diabetes* 2009;58:203-208.
249. Caballero F, Fernandez A, Matias N, Martinez L, Fucho R, Elena M, Caballeria J, et al. Specific contribution of methionine and choline in nutritional nonalcoholic steatohepatitis: impact on mitochondrial S-adenosyl-L-methionine and glutathione. *J Biol Chem* 2010;285:18528-18536.
250. Gorden DL, Ivanova PT, Myers DS, McIntyre JO, VanSaun MN, Wright JK, Matrisian LM, et al. Increased diacylglycerols characterize hepatic lipid changes in progression of human nonalcoholic fatty

## References

---

- liver disease; comparison to a murine model. *PLoS One* 2011;6:e22775.
251. Vinaixa M, Rodriguez MA, Rull A, Beltran R, Blade C, Brezmes J, Canellas N, et al. Metabolomic assessment of the effect of dietary cholesterol in the progressive development of fatty liver disease. *J Proteome Res* 2010;9:2527-2538.
252. Yamaguchi K, Yang L, McCall S, Huang J, Yu XX, Pandey SK, Bhanot S, et al. Inhibiting triglyceride synthesis improves hepatic steatosis but exacerbates liver damage and fibrosis in obese mice with nonalcoholic steatohepatitis. *Hepatology* 2007;45:1366-1374.
253. Cole LK, Jacobs RL, Vance DE. Tamoxifen induces triacylglycerol accumulation in the mouse liver by activation of fatty acid synthesis. *Hepatology* 2010;52:1258-1265.
254. Letteron P, Fromenty B, Terris B, Degott C, Pessayre D. Acute and chronic hepatic steatosis lead to in vivo lipid peroxidation in mice. *J Hepatol* 1996;24:200-208.
255. Vitins AP, Kienhuis AS, Speksnijder EN, Roodbergen M, Luijten M, van der Ven LT. Mechanisms of amiodarone and valproic acid induced liver steatosis in mouse in vivo act as a template for other hepatotoxicity models. *Arch Toxicol* 2014;88:1573-1588.
256. Antherieu S, Rogue A, Fromenty B, Guillouzo A, Robin MA. Induction of vesicular steatosis by amiodarone and tetracycline is associated with up-regulation of lipogenic genes in HepaRG cells. *Hepatology* 2011;53:1895-1905.
257. Amacher DE. Strategies for the early detection of drug-induced hepatic steatosis in preclinical drug safety evaluation studies. *Toxicology* 2011;279:10-18.
258. Leamy AK, Egnatchik RA, Young JD. Molecular mechanisms and the role of saturated fatty acids in the progression of non-alcoholic fatty liver disease. *Prog Lipid Res* 2013;52:165-174.
259. Neuschwander-Tetri BA. Hepatic lipotoxicity and the pathogenesis of nonalcoholic steatohepatitis: the central role of nontriglyceride fatty acid metabolites. *Hepatology* 2010;52:774-788.
260. Listenberger LL, Han X, Lewis SE, Cases S, Farese RV, Jr., Ory DS, Schaffer JE. Triglyceride accumulation protects against fatty acid-induced lipotoxicity. *Proc Natl Acad Sci U S A* 2003;100:3077-3082.
261. Barr J, Caballeria J, Martinez-Arranz I, Dominguez-Diez A, Alonso C, Muntane J, Perez-Cormenzana M, et al. Obesity-dependent metabolic signatures associated with nonalcoholic fatty liver disease progression. *J Proteome Res* 2012;11:2521-2532.
262. Barr J, Vazquez-Chantada M, Alonso C, Perez-Cormenzana M, Mayo R, Galan A, Caballeria J, et al. Liquid chromatography-mass spectrometry-based parallel metabolic profiling of human and mouse model serum reveals putative biomarkers associated with the progression of nonalcoholic fatty liver disease. *J Proteome Res* 2010;9:4501-4512.

## References

---

263. Kim HJ, Kim JH, Noh S, Hur HJ, Sung MJ, Hwang JT, Park JH, et al. Metabolomic analysis of livers and serum from high-fat diet induced obese mice. *J Proteome Res* 2011;10:722-731.
264. Cauwels A, Janssen B, Waeytens A, Cuvelier C, Brouckaert P. Caspase inhibition causes hyperacute tumor necrosis factor-induced shock via oxidative stress and phospholipase A2. *Nat Immunol* 2003;4:387-393.
265. Schmid PC, Deli E, Schmid HH. Generation and remodeling of phospholipid molecular species in rat hepatocytes. *Arch Biochem Biophys* 1995;319:168-176.
266. Shinzawa K, Tsujimoto Y. PLA2 activity is required for nuclear shrinkage in caspase-independent cell death. *The Journal of cell biology* 2003;163:1219-1230.
267. Han MS, Park SY, Shinzawa K, Kim S, Chung KW, Lee JH, Kwon CH, et al. Lysophosphatidylcholine as a death effector in the lipoapoptosis of hepatocytes. *J Lipid Res* 2008;49:84-97.
268. Araya J, Rodrigo R, Videla LA, Thielemann L, Orellana M, Pettinelli P, Poniachik J. Increase in long-chain polyunsaturated fatty acid n - 6/n - 3 ratio in relation to hepatic steatosis in patients with non-alcoholic fatty liver disease. *Clin Sci (Lond)* 2004;106:635-643.
269. Puri P, Wiest MM, Cheung O, Mirshahi F, Sargeant C, Min HK, Contos MJ, et al. The plasma lipidomic signature of nonalcoholic steatohepatitis. *Hepatology* 2009;50:1827-1838.
270. Bishop W, Bell R. Functions of diacylglycerol in glycerolipid metabolism, signal transduction and cellular transformation. *Oncogene research* 1988;2:205-218.
271. Nishizuka Y. Protein kinase C and lipid signaling for sustained cellular responses. *FASEB J* 1995;9:484-496.
272. Villanueva CJ, Monetti M, Shih M, Zhou P, Watkins SM, Bhanot S, Farese RV, Jr. Specific role for acyl CoA:Diacylglycerol acyltransferase 1 (Dgat1) in hepatic steatosis due to exogenous fatty acids. *Hepatology* 2009;50:434-442.
273. Yamaguchi K, Yang L, McCall S, Huang J, Yu XX, Pandey SK, Bhanot S, et al. Diacylglycerol acyltransferase 1 anti-sense oligonucleotides reduce hepatic fibrosis in mice with nonalcoholic steatohepatitis. *Hepatology* 2008;47:625-635.
274. Kennedy EP, Weiss SB. The function of cytidine coenzymes in the biosynthesis of phospholipides. *J Biol Chem* 1956;222:193-214.
275. Gibellini F, Smith TK. The Kennedy pathway--De novo synthesis of phosphatidylethanolamine and phosphatidylcholine. *IUBMB Life* 2010;62:414-428.
276. Browning JD, Horton JD. Molecular mediators of hepatic steatosis and liver injury. *J Clin Invest* 2004;114:147-152.
277. Nakamura S, Takamura T, Matsuzawa-Nagata N, Takayama H, Misu H, Noda H, Nabemoto S, et al. Palmitate induces insulin resistance

## References

---

- in H4IIEC3 hepatocytes through reactive oxygen species produced by mitochondria. *J Biol Chem* 2009;284:14809-14818.
278. Josephine A, Nithya K, Amudha G, Veena CK, Preetha SP, Varalakshmi P. Role of sulphated polysaccharides from *Sargassum Wightii* in Cyclosporine A-induced oxidative liver injury in rats. *BMC Pharmacol* 2008;8:4.
279. Luo Y, Rana P, Will Y. Cyclosporine A and palmitic acid treatment synergistically induce cytotoxicity in HepG2 cells. *Toxicol Appl Pharmacol* 2012;261:172-180.
280. Illsinger S, Janzen N, Lucke T, Bednarczyk J, Schmidt KH, Hoy L, Sander J, et al. Cyclosporine A: impact on mitochondrial function in endothelial cells. *Clin Transplant* 2011;25:584-593.
281. Lemmi CA, Miller RL, Rajfer J. Inhibition of fatty acid-supported mitochondrial respiration by cyclosporine. *Biochem Med Metab Biol* 1990;44:266-270.
282. Armstrong KA, Hiremagalur B, Haluska BA, Campbell SB, Hawley CM, Marks L, Prins J, et al. Free fatty acids are associated with obesity, insulin resistance, and atherosclerosis in renal transplant recipients. *Transplantation* 2005;80:937-944.
283. Hilgendorf C, Ahlin G, Seithel A, Artursson P, Ungell AL, Karlsson J. Expression of thirty-six drug transporter genes in human intestine, liver, kidney, and organotypic cell lines. *Drug Metab Dispos* 2007;35:1333-1340.
284. Ulvestad M, Nordell P, Asplund A, Rehnstrom M, Jacobsson S, Holmgren G, Davidson L, et al. Drug metabolizing enzyme and transporter protein profiles of hepatocytes derived from human embryonic and induced pluripotent stem cells. *Biochem Pharmacol* 2013;86:691-702.
285. Liu X, LeCluyse EL, Brouwer KR, Gan LS, Lemasters JJ, Stieger B, Meier PJ, et al. Biliary excretion in primary rat hepatocytes cultured in a collagen-sandwich configuration. *Am J Physiol* 1999;277:G12-21.
286. Liu X, LeCluyse EL, Brouwer KR, Lightfoot RM, Lee JI, Brouwer KL. Use of Ca<sup>2+</sup> modulation to evaluate biliary excretion in sandwich-cultured rat hepatocytes. *J Pharmacol Exp Ther* 1999;289:1592-1599.
287. Marion TL, Leslie EM, Brouwer KL. Use of sandwich-cultured hepatocytes to evaluate impaired bile acid transport as a mechanism of drug-induced hepatotoxicity. *Molecular pharmaceutics* 2007;4:911-918.
288. Swift B, Pfeifer ND, Brouwer KL. Sandwich-cultured hepatocytes: an in vitro model to evaluate hepatobiliary transporter-based drug interactions and hepatotoxicity. *Drug Metab Rev* 2010;42:446-471.
289. Antherieu S, Bachour-El Azzi P, Dumont J, Abdel-Razzak Z, Guguen-Guillouzo C, Fromenty B, Robin MA, et al. Oxidative stress plays a



## References

---

- major role in chlorpromazine-induced cholestasis in human HepaRG cells. *Hepatology* 2013;57:1518-1529.
290. Antherieu S, Chesne C, Li R, Guguen-Guillouzo C, Guillouzo A. Optimization of the HepaRG cell model for drug metabolism and toxicity studies. *Toxicol In Vitro* 2012;26:1278-1285.
  291. Sharanek A, Bachour-El Azzi P, Al-Attrache H, Savary CC, Humbert L, Rainteau D, Guguen-Guillouzo C, et al. Different Dose-Dependent Mechanisms Are Involved in Early Cyclosporine A-Induced Cholestatic Effects in HepaRG Cells. *Toxicol Sci* 2014.
  292. Hostetler KY. Molecular studies of the induction of cellular phospholipidosis by cationic amphiphilic drugs. *Fed Proc* 1984;43:2582-2585.
  293. Reasor MJ, McCloud CM, Beard TL, Ebert DC, Kacew S, Gardner MF, Aldern KA, et al. Comparative evaluation of amiodarone-induced phospholipidosis and drug accumulation in Fischer-344 and Sprague-Dawley rats. *Toxicology* 1996;106:139-147.
  294. Kodavanti UP, Mehendale HM. Cationic amphiphilic drugs and phospholipid storage disorder. *Pharmacol Rev* 1990;42:327-354.
  295. Anderson N, Borlak J. Drug-induced phospholipidosis. *FEBS Lett* 2006;580:5533-5540.
  296. Costa-Jussa FR, Corrin B, Jacobs JM. Amiodarone lung toxicity: a human and experimental study. *J Pathol* 1984;144:73-79.
  297. Abe A, Hiraoka M, Shayman JA. A role for lysosomal phospholipase A2 in drug induced phospholipidosis. *Drug metabolism letters* 2007;1:49-53.
  298. Mingeot-Leclercq M-P, Piret J, Brasseur R, Tulkens PM. Effect of acidic phospholipids on the activity of lysosomal phospholipases and on their inhibition by aminoglycoside antibiotics—I: Biochemical analysis. *Biochemical pharmacology* 1990;40:489-497.
  299. Pessayre D, Larrey D: Drug-induced liver injury. In: Rodés J, Benhamou J-P, Blei AT, Reichen JR, Manocchia M, eds. *Textbook of hepatology: from basic science to clinical practice*. 3rd edition ed: Malden: Wiley-Blackwell Publishing., 2007.
  300. Park S, Choi YJ, Lee BH. In vitro validation of drug-induced phospholipidosis. *J Toxicol Sci* 2012;37:261-267.
  301. Shayman JA, Abe A. Drug induced phospholipidosis: an acquired lysosomal storage disorder. *Biochim Biophys Acta* 2013;1831:602-611.
  302. Reasor MJ. Phospholipidosis in the alveolar macrophage induced by cationic amphiphilic drugs. *Fed Proc* 1984;43:2578-2581.
  303. Alakoskela JM, Vitovic P, Kinnunen PK. Screening for the drug-phospholipid interaction: correlation to phospholipidosis. *ChemMedChem* 2009;4:1224-1251.
  304. Baronas ET, Lee JW, Alden C, Hsieh FY. Biomarkers to monitor drug-induced phospholipidosis. *Toxicol Appl Pharmacol* 2007;218:72-78.

## References

---

305. Van Meer G, Voelker DR, Feigenson GW. Membrane lipids: where they are and how they behave. *Nature reviews molecular cell biology* 2008;9:112-124.
306. Malhi H, Gores GJ. Molecular mechanisms of lipotoxicity in nonalcoholic fatty liver disease. *Semin Liver Dis* 2008;28:360-369.
307. Yetukuri L, Katajamaa M, Medina-Gomez G, Seppanen-Laakso T, Vidal-Puig A, Oresic M. Bioinformatics strategies for lipidomics analysis: characterization of obesity related hepatic steatosis. *BMC Syst Biol* 2007;1:12.
308. Minehira K, Young SG, Villanueva CJ, Yetukuri L, Oresic M, Hellerstein MK, Farese RV, et al. Blocking VLDL secretion causes hepatic steatosis but does not affect peripheral lipid stores or insulin sensitivity in mice. *J Lipid Res* 2008;49:2038-2044.
309. James SJ, Cutler P, Melnyk S, Jernigan S, Janak L, Gaylor DW, Neubrandner JA. Metabolic biomarkers of increased oxidative stress and impaired methylation capacity in children with autism. *Am J Clin Nutr* 2004;80:1611-1617.
310. Sanayama Y, Nagasaka H, Takayanagi M, Ohura T, Sakamoto O, Ito T, Ishige-Wada M, et al. Experimental evidence that phenylalanine is strongly associated to oxidative stress in adolescents and adults with phenylketonuria. *Mol Genet Metab* 2011;103:220-225.
311. Syslova K, Kacer P, Kuzma M, Pankracova A, Fenclova Z, Vlckova S, Lebedova J, et al. LC-ESI-MS/MS method for oxidative stress multimarker screening in the exhaled breath condensate of asbestosis/silicosis patients. *J Breath Res* 2010;4:017104.
312. Delatour T, Richoz J, Vouros P, Turesky RJ. Simultaneous determination of 3-nitrotyrosine and tyrosine in plasma proteins of rats and assessment of artifactual tyrosine nitration. *J Chromatogr B Analyt Technol Biomed Life Sci* 2002;779:189-199.
313. Valavanidis A, Vlachogianni T, Fiotakis C. 8-hydroxy-2'-deoxyguanosine (8-OHdG): A critical biomarker of oxidative stress and carcinogenesis. *J Environ Sci Health C Environ Carcinog Ecotoxicol Rev* 2009;27:120-139.
314. Lykkesfeldt J. Malondialdehyde as biomarker of oxidative damage to lipids caused by smoking. *Clin Chim Acta* 2007;380:50-58.
315. Serviddio G, Bellanti F, Giudetti AM, Gnoni GV, Capitanio N, Tamborra R, Romano AD, et al. Mitochondrial oxidative stress and respiratory chain dysfunction account for liver toxicity during amiodarone but not dronedarone administration. *Free Radic Biol Med* 2011;51:2234-2242.
316. Dello SA, Neis EP, de Jong MC, van Eijk HM, Kicken CH, Olde Damink SW, Dejong CH. Systematic review of ophthalmate as a novel biomarker of hepatic glutathione depletion. *Clinical Nutrition* 2013;32:325-330.
317. Orłowski M, Wilk S. Synthesis of ophthalmic acid in liver and kidney in vivo. *Biochem J* 1978;170:415-419.

## References

---

318. Geenen S, du Preez FB, Snoep JL, Foster AJ, Sarda S, Kenna JG, Wilson ID, et al. Glutathione metabolism modeling: a mechanism for liver drug-robustness and a new biomarker strategy. *Biochim Biophys Acta* 2013;1830:4943-4959.
319. Ballatori N, Dutczak WJ. Identification and characterization of high and low affinity transport systems for reduced glutathione in liver cell canalicular membranes. *J Biol Chem* 1994;269:19731-19737.
320. Golli-Bennour EE, Bouslimi A, Zouaoui O, Nouira S, Achour A, Bacha H. Cytotoxicity effects of amiodarone on cultured cells. *Exp Toxicol Pathol* 2012;64:425-430.
321. Rezzani R, Buffoli B, Rodella L, Stacchiotti A, Bianchi R. Protective role of melatonin in cyclosporine A-induced oxidative stress in rat liver. *Int Immunopharmacol* 2005;5:1397-1405.
322. Yuce A, Atessahin A, Ceribasi AO. Amelioration of cyclosporine A-induced renal, hepatic and cardiac damages by ellagic acid in rats. *Basic Clin Pharmacol Toxicol* 2008;103:186-191.
323. Letteron P, Sutton A, Mansouri A, Fromenty B, Pessayre D. Inhibition of microsomal triglyceride transfer protein: another mechanism for drug-induced steatosis in mice. *Hepatology* 2003;38:133-140.
324. Fromenty B, Fisch C, Labbe G, Degott C, Deschamps D, Berson A, Letteron P, et al. Amiodarone inhibits the mitochondrial beta-oxidation of fatty acids and produces microvesicular steatosis of the liver in mice. *J Pharmacol Exp Ther* 1990;255:1371-1376.
325. Felser A, Blum K, Lindinger PW, Bouitbir J, Krahenbuhl S. Mechanisms of hepatocellular toxicity associated with dronedarone-a comparison to amiodarone. *Toxicol Sci* 2013;131:480-490.
326. Spaniol M, Bracher R, Ha HR, Follath F, Krahenbuhl S. Toxicity of amiodarone and amiodarone analogues on isolated rat liver mitochondria. *J Hepatol* 2001;35:628-636.
327. Grattagliano I, Portincasa P, Palmieri VO, Palasciano G. Overview on the mechanisms of drug-induced liver cell death. *Ann Hepatol* 2002;1:162-168.
328. Yano T, Itoh Y, Yamada M, Egashira N, Oishi R. Combined treatment with L-carnitine and a pan-caspase inhibitor effectively reverses amiodarone-induced injury in cultured human lung epithelial cells. *Apoptosis* 2008;13:543-552.
329. Amacher DE, Martin BA. Tetracycline-induced steatosis in primary canine hepatocyte cultures. *Fundam Appl Toxicol* 1997;40:256-263.
330. Freneaux E, Labbe G, Letteron P, The Le D, Degott C, Geneve J, Larrey D, et al. Inhibition of the mitochondrial oxidation of fatty acids by tetracycline in mice and in man: possible role in microvesicular steatosis induced by this antibiotic. *Hepatology* 1988;8:1056-1062.
331. Rodriguez LC, Araujo CR, Posleman SE, Rey Mdel R. Hepatotoxic effect of cyclosporin A in the mitochondrial respiratory chain. *J Appl Toxicol* 2007;27:310-317.

## References

---

332. Germano D, Uteng M, Pognan F, Chibout SD, Wolf A. Determination of liver specific toxicities in rat hepatocytes by high content imaging during 2-week multiple treatment. *Toxicol In Vitro* 2014.
333. Cheng F, Theodorescu D, Schulman IG, Lee JK. In vitro transcriptomic prediction of hepatotoxicity for early drug discovery. *J Theor Biol* 2011;290:27-36.
334. Yang Y, Abel SJ, Ciurlionis R, Waring JF. Development of a toxicogenomics in vitro assay for the efficient characterization of compounds. *Pharmacogenomics* 2006;7:177-186.
335. Thome-Kromer B, Bonk I, Klatt M, Nebrich G, Taufmann M, Bryant S, Wacker U, et al. Toward the identification of liver toxicity markers: a proteome study in human cell culture and rats. *Proteomics* 2003;3:1835-1862.
336. Flynn TJ, Ferguson MS. Multiendpoint mechanistic profiling of hepatotoxicants in HepG2/C3A human hepatoma cells and novel statistical approaches for development of a prediction model for acute hepatotoxicity. *Toxicol In Vitro* 2008;22:1618-1631.
337. Persson M, Løye AF, Mow T, Hornberg JJ. A high content screening assay to predict human drug-induced liver injury during drug discovery. *Journal of pharmacological and toxicological methods* 2013;68:302-313.
338. O'Brien PJ. High-content analysis in toxicology: screening substances for human toxicity potential, elucidating subcellular mechanisms and in vivo use as translational safety biomarkers. *Basic Clin Pharmacol Toxicol* 2014;115:4-17.
339. Nioi P, Perry BK, Wang E-J, Gu Y-Z, Snyder RD. In Vitro Detection of Drug-Induced Phospholipidosis Using Gene Expression and Fluorescent Phospholipid-Based Methodologies. *Toxicological sciences* 2007;99:162-173.
340. Shahane SA, Huang R, Gerhold D, Baxa U, Austin CP, Xia M. Detection of phospholipidosis induction: a cell-based assay in high-throughput and high-content format. *J Biomol Screen* 2014;19:66-76.
341. Tilmant K, Gerets HH, Dhalluin S, Hanon E, Depelchin O, Cossu-Leguille C, Vasseur P, et al. Comparison of a genomic and a multiplex cell imaging approach for the detection of phospholipidosis. *Toxicol In Vitro* 2011;25:1414-1424.
342. Drenckhahn D, Kleine L, Lullmann-Rauch R. Lysosomal alterations in cultured macrophages exposed to anorexigenic and psychotropic drugs. *Lab Invest* 1976;35:116-123.
343. Atienzar F, Gerets H, Dufrane S, Tilmant K, Cornet M, Dhalluin S, Ruty B, et al. Determination of phospholipidosis potential based on gene expression analysis in HepG2 cells. *Toxicol Sci* 2007;96:101-114.
344. Kasahara T, Tomita K, Murano H, Harada T, Tsubakimoto K, Ogihara T, Ohnishi S, et al. Establishment of an in vitro high-throughput

## References

---

- screening assay for detecting phospholipidosis-inducing potential. *Toxicol Sci* 2006;90:133-141.
345. van de Water FM, Havinga J, Ravesloot WT, Horbach GJ, Schoonen WG. High content screening analysis of phospholipidosis: validation of a 96-well assay with CHO-K1 and HepG2 cells for the prediction of in vivo based phospholipidosis. *Toxicol In Vitro* 2011;25:1870-1882.
346. Matsumoto T, Terai S, Oishi T, Kuwashiro S, Fujisawa K, Yamamoto N, Fujita Y, et al. Medaka as a model for human nonalcoholic steatohepatitis. *Disease models & mechanisms* 2010;3:431-440.
347. Vliegenthart A, Tucker C, Del Pozo J, Dear J. Zebrafish as model organisms for studying drug induced liver injury. *Br J Clin Pharmacol* 2014.
348. Sheridan MA. Lipid dynamics in fish: aspects of absorption, transportation, deposition and mobilization. *Comp Biochem Physiol B* 1988;90:679-690.
349. Brown WD, Tappel AL. Fatty acid oxidation by carp liver mitochondria. *Arch Biochem Biophys* 1959;85:149-158.
350. Hardman RC, Volz DC, Kullman SW, Hinton DE. An in vivo Look at Vertebrate Liver Architecture: Three- Dimensional Reconstructions from Medaka (*Oryzias latipes*). *The Anatomical Record* 2007;290:770-782.
351. Kotronen A, Seppanen-Laakso T, Westerbacka J, Kiviluoto T, Arola J, Ruskeepaa AL, Yki-Jarvinen H, et al. Comparison of lipid and fatty acid composition of the liver, subcutaneous and intra-abdominal adipose tissue, and serum. *Obesity (Silver Spring)* 2010;18:937-944.
352. Holtta-Vuori M, Salo VT, Nyberg L, Brackmann C, Enejder A, Panula P, Ikonen E. Zebrafish: gaining popularity in lipid research. *Biochem J* 2010;429:235-242.
353. Henderson RJ, Tocher DR. The lipid composition and biochemistry of freshwater fish. *Prog Lipid Res* 1987;26:281-347.
354. Rhee JS, Kim BM, Choi BS, Choi IY, Wu RS, Nelson DR, Lee JS. Whole spectrum of cytochrome P450 genes and molecular responses to water-accommodated fractions exposure in the marine medaka. *Environ Sci Technol* 2013;47:4804-4812.
355. Goldstone JV, McArthur AG, Kubota A, Zanette J, Parente T, Jonsson ME, Nelson DR, et al. Identification and developmental expression of the full complement of Cytochrome P450 genes in Zebrafish. *BMC Genomics* 2010;11:643.
356. Parg C, Seng WL, Semino C, McGrath P. Zebrafish: a preclinical model for drug screening. *Assay Drug Dev Technol* 2002;1:41-48.
357. Driessen M, Kienhuis AS, Vitins AP, Pennings JL, Pronk TE, Brandhof EJ, Roodbergen M, et al. Gene expression markers in the zebrafish embryo reflect a hepatotoxic response in animal models and humans. *Toxicol Lett* 2014;230:48-56.

## References

358. Hill AJ, Teraoka H, Heideman W, Peterson RE. Zebrafish as a model vertebrate for investigating chemical toxicity. *Toxicological sciences* 2005;86:6-19.
359. Asaoka Y, Terai S, Sakaida I, Nishina H. The expanding role of fish models in understanding non-alcoholic fatty liver disease. *Dis Model Mech* 2013;6:905-914.
360. Hagey LR, Lida T, Tamegai H, Ogawa S, Une M, Asahina K, Mushiake K, et al. Major biliary bile acids of the medaka (*Oryzias latipes*): 25R- and 25S-epimers of 3 $\alpha$ ,7 $\alpha$ ,12 $\alpha$ -trihydroxy-5 $\beta$ -cholestanoic acid. *Zoolog Sci* 2010;27:565-573.
361. Hofmann AF, Hagey LR. Bile acids: chemistry, pathochemistry, biology, pathobiology, and therapeutics. *Cell Mol Life Sci* 2008;65:2461-2483.
362. Hofmann AF, Hagey LR, Krasowski MD. Bile salts of vertebrates: structural variation and possible evolutionary significance. *J Lipid Res* 2010;51:226-246.
363. Hardman R, Kullman S, Yuen B, Hinton DE. Non invasive high resolution in vivo imaging of alpha-naphthylisothiocyanate (ANIT) induced hepatobiliary toxicity in STII medaka. *Aquat Toxicol* 2008;86:20-37.
364. den Boer M, Voshol PJ, Kuipers F, Havekes LM, Romijn JA. Hepatic steatosis: a mediator of the metabolic syndrome. Lessons from animal models. *Arterioscler Thromb Vasc Biol* 2004;24:644-649.
365. Donnelly KL, Smith CI, Schwarzenberg SJ, Jessurun J, Boldt MD, Parks EJ. Sources of fatty acids stored in liver and secreted via lipoproteins in patients with nonalcoholic fatty liver disease. *J Clin Invest* 2005;115:1343-1351.
366. Kuwashiro S, Terai S, Oishi T, Fujisawa K, Matsumoto T, Nishina H, Sakaida I. Telmisartan improves nonalcoholic steatohepatitis in medaka (*Oryzias latipes*) by reducing macrophage infiltration and fat accumulation. *Cell and tissue research* 2011;344:125-134.
367. Tserng KY, Jin SJ. Metabolic origin of urinary 3-hydroxy dicarboxylic acids. *Biochemistry* 1991;30:2508-2514.
368. Buness A, Roth A, Herrmann A, Schmitz O, Kamp H, Busch K, Suter L. Identification of metabolites, clinical chemistry markers and transcripts associated with hepatotoxicity. *PLoS One* 2014;9:e97249.
369. Kalhan SC, Guo L, Edmison J, Dasarathy S, McCullough AJ, Hanson RW, Milburn M. Plasma metabolomic profile in nonalcoholic fatty liver disease. *Metabolism* 2011;60:404-413.
370. Vermeulen NP, Bessems JG, Van de Straat R. Molecular aspects of paracetamol-induced hepatotoxicity and its mechanism-based prevention. *Drug Metab Rev* 1992;24:367-407.
371. Dahlin DC, Miwa GT, Lu AY, Nelson SD. N-acetyl-p-benzoquinone imine: a cytochrome P-450-mediated oxidation product of acetaminophen. *Proc Natl Acad Sci U S A* 1984;81:1327-1331.

## References

---

372. Hinson JA, Reid AB, McCullough SS, James LP. Acetaminophen-induced hepatotoxicity: role of metabolic activation, reactive oxygen/nitrogen species, and mitochondrial permeability transition. *Drug Metab Rev* 2004;36:805-822.
373. Reilly TP, Bourdi M, Brady JN, Pise-Masison CA, Radonovich MF, George JW, Pohl LR. Expression profiling of acetaminophen liver toxicity in mice using microarray technology. *Biochem Biophys Res Commun* 2001;282:321-328.
374. Ruepp SU, Tonge RP, Shaw J, Wallis N, Pognan F. Genomics and proteomics analysis of acetaminophen toxicity in mouse liver. *Toxicol Sci* 2002;65:135-150.
375. Aleo MD, Luo Y, Swiss R, Bonin PD, Potter DM, Will Y. Human drug-induced liver injury severity is highly associated with dual inhibition of liver mitochondrial function and bile salt export pump. *Hepatology* 2014;60:1015-1022.
376. BOTHAM KM, BOYD GS. The Metabolism of Chenodeoxycholic Acid to  $\beta$ -Muricholic Acid in Rat Liver. *European Journal of Biochemistry* 1983;134:191-196.
377. Eyssen H, De Pauw G, Stragier J, Verhulst A. Cooperative formation of omega-muricholic acid by intestinal microorganisms. *Applied and environmental microbiology* 1983;45:141-147.
378. Matschiner JT, Mahowald TA, Elliott WH, Doisy E, Hsia S, Doisy EA. Bile acids I. Two new acids from rat bile. *Journal of Biological Chemistry* 1957;225:771-780.
379. Elliott WH, Hyde PM. Metabolic pathways of bile acid synthesis. *The American journal of medicine* 1971;51:568-579.
380. Mahowald TA, Matschiner JT, Hsia S, Richter R, Doisy E, Elliott WH, Doisy EA. BILE ACIDS II. METABOLISM OF DEOXYCHOLIC ACID-24-C14 AND CHENODEOXYCHOLIC ACID-24-C14 IN THE RAT. *Journal of Biological Chemistry* 1957;225:781-794.
381. Li T, Chiang JY. Bile Acid signaling in liver metabolism and diseases. *J Lipids* 2012;2012:754067.
382. Ridlon JM, Kang DJ, Hylemon PB. Bile salt biotransformations by human intestinal bacteria. *J Lipid Res* 2006;47:241-259.
383. Want EJ, Coen M, Masson P, Keun HC, Pearce JT, Reilly MD, Robertson DG, et al. Ultra performance liquid chromatography-mass spectrometry profiling of bile acid metabolites in biofluids: application to experimental toxicology studies. *Anal Chem* 2010;82:5282-5289.
384. García-Cañaveras JC, Donato MT, Lahoz A: Ultra-Performance Liquid Chromatography-Mass Spectrometry Targeted Profiling of Bile Acids: Application to Serum, Liver Tissue, and Cultured Cells of Different Species. In: Raftery D, ed. *Mass Spectrometry in Metabolomics*. Volume 1198: Springer New York, 2014; 233-247.
385. Reed DJ. Glutathione: toxicological implications. *Annu Rev Pharmacol Toxicol* 1990;30:603-631.

### LIST OF FIGURES

<b>Figure 1.1.</b> A) Diagram of the basic hepatic lobule and the acinus substructure. B) Diagram illustrating the basic structure and composition of liver sinusoids.	28
<b>Figure 1.2.</b> Schematic representation of the different steps involved in the initiation, development and resolution of drug-induced liver damage.	34
<b>Figure 1.3.</b> Representation of the ' <i>omics cascade</i> ' along with the figures of the estimated number of components belonging to each of the levels.	51
<b>Figure 1.4.</b> Scheme of a general workflow in a metabolomics study.	52
<b>Figure 1.5.</b> Scheme of the proposed global metabolite profile strategy.	55
<b>Figure 2.1.</b> A) Precellys 24 Dual equipped with a Cryolys cooler. B) Savant SpeedVac connected to an oil-free vacuum pump and a refrigerated vapor trap.	67
<b>Figure 2.2.</b> LC-MS metabolomic platforms employed. A) Instrument employed for untargeted metabolomic studies: a Waters Acquity UPLC system coupled to a Waters Synapt HDMS QToF mass spectrometer. B) Instrument employed for targeted metabolomic studies: a Waters Acquity UPLC system coupled to a Waters Xevo TQ-S mass spectrometer.	68
<b>Figure 2.3.</b> Schematic representation of the most important steps performed during data processing.	76
<b>Figure 2.4.</b> Workflow of data analysis strategy.	78
<b>Figure 2.5.</b> Simulated example of the application of boxplot of intensity distribution (A), PCA (B) and HCA (C) for the detection of outliers.	81
<b>Figure 2.6.</b> Cross-validation and permutation testing strategies for model optimization and validation.	85
<b>Figure 2.7.</b> Fundamental equations of PLS-DA.	87
<b>Figure 2.8.</b> Values of $R^2$ , $Q^2$ and misclassification error as a function of the number of LVs employed to build the PLS-DA model using the simulated data described in <b>Section 2.5.2.</b>	89



## List of Figures

---

- Figure 2.9.** Values obtained for the AUROC (green) and misclassification error (red) versus the number of retained variables using the simulated data described in **Section 2.5.2** based on the bootstrapped resampling coupled to VIP ranking strategy. 90
- Figure 2.10.** Scores (A) and loadings (B) plots corresponding to the PLS-DA model developed using the top 4 ranked variables and 1LV using the simulated data described in **Section 2.5.2** and a bootstrapping coupled to VIP-based ranking and variable selection strategy. 91
- Figure 2.11.** Permutations tests (n=1000) for  $R^2$  (A),  $Q^2$  (B), misclassification error (C) and AUROC (D) corresponding to the PLS-DA model developed using the top 4 ranked variables and 1LV from the simulated data described in **Section 2.5.2** and a bootstrapping coupled to VIP-based ranking and variable selection strategy. 92
- Figure 2.12.** HepG2 cells cultured at low (panel A) and high (panel B) densities. 93
- Figure 2.13.** Schematic representation of the parameters evaluated during sample processing and analysis strategy optimization. 96
- Figure 2.14.** Sample processing strategies tested during the development and optimization phase. 102
- Figure 2.15.** Adult medaka (*Oryzias latipes*). 107
- Figure 2.16.** Chromatograms corresponding to the targeted LC-MS/MS analysis of BAs. A) Non conjugated BAs. B) Glycine-conjugated BAs. C) Taurine-conjugated BAs. D) Deuterium-labeled IS. 117
- Figure 2.17.** Chromatograms corresponding to the targeted LC-MS/MS analysis of OS markers and related compounds. A) Sulphur containing and related compounds; B) Markers of OS damage to proteins; C) Markers of OS damage to DNA; D) MDA; E) IS. 123
- Figure 2.18.** Chromatograms corresponding to the targeted LC-MS/MS analysis of  $\gamma$ -glutamyl dipeptides and related compounds. A) IS Phe-D5; B) Aminoacids; C) Ophthalmic acid; D)  $\gamma$ -Glutamyl dipeptides; E) Compounds detected as NEM derivates; F) Oxidized compounds. 127
- Formula 2.1.** Expression to calculate mass resolution using the full width at half maximum (FWHM) approximation. 70

## List of Figures

---

<b>Formula 2.2.</b> Expression employed to calculate mass error in parts per million (ppm).	70
<b>Figure 3.1.</b> Analysis queue example in LC-MS untargeted metabolomic study.	135
<b>Figure 3.2.</b> The peak area (upper panel), mass error (middle panel) and retention time (RT, lower panel) for the IS sulfadimethoxine and reserpine spiked in the problem samples	136
<b>Figure 3.3.</b> Peak area (arbitrary units) variation along sample batch analysis for the different IS spiked in the pooled QC	137
<b>Figure 3.4.</b> Mass error (ppm) variation along sample batch analysis for the different IS spiked in the pooled QC.	138
<b>Figure 3.5.</b> Retention time (RT, expressed in minutes) variation along sample batch analysis for the different IS spiked in the pooled QC.	139
<b>Figure 3.6.</b> PCA scores plot showing the natural interrelationship among the different QC and problem samples included in the example study.	140
<b>Figure 3.7.</b> Venn diagrams showing the overlap between the different analytical conditions with respect to polar (A) and lipidic metabolites (B) in sample analysis optimization.	145
<b>Figure 3.8.</b> The PCA scores plot showing the natural interrelationship among the different extracts in metabolome extraction optimization.	147
<b>Figure 3.9.</b> Workflow of the optimized sample processing and analysis strategy for the analysis of the endometabolome of HepG2 cells.	152
<b>Figure 3.10.</b> PCA scores plots corresponding to data obtained from HepG2 cells treated with hepatotoxins acting through different mechanisms of toxicity and analyzed using the generic metabolomic strategy. A) Control vs OS. B) Control vs Steatosis. C) Control vs Cholestasis. D) Control vs Phospholipidosis.	156
<b>Figure 3.11.</b> Boxplots showing the most important changes associated to generic hepatotoxicity in HepG2 cells analyzed following the generic untargeted metabolomic analysis strategy.	159
<b>Figure 3.12.</b> Boxplots showing the most important changes associated to OS treatment in HepG2 cells analyzed using the generic untargeted strategy.	160

## List of Figures

---

<b>Figure 3.13.</b> $\gamma$ -glutamyl cycle.	162
<b>Figure 3.14.</b> Hypothesis postulated by Soga et al to explain the accumulation of $\gamma$ -glutamyl dipeptides under OS conditions.	163
<b>Figure 3.15.</b> Boxplots showing the most important changes associated to steatosis treatment in HepG2 cells analyzed using the generic untargeted metabolomic analysis strategy.	165
<b>Figure 3.16.</b> Main lipidic pathways showing alterations as a result of drug-induced steatosis.	167
<b>Figure 3.17.</b> Boxplots showing the most important changes associated to HepG2 cells exposed to cyclosporine A and analyzed using the generic untargeted metabolomic strategy.	170
<b>Figure 3.18.</b> Boxplots showing the most important changes associated to HepG2 cells treated with phospholipidogenic drugs and analyzed following the untargeted metabolomic strategy.	172
<b>Figure 3.19.</b> PCA scores plots corresponding to the lipidomic analysis of HepG2 cells preloaded with a mixture of free FAs and treated with phospholipidogenic and steatogenic compounds. <b>A)</b> Control vs phospholipidosis . <b>B)</b> Control vs steatosis . <b>C)</b> All groups together.	176
<b>Figure 3.20.</b> Boxplots showing the changes induced in the levels of PLs and LysoPLs as a result of the treatment with steatosis and phospholipidosis-inducing drugs in HepG2 cells previously incubated with a mixture of free FAs.	178
<b>Figure 3.21.</b> Boxplots showing the changes induced in the lipidome (except phospholipids) as a result of the treatment with steatosis and phospholipidosis-inducing drugs in HepG2 cells previously incubated with a mixture of FA.	179
<b>Figure 3.22.</b> Boxplots showing the differences in palmitic and oleic acid distribution in lipidic species as a result of drug-induced steatosis in HepG2 cells pre-incubated with a mix of palmitic and oleic acids and analyzed using a lipidomic strategy.	181
<b>Figure 3.23.</b> Boxplots showing the results obtained with the targeted analysis of OS markers (GSH/GSSG, upper panel; ophthalmic acid, middle panel; and MDA, lower panel) for HepG2 cells treated with control compounds , tert-butyl hydroperoxide , amiodarone , tetracycline and cyclosporine (blue).	185

## List of Figures

---

- Figure 3.24.** Model parameters optimization using the data obtained with the generic untargeted metabolomic analysis of HepG2 treated with either non-toxic or hepatotoxic compounds. **A)** Selection of the number of LVs. **B)** Selection of the variables to be included in the final model. 189
- Figure 3.25.** Summary of the results provided by the PLS-DA model built using 2 LVs and the top-ranked 8 variables based on the data obtained with the generic untargeted metabolomic analysis of HepG2 treated with either non-toxic or hepatotoxic compounds. **A)** Scores plot. **B)** Loadings plot. **C)** Permutation test for the misclassification error. **D)** Permutation test for the AUROC. 190
- Figure 3.26.** Model parameters optimization using the data obtained with the generic untargeted metabolomic analysis of HepG2 treated with either non-toxic or hepatotoxic compounds acting through different mechanism of hepatotoxicity (i.e. OS, phospholipidosis and steatosis). **A)** Selection of the number of LVs. **B)** Selection of the variables to be included in the final model. 192
- Figure 3.27.** Summary of the results provided by the PLS-DA model built using 3 LVs and the top-22 ranked variables based on the data obtained with the generic untargeted metabolomic analysis of HepG2 treated with either non-toxic or hepatotoxic compounds acting through different mechanism of hepatotoxicity (i.e. OS, phospholipidosis and steatosis). **A)** Scores plot. **B)** Permutation test for the misclassification error. **C)** Permutation test for the multiclass AUROC. 193
- Figure 3.28.** Model parameters optimization using the data obtained with the lipidomic analysis of HepG2 treated with either non-toxic or hepatotoxic compounds inducing steatosis or phospholipidosis in the presence of an external source of FA. and using those lipidic compounds containing only FA(16:0) and/or FA(18:1) moieties. **A)** Selection of the number of LVs. **B)** Selection of the variables to be included in the model. 196
- Figure 3.29.** Summary of the results provided by the PLS-DA model built using 2 LVs and the top-ranked 8 variables based on the data obtained with the lipidomic analysis of HepG2 treated with either non-toxic or hepatotoxic compounds inducing steatosis or phospholipidosis in the presence of an external source of FA. **A)** Scores plot. **B)** Loadings plot. **C)** Permutation test for the misclassification error. **D)** Permutation test for the AUROC. 197

## List of Figures

---

- Figure 3.30.** Scores plots corresponding to the PCA performed using the data obtained from the metabolomic analysis of liver of medaka treated either with control (i.e. non-toxic) or hepatotoxic compounds acting through different mechanisms of toxicity (i.e. cholestasis, phospholipidosis and steatosis). **A)** Control vs cholestasis. **B)** Control vs Phospholipidosis. **C)** Control vs Steatosis. 202
- Figure 3.31.** Boxplots showing the most important changes associated to generic hepatotoxicity in the liver of medaka analyzed following the generic untargeted metabolomic analysis strategy. 204
- Figure 3.32.** Boxplots showing the most important changes associated to cholestasis treatment in the liver of medaka analyzed following a generic untargeted analysis strategy. 205
- Figure 3.33.** Boxplots showing the most important changes associated to phospholipidosis treatment in the liver of medaka analyzed following a generic untargeted analysis strategy. 208
- Figure 3.34.** Boxplots showing the most important changes associated to steatosis treatment in the liver of medaka analyzed following a generic untargeted analysis strategy. 208
- Figure 3.35.** Model parameters optimization using the data obtained with generic untargeted metabolomic analysis of the liver of medaka treated with either non-toxic or hepatotoxic compounds. **A)** Selection of the number of LVs. **B)** Selection of the variables to be included in the final model. 212
- Figure 3.36.** Summary of the results provided by the PLS-DA model built using 2 LVs and the top-ranked 6 variables based on the data obtained with the generic untargeted metabolomic analysis of livers from medaka treated with either non-toxic or hepatotoxic compounds. **A)** Scores plot. **B)** Loadings plot. **C)** Permutation test for the misclassification error. **D)** Permutation test for the AUROC. 213
- Figure 3.37.** Model parameters optimization using the data obtained with generic untargeted metabolomic analysis of the liver of medaka treated with either non-toxic or hepatotoxic compounds acting through different mechanism of hepatotoxicity (i.e. cholestasis, phospholipidosis and steatosis). **A)** Selection of the number of LVs. **B)** Selection of the variables to be included in the final model. 214

## List of Figures

---

- Figure 3.38.** Summary of the results provided by the PLS-DA model built using 3 LVs and the top-23 ranked variables based on the data obtained with the generic untargeted metabolomic analysis of livers of medaka treated with either non-toxic or hepatotoxic compounds acting through different mechanism of hepatotoxicity (i.e. cholestasis, phospholipidosis and steatosis). **A)** Scores plot. **B)** Permutation test for the misclassification error. **C)** Permutation test for the multiclass AUROC. 215
- Figure 3.39.** Scores plots corresponding to the PCA performed using the data obtained from the metabolomic analysis of liver and serum of rats dosed either vehicle (i.e. control, green) or model hepatotoxins (i.e. paracetamol and tetracycline), 217
- Figure 3.40.** Boxplots showing the most important changes associated to tetracycline treatment in the liver of rats. 219
- Figure 3.41.** Boxplots showing the most important changes associated to tetracycline treatment in the serum of rats. 220
- Figure 3.42.** Boxplots showing the most important changes associated to paracetamol treatment in the liver of rats. 222
- Figure 3.43.** Summary of BA metabolism and transport processes. 225
- Figure 3.44.** BA composition in the serum of rats as a result of the indicated treatments. Results expressed as percentage of the indicated group of BA (non-conjugated, glycine-conjugated and taurine-conjugated) with respect the total pool of BA. 227



## LIST OF TABLES

<b>Table 1.1.</b> <i>In vitro</i> models for hepatotoxicity studies.	44
<b>Table 2.1.</b> Figures of the different strategies employed for variable selection over the simulated data described in <b>Section 2.5.2</b> .	83
<b>Table 2.2.</b> Model hepatotoxins included in the HepG2 cell studies classified by their mechanism of hepatotoxicity.	95
<b>Table 2.3.</b> Model hepatotoxins included in the study using <i>Oryzias latipes</i> .	108
<b>Table 2.4.</b> Mass spectrometer setup for the quantification of selected bile acids.	116
<b>Table 2.5.</b> Mass spectrometer setup for the quantification of selected oxidative stress markers.	120
<b>Table 2.6.</b> Mass spectrometer setup for the quantification of selected $\gamma$ -glutamyl dipeptides and related compounds.	126
<b>Table 3.1.</b> Summary of the metabolites detected by each extract under the different analytical conditions.	144
<b>Table 3.2.</b> Summary of the metabolites detected with each sample processing strategy under each analytical condition.	150
<b>Table 3.3.</b> Values of fold of change for control vs treated cells for each of the lipid classes and treatments.	183
<b>Table 3.4.</b> Clinical laboratory analysis of serum samples from rats treated with hepatotoxic compounds.	216
<b>Table 3.5.</b> BA concentration (expressed as nM) in the serum of rats as a result of the indicated treatments.	226
<b>Table 3.6.</b> $\gamma$ -glutamyl dipeptides and related compounds concentration (expressed as nM) in the serum of rats as a result of the indicated treatments.	229





### LIST OF PUBLICATIONS

1. **García-Cañaveras JC**, Donato MT, Castell JV, Lahoz A. A comprehensive untargeted metabolomic analysis of human steatotic liver tissue by RP and HILIC chromatography coupled to mass spectrometry reveals important metabolic alterations. *J Proteome Res* 2011;10:4825-4834.
2. Quintás G, Portillo N, **García-Cañaveras JC**, Castell JV, Ferrer A, Lahoz A. Chemometric approaches to improve PLSDA model outcome for predicting human non-alcoholic fatty liver disease using UPLC-MS as a metabolic profiling tool. *Metabolomics* 2012;8:86-98.
3. **García-Cañaveras JC**, Donato MT, Castell JV, Lahoz A. Targeted profiling of circulating and hepatic bile acids in human, mouse, and rat using a UPLC-MRM-MS-validated method. *J Lipid Res* 2012;53:2231-2241.
4. Leon Z, **García-Cañaveras JC**, Donato MT, Lahoz A. Mammalian cell metabolomics: experimental design and sample preparation. *Electrophoresis* 2013;34:2762-2775.
5. Carretero A, León Z, **García-Cañaveras JC**, Zaragoza Á, Gómez-Lechón MJ, Donato MT, Lahoz A. In vitro/in vivo screening of oxidative homeostasis and damage to DNA, protein, and lipids using UPLC/MS-MS. *Anal Bioanal Chem* 2014;406:5465-5476.
6. Cortes M, Pareja E, **García-Cañaveras JC**, Donato MT, Montero S, Mir J, Castell JV, Lahoz A. Metabolomics discloses donor liver biomarkers associated with early allograft dysfunction. *J Hepatol* 2014;61:564-574.

## List of Publications

---

7. **García-Cañaveras JC**, Donato MT, Lahoz A: Ultra-Performance Liquid Chromatography-Mass Spectrometry Targeted Profiling of Bile Acids: Application to Serum, Liver Tissue, and Cultured Cells of Different Species. In: Raftery D, ed. Mass Spectrometry in Metabolomics. Volume 1198: Springer New York, 2014; 233-247.



Instituto de  
**Investigación**  
Sanitaria LaFe